Distribution Agreement

In presenting this thesis or dissertation as a partial fulfillment of the requirements for an advanced degree from Emory University, I hereby grant to Emory University and its agents the non-exclusive license to archive, make accessible, and display my thesis or dissertation in whole or in part in all forms of media, now or hereafter known, including display on the world wide web. I understand that I may select some access restrictions as part of the online submission of this thesis or dissertation. I retain all ownership rights to the copyright of the thesis or dissertation. I also retain the right to use in future works (such as articles or books) all or part of this thesis or dissertation.

Signature:

_____ _____

Laura E. Newman Date

The small GTPase ARL2 is a novel regulator of mitochondrial fusion

By

Laura E. Newman
Doctor of Philosophy

Graduate Division of Biological and Biomedical Science
Biochemistry, Cell, and Developmental Biology

_____
Richard A. Kahn, Ph.D.
Advisor

_____
Lawrence H. Boise, Ph.D.
Committee Member

_____
John R. Hepler, Ph.D.
Committee Member

_____
Zixu Mao, M.D., Ph.D.
Committee Member

_____
James Q. Zheng, Ph.D.
Committee Member

Accepted:

_____
Lisa A. Tedesco, Ph.D.
Dean of the James T. Laney School of Graduate Studies

_____
Date

The small GTPase ARL2 is a novel regulator of mitochondrial fusion

By

Laura E. Newman
B.S., Indiana University Bloomington, 2009

Advisor: Richard A. Kahn, Ph.D.

An abstract of
A dissertation submitted to the Faculty of the
James T. Laney School of Graduate Studies of Emory University
in partial fulfillment of the requirements for the degree of
Doctor of Philosophy
in Graduate Division of Biological and Biomedical Sciences
Biochemistry, Cell, and Developmental Biology
2016

Abstract

The small GTPase ARL2 is a novel regulator of mitochondrial fusion
By Laura E. Newman

ARL2 is a small GTPase and member of the ARF family of GTPases. ARL2 is ubiquitous, conserved across eukaryotes, predicted to be present in the last eukaryotic common ancestor, and essential in three model organisms. ARL2 is unusual among regulatory GTPases in that it localizes to several places in the cell, including cytosol, centrosomes, the nucleus, and mitochondria. Though its actions at the other locations have been documented, its functions in mitochondria are poorly described. In this dissertation, I document our research that has expanded our knowledge of mitochondrial functions of ARL2. We show that ARL2 is required for mitochondrial morphology, motility, and ATP production. In addition, we show that the ARL2 GAP ELMOD2 is also required for mitochondrial morphology and motility, but not ATP production. Based on these data, we model two pathways in mitochondria regulated by ARL2: one regulating morphology and motility with ELMOD2 as the likely ARL2 effector, and the other regulating ATP production without ELMOD2. To further study regulation of morphology by ARL2, we developed plasmids for targeting exogenous proteins to either the mitochondrial intermembrane space or matrix, under the control of variable strength CMV promoters. I then used these plasmids to demonstrate that ARL2 regulates mitochondrial morphology from the intermembrane space. Additionally, I show that ARL2 regulates mitochondrial fusion upstream of the mitofusins. We expand upon these studies to show that the amount of ARL2 and ELMOD2 in mitochondria is responsive to the fusogenic activity of MFN2, as well as cellular stressors leading to mitochondrial hyperfusion. These observations further support a role for ARL2 and ELMOD2 in mitochondrial fusion. Finally, I provide preliminary data that ARL2 regulates ATP levels via cristae morphology, that ARL2 also regulates mitochondrial motility, and that ARL2 is phosphorylated in cells. From this research, I conclude that ARL2, and likely ELMOD2, are novel regulators of mitochondrial fusion. Future research will focus on identifying novel mitochondrial binding partners of ARL2 and ELMOD2, with the goal of elucidating the mechanism by which ARL2 regulates mitochondrial fusion.

The small GTPase ARL2 is a novel regulator of mitochondrial fusion

By

Laura E. Newman
B.S., Indiana University Bloomington, 2009

Advisor: Richard A. Kahn, Ph.D.

A dissertation submitted to the Faculty of the
James T. Laney School of Graduate Studies of Emory University
in partial fulfillment of the requirements for the degree of
Doctor of Philosophy
in Graduate Division of Biological and Biomedical Sciences
Biochemistry, Cell, and Developmental Biology
2016

Table of Contents

Abbreviations

ANT1	Adenine nucleotide transporter 1, aka AAC
ARL2	ADP ribosylation factor like 2
ARL3	ADP ribosylation factor like 3
BART	Binder of ARL2, aka ARL2 binding protein (ARL2BP)
BN-PAGE	Blue native polyacrylamide gel electrophoresis
CCCP	Carbonyl cyanide 3-chlorophenylhydrazone
CMV	Cytomegalovirus, referring to the promoter
DRP1	Dynamin related protein 1
ELMOD2	ELMO [engulfment and cell motility] domain containing protein 2
EM	Electron microscopy
ER	Endoplasmic reticulum
ERMES	ER mitochondrial encounter structure
FBS	Fetal bovine serum
FIS1	Mitochondrial fission 1 protein
GAP	GTPase activating protein
GEF	Guanine nucleotide exchange factor
GFP	Green fluorescent protein

IMS	Intermembrane space [mitochondria]
IP	Immunoprecipitation
HSP60	Heat shock protein 60
MEF	Mouse embryonic fibroblast
MEF2D	Myocyte enhancer factor 2D
MFF	Mitochondrial fission factor
MFN1	Mitofusin 1
MFN2	Mitofusin 2
MICOS	Mitochondrial contact site and cristae organizing system, previously known as MINOS and MitOS
MiD49	Mitochondrial elongation factor 2
MiD51	Mitochondrial elongation factor 1
MIGA	Mitoguardin
MLS	Mitochondrial localization sequence
mtDNA	Mitochondrial DNA
OCT	Ornithine carbamoyltransferase (or the 32 residue leader sequence derived from the human protein)
OPA1	Optic atrophy protein 1
PAGFP	Photoactivatable GFP

PTM	Post-translational modification
RIN1	Rab and ras interactor 1
ROS	Reactive oxygen species
SDS-PAGE	Sodium dodecyl sulfate polyacrylamide gel electrophoresis
SIM	Structured illumination microscopy
siRNA	short interfering RNA
SMAC	second mitochondria-derived activator of caspases, or the 59 residue leader sequence derived from the human protein; aka Diablo
SMAD2	Mothers against decapentaplegic homolog 2
STAT3	Signal transducer and activator of transcription 3
VDAC	Voltage dependent anion carrier

Chapter 1: Introduction

1. Mitochondria

Mitochondria are essential organelles within all eukaryotic cells. They have critical roles in a variety of important functions, including ATP generation, apoptosis, lipid synthesis, and calcium buffering. Mitochondria also figure prominently in the evolutionary origins of eukaryotes: according to the endosymbiotic theory, mitochondria were a one-celled prokaryote that were either engulfed by or infected another cell, which became the last eukaryotic common ancestor. Over time, most mitochondrial genes were transferred to the nucleus, although mitochondria retain some of their original DNA (Zimorski et al., 2014). Mitochondria are also unique organelles in that they are surrounded by two membranes (Figure 1). The mitochondrial outer membrane houses machinery important for several mitochondrial functions, including mitochondrial import, motility, mitophagy, lipid biosynthesis, and outer membrane fusion. In contrast to the outer membrane, the inner membrane is highly invaginated, and these invaginations are called cristae (Figure 1). The electron transport chain, a collection of five complexes (Complex I-V) that generate ATP, localizes discretely to cristae, with Complex V forming dimers at the tips of cristae invaginations and are important determinants of membrane curvature at that site (Paumard et al., 2002; Habersetzer et al., 2013; Wilkens et al., 2013). Between the two membranes is the intermembrane space (IMS), which contains proteins important for electron transport chain function and apoptosis. Finally, the matrix is the innermost space within mitochondria, bounded by the inner membrane, and houses mitochondrial DNA.

Over the course of eukaryotic evolution, most genes encoding mitochondrial proteins have moved into the genomic DNA and mitochondrial functions have been integrated into cellular homeostasis and functions in all parts of the cell. Given their complex organization as well as evolutionary origins, how mitochondria communicate with the rest of the cell is a major

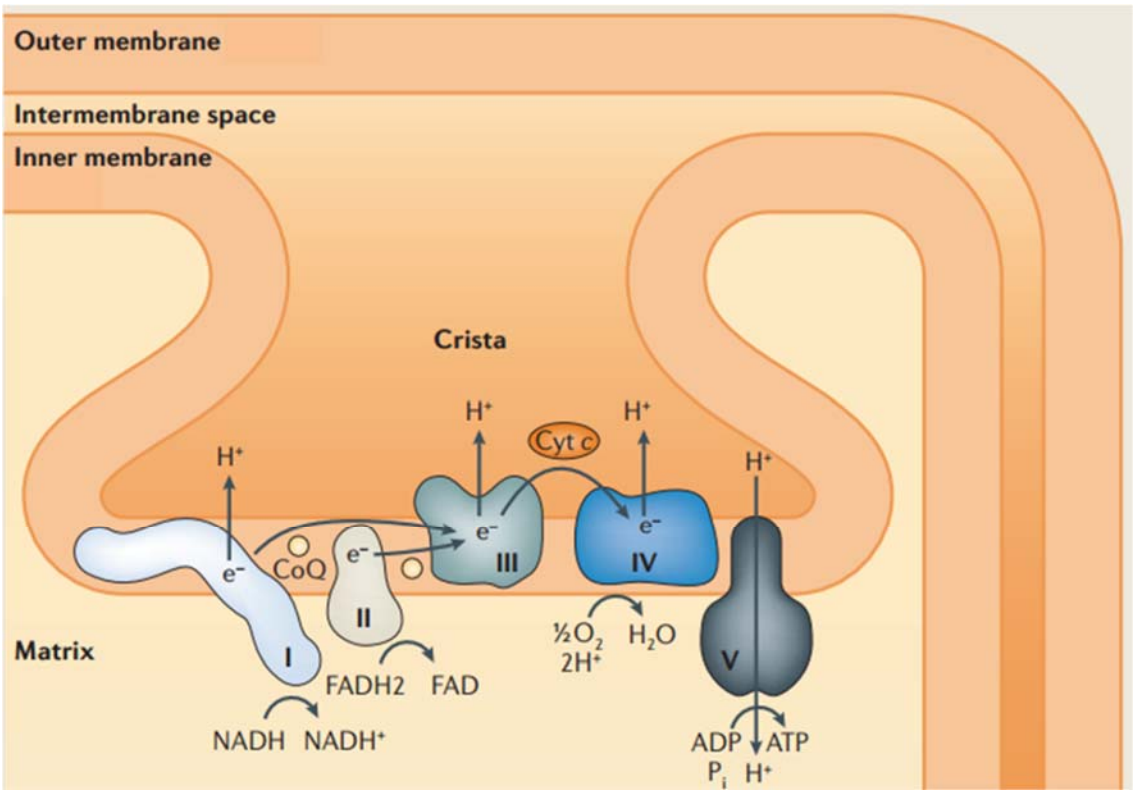

Figure 1. Schematic of mitochondrial structure. Mitochondria possess both an outer membrane, as well as an inner membrane. The intermembrane space (IMS) exists between the two membranes. The inner membrane is highly invaginated, and the invaginations are called cristae. The electron transport chain (complexes I, II, III, IV, and V) localize to cristae membranes. Finally, the matrix is the space within the inner membrane. Figure cropped from Box 1 in Mishra and Chan, 2014. Reprinted with permission (details at end of dissertation).

unanswered question in mitochondrial biology. There are several examples in which small molecules (adenine nucleotides, calcium or intermediates of metabolism) are exchanged across mitochondrial membranes impacting cell metabolism and functions. But very few examples exist of protein-based cell signals emanating from the mitochondria (e.g, cytochrome c release during apoptosis) or targeted to mitochondria to alter its functions. A few examples of the latter also exist: the transcription factors STAT3 (Wegrzyn et al., 2009a) and MEF2D (She et al., 2011), which both localize to the nucleus, also localize to mitochondria, where they modulate respiratory complexes. Several DNA repair proteins also localize to both the nucleus and mitochondria (Bauer et al., 2015). Additionally, fumarase, an enzyme in the tricarboxylic acid cycle in mitochondria, has a separate role in response to DNA damage (Yogev et al., 2011). Though there are a few examples of proteins retro-translocating from within mitochondria back to the cytosol, it is thought that most proteins imported into mitochondria are eventually degraded there, though a few examples of retro-translocation exist (Yamano and Youle, 2013; Bragoszewski et al., 2015). Therefore, mitochondria use other molecules, such as ROS, in retrograde signaling to other parts of the cell. These molecules are able to cross the outer membrane through VDAC, where they can modify other proteins and communicate with other organelles, such as the nucleus (Shadel and Horvath, 2015).

2. Mitochondrial dynamics

Mitochondria are dynamic organelles in that they constantly move and modify their shape in response to cellular demand. Mitochondrial shape is important for function, highly dynamic, varies amongst different cell types to meet acute energy or other demands, and is responsive to cellular stress (Mishra and Chan, 2014). Mitochondria can appear tubular and thread-like, termed “elongated,” or they can appear small and spherical (“fragmented”) (see examples in Figure 2). Larger mitochondria contain more cristae, and are thus capable of higher ATP production. In support of this idea, mitochondria elongate during conditions of glucose

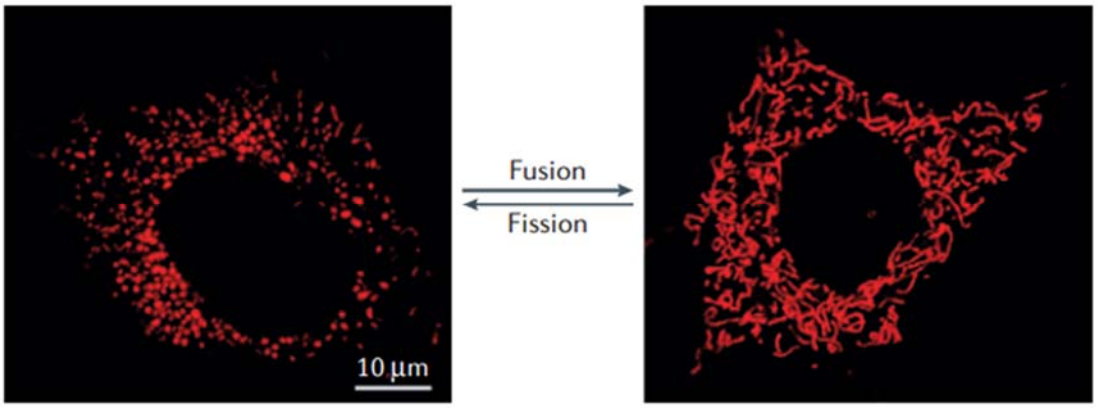

Figure 2. **Mitochondrial shape varies as a result of fission and fusion**. Mitochondrial morphology can appear fragmented (left), elongated (right), or can appear intermediate between the two. Morphology is regulated by fission and fusion, which are two opposing processes. Fragmented mitochondria appear small and spherical, and can result from either too little fusion or too much fission. In contrast, elongated mitochondria appear long, tubular, and thread-like, and can result from either a decrease in fission or an increase in fusion. Figure cropped from Figure 1 from Mishra and Chan, 2014. Reprinted with permission (details at end of dissertation).

starvation, to maintain ATP levels (Gomes et al., 2011; Mishra et al., 2014). Fusion is also important for maintenance of mtDNA and mixing of mitochondrial contents (Chen et al., 2007; Song et al., 2009; Chen et al., 2010; Chan, 2012). On the other hand, mitochondrial fragmentation is required for efficient trafficking (Saotome et al., 2008), apoptosis (Frank et al., 2001), equal distribution of mitochondria into daughter cells during mitosis (Taguchi et al., 2007), and segregation of dysfunctional mitochondria for elimination by mitophagy (Tanaka et al., 2010). Mitochondrial shape is regulated by two opposing processes – fission and fusion. Fission is mitochondrial division, while fusion involves mitochondria joining and mixing contents. Fragmented mitochondria can result from either an increase in fission or decrease in fusion, whereas elongation can result from the opposite. Therefore, the overall mitochondrial shape within the cell is the result of the balance of fission and fusion (Chan, 2012). Despite the clear importance of these processes to the activities of mitochondria and health of the cell, we have only incomplete understandings of each process.

2.1 Mitochondrial fission

Mitochondrial fission is mediated by machinery present on or recruited to the outer mitochondrial membrane. Fission is driven by recruitment of DRP1, a large dynamin-related GTPase, from the cytosol to the mitochondrial outer membrane. Once DRP1 is localized to the outer membrane, it oligomerizes, forming a ring that constricts mitochondria and promotes division (Smirnova et al., 1998; Labrousse et al., 1999; Smirnova et al., 2001). DRP1 is recruited to mitochondria primarily by MFF, but can also be independently recruited by FIS1, MiD49, and MiD51 (Yoon et al., 2003; Yu et al., 2005; Otera et al., 2010; Palmer et al., 2011). The upstream events leading to mitochondrial fission are still unclear. The endoplasmic reticulum (ER) makes contacts at specific sites where DRP1 is later recruited prior to fission, suggesting a role for ER in upstream events leading to fission (Friedman et al., 2011). Additionally, a recent study demonstrated that division of mtDNA nucleoids also occurs at sites of ER-mediated constriction

prior to fission (Lewis et al., 2016). However, the upstream events for both ER and mtDNA in fission are unknown. Therefore, more work on the regulation of fission and the underlying mechanisms is required.

2.2 Mitochondrial fusion

Mitochondrial fusion is regulated by three dynamin-related GTPases: OPA1, and the two mitofusins, MFN1 and MFN2, each of which are transmembrane proteins. OPA1 localizes to and promotes inner membrane fusion, and also regulates cristae morphology (Cipolat et al., 2004; Griparic et al., 2004). Outer membrane fusion is mediated by MFN1 and MFN2, which are localized in the outer membrane (Chen et al., 2003; Chen et al., 2005). MFNs are thought to act in trans, on adjacent mitochondria, to form specific attachments or tethers that promote fusion. Though both MFNs promote outer membrane fusion, MFN1 has stronger tethering and fusion activity in vitro (Ishihara et al., 2004). MFN2 also differs from MFN1 in that it has additional signaling and metabolic roles (Bach et al., 2003; Chen et al., 2005; Pich et al., 2005; Mourier et al., 2015), and also acts as a tether between mitochondria and the ER (de Brito and Scorrano, 2008), though this has recently been contested (Cosson et al., 2012; Filadi et al., 2015). MFNs are ubiquitiously expressed, though MFN2 is the predominant mitofusin in heart, skeletal muscle, and the brain (Eura et al., 2003; Santel et al., 2003).

The importance of mitochondrial fusion is underscored by the fact that mutations in mitochondrial proteins involved in fusion are associated with human diseases. Mutations in MFN2 cause Charcot-Marie-Tooth Type 2A (Zuchner et al., 2004), while mutations in OPA1 are linked to dominant optic atrophy (Alexander et al., 2000; Delettre et al., 2000). Additionally, *mfn1*$^{-/-}$ and *mfn2*$^{-/-}$ mice are embryonic lethal due to defective placental development (Chen et al., 2003). Conditional deletion of MFN2 after placental development results in cerebellar defects and mice die by day P17 (Chen et al., 2007). Deletion of OPA1 also results in embryonic lethality

(Alavi et al., 2007; Davies et al., 2007). Therefore, a better understanding of mitochondrial fusion will also improve our understanding of the cellular processes that underlie these, and other, human diseases.

Fusion of the outer and inner mitochondrial membranes occurs sequentially, with outer membrane fusion necessarily occurring before inner membrane fusion (Song et al., 2009; Mishra et al., 2014) (Figure 3). MFN1 and MFN2 promote outer membrane fusion by oligomerizing; both homo-oligomers and hetero-oligomers are capable of promoting fusion. MFN first form cis oligomers on one mitochondrion, which is regulated by the binding of GTP. Next, MFN cis oligomers form larger trans oligomers and tether opposing mitochondria, which requires GTP hydrolysis (Ishihara et al., 2004). Downstream of MFNs, mitoPLD converts cardiolipin to phosphatidic acid on the opposing mitochondrial membrane, and this step is required for outer membrane fusion to proceed (Choi et al., 2006). MIGAs have recently been implicated in fusion downstream of MFNs by influencing dimerization of mitoPLD (Zhang et al., 2016). After outer membrane fusion is complete, OPA1 homo-oligomerizes to promote inner membrane fusion, though details of this mechanism are still missing (Cipolat et al., 2004; Escobar-Henriques and Anton, 2013; Mishra et al., 2014).

2.3 Mitochondrial motility

Mitochondria constantly move to areas of the cell to supply ATP or calcium. In eukaryotic cells, mitochondria traffic primarily along microtubules, though they can traffic along actin filaments and also interact with intermediate filaments (Boldogh and Pon, 2007). For plus-end directed motility along microtubules, attachment to kinesin and microtubules is mediated by MIRO and Milton. MIRO is a calcium sensitive GTPase, with two GTPase domains, that localizes to the outer mitochondrial membrane (Fransson et al., 2003). MIRO regulates mitochondrial motility in response to local calcium concentration (Wang and Schwarz, 2009).

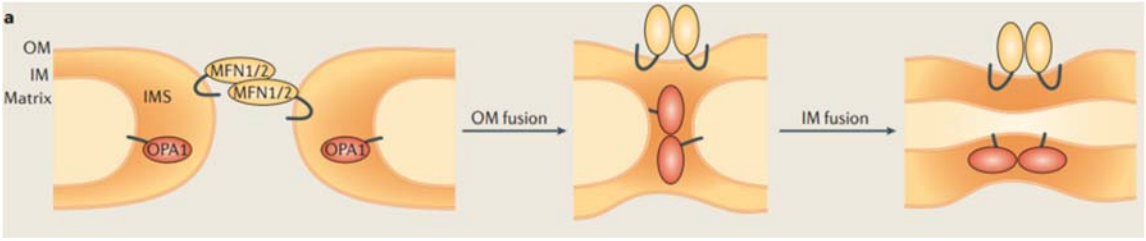

Figure 3. Summary of mitochondrial fusion. Mitochondrial fusion is controlled by three large, dynamin-related GTPases and occurs in two steps. First, fusion of the outer membrane is mediated by MFN1 and MFN2. MFN1 and MFN2 can homo- or hetero-oligomerize to drive outer membrane fusion. In the second step, inner membrane fusion is mediated by homo-oligomerization of OPA1. Figure cropped from Box 2 in Mishra and Chan, 2014. Reprinted with permission (details at end of dissertation).

Attachment of MIRO to kinesin is mediated by Milton (fly homolog, mammalian orthologs are TRAK1 and TRAK2, also known as GRIF1) (Glater et al., 2006). Finally, kinesins (both KIF1B and KIF5B) are plus-end directed motor proteins that transport mitochondria (Hirokawa and Takemura, 2005). Minus-end directed motility occurs via dynein and dynactin (Varadi et al., 2004). Interestingly, the motility machinery interacts with mitochondrial fission and fusion machinery. Overexpression of a subunit of dynactin, dynamitin (p50), disrupts DRP1 recruitment to mitochondria, and two dynactin subunits co-immunoprecipitate with DRP1 (Varadi et al., 2004). In addition, both MFN1 and MFN2 co-immunoprecipitate with MIRO1, and deletion of MFN2 adversely affects mitochondrial motility (Chen et al., 2003; Misko et al., 2010). Therefore, there is likely crosstalk between mitochondrial motility and fission/fusion.

3. Regulation of mitochondrial fusion

3.1 Regulation of OPA1

Fusogenic activity of OPA1 is regulated by its proteolytic cleavage, resulting in the generation of a complex collection of OPA1 proteins. Loss of membrane potential activates the inner membrane protease OMA1, which cleaves and inactivates OPA1, preventing mitochondrial fusion (Griparic et al., 2007; Ehses et al., 2009; Head et al., 2009). OPA1 is also cleaved by YME1L, another inner membrane protease, at a different site from OMA1 cleavage. Cleavage of OPA1 by YME1L is proposed to occur in response to respiratory activity, and the cleaved form stimulates fusion (Song et al., 2007; Mishra et al., 2014). However, another study found that cleavage by YME1L and the short form of OPA1 are both dispensable for mitochondrial fusion (Anand et al., 2014), so the role of OPA1 proteolytic cleavage by YME1L requires further study. Besides proteolytic cleavage by proteases embedded in the inner mitochondrial membrane, no other regulatory factors of OPA1 have been identified.

3.2 Regulation of MFNs

To date, only a few proteins have been found to regulate MFNs. MIB binds to MFNs and negatively regulates their activity through an unknown mechanism (Eura et al., 2006). Additionally, Bax stimulates fusion via MFN2, but not MFN1 (Hoppins et al., 2011b). SMAD2 also stimulates MFN2 fusogenic activity by binding to MFN2 and recruiting RIN1, which is proposed to act as an MFN2 GEF (Kumar et al., 2016). MFNs are also regulated by post-translational modifications. MFN1 is phosphorylated during cell death, which inhibits its fusogenic activity and leads to mitochondrial fragmentation (Pyakurel et al., 2015). MFN1 is also deacetylated during glucose starvation, increasing its activity (Lee et al., 2014). Mitofusins also form disulfide bonds during oxidative stress, promoting cis-oligomerization and fusion (Shutt et al., 2012). Finally, MFNs are ubiquitinated by Parkin during mitophagy, leading to their degradation and inhibition of mitochondrial fusion (Tanaka et al., 2010). All of the known regulation of MFNs occurs from the cytosolic face of the outer membrane, consistent with the proposed topology of MFNs. MFNs have two transmembrane domains, so that both the N and C termini of MFNs face the cytosol, with a loop of 2-3 amino acids exposed to the IMS (Rojo et al., 2002). To date, no MFN regulatory factors from the IMS have been identified.

4. ARL2 and ELMOD2

ARL2 is a member of the ARF family of regulatory GTPases (Clark et al., 1993). ARL2 is ubiquitously expressed, very highly conserved across eukaryotes, and predicted to be present in the last eukaryotic common ancestor (Li et al., 2004). Additionally, ARL2 is essential in *S. pombe* (Radcliffe et al., 2000), *C. elegans* (Antoshechkin and Han, 2002), and *A. thaliana* (McElver et al., 2000), though is not essential in *S. cerevisiae* (Hoyt et al., 1990). Regulatory GTPases act as molecular switches, with guanine nucleotide exchange factors (GEFs) required for their activation and GTPase activating proteins (GAPs) acting as both effectors and terminators of the activated state. ELMOD2 was the first ARL2 GAP discovered, and the closely related family members

ELMOD1 and ELMOD3 also have GAP activity against ARL2 (Bowzard et al., 2007; Ivanova et al., 2014). However, no GEF for ARL2 has been identified.

ARL2 is unusual for a regulatory GTPase in that it localizes to several places in the cell, and has essential functions associated with each location. An estimated 90% of ARL2 is cytosolic, where it is bound to the tubulin chaperone Cofactor D and regulates tubulin folding (Bhamidipati et al., 2000; Sharer et al., 2002; Shern et al., 2003; Zhou et al., 2006; Tian et al., 2010). ARL2 and Cofactor D also localize to centrosomes and are implicated in recruitment of γ-tubulin ring complex, tubulin polymerization, and mitotic spindle organization (Zhou et al., 2006; Cunningham and Kahn, 2008). ARL2 also localizes to the nucleus, where it regulates transcriptional activation of STAT3 along with its effector BART. Finally, ARL2 and its paralog ARL3 regulate trafficking of farnesylated cargo (Ismail et al., 2011).

We have also described roles for ARL2 in mitochondria. Based on subcellular fractionation of cells, 5-10% of cellular ARL2 is associated with mitochondria, and further fractionation of mitochondria reveals a pool of ARL2 associated with the IMS as well as the matrix (Sharer et al., 2002). ARL2 and its effector BART together bind to the adenine nucleotide transporter 1 (ANT1), which exchanges mitochondrial ATP for cytosolic ADP across the inner mitochondrial membrane. Strikingly, the amount of mitochondrial ARL2 is increased specifically in cardiac and skeletal muscle of *ant1*$^{-/-}$ knockout mice (Sharer et al., 2002). These mice display cardiomyopathy, muscle weakness, and exercise intolerance (Graham et al., 1997), suggesting that mitochondrial roles of ARL2 are important for cardiac and skeletal muscle function. Another study identified ARL2 as a target of four microRNAs with high expression in the heart (Nishi et al., 2010), two of which (miR-15b and -195) are up-regulated in cardiac hypertrophy (van Rooij et al., 2006; Sayed et al., 2007). Overexpression of these microRNAs in rat neonatal cardiomyocytes lowered expression of ARL2, which was correlated with lower ATP levels and abnormal mitochondrial morphology (Nishi et al., 2010). Therefore, ARL2 may play an important

role in regulation of ATP levels and mitochondrial morphology, particularly in muscle tissues.

In this dissertation, I describe results of our research that have resulted in an expansion in our knowledge of mitochondrial functions of ARL2. In chapter two, we show that ARL2 is required for mitochondrial morphology, motility, and ATP production. We also show that loss of ELMOD2 affects mitochondrial morphology and motility, but not ATP production. From these observations, we model two pathways in mitochondria regulated by ARL2: one regulating morphology and motility with ELMOD2 as the likely ARL2 effector, and the other regulating ATP production independently of ELMOD2. In chapter three, we develop plasmids for targeting exogenous proteins to either the mitochondrial IMS or matrix, under the control of variable strength CMV promoters. These plasmids are used in chapter four to show that ARL2 regulates mitochondrial morphology from the IMS. In chapter four, I show that ARL2 regulates mitochondrial fusion upstream of the mitofusins. We expand upon these studies in chapter five to demonstrate that the amount of ARL2 and ELMOD2 in mitochondria is responsive to MFN2 and cellular stressors, further supporting a role for ARL2 and ELMOD2 in mitochondrial fusion. Chapter six summarizes my unpublished data concerning ARL2 and mitochondria, in which I provide preliminary data that ARL2 regulates ATP levels via cristae morphology, and that ARL2 also regulates mitochondrial motility. Finally, in chapter seven I show that ARL2 is phosphorylated in cells, though the functional significance of this phosphorylation remains to be determined. The last chapter is a discussion of the impact and significance of my findings.

References

Alavi, M.V., Bette, S., Schimpf, S., Schuettauf, F., Schraermeyer, U., Wehrl, H.F., Ruttiger, L., Beck, S.C., Tonagel, F., Pichler, B.J., Knipper, M., Peters, T., Laufs, J., and Wissinger, B. (2007). A splice site mutation in the murine Opa1 gene features pathology of autosomal dominant optic atrophy. Brain 130, 1029-1042.

Alexander, C., Votruba, M., Pesch, U.E., Thiselton, D.L., Mayer, S., Moore, A., Rodriguez, M., Kellner, U., Leo-Kottler, B., Auburger, G., Bhattacharya, S.S., and Wissinger, B. (2000). OPA1, encoding a dynamin-related GTPase, is mutated in autosomal dominant optic atrophy linked to chromosome 3q28. Nat Genet 26, 211-215.

Anand, R., Wai, T., Baker, M.J., Kladt, N., Schauss, A.C., Rugarli, E., and Langer, T. (2014). The i-AAA protease YME1L and OMA1 cleave OPA1 to balance mitochondrial fusion and fission. J Cell Biol 204, 919-929.

Antoshechkin, I., and Han, M. (2002). The C. elegans evl-20 gene is a homolog of the small GTPase ARL2 and regulates cytoskeleton dynamics during cytokinesis and morphogenesis. Dev Cell 2, 579-591.

Bach, D., Pich, S., Soriano, F.X., Vega, N., Baumgartner, B., Oriola, J., Daugaard, J.R., Lloberas, J., Camps, M., Zierath, J.R., Rabasa-Lhoret, R., Wallberg-Henriksson, H., Laville, M., Palacin, M., Vidal, H., Rivera, F., Brand, M., and Zorzano, A. (2003). Mitofusin-2 determines mitochondrial network architecture and mitochondrial metabolism. A novel regulatory mechanism altered in obesity. J Biol Chem 278, 17190-17197.

Bauer, N.C., Corbett, A.H., and Doetsch, P.W. (2015). The current state of eukaryotic DNA base damage and repair. Nucleic Acids Res 43, 10083-10101.

Bhamidipati, A., Lewis, S.A., and Cowan, N.J. (2000). ADP ribosylation factor-like protein 2 (Arl2) regulates the interaction of tubulin-folding cofactor D with native tubulin. J Cell Biol 149, 1087-1096.

Boldogh, I.R., and Pon, L.A. (2007). Mitochondria on the move. Trends Cell Biol 17, 502-510.

Bowzard, J.B., Cheng, D., Peng, J., and Kahn, R.A. (2007). ELMOD2 is an Arl2 GTPase-activating protein that also acts on Arfs. J Biol Chem 282, 17568-17580.

Bragoszewski, P., Wasilewski, M., Sakowska, P., Gornicka, A., Böttinger, L., Qiu, J., Wiedemann, N., and Chacinska, A. (2015). Retro-translocation of mitochondrial intermembrane space proteins. Proceedings of the National Academy of Sciences 112, 7713-7718.

Chan, D.C. (2012). Fusion and fission: interlinked processes critical for mitochondrial health. Annu Rev Genet 46, 265-287.

Chen, H., Chomyn, A., and Chan, D.C. (2005). Disruption of fusion results in mitochondrial heterogeneity and dysfunction. J Biol Chem 280, 26185-26192.

Chen, H., Detmer, S.A., Ewald, A.J., Griffin, E.E., Fraser, S.E., and Chan, D.C. (2003). Mitofusins Mfn1 and Mfn2 coordinately regulate mitochondrial fusion and are essential for embryonic development. J Cell Biol 160, 189-200.

Chen, H., McCaffery, J.M., and Chan, D.C. (2007). Mitochondrial fusion protects against neurodegeneration in the cerebellum. Cell 130, 548-562.

Chen, H., Vermulst, M., Wang, Y.E., Chomyn, A., Prolla, T.A., McCaffery, J.M., and Chan, D.C. (2010). Mitochondrial fusion is required for mtDNA stability in skeletal muscle and tolerance of mtDNA mutations. Cell 141, 280-289.

Choi, S.Y., Huang, P., Jenkins, G.M., Chan, D.C., Schiller, J., and Frohman, M.A. (2006). A common lipid links Mfn-mediated mitochondrial fusion and SNARE-regulated exocytosis. Nature cell biology 8, 1255-1262.

Cipolat, S., de Brito, O.M., Dal Zilio, B., and Scorrano, L. (2004). OPA1 requires mitofusin 1 to promote mitochondrial fusion. Proc Natl Acad Sci U S A 101, 15927-15932.

Clark, J., Moore, L., Krasinskas, A., Way, J., Battey, J., Tamkun, J., and Kahn, R.A. (1993). Selective amplification of additional members of the ADP-ribosylation factor (ARF) family:

cloning of additional human and Drosophila ARF-like genes. Proc Natl Acad Sci U S A 90, 8952-8956.

Cosson, P., Marchetti, A., Ravazzola, M., and Orci, L. (2012). Mitofusin-2 independent juxtaposition of endoplasmic reticulum and mitochondria: an ultrastructural study. PLoS One 7, e46293.

Cunningham, L.A., and Kahn, R.A. (2008). Cofactor D functions as a centrosomal protein and is required for the recruitment of the gamma-tubulin ring complex at centrosomes and organization of the mitotic spindle. J Biol Chem 283, 7155-7165.

Davies, V.J., Hollins, A.J., Piechota, M.J., Yip, W., Davies, J.R., White, K.E., Nicols, P.P., Boulton, M.E., and Votruba, M. (2007). Opa1 deficiency in a mouse model of autosomal dominant optic atrophy impairs mitochondrial morphology, optic nerve structure and visual function. Hum Mol Genet 16, 1307-1318.

de Brito, O.M., and Scorrano, L. (2008). Mitofusin 2 tethers endoplasmic reticulum to mitochondria. Nature 456, 605-610.

Delettre, C., Lenaers, G., Griffoin, J.M., Gigarel, N., Lorenzo, C., Belenguer, P., Pelloquin, L., Grosgeorge, J., Turc-Carel, C., Perret, E., Astarie-Dequeker, C., Lasquellec, L., Arnaud, B., Ducommun, B., Kaplan, J., and Hamel, C.P. (2000). Nuclear gene OPA1, encoding a mitochondrial dynamin-related protein, is mutated in dominant optic atrophy. Nat Genet 26, 207-210.

Ehses, S., Raschke, I., Mancuso, G., Bernacchia, A., Geimer, S., Tondera, D., Martinou, J.C., Westermann, B., Rugarli, E.I., and Langer, T. (2009). Regulation of OPA1 processing and mitochondrial fusion by m-AAA protease isoenzymes and OMA1. J Cell Biol 187, 1023-1036.

Escobar-Henriques, M., and Anton, F. (2013). Mechanistic perspective of mitochondrial fusion: tubulation vs. fragmentation. Biochim Biophys Acta 1833, 162-175.

Eura, Y., Ishihara, N., Oka, T., and Mihara, K. (2006). Identification of a novel protein that regulates mitochondrial fusion by modulating mitofusin (Mfn) protein function. Journal of Cell Science 119, 4913-4925.

Eura, Y., Ishihara, N., Yokota, S., and Mihara, K. (2003). Two mitofusin proteins, mammalian homologues of FZO, with distinct functions are both required for mitochondrial fusion. J Biochem 134, 333-344.

Filadi, R., Greotti, E., Turacchio, G., Luini, A., Pozzan, T., and Pizzo, P. (2015). Mitofusin 2 ablation increases endoplasmic reticulum-mitochondria coupling. Proc Natl Acad Sci U S A 112, E2174-2181.

Frank, S., Gaume, B., Bergmann-Leitner, E.S., Leitner, W.W., Robert, E.G., Catez, F., Smith, C.L., and Youle, R.J. (2001). The role of dynamin-related protein 1, a mediator of mitochondrial fission, in apoptosis. Dev Cell 1, 515-525.

Fransson, A., Ruusala, A., and Aspenstrom, P. (2003). Atypical Rho GTPases have roles in mitochondrial homeostasis and apoptosis. J Biol Chem 278, 6495-6502.

Friedman, J.R., Lackner, L.L., West, M., DiBenedetto, J.R., Nunnari, J., and Voeltz, G.K. (2011). ER Tubules Mark Sites of Mitochondrial Division. Science 334, 358-362.

Glater, E.E., Megeath, L.J., Stowers, R.S., and Schwarz, T.L. (2006). Axonal transport of mitochondria requires milton to recruit kinesin heavy chain and is light chain independent. J Cell Biol 173, 545-557.

Gomes, L.C., Di Benedetto, G., and Scorrano, L. (2011). During autophagy mitochondria elongate, are spared from degradation and sustain cell viability. Nature cell biology 13, 589-598.

Graham, B.H., Waymire, K.G., Cottrell, B., Trounce, I.A., MacGregor, G.R., and Wallace, D.C. (1997). A mouse model for mitochondrial myopathy and cardiomyopathy resulting from a deficiency in the heart/muscle isoform of the adenine nucleotide translocator. Nat Genet 16, 226-234.

Griparic, L., Kanazawa, T., and van der Bliek, A.M. (2007). Regulation of the mitochondrial dynamin-like protein Opa1 by proteolytic cleavage. J Cell Biol 178, 757-764.

Griparic, L., van der Wel, N.N., Orozco, I.J., Peters, P.J., and van der Bliek, A.M. (2004). Loss of the intermembrane space protein Mgm1/OPA1 induces swelling and localized constrictions along the lengths of mitochondria. J Biol Chem 279, 18792-18798.

Habersetzer, J., Larrieu, I., Priault, M., Salin, B., Rossignol, R., Brethes, D., and Paumard, P. (2013). Human F1F0 ATP synthase, mitochondrial ultrastructure and OXPHOS impairment: a (super-)complex matter? PLoS One 8, e75429.

Head, B., Griparic, L., Amiri, M., Gandre-Babbe, S., and van der Bliek, A.M. (2009). Inducible proteolytic inactivation of OPA1 mediated by the OMA1 protease in mammalian cells. J Cell Biol 187, 959-966.

Hirokawa, N., and Takemura, R. (2005). Molecular motors and mechanisms of directional transport in neurons. Nat Rev Neurosci 6, 201-214.

Hoppins, S., Edlich, F., Cleland, M.M., Banerjee, S., McCaffery, J.M., Youle, R.J., and Nunnari, J. (2011). The soluble form of Bax regulates mitochondrial fusion via MFN2 homotypic complexes. Mol Cell 41, 150-160.

Hoyt, M.A., Stearns, T., and Botstein, D. (1990). Chromosome instability mutants of Saccharomyces cerevisiae that are defective in microtubule-mediated processes. Mol Cell Biol 10, 223-234.

Ishihara, N., Eura, Y., and Mihara, K. (2004). Mitofusin 1 and 2 play distinct roles in mitochondrial fusion reactions via GTPase activity. J Cell Sci 117, 6535-6546.

Ismail, S.A., Chen, Y.-X., Rusinova, A., Chandra, A., Bierbaum, M., Gremer, L., Triola, G., Waldmann, H., Bastiaens, P.I.H., and Wittinghofer, A. (2011). Arl2-GTP and Arl3-GTP regulate a GDI-like transport system for farnesylated cargo. Nat Chem Biol 7, 942-949.

Ivanova, A.A., East, M.P., Yi, S.L., and Kahn, R.A. (2014). Characterization of Recombinant ELMOD Proteins as GTPase Activating Proteins (GAPs) for ARF Family GTPases. J Biol Chem.

Kumar, S., Pan, Christopher C., Shah, N., Wheeler, Sarah E., Hoyt, Kari R., Hempel, N., Mythreye, K., and Lee, Nam Y. (2016). Activation of Mitofusin2 by Smad2-RIN1 Complex during Mitochondrial Fusion. Molecular Cell 62, 520-531.

Labrousse, A.M., Zappaterra, M.D., Rube, D.A., and van der Bliek, A.M. (1999). C. elegans dynamin-related protein DRP-1 controls severing of the mitochondrial outer membrane. Mol Cell 4, 815-826.

Lee, J.-Y., Kapur, M., Li, M., Choi, M.-C., Choi, S., Kim, H.-J., Kim, I., Lee, E., Taylor, J.P., and Yao, T.-P. (2014). MFN1 deacetylation activates adaptive mitochondrial fusion and protects metabolically challenged mitochondria. J Cell Science 127, 4954-4963.

Lewis, S.C., Uchiyama, L.F., and Nunnari, J. (2016). ER-mitochondria contacts couple mtDNA synthesis with mitochondrial division in human cells. Science 353.

Li, Y., Kelly, W.G., Logsdon, J.M., Jr., Schurko, A.M., Harfe, B.D., Hill-Harfe, K.L., and Kahn, R.A. (2004). Functional genomic analysis of the ADP-ribosylation factor family of GTPases: phylogeny among diverse eukaryotes and function in C. elegans. FASEB J 18, 1834-1850.

McElver, J., Patton, D., Rumbaugh, M., Liu, C., Yang, L.J., and Meinke, D. (2000). The TITAN5 gene of Arabidopsis encodes a protein related to the ADP ribosylation factor family of GTP binding proteins. Plant Cell 12, 1379-1392.

Mishra, P., Carelli, V., Manfredi, G., and Chan, David C. (2014). Proteolytic Cleavage of Opa1 Stimulates Mitochondrial Inner Membrane Fusion and Couples Fusion to Oxidative Phosphorylation. Cell Metabolism 19, 630-641.

Mishra, P., and Chan, D.C. (2014). Mitochondrial dynamics and inheritance during cell division, development and disease. Nat Rev Mol Cell Biol 15, 634-646.

Misko, A., Jiang, S., Wegorzewska, I., Milbrandt, J., and Baloh, R.H. (2010). Mitofusin 2 is necessary for transport of axonal mitochondria and interacts with the Miro/Milton complex. J Neurosci 30, 4232-4240.

Mourier, A., Motori, E., Brandt, T., Lagouge, M., Atanassov, I., Galinier, A., Rappl, G., Brodesser, S., Hultenby, K., Dieterich, C., and Larsson, N.G. (2015). Mitofusin 2 is required to maintain mitochondrial coenzyme Q levels. J Cell Biol 208, 429-442.

Nishi, H., Ono, K., Iwanaga, Y., Horie, T., Nagao, K., Takemura, G., Kinoshita, M., Kuwabara, Y., Mori, R.T., Hasegawa, K., Kita, T., and Kimura, T. (2010). MicroRNA-15b modulates cellular ATP levels and degenerates mitochondria via Arl2 in neonatal rat cardiac myocytes. J Biol Chem 285, 4920-4930.

Otera, H., Wang, C., Cleland, M.M., Setoguchi, K., Yokota, S., Youle, R.J., and Mihara, K. (2010). Mff is an essential factor for mitochondrial recruitment of Drp1 during mitochondrial fission in mammalian cells. J Cell Biol 191, 1141-1158.

Palmer, C.S., Osellame, L.D., Laine, D., Koutsopoulos, O.S., Frazier, A.E., and Ryan, M.T. (2011). MiD49 and MiD51, new components of the mitochondrial fission machinery. Embo Rep 12, 565-573.

Paumard, P., Vaillier, J., Coulary, B., Schaeffer, J., Soubannier, V., Mueller, D.M., Brethes, D., di Rago, J.P., and Velours, J. (2002). The ATP synthase is involved in generating mitochondrial cristae morphology. EMBO J 21, 221-230.

Pich, S., Bach, D., Briones, P., Liesa, M., Camps, M., Testar, X., Palacin, M., and Zorzano, A. (2005). The Charcot-Marie-Tooth type 2A gene product, Mfn2, up-regulates fuel oxidation through expression of OXPHOS system. Hum Mol Genet 14, 1405-1415.

Pyakurel, A., Savoia, C., Hess, D., and Scorrano, L. (2015). Extracellular Regulated Kinase Phosphorylates Mitofusin 1 to Control Mitochondrial Morphology and Apoptosis. Molecular Cell 58, 244-254.

Radcliffe, P.A., Vardy, L., and Toda, T. (2000). A conserved small GTP-binding protein Alp41 is essential for the cofactor-dependent biogenesis of microtubules in fission yeast. FEBS Lett 468, 84-88.

Rojo, M., Legros, F., Chateau, D., and Lombès, A. (2002). Membrane topology and mitochondrial targeting of mitofusins, ubiquitous mammalian homologs of the transmembrane GTPase Fzo. Journal of Cell Science 115, 1663-1674.

Santel, A., Frank, S., Gaume, B., Herrler, M., Youle, R.J., and Fuller, M.T. (2003). Mitofusin-1 protein is a generally expressed mediator of mitochondrial fusion in mammalian cells. J Cell Sci 116, 2763-2774.

Saotome, M., Safiulina, D., Szabadkai, G., Das, S., Fransson, A., Aspenstrom, P., Rizzuto, R., and Hajnoczky, G. (2008). Bidirectional Ca2+-dependent control of mitochondrial dynamics by the Miro GTPase. Proc Natl Acad Sci U S A 105, 20728-20733.

Sayed, D., Hong, C., Chen, I.Y., Lypowy, J., and Abdellatif, M. (2007). MicroRNAs play an essential role in the development of cardiac hypertrophy. Circ Res 100, 416-424.

Shadel, G.S., and Horvath, T.L. (2015). Mitochondrial ROS signaling in organismal homeostasis. Cell 163, 560-569.

Sharer, J.D., Shern, J.F., Van Valkenburgh, H., Wallace, D.C., and Kahn, R.A. (2002). ARL2 and BART enter mitochondria and bind the adenine nucleotide transporter. Mol Biol Cell 13, 71-83.

She, H., Yang, Q., Shepherd, K., Smith, Y., Miller, G., Testa, C., and Mao, Z. (2011). Direct regulation of complex I by mitochondrial MEF2D is disrupted in a mouse model of Parkinson disease and in human patients. The Journal of Clinical Investigation 121, 930-940.

Shern, J.F., Sharer, J.D., Pallas, D.C., Bartolini, F., Cowan, N.J., Reed, M.S., Pohl, J., and Kahn, R.A. (2003). Cytosolic Arl2 is complexed with cofactor D and protein phosphatase 2A. J Biol Chem 278, 40829-40836.

Shutt, T., Geoffrion, M., Milne, R., and McBride, H.M. (2012). The intracellular redox state is a core determinant of mitochondrial fusion. Embo Rep 13, 909-915.

Smirnova, E., Griparic, L., Shurland, D.L., and van der Bliek, A.M. (2001). Dynamin-related protein Drp1 is required for mitochondrial division in mammalian cells. Mol Biol Cell 12, 2245-2256.

Smirnova, E., Shurland, D.L., Ryazantsev, S.N., and van der Bliek, A.M. (1998). A human dynamin-related protein controls the distribution of mitochondria. J Cell Biol 143, 351-358.

Song, Z., Chen, H., Fiket, M., Alexander, C., and Chan, D.C. (2007). OPA1 processing controls mitochondrial fusion and is regulated by mRNA splicing, membrane potential, and Yme1L. J Cell Biol 178, 749-755.

Song, Z., Ghochani, M., McCaffery, J.M., Frey, T.G., and Chan, D.C. (2009). Mitofusins and OPA1 mediate sequential steps in mitochondrial membrane fusion. Mol Biol Cell 20, 3525-3532.

Taguchi, N., Ishihara, N., Jofuku, A., Oka, T., and Mihara, K. (2007). Mitotic Phosphorylation of Dynamin-related GTPase Drp1 Participates in Mitochondrial Fission. Journal of Biological Chemistry 282, 11521-11529.

Tanaka, A., Cleland, M.M., Xu, S., Narendra, D.P., Suen, D.F., Karbowski, M., and Youle, R.J. (2010). Proteasome and p97 mediate mitophagy and degradation of mitofusins induced by Parkin. J Cell Biol 191, 1367-1380.

Tian, G., Thomas, S., and Cowan, N.J. (2010). Effect of TBCD and its regulatory interactor Arl2 on tubulin and microtubule integrity. Cytoskeleton (Hoboken) 67, 706-714.

van Rooij, E., Sutherland, L.B., Liu, N., Williams, A.H., McAnally, J., Gerard, R.D., Richardson, J.A., and Olson, E.N. (2006). A signature pattern of stress-responsive microRNAs that can evoke cardiac hypertrophy and heart failure. Proc Natl Acad Sci U S A 103, 18255-18260.

Varadi, A., Johnson-Cadwell, L.I., Cirulli, V., Yoon, Y., Allan, V.J., and Rutter, G.A. (2004). Cytoplasmic dynein regulates the subcellular distribution of mitochondria by controlling the recruitment of the fission factor dynamin-related protein-1. J Cell Sci 117, 4389-4400.

Wang, X., and Schwarz, T.L. (2009). The mechanism of Ca2+ -dependent regulation of kinesin-mediated mitochondrial motility. Cell 136, 163-174.

Wegrzyn, J., Potla, R., Chwae, Y.-J., Sepuri, N.B.V., Zhang, Q., Koeck, T., Derecka, M., Szczepanek, K., Szelag, M., Gornicka, A., Moh, A., Moghaddas, S., Chen, Q., Bobbili, S., Cichy, J., Dulak, J., Baker, D.P., Wolfman, A., Stuehr, D., Hassan, M.O., Fu, X.-Y., Avadhani, N., Drake, J.I., Fawcett, P., Lesnefsky, E.J., and Larner, A.C. (2009). Function of Mitochondrial Stat3 in Cellular Respiration. Science 323, 793-797.

Wilkens, V., Kohl, W., and Busch, K. (2013). Restricted diffusion of OXPHOS complexes in dynamic mitochondria delays their exchange between cristae and engenders a transitory mosaic distribution. J Cell Sci 126, 103-116.

Yamano, K., and Youle, R.J. (2013). PINK1 is degraded through the N-end rule pathway. Autophagy 9, 1758-1769.

Yogev, O., Naamati, A., and Pines, O. (2011). Fumarase: a paradigm of dual targeting and dual localized functions. FEBS Journal 278, 4230-4242.

Yoon, Y., Krueger, E.W., Oswald, B.J., and McNiven, M.A. (2003). The mitochondrial protein hFis1 regulates mitochondrial fission in mammalian cells through an interaction with the dynamin-like protein DLP1. Mol Cell Biol 23, 5409-5420.

Yu, T., Fox, R.J., Burwell, L.S., and Yoon, Y. (2005). Regulation of mitochondrial fission and apoptosis by the mitochondrial outer membrane protein hFis1. J Cell Sci 118, 4141-4151.

Zhang, Y., Liu, X., Bai, J., Tian, X., Zhao, X., Liu, W., Duan, X., Shang, W., Fan, H.Y., and Tong, C. (2016). Mitoguardin Regulates Mitochondrial Fusion through MitoPLD and Is Required for Neuronal Homeostasis. Mol Cell 61, 111-124.

Zhou, C., Cunningham, L., Marcus, A.I., Li, Y., and Kahn, R.A. (2006). Arl2 and Arl3 regulate different microtubule-dependent processes. Mol Biol Cell 17, 2476-2487.

Zimorski, V., Ku, C., Martin, W.F., and Gould, S.B. (2014). Endosymbiotic theory for organelle origins. Current Opinion in Microbiology 22, 38-48.

Zuchner, S., Mersiyanova, I.V., Muglia, M., Bissar-Tadmouri, N., Rochelle, J., Dadali, E.L., Zappia, M., Nelis, E., Patitucci, A., Senderek, J., Parman, Y., Evgrafov, O., Jonghe, P.D., Takahashi, Y., Tsuji, S., Pericak-Vance, M.A., Quattrone, A., Battaloglu, E., Polyakov, A.V., Timmerman, V., Schroder, J.M., and Vance, J.M. (2004). Mutations in the mitochondrial GTPase mitofusin 2 cause Charcot-Marie-Tooth neuropathy type 2A. Nat Genet 36, 449-451.

Chapter 2: The ARL2 GTPase is required for mitochondrial morphology, motility, and maintenance of ATP levels

This chapter was published as:

Newman, L.E., C.-j. Zhou, S. Mudigonda, A.L. Mattheyses, E. Paradies, C.M.T. Marobbio, and R.A. Kahn. 2014. The ARL2 GTPase Is Required for Mitochondrial Morphology, Motility, and Maintenance of ATP Levels. PLoS One. 9:e99270.

Abstract

ARF-like 2 (ARL2) is a member of the ARF family and RAS superfamily of regulatory GTPases, predicted to be present in the last eukaryotic common ancestor, and essential in a number of model genetic systems. Though best studied as a regulator of tubulin folding, we previously demonstrated that ARL2 partially localizes to mitochondria. Here, we show that ARL2 is essential to a number of mitochondrial functions, including mitochondrial morphology, motility, and maintenance of ATP levels. We compare phenotypes resulting from ARL2 depletion and expression of dominant negative mutants and use these to demonstrate that the mitochondrial roles of ARL2 are distinct from its roles in tubulin folding. Testing of current models for ARL2 actions at mitochondria failed to support them. Rather, we found that knockdown of the ARL2 GTPase activating protein (GAP) ELMOD2 phenocopies two of three phenotypes of ARL2 siRNA, making it a likely effector for these actions. These results add new layers of complexity to ARL2 signaling, highlighting the need to deconvolve these different cell functions. We hypothesize that ARL2 plays essential roles inside mitochondria along with other cellular functions, at least in part to provide coupling of regulation between these essential cell processes.

Introduction

GTPases in the RAS superfamily have emerged not only as regulators of many specific signaling and metabolic pathways but also provide integration between pathways through the use of common GTPases or effectors. ADP-ribosylation factor-like 2 (ARL2), within the ARF family of ~30 genes/proteins in mammals, is one such regulator and is the focus of this study. ARL2 is highly conserved in eukaryotes and ubiquitously expressed (Clark et al., 1993). It plays roles in both the regulation of tubulin folding and microtubule destruction (Bhamidipati et al., 2000; Tian et al., 2010), and is found in cytosol tightly bound to the tubulin specific co-chaperone, cofactor D, which shares those activities. Mutations in both ARL2 and cofactor D have been identified in a number of genetic screens linked to microtubules in model organisms that include S. cerevisiae,

S. pombe, A. thaliana, and C. elegans (Antoshechkin and Han, 2002; Hoyt et al., 1990; McElver et al., 2000; Price et al., 2010; Radcliffe et al., 2000; Stearns et al., 1990). Using stable variants of human breast adenocarcinoma lines, Beghin, et al (Beghin et al., 2007; Beghin et al., 2008) showed that ARL2 protein content influences cell morphology (or cell spreading), soluble tubulin pools, microtubule dynamics, cell cycle progression, and chemosensitivity. ARL2 has also been proposed to regulate aspects of STAT3 signaling through actions in the nucleus (Muromoto et al., 2008). In addition to its localizations in the nucleus and cytosol, we have shown that ARL2 is also localized inside mitochondria, as ARL2-specific antibodies localized it to mitochondria in a number of different cell lines and tissues (Sharer et al., 2002). Thus, we set out to examine its role(s) in mitochondria both to better understand its cellular functions and also to provide potential insights into how these different essential cell roles may be integrated, as defects in any of the processes linked to ARL2 dysfunction are hallmarks of the transformed state, cancer, and a host of human diseases.

The mitochondrial pool of ARL2 is estimated to be ~10% of total cellular ARL2, though that percentage also appears to be subject to regulatory influences (Nishi et al., 2010; Sharer et al., 2002). We earlier concluded that ARL2 was present in the inner membrane space (IMS) of mitochondria and a recent proteomic study confirmed our conclusions, using spatially restricted enzymatic tagging in human embryonic kidney cells (Rhee et al., 2013). Our previous studies also localized the ARL2 effector Binder of ARL2 (BART, or ARL2BP) (Sharer and Kahn, 1999; Sharer et al., 2002) to mitochondria. Binding of ARL2 to BART is promoted by activation of the ARL2, via its binding to GTP. The ARL2(GTP)-BART complex binds the adenine nucleotide transporter, ANT1, in an in vitro gel overlay assay (Sharer et al., 2002) though the consequences of this association to ANT activity are unknown. Thus, while ARL2 clearly localizes to mitochondria, its function(s) there are poorly understood. The ARF and RAS families of GTPases are predicted to have arisen in prokaryotes (Dong et al., 2007) and thus specific roles in mitochondrial biology may be among the most ancient signaling pathways known to have

survived the emergence of eukaryotes. Therefore, a role for a nuclear encoded regulatory GTPase inside mitochondria is expected to provide potentially important insights into both mitochondrial and evolutionary biology.

The presence of ARL2 in multiple cellular locations and its proposed regulation of multiple cellular processes are consistent with other RAS superfamily and ARF family members displaying such characteristics. Indeed, the challenge to researchers has changed from earlier attempts to identify the signaling pathway regulated by a GTPase to deconvolution of the multiple processes that lie downstream. In efforts to develop models for ARL2 signaling pathways, we purified the only known ARL2 GAPs, ELMOD1-3 (Bowzard et al., 2007). ELMOD proteins are highly conserved in eukaryotic evolution, predicted to be present in the last eukaryotic common ancestor and the defining ELMO domain was shown to be the ARL2 GAP domain (East et al., 2012). Roles for at least two of the three ELMOD proteins in deafness in mammals (Jaworek et al., in press; Johnson et al., 2012) further highlight the need to understand ARL2 regulation and cellular functions. Similarly, it is common in GTPase families for each protein to have close paralogs that may share overlapping functions. Therefore, it is important to also discriminate between roles for each GTPase within a family as new functions emerge. The closest ARL2 paralog is ARL3, which shares 53% identity with ARL2, which has distinct functions (Hanzal-Bayer et al., 2005; Ismail et al., 2012; Ismail et al., 2011; Veltel et al., 2008b; Zhou et al., 2006) yet is also a substrate for ELMODs as GAPs (Bowzard et al., 2007).

As is common in GTPase research, we took advantage of previously described (Zhou et al., 2006) dominant activating (ARL2[Q70L] and inactivating (ARL2[T30N]) point mutants to test for effects of excessive or loss of ARL2 activities. These mutants are homologous to dominant activating (Q61L) or dominant inactivating (S17N) mutants of Ras proteins (Bollag and McCormick, 1991; Feig, 1999; Scheffzek et al., 1997) or Q71L and T31N mutants of ARFs (e.g., see Zhang, et al (Zhang et al., 1994)). Dominant activating mutants are persistently active because the mutated glutamine is involved in hydrolysis of the γ-phosphate of bound GTP and its loss

leads to reduced ability to hydrolyze GTP in the presence of the GTPase activating protein (GAP). The dominant inactivating (or dominant negative) mutants are thought to bind their cognate guanine nucleotide exchange factor (GEF) but bind GTP poorly, leading to a more stable GTPase-GEF complex that prevents activation of endogenous GEF substrate(s). We also employ short interfering RNAs (siRNAs) to knock down protein expression in cultured cells to identify phenotypes resulting from the deficiency of the specific protein under study. Because knockdown of a protein can be incomplete and varies with time after expression or transfection of the siRNA, it is not uncommon to see different phenotypes, or more severe phenotypes, with expression of the dominant negative mutants. Therefore, comparing effects of each approach has also proven instructive due to their distinct mechanisms of action. Here we document roles for ARL2 in mitochondrial functions by comparing phenotypes of mitochondria in cells either deficient for ARL2 or expressing dominant negative ARL2 and develop novel models for ARL2 actions at mitochondria. Particular attention was paid to resolve effects of ARL2 on microtubules from those on mitochondria to allow current and future efforts to determine mechanisms of each as well as develop models for integration of these different essential functions.

Materials and Methods

Cell Culture: Human cervical carcinoma (HeLa) were grown in DMEM supplemented with 10% fetal bovine serum (Invitrogen, Carlsbad, CA) and 2 mM glutamine at 37°C in the presence of 5% CO2. Cells were obtained from ATCC.

Antibodies: Affinity-purified rabbit, polyclonal ARL2 (R-86336) or BART (R-46712) antibodies were prepared as described in Sharer et al. (Sharer et al., 2002). Monoclonal antibodies directed against cytochrome-c and TOM20 were purchased from BD Transduction Laboratories (Lexington, KY). Mouse monoclonal antibodies to actin and α tubulin were purchased from Sigma (St. Louis, MS). A rabbit polyclonal antibody to GFP was purchased from Abcam.(Cambridge, MA). Mouse monoclonal ADI-SPA-807, directed against HSP60, was

purchased from Stressgen (now Enzo Life Sciences). To probe electron transport chain complexes, we used a cocktail of 5 antibodies that recognized NDUFA9 (Complex I), core protein 2 (Complex II), UQCRC2 (Complex III), subunit IV (Complex IV), and subunit alpha (Complex V), purchased from Mitosciences (catalog # MS603). ARL3 (Zhou et al., 2006) and ELMOD2 antibodies were raised in rabbits against purified, bacterially expressed human proteins and characterized in our lab. All such antibodies (including those directed against ARL2) at a minimum react with the purified antigen as well as a band of the correct electrophoretic mobility in lysates from cells over-expressing the antigen in immunoblots, while the pre-immune sera do not. Also, the appropriate band is effectively competed by prior incubation of the antiserum with antigen.

Plasmids: Plasmids directing expression of human ARL2, ARL2[T30N], or ARL2[Q70L] in the pcDNA3.1 backbone have been described previously (Zhou et al., 2006). Site directed mutagenesis was used to generate the K71R mutation in the same vector; work was performed at the Emory Cloning Core. Each was sequence verified. GFP-DRP1[K38A] (Young et al., 2010) was a gift from Dr. Edward Bampton (University of Leicester, UK).GFP-Mito and DsRed-Mito were provided by Dr. James Zheng (Emory University). The source of RAB5-GFP and RAB7-GFP plasmids were Dr. Allan Levey (Emory University) and Dr. Richard Pagano (Mayo Clinic, MN), respectively. The coding sequence of bovine ANT1/AAC1 (SLC25A4) was amplified by PCR from total bovine heart cDNA. The oligonucleotide primers were synthesized corresponding to the extremities of the coding sequence (accession NM174658.2), with NdeI and HindIII sites added. The amplified product was cloned into pET21b for expression in E. coli and the sequence was verified.

siRNAs: siRNAs were obtained from Dharmacon (Lafayette, CO), with the exception of individual ELMOD2 siRNAs, which were obtained from Sigma (St. Louis, MS). Catalog numbers are as follows: ARL2 siRNA #1 J-011585-05 (CAACCAUCCUGAAGAAGUU), ARL2 siRNA #2 J-011585-06 (GAGCAACCCUCCUCAUCUU), BART siRNA #1 J-013074-04, #2 J-

013074-12, Arl3 SmartPool L-011813-00, ELMOD2 SmartPool L-016104-00. Individual ELMODs siRNAs were ordered from Sigma with the following modifications: 5' amine C6, 3' PHOS, 3' dT overhang, and 2' verite. The sequences were (#2) AUAUAAAUUCUGUUGAAUG and (#3) UCAAUUUAAUACAAAUACC, directed against the 3' UTR.

Transfection with siRNA and plasmids: Cells were grown in six-well culture dishes to 70-90% confluence. Plasmids (2 μg of pcDNA3.1 or pcDNA3.1 carrying indicated inserts and Mito-GFP; 2:1 ratio) were co-transfected using LipofectAMINE and Plus reagents (Invitrogen) according to the manufacturer's instructions. siRNAs (25 nM) were transfected into HeLa cells using Dharmafect transfection reagent #1 (Dharmacon, Lafayette, CO) following the company's instructions. For some experiments, transfections were performed sequentially first with plasmid DNA followed 5 hours later by transfection of the ARL2 siRNA, to minimize cell toxicity evident from co-transfections. We consistently observed at least 70% transfection efficiency, using expression of fluorescence-tagged proteins to score.

Immunofluorescence analyses: Cells were grown on Matrigel-coated coverslips. For imaging mitochondria and ARL2, cells were fixed in 4% paraformaldehyde followed by permeabilization with 0.1% (v/v) Triton X-100 in PBS. Incubation with primary antibodies was carried out in PBS containing 1% (w/v) BSA, at 4°C overnight. Secondary antibodies (Alexa fluorophores, Invitrogen) were incubated in the same buffer for 1 hour at room temperature. Cells were examined using a Zeiss LSM 510 microscope (Thornwood, NY) using 100× objective with laser excitation at 488 or 543 nm. To visualize microtubules, we used PHEMO fixation (3.7% (v/v) paraformaldehyde, 0.05% (v/v) glutaraldehyde, 0.5% (v/v) Triton X-100 in 68 mM PIPES, 25 mM HEPES, 15 mM EGTA, 3 mM MgCl2, 10% (v/v) dimethylsulfoxide, pH 6.8) for 10 minutes at room temperature, as described in Mabjeesh et al (Mabjeesh et al., 2003). Cells were then stained and imaged as described above.

The sub-mitochondrial location of ARL2 was investigated by the use of differential permeabilization of fixed HeLa cells with increasing concentrations of digitonin, as described

previously (Jeyaraju et al., 2006; Otera et al., 2005). Briefly, cells were used at ~70% confluence. Prior to fixation, cells were treated with 0.1% (w/v) saponin in growth media for 1 min. on ice. This pre-permeabilization fixation decreased background, cytosolic staining of ARL2, BART, and ELMOD2, making endogenous mitochondria-associated protein easier to detect. Cells were then immediately fixed in 4% paraformaldehyde for 15 minutes at room temperature. Fixed cells were then permeabilized with 0.2 or 1.0 mg/mL digitonin in PBS for 10 minutes at room temperature, and immunofluorescence was performed as previously described.

Live cell imaging: Cells were imaged for 8 hours, starting 24 hours after transfection, for both siRNA and overexpression experiments. Cells already displaying mitochondrial fragmentation at the beginning of the imaging period were excluded from analysis. Live cell imaging was performed using a Nikon A1R confocal microscope, enclosed in a heating chamber at 37°C with 5% CO2 perfused over the plate holder. Cells were plated on 35 mm live-cell imaging dishes and imaged using a 63X (NA 1.4) objective. Time-lapse images were taken every 20 seconds over a period of 8 hours or as indicated. For experiments using only GFP-labeled proteins, the fluorophore was excited using the 488-nm line of an Ar ion laser. For time-lapse sequences where dual labels were used (Lysotracker red; Molecular Probes, OR; and GFP-Mito), the fluorophores were sequentially excited with the 488 and 543 laser lines and emission signals were separated using an electronically controlled emission discrimination filter with the appropriate filter sets. To monitor lysosome movements, LysoTracker Red (Molecular Probes) was added to cells 30 minutes prior to imaging. To visualize early or late endosome motility we expressed GFP-RAB5 or GFP-RAB7, respectively.

Mitochondrial Morphology Assays: Alterations in mitochondrial morphology were generally observed as changes in the length of the organelle and the distribution of mitochondria in the cell. Acquired images of cells stained with mitochondria markers (cytochrome c, TOM20, HSP60, etc.) were analyzed using NIH Image J software (Wayne Rasband, NIH). Multinucleated cells were excluded from this analysis. For quantitative analyses, cells were classified according

to their mitochondrial morphology into four different groups: tubular (if most mitochondria were filamentous); perinuclear (mitochondrial aggregates were located near the nucleus); fragmentation (all mitochondria were fragmented and no filamentous mitochondria were found) and intermediate (a mixture of short tubular and fragmented forms). For each experiment at least 200 cells were scored from three different experiments in the analysis and values are represented as means ± one standard deviation (1 SD) of three independent experiments. Statistical analysis was determined using Student's t test. A value of $p<0.05$ was considered significant unless otherwise indicated.

For 3D imaging, 20-22 Z-sections of mito-GFP-expressing cells were obtained at 0.2-μm intervals through the entire cell using a piezo-electric focus motor mounted onto the objective lens of a Nikon Widefield microscope. Subsequent image restoration was achieved with Huygens Essential (SVI, Netherlands) deconvolution software, using the deconvolution algorithm with a computed point spread function. Image analysis and processing was performed with ImageJ (NIH; http://rsb.info.nih.gov/ij).

Tracking of Mitochondrial Movements: Images were subjected to motility analysis by generating kymographs using the plug-in MTrackJ (Meijering, E., University Medical Center of Rotterdam, Netherlands; http://www.imagescience.org/meijering/software/mtrackj/) and ImageJ (NIH) (Abramoff et al., 2004). Kymographs of mitochondria in time lapse images from HeLa cells expressing mito-GFP were produced using ImageJ, as described previously (Miller and Sheetz, 2004). Motile mitochondria were identified as moving objects in movies and diagonal lines in the kymographs. The velocity of the motile mitochondria was extracted from the kymographs. The displacement of a mitochondrion from one frame to the next was converted from pixels to real distances by calibrating the x-y axes of the analyzed images in MTtrackJ. For tubular mitochondria, the ends were tracked whereas for fragmented mitochondria the center was tracked. The obtained x-y-t tracking coordinates of mitochondrial movements were analyzed with Excel-based software. The start of a run was defined by a minimal displacement of 0.1 μm/sec.

Mitochondria were classified as either moving or stationary based on whether they achieved a displacement of >1 μm and also by the vertical straight lines in the kymographs. Tracks of the ends of different mitochondria in a one hour period are shown in different colors and explained in the legends. All the values are means ± 1 standard deviation of randomly selected mitochondria; at least 8 individual cells were analyzed.

Determination of cellular and mitochondrial ATP: ATP concentrations were measured using the ENLITEN ATP Assay Bioluminescence Detection Kit (Promega), according to the manufacturer's instructions. Briefly, HeLa cells were grown in six well plates (3 wells/condition) and transfected as described above. Cells were seeded to ensure densities at the time of harvest of between 40-80%, and similar densities between experimental and control cells. Cells were collected by trypsin at the times indicated and concentrated by centrifugation. Samples were prepared by resuspending cells in water and boiling for 5 minutes, followed by centrifugation (15 min at 14,000xg) to pellet cell debris. Supernatant (S14; 10 μL) was added to a tube containing 100 μL reconstituted luciferin/luciferase reagent, and ATP levels were determined by luminometer, and quantified using an ATP standard curve (10-7 - 10-10 M). Reactions were carried out in triplicates (3/well) and averaged. Protein concentrations were determined for the same samples to allow ATP levels to be normalized to cell protein. ATP concentrations were expressed as the percentage of controls as the absolute values differed between experiments. All values are reported as mean ± 1 standard deviation.

Blue Native Polyacrylamide Gel Electrophoresis (BN-PAGE): 4-16% BN-PAGE gels were purchased (Invitrogen) and electrophoresis was carried out according to manufacturer's instructions. Molecular weight standards for native gels were purchased from Invitrogen (cat#LC0725).

Expression and purification of recombinant proteins: ARL2 and BART-His were expressed from pET3C plasmids. Plasmids were transformed into BL21(DE3) cells and protein expression was achieved by growth in Studier's auto-induction medium (Studier, 2005), as

described earlier for wild type ARL2 (Bowzard et al., 2007; Bowzard et al., 2005). Bovine ANT1 was purified as inclusion bodies from E. coli as described previously, except that the host cells were E. coli C0214(DE3) (Fiermonte et al., 2009; Marobbio et al., 2003). Inclusion bodies were purified on a sucrose density gradient, and ANT1 was purified by centrifugation and washing (Marobbio et al., 2003) prior to solubilization in Sarkosyl and reconstitution into proteoliposomes.

ADP/ATP transport assays: The recombinant ANT1 (10 µg) in 1.7% Sarkosyl was reconstituted into liposomes in the presence of 10 mM ADP, 5 mM MgCl2 and 10 mM PIPES pH 7.0, as described previously (Fiermonte et al., 2009; Palmieri et al., 1995). External substrate was removed from proteoliposomes on Sephadex G-75 columns pre-equilibrated with 50 mM NaCl and 10 mM PIPES, pH 7.0. The amount of ANT1 incorporated into liposomes was measured as described previously (Agrimi et al., 2004); in all experiments, it was ~20%. Purified recombinant ARL2 or ARL2 and BART-His (30 µg each) were pre-incubated with 5 mM MgCl2, and 20 µM GTP or GDP for 20 min, prior to addition to the proteoliposome mixture. Transport at 25°C was started by adding [14C]-ADP (Perkin Elmer) to substrate-loaded proteoliposomes (exchange), and terminated after 1 minute by addition of 20 mM pyridoxal 5′-phosphate and 20 mM bathophenanthroline according to the 'inhibitor stop' method (Palmieri and Klingenberg, 1979). The external substrate was removed, and the radioactivity in the liposomes was measured (Palmieri et al., 1995). The initial transport rate was calculated from the radioactivity taken up by proteoliposomes after 1 min (in the initial linear range of substrate uptake). All values are reported as mean ± 1 standard deviation.

Results

To explore the functional role of ARL2 in mitochondria, we initially used two separate approaches to deplete cells of ARL2 activity: knockdown by siRNA and expression of a dominant negative mutant. In the first of these we tested multiple, sequence-independent

synthetic siRNAs and plasmid-based shRNAs; including two Dharmacon pools of synthetic RNAs and eight pSUPER-based plasmids (Zhou et al., 2006) to direct expression of shRNAs to knockdown ARL2. The two most effective reagents at reducing ARL2 protein levels (Figure 1A) proved to be commercially available, synthetic RNAs (siRNA #1 and #2) from the SmartPool (Dharmacon) of four siRNAs. Controls for specificity of knockdown include the sequence independence of the RNAs, mock transfected cells, and use of siRNAs directed against the closest ARL2 paralog, ARL3, which lack each of the activities described here for ARL2. ARL2[T30N] is a previously described dominant negative mutant that has decreased affinity for guanine nucleotides (Hanzal-Bayer et al., 2005) and is thus predicted to bind ARL2 GEF(s) and prevent their acting on endogenous ARL2. The key control for effects of ARL2[T30N] expression is comparison to wild type ARL2 over-expression, which consistently is found at higher levels than ARL2[T30N] in cell homogenates, assessed by immunoblotting with ARL2 specific antisera. We believe this is the result of a shorter half-life of the mutant, secondary to its impaired guanine nucleotide binding (Hanzal-Bayer et al., 2005) but have not tested this conclusion.

Loss of ARL2 activity causes mitochondrial fragmentation

We found that decreasing ARL2 activity in cells using a couple different strategies resulted in fragmentation of mitochondria. HeLa cells were co-transfected with plasmids directing expression of mito-GFP with either wild type ARL2 or ARL2[T30N], and mitochondrial morphologies were observed 24 hours later, as described under Materials and Methods. HeLa cells overexpressing ARL2 and mito-GFP displayed no differences in mitochondrial morphology. In contrast, we found that expression of ARL2[T30N] dramatically altered mitochondrial morphology, leading to fragmented structures that were evident by standard epifluorescence imaging. Even more striking were the deconvolved images of cytochrome c staining in z stacks of control HeLa cells or those expressing ARL2[T30N], as shown in Figure 1B. Extended, branching tubular mitochondrial structures are evident and common in control cells. These are

lost in cells expressing ARL2[T30N] and replaced by much smaller structures that appear spherical, despite the fact that this mutant is expressed to lower levels than wild type ARL2. We observe the same phenotype when ARL2[T30N] is expressed in other cell lines, including C2C12, COS7, and MCF7, so we believe these results are applicable to different cell types. Like expression of ARL2[T30N], knockdown of ARL2 by siRNA also caused mitochondria to fragment. Mitochondrial morphologies in cells with compromised ARL2 activity were similar whether cells were stained with antibodies to TOM20 (marker of the outer membrane), cytochrome c (marker of the intermembrane space), or HSP60 (a marker of the mitochondrial matrix). In addition to changes in mitochondrial morphology, we also noted that cells deficient in ARL2 activity, either resulting from depletion by siRNA or expression of ARL2[T30N], appear to be smaller than controls. This size difference was not quantified or explored further in the current study but was reported earlier in related studies (Beghin et al., 2007; Beghin et al., 2008; Zhou et al., 2006).

To quantify the effects on mitochondrial morphology we scored mitochondrial networks in transfected cells as having one of three phenotypes: (1) “tubular” = long, tubular and branched structures, (2) “intermediate” = a mixture of tubular and fragmented phenotypes, and (3) “fragmented” = mainly small and round structures with no tubular or branched structures (Figure 1C). The tubular and intermediate phenotypes are commonly observed in control cells, accounting for ~90% of all cells. In contrast, cells transfected with ARL2[T30N] or ARL2 siRNA displayed fragmentation in ~50% of cells (Figure 1D). Thus, mitochondrial fragmentation is a readily scored phenotype that accompanies loss of ARL2 activity.

Mitochondrial fragmentation can result from either a loss of fusion or increase in fission (Chan, 2006). To distinguish between these two activities, we used the dominant negative mutant of the fission component DRP1, DRP1[K38A], as previously described (Young et al., 2010). Expression of DRP1[K38A] blocks mitochondrial fission, while fusion proceeds normally, leading to elongated mitochondria. Therefore, mitochondria should only fragment with

expression of DRP1[K38A] if fusion is impaired, as DRP1[K38A] should block fission. GFP or GFP-DRP1[K38A] was co-expressed with empty vector or those expressing ARL2 or ARL2[T30N], and mitochondrial morphologies in GFP positive cells were scored. Expression of DRP1[K38A] resulted in mitochondria with increased apparent length and interconnectivity when co-expressed with either empty vector (not shown) or wild-type ARL2 (Figure 2A, top right panel), compared to cells co-expressing GFP and pcDNA (not shown) or wild-type ARL2 (Figure 2A, top left panel). Co-expression of GFP-DRP1[K38A] reversed mitochondrial fragmentation caused by ARL2[T30N] (Figure 2A, bottom right panel), despite the fact that ARL2[T30N] caused mitochondrial fragmentation when co-transfected with GFP alone (Figure 2A, bottom left panel).Cells co-transfected with GFP-DRP1[K38A] and empty vector, ARL2 wild type, or ARL2[T30N] were scored for fragmented mitochondria, and we observed no statistically significant differences (Figure 2B). Both ARL2 and ARL2[T30N] expressed to similar levels, regardless of co-expression with GFP alone or GFP-DRP1[K38A] (Figure S1). Because DRP1[K38A] blocks mitochondrial fission, we interpret these findings as indirect evidence that a loss in ARL2 activity alters mitochondrial morphology by increasing fission at a step that is upstream of the actions of DRP1. Stated another way, we believe that ARL2 may act to down-regulate fission such that its loss results in increased fission.

Mitochondrial motility is specifically compromised in cells deficient in ARL2 activity

In addition to the fragmentation of mitochondria there was an increase in perinuclear clustering of mitochondria in cells depleted for ARL2 (Figure 3A,B) or expressing ARL2[T30N]. This clustering was most readily seen as an absence, or clearly diminished density, of mitochondria in the cell periphery as mitochondria in control cells typically appear to have a higher density near the nucleus for a number of reasons (e.g., thickness of the cell). This perinuclear clustering with loss of peripheral mitochondria was almost completely absent in control cells (0.9%) but was seen in 23.7 ± 0.5% of cells depleted of ARL2.

In efforts to gain further insights into possible relationships between fragmentation and clustering of mitochondria we performed time-lapse imaging. Control cells, expressing only mito-GFP, were characterized by mitochondria moving in a bidirectional fashion with thread-like morphology that displayed readily observable fusion and fission events. Substantial mitochondrial fragmentation, perinuclear clustering, or sustained loss of motility were rare in controls. In contrast, cells depleted of ARL2 by siRNA displayed mitochondrial fragmentation (52.3 ± 6.5%), with or without clustering, by the end of the eight hour imaging window. Perinuclear clustering of mitochondria occurred in 16 ± 3.1% of imaged cells, resulting from directed movement of the fragmented mitochondria inward, with a near complete absence of outward movement. And in a similar percentage of cells (14.1 ± 4.6%), we observed loss of mitochondrial motility, with fragmented mitochondria simply stopping their directed movement throughout the cell but retaining localized movement. The remaining (~70%) transfected cells displayed bidirectional, motile, fragmented mitochondria. Thus, perinuclear clustering resulted from a loss in outward mitochondrial motility and occurred after mitochondrial fragmentation. Kymographs of mitochondria in time lapse images from mito-GFP expressing HeLa cells were produced using ImageJ, as described previously (Miller and Sheetz, 2004). Motile mitochondria were identified as moving objects in movies and diagonal lines in the kymographs (Figure 4A,B). Mean velocity of motile mitochondria was quantified using ImageJ to track individual mitochondria and dividing displacement distance by time (Figure 4C). Rates of mitochondrial motility in ARL2 siRNA cells (0.23 ± 0.01 μm/sec; 28 mitochondria from 8 cells) were less than half those in control cells (0.65 ± 0.08 μm/sec; 51 mitochondria from 8 cells) when averaged over the eight hour imaging window (Figure 4C). These control rates from this experiment of mitochondrial transport are very similar to previously reported values (Beltran-Parrazal et al., 2006; Fehrenbacher et al., 2004; Miller and Sheetz, 2004).

We also observed changes in mitochondrial motility in cells expressing ARL2[T30N]. HeLa cells expressing mito-GFP or mito-GFP and ARL2 were imaged as described above. No

differences in the overall distribution, length, or motility of mitochondria were evident by visual inspection, and there was no significant difference between the average rate of movement in controls (0.77 ± 0.12 μm/sec) and ARL2-expressing cells (0.71 ± 0.14 μm/sec). In contrast to controls, but similar to cells depleted for ARL2, cells expressing ARL2[T30N] displayed mitochondria that were fragmented and arrested in their motility. The mean velocity of mitochondria in ARL2[T30N] expressing cells was 0.37 ± 0.7 μm/second, a 48% decrease ($p<0.01$) from ARL2 over-expressing cells (Figure 4C). Together these data reveal that loss of ARL2 activity, through either ARL2 depletion or expression of ARL2[T30N], causes a significant decrease in the average rate of mitochondrial movements.

Transport of other organelles, e.g., lysosomes and endosomes, also occurs along microtubules but these were not affected by depletion of ARL2. The rate of movement of lysosomes (determined as described in Materials and Methods) was found to be the same in control (0.46 ± 0.06 μm/sec; average of five cells/experiment, repeated three times) and ARL2 siRNA cells (0.42 ± 0.04 μm/sec) (Figure 4C) and was comparable to previously reported values (Brown, 2003). The movements of early and late endosomes (visualized by GFP-RAB5 or RAB7, respectively) over the imaging period were indistinguishable between control and ARL2 siRNA cells upon visual inspection, so we did not quantify further. To further ensure that mitochondria movements were compromised under conditions in which lysosome and endosome mobilities were preserved, we also performed experiments in which we tracked both mitochondria and lysosomes in the same cells; comparing controls to either ARL2 depletion or ARL2[T30N] expression. In each case we observed instances in which mitochondrial motility was slowed by the loss of ARL2 activity (either ARL2 siRNA or ARL2[T30N]), yet lysosomal and endosomal traffic continued without evident change. Thus, depletion of ARL2 resulted in a motility defect that was specific to mitochondria and was not shared by other organelles, which traffic along similar cytoskeletal elements.

Mitochondrial phenotypes from loss of ARL2 activity are not secondary to changes in microtubules

Previous work in our lab had described effects of the dominant active mutant ARL2[Q70L] to cause the loss of microtubules (Zhou et al., 2006). In addition, work by our lab and others describes a role for ARL2 in regulation of microtubule destruction through the tubulin co-chaperone cofactor D (Bhamidipati et al., 2000; Cunningham and Kahn, 2008; Shern et al., 2003; Tian et al., 2010). Given ARL2's well-established role as a regulator of tubulin folding and microtubule dynamics (Antoshechkin and Han, 2002; Bhamidipati et al., 2000; Hoyt et al., 1990; McElver et al., 2000; Price et al., 2010; Radcliffe et al., 2000; Stearns et al., 1990; Tian et al., 2010), we wanted to clearly distinguish between direct effects of the GTPase on mitochondria as opposed to possible indirect effects resulting from changes in microtubules.

In an unrelated study we had generated a point mutant that helped us to more clearly resolve these two functions of ARL2, a conservative point mutant of ARL2, Lys71-Arg71 or ARL2[K71R]. We expressed ARL2[K71R] in HeLa cells, using the same pcDNA3-based vectors used above for wild type and ARL2[T30N], and assayed effects on mitochondria. ARL2[K71R] also caused mitochondria to fragment and cluster around the nucleus when assessed 24 or 48 hours after transfection. Thus, by these criteria ARL2[K71R] appears to act in a dominant negative fashion, indistinguishably from ARL2[T30N] or ARL2 siRNA. ARL2[K71R] was expressed to the same levels as ARL2, each of which are higher than the T30N mutant, as determined by immunoblotting of whole cell lysates. Thus, ARL2[K71R] phenocopies ARL2[T30N] and ARL2 siRNA in promoting mitochondrial fragmentation and perinuclear clustering.

When we compared the microtubule staining profiles of mock transfected cells with those expressing ARL2 or ARL2[K71R], and those depleted for ARL2, we found that microtubule profiles were indistinguishable at all times examined (Figure 5; 48 hours); characterized by meshwork staining throughout the cytosol, extending to the cell periphery. In contrast, only cells

expressing ARL2[T30N] or ARL2[Q70L] displayed a clearly reduced density of microtubules (Figure 5). This effect on microtubules was seen 48 hours after transfection (Figure 5), which is later than when we observe mitochondrial defects (24 hours). The strongest effect on loss of microtubules was seen with expression of the dominant active mutant, ARL2[Q70L] (Figure 5) (Zhou et al., 2006), which had no effects on mitochondrial fragmentation or clustering (data not shown).

Thus, the two point mutants ([T30N] and [K71R]) whose expression cause very similar changes to mitochondrial morphology and clustering have very different effects on microtubules. Additionally, knockdown of ARL2 by siRNA did not alter microtubule density. Lastly, we showed that endosomal and lysosomal motility are not compromised at the same times that we observe mitochondrial motility loss. Taken together (see summary in Table I), these results strengthen our conclusions that ARL2 regulates multiple aspects of mitochondrial function and does so independently of its role(s) in tubulin or microtubule dynamics.

ARL2 siRNA, but not ARL2[T30N], causes loss of cellular ATP

Given that loss of ARL2 activity, via siRNA-mediated knockdown or expression of ARL2[T30N], causes changes to mitochondrial morphology and motility, we next asked if loss of ARL2 activity compromised ATP production. Depletion of ARL2 by siRNAs in HeLa cells resulted in a dramatic (40-50% of controls) loss of cellular ATP (Figure 6A) 2-4 days after transfection. There was a good qualitative agreement between effectiveness in knockdown of protein expression, assessed by Western blotting of total cell lysates, and effects on ATP levels, with siRNA #1 slightly better than the pool, and siRNA #2 least effective (compare Figure 1A and Figure 6A). The 40-60% decrease in ATP levels is comparable to what has been reported previously after treatment with potent inhibitors of glycolysis or oxidative phosphorylation. In contrast, we saw no significant changes (93% ± 19%) in cellular ATP 24 hours after transfection with ARL2 siRNA, despite the fact that mitochondria were already fragmented and clustered at

this time point, suggesting that the ATP loss occurs after mitochondrial morphology and motility have already been compromised.

Depletion of cellular ARL2 activities through siRNA resulted in decreased numbers of cells compared to controls. This was thought not to be the result of apoptosis or loss of mitochondrial membrane potential as we saw no evidence of release of cytochrome c from the IMS or changes in mitochondrial staining with JC-1 or MitoTracker Red CMXRos, two mitochondrial membrane potential-sensitive dyes. Nor did we observe nuclear blebbing. Differences in cell number between ARL2 knockdown and controls increased with time and may result from a combination of increased doubling times and necrosis as previously reported for other mitochondrial proteins (An et al., 2012; Darshi et al., 2011), though these were not pursued further.

In contrast to ARL2 siRNA, we found that over-expression of wild type human ARL2 (102.3 ± 9.2%) or expression of the dominant negative mutant, ARL2[T30N] (86.8 ± 9.9%) or ARL2[K71R] (115 ± 11%), had no statistically significant effect on ATP levels in HeLa cells after 48 hours, when compared to empty vector controls (Figure 6B). Therefore, we conclude that the changes in mitochondrial morphology and motility accompanying the loss of ARL2 are not secondary to the loss of ATP in cells. These data also highlight the important functional differences between the absence of ARL2 in cells (knockdown) and the presence of a dominant negative mutant, as they act via distinct mechanisms yet share a subset of phenotypes.

Changes in ARL3 levels or activity have no effect on mitochondria

ARL3 is the closest paralog to ARL2 in humans, sharing 53% identity and 72% homology. With previous evidence of both shared and distinct functions in cells (Ismail et al., 2011; Zhou et al., 2006), we tested for effects of ARL3 siRNA or expression of dominant negative ARL3[T31N] on mitochondria. We reported previously the characterization of ARL3 siRNA reagents and their effects on Golgi, microtubules, and cytokinesis but did not specifically

examine mitochondria in the earlier study (Zhou et al., 2006). When ARL3 was depleted using an ARL3 SmartPool (Dharmacon) in HeLa cells, we observed no changes in mitochondrial morphology or localization after staining of fixed cells with HSP60 or cytochrome c 48 hours after transfection (data not shown). Similarly, expression of either wild type ARL3 or the dominant negative ARL3[T31N] had no evident effects on mitochondrial morphology or localization in cells. As the distribution of mitochondria was indistinguishable from controls, we did not attempt to quantify mitochondrial motility in either case. We assayed total cellular ATP levels in mock or ARL3 knockdown cells and found no statistically significant differences. Finally, staining of HeLa cells using fixation and permeabilization conditions that are positive for ARL2 in mitochondria failed to reveal any evidence for a pool of ARL3 associated with mitochondria, using our ARL3-specific antisera that is useful in localization to other sites (Zhou et al., 2006). Thus, we conclude that ARL3 does not share with ARL2 any of the activities described here with regard to mitochondrial functions. Rather, these results further highlight the specificity of these effects to ARL2.

ARL2 is present in the mitochondrial matrix

Studies in our lab demonstrated that ARL2 from different cells (HeLa, sf295) or tissues (brain, liver, kidney, spleen, heart) partially localizes to mitochondria, as visualized by indirect immunofluorescence microscopy with specific antibodies and by cell fractionation (Sharer et al., 2002). In that fractionation study, the mitochondria-associated ARL2 was shown to be resistant to protease treatment, unless detergent was added to solubilize the mitochondrial membranes, revealing there to be a pool of ARL2 inside the organelle. Results from sub-mitochondrial fractionation were interpreted as evidence that ARL2 was present in the intermembrane space (IMS) (Sharer, 2005). With evidence for a role for ARL2 in three mitochondrial phenotypes, we re-opened the question of localization within mitochondria using independent methods to determine the localization of ARL2 inside mitochondria.

We used cBid-induced permeabilization of the outer membrane (Madesh et al., 2002) of cultured HeLa cells to test whether ARL2 exists in the IMS in a freely diffusible form. Addition of purified cBid (10 nM; a kind gift of Dr. David Andrews, McMaster University, Canada) to HeLa cells in which the plasma membrane had been permeabilized with 0.2% saponin resulted in essentially complete release of cytochrome c from mitochondria within 15 minutes, as visualized by staining of fixed cells (Figure S2). In contrast, ARL2 staining in mitochondria was retained in HeLa cells treated with cBid under these same conditions (Figure S2). We conclude from these results that ARL2 is unlikely to be free in the IMS and more likely is either bound tightly to another protein(s) on the inner or outer mitochondrial membranes or resides in the matrix of the mitochondria.

We then used increasing concentrations of digitonin on fixed cells and looked for the appearance of staining for cytochrome c (as a marker of the IMS), or HSP60 (as a marker of the matrix). Treatment with 0.02% digitonin permeabilized the plasma membrane and outer mitochondrial membrane, as revealed by the appearance of cytochrome c staining (Figure 7, top row). However, no mitochondrial staining for ARL2 or HSP60 was evident (top two rows) under this condition, consistent with the lack of permeabilization of the inner mitochondrial membrane. In contrast, treatment with 0.06 - 0.1% digitonin led to the emergence of staining for both ARL2 and HSP60 (Figure 7, bottom row). Intermediate concentrations of digitonin were also tested and in every case we found a strong correlation between the appearance of ARL2 and HSP60 staining (data not shown). Note that digitonin also permeabilized the nuclear envelope, revealing ARL2 staining within the nucleus, as previously reported (Zhou et al., 2006); however, the mitochondrial staining is readily distinguished from the nuclear pool (Figure 7, bottom panels). While these data cannot exclude the presence of some ARL2 in other compartments, including the IMS, we conclude that there exists a mitochondrial pool of ARL2 in the matrix.

Neither ANT1 nor BART mediate the mitochondrial effects of ARL2

The direct binding of the ARL2(GTP)-BART complex to ANT1 in our gel overlay assay (Sharer et al., 2002) identified the ADP-ATP transporter ANT1 as a potential mediator of the ARL2 effects described above. A prediction from those data was that ARL2 positively regulates ANT transporter activity, and that the absence of ARL2(GTP)-BART binding to ANT causes a decrease in ATP/ADP transport, leading to an accumulation of ADP in the cytosol and falling ATP levels. In support of this idea, another group showed that BART knockdown lowered ATP levels and that ARL2 knockdown led to a decrease in ANT transporter activity in isolated mitochondria (Nishi et al., 2010). To test this model we used a reconstitution assay for transport proteins, as described previously (Palmieri et al., 1995). The bovine ADP/ATP carrier, isoform 1 (ANT1 or AAC1/SLC25A4), was reconstituted into liposomes, as described under Materials and Methods, and the rate of adenine nucleotide exchange was measured. No differences in the rate of transport were seen upon inclusion of up to 30 μg ARL2 or BART in the reconstitution assay. Using external and internal ADP concentrations of 0.02 and 10 mM, respectively, the transport activity of reconstituted ANT1 was 73.2 ± 8.1 μmol/min/g protein in controls (i.e., in the absence of either ARL2 or BART). The activity was no different in the presence of BART (71.5 ± 8.7 μmol/min/g protein), or ARL2 alone (75.0 ± 10.2 μmol/min/g protein) or the ARL2(GTP)-BART complex (72.6 ± 11.2 μmol/min/g protein) or ARL2(GDP)/BART (70.1 ± 9.4 μmol/min/g protein).

Any in vitro reconstitution may fail to replicate a response seen in cells as a result of the absence of a required component that is unknown. BART is the only known classical ARL2 effector in mitochondria, and was required for ARL2 binding to ANT1 in our gel overlay assay (Sharer et al., 2002). Thus, to further test the possibility that the effects of ARL2 siRNA on ATP levels were mediated by loss of ARL2 binding to BART (and therefore ANT1), we performed knockdowns of BART in HeLa cells. Four siRNAs against BART (Dharmacon) each decreased BART levels by an estimated 80%, as judged by immunoblotting of cell homogenates up to four days after transfection. With successful depletion of BART protein from HeLa cells, we looked

for effects on mitochondrial morphology and ATP levels in cells. HeLa cells were fixed on days 1-3 after transfection with the siRNAs and stained with an antibody to cytochrome c to image mitochondria. No differences were apparent in overall mitochondrial morphology or localization in cells, as determined by visual inspection. Total cellular pools of ATP in BART siRNA cells were not significantly different from control cells after 48 hours of knockdown (96.5 ± 9.7% of control levels for BART siRNA #1, and 106.6 ± 1.4% for BART siRNA #2). Thus, despite the fact that a pool of BART is found within mitochondria and our previously published data revealed that BART was required for ARL2(GTP) to bind ANT1 in a gel overlay assay, these data fail to support a role for ANT1 or BART in mediating effects of ARL2 on ATP levels, mitochondria morphology, or motility in HeLa cells.

With the lack of evidence in ARL2(GTP)-BART regulation of ANT1, we sought another explanation for the large ATP loss observed with ARL2 siRNA. There is precedent for proteins with well-established roles outside of mitochondria, but with smaller pools inside mitochondria, also having critical roles in maintenance of ATP levels and stability of electron chain complexes (e.g., MEF2 (She et al., 2011) and STAT3 (Wegrzyn et al., 2009)). Thus, we tested for changes in the abundance of complexes I-V in mitochondria after depletion of ARL2. We monitored the levels of each complex using non-denaturing blue native-polyacrylamide gels to resolve the complexes and antibodies to a component of each complex (see Materials and Methods for details) to estimate the abundance of each and found no differences of any of these five complexes in ARL2 siRNA cells compared to mock transfected controls.

Knockdown of the ARL2 GAP, ELMOD2, phenocopies ARL2 point mutants

We next explored the possibility that one or more of the three recently identified ARL2 GAPs, ELMOD1-3 (Bowzard et al., 2007; East et al., 2012; Jaworek et al., in press), may localize to mitochondria and act downstream of ARL2. Little is known of the functions of these three proteins in cells and GAP activity is the only known biochemical activity for any of them (East et

al., 2012; Ivanova et al., 2014). Because ARF family GAPs are often found to have effector functions (East and Kahn, 2011), we explored the potential for ELMOD proteins as effectors for ARL2 in mitochondria. We developed a rabbit polyclonal antibody to human ELMOD2 and found specific localization of endogenous protein to mitochondria in HeLa (Figure 8) and other cells (e.g., COS7, SH-SY5Y; Supplementary Figure S3). The specificity of our rabbit polyclonal antibody to ELMOD2 and mitochondrial staining was confirmed in control studies testing pre-immune serum and antigen competition on fixed cells (Figure S3). Specific localization to mitochondria was further confirmed by expression in HeLa cells of epitope (HA) tagged ELMOD2-HA as antibodies to the epitope tag overlapped extensively with mitochondrial markers, cytochrome c or HSP60 (data not shown). Using the same method described above of increasing concentrations of digitonin to solubilize different mitochondrial membranes we found that at least some of this mitochondria localized ELMOD2 is present in the mitochondrial matrix (Figure S4).

We next tested commercial siRNA reagents to allow us to evaluate a functional role for ELMOD2 in mitochondria. Dharmacon's Smart Pool of four siRNAs as well as two individual siRNAs purchased from Sigma Chemical Co were found to effectively deplete ELMOD2 protein, as assayed by immunoblot. Each of these siRNAs effectively depleted cells of ELMOD2 on days 2 (Figure 9A) or 3 (data not shown). When cells were fixed at these time points and imaged with mitochondrial markers we found them to be fragmented and concentrated around the nucleus (Figure 9B) similar to phenotypes described above for ARL2 knockdown. When assayed for total cellular ATP levels at 48 hours we found no significant differences between controls and ELMOD2 siRNA (98.4 ± 7.0% for siRNA #2, 98.7 ± 10% for siRNA #3). These data are consistent with a model in which ELMOD2 acts downstream of ARL2 in regulating mitochondrial morphology and motility, but not in its actions required for maintenance of ATP pools.

Discussion

We provide evidence that ARL2 acts in mitochondria to regulate mitochondrial morphology, motility, and ATP production. Differences between the consequences of ARL2 siRNA compared to expression of two different dominant acting point mutants allowed us to cleanly resolve effects on ATP levels or microtubules from those on mitochondria morphology or motility (summarized in Table 1). Thus, ARL2 has been shown to have a distinct and essential role in mitochondria that expands its known roles in eukaryotic cell biology. These roles at least provide an opportunity for coordinate regulation of energy metabolism and the cytoskeleton, with likely links to cell division. Together, our data lead us to propose the existence of two actions of ARL2 relevant to mitochondrial physiology that are each distinct from effects on tubulin or microtubules; one impacting inner membrane ultrastructure with consequences to ATP production and one involving ELMOD2 that results in changes in morphology and motility. These models are discussed in more detail below.

The effects of ARL2 siRNAs on ATP pools are consistent with the previously described (Nishi et al., 2010; Wang et al., 2011) effects of microRNAs (miRNAs) that target ARL2 and lead us to conclude both that ARL2 is required for maintenance of ATP levels and that at least some tissues have the means to modulate ARL2 levels post-transcriptionally. Four or more microRNAs may target ARL2 mRNA in cardiac tissues (Nishi et al., 2010; Wang et al., 2011), and depletion of ARL2 in neonatal ventricular myocytes also lowered ATP levels (Nishi et al., 2010). Earlier, we found that levels of mitochondrial ARL2 (no changes in total tissue ARL2) increased several fold in mice deleted for the adenine nucleotide transporter, ANT1, but only in cardiac and skeletal muscle (Sharer et al., 2002), indicating the existence of regulated import of ARL2 into mitochondria that may be tissue specific. With (i) the levels of cellular ARL2 under regulation by miRNAs; (ii) the regulated import of ARL2 into mitochondria, via unknown mechanisms; and (iii) the ancient and highly conserved nature of ARL2 and its ubiquitous expression, we believe that ARL2 plays fundamental roles in energy metabolism in mitochondria

of all eukaryotic cells, though ARL2 function may be particularly important in those cells with high energy demands, e.g., cardiac and skeletal muscle cells. This requirement for ARL2 in the maintenance of ATP pools may explain its essential nature, previously described in a number of organisms, though in those studies clear resolution from effects on microtubules and cell division was not achieved.

In addition to effects on ATP levels, changes in ARL2 activity cause fragmentation of mitochondria and specific loss of mitochondrial motility. We interpret the observation that fragmentation of mitochondria was prevented in cells expressing both ARL2[T30N] and DRP1[K38A], which inhibits mitochondrial fission, as evidence that the ARL2 mutant alone promotes mitochondrial fission, a process that is thought to require attachment to mitochondria and motility (Boldogh and Pon, 2007), and that ARL2 acts upstream of DRP1 to do so. Miro is a calcium-sensitive GTPase (Boldogh and Pon, 2007; Wang and Schwarz, 2009) that is involved in mitochondrial motility and ELMOD2 is a GAP for ARL2 with broad specificity, so far restricted to the ARF family, but may be worth exploring (Bowzard et al., 2007) for possible functional connections. These effects were clearly resolved from changes in ATP levels as they were evident in cells expressing ARL2[T30N] or ARL2[K71R], which do not alter ATP levels, and thus are not simply secondary consequences of falling ATP. In addition, substantial changes in morphology and motility were evident within 24 hours, at which point we saw no statistically significant changes in ATP levels. We believe the order of events resulting from loss of ARL2 is fragmentation, loss of motility, and then loss of ATP.

Because changes in ARL2 activity (e.g., expression of the dominant active mutant ARL2[Q70L] or ARL2[T30N]) can also result in changes in microtubule density in cells and mitochondria travel along microtubules, it was important to cleanly resolve these two activities. The result that depletion of ARL2 (siRNA) or expression of ARL2[K71R] each cause mitochondrial fragmentation and loss of motility without changes in microtubules is evidence that ARL2 activity is required for maintenance of mitochondrial morphology and motility

independently of effects on microtubules. In addition, the fact that endosomes and lysosomes, which also traffic along microtubules, were found to travel at undisturbed rates in the same cells that lost mitochondrial motility is strong evidence of a specific defect at mitochondria and argues further against changes in microtubules or ATP levels as primary defects.

Our conclusion that ARL2 is required for mitochondrial morphology, motility, and ATP production led us to test our previous model, that ARL2 is an activator of ATP/ADP transporters in the inner mitochondrial membrane (Nishi et al., 2010; Sharer et al., 2002). Our earlier in vitro data demonstrated direct binding of ANT1 by the ARL2(GTP)-BART complex, but no functional evidence of effects on transporter activities. Here we used reconstitution assays of ANT1 in proteoliposomes and failed to see any changes in transporter activity upon addition of ARL2, BART, or the ARL2(GTP)-BART complex. We also found that depletion of BART had no effects on ATP levels or mitochondrial morphology in the same cell line in which depletion of ARL2 did. This is in contrast to Nishi, et al (Nishi et al., 2010), who reported that BART siRNA lowered ATP levels, though we cannot currently explain the different outcomes. Thus, we found no evidence that BART is a mediator of the required roles of ARL2 in maintenance of ATP levels, mitochondria fragmentation, or motility, despite its presence in the matrix. Though our results do not rule out other, currently unknown, roles for ANT and BART in ARL2 signaling, we conclude that our mitochondrial phenotypes resulting from the loss of ARL2 are not mediated by either ANT1 or BART.

In contrast to BART, the evidence that ELMOD2 siRNA phenocopied two of three effects described for ARL2 siRNA, and that both proteins are present in the matrix, is consistent with ELMOD2 being an effector of ARL2 in mitochondria; potentially in regulating morphology and motility but not ATP levels. ELMOD2 is an ARF family GAP with broad substrate specificity within the ARF family (Bowzard et al., 2007; Ivanova et al., 2014) and is predicted to act immediately downstream of a GTPase. While some shared binding partners and activities have been previously described for ARL2 and ARL3 (Ismail et al., 2011; Van Valkenburgh et al.,

2001; Veltel et al., 2008a), we found no evidence of ARL3 localizing to mitochondria or affecting its functions, which suggests a high degree of specificity to ARL2 in its mitochondrial roles and also leaving ELMOD2 as the most likely GAP and effector for at least a subset of ARL2 actions in mitochondria.

We showed that ARL2 is present in the mitochondrial matrix using two different approaches. cBid addition to permeabilized HeLa cells released cytochrome c but retained ARL2 in mitochondria. This result is consistent with ARL2 localizing to the matrix but it is likely that ARL2 is also present in the IMS. Increasing concentrations of digitonin selectively permeabilized outer and inner mitochondrial membranes and ARL2 staining was seen only after permeabilization of the inner mitochondrial membrane, the same condition required to visualize HSP60, a well-documented matrix protein. In contrast, cytochrome c (an IMS protein) staining of mitochondria was seen at lower concentrations of digitonin. The digitonin permeabilization approach does not rule out the presence of ARL2 in the IMS if that pool of the GTPase is not fixed well by paraformaldehyde. Thus, we conclude that a pool of mitochondria-associated ARL2 is in the matrix, though we cannot exclude the possibility that some ARL2 is also in the IMS. Indeed, we believe there is a pool of ARL2 in the IMS, based upon our earlier sub-mitochondria fractionation data (Sharer et al., 2002) and more recent techniques that combine proteomics with spatially restricted protein tagging (Rhee et al., 2013); each of which concluded that ARL2 is in the IMS. Because ARL2 is present in mitochondria in amounts that preclude a stoichiometric binding to any of the complexes of the electron transport chain or transporters and is not found in any stable complexes, it is likely that ARL2 actions in the matrix are catalytic or regulatory and transient in nature, rather than as a stoichiometric component of a complex (Phillips et al., 2010). How then does the depletion of ARL2 cause these mitochondrial defects? We believe the best model is that ARL2 is involved in remodeling of the inner mitochondrial membrane, likely at crista junctions (van der Laan et al., 2012; Zick et al., 2009). Knockdown of either of the inner membrane proteins ChChd3 (Darshi et al., 2011) or ChChd6 (An et al., 2012) results in

mitochondrial fragmentation, perinuclear clustering, and loss of cell proliferation (An et al., 2012; Darshi et al., 2011) and ATP levels. ChChd3 siRNA also decreased cell proliferation without increasing apoptosis, again similar to ARL2 siRNA. The two ChChd proteins bind to each other and to Mitofilin, a core component of the MINOS (Zerbes et al., 2012) or MitOS (Alkhaja et al., 2012; Harner et al., 2011; Hoppins et al., 2011; von der Malsburg et al., 2011) complex that is key to crista junction formation and stabilization. The model for ARL2 affecting inner membrane remodeling also derives from analogy to the actions of the ARF (and ARL1) proteins, which are intimately involved in vesicle biogenesis and membrane remodeling at the Golgi and endosomes (Donaldson and Jackson, 2011; Gillingham and Munro, 2007; Inoue and Randazzo, 2007; Kahn, 2009; Tsai et al., 2013). Thus, the intimate contact of ARF family members with membranes (Liu et al., 2009), ability to alter membrane curvature, their recruitment of other proteins with similar membrane sensing and modifying activities, and ability to alter localized phospholipid metabolism may be a more widespread feature of the ARF family than previously appreciated. These are very challenging issues to explore on the inner mitochondrial membrane, but research in this area is increasingly active and productive, since the identification of the MINOS complex. The hypothesis that ARL2 may be a component of the MINOS complex or regulate cristae morphology is currently under investigation in our lab.

When our latest observations are combined with earlier studies, we conclude that ARL2 is an important component of several cellular processes, including (i) regulation of ATP levels in mitochondria, likely in the matrix, (ii) regulation of mitochondrial fission and motility, (iii) at centrosomes, in concert with cofactor D, to regulate the growth of microtubules and mitotic spindles (Beghin et al., 2007; Beghin et al., 2008; Cunningham and Kahn, 2008; Fanarraga et al., 2010; Zhou et al., 2006), (iv) in the nucleus to regulate STAT3 and perhaps other transcriptional responses (Muromoto et al., 2008), and in the cytosol to (v) regulate the folding of tubulin heterodimers (Bhamidipati et al., 2000; Tian et al., 2010), and (vi) the shuttling and release of farnesylated proteins (Ismail et al., 2011). With the dissection of these different functions of

ARL2 and the growing list of reagents allowing their clear resolution we are poised to understand the mechanisms of these actions at the molecular level, though some of them are expected to be challenging to document due to the limited understanding of the process itself (e.g., crista junction regulation). The fact that ARL2 is linked to so many different essential cellular functions and increasingly to human diseases drives further exploration into the mechanistic details of each of these actions.

Acknowledgements: We are grateful to Dr. David Andrews (McMaster University, Canada), for the gift of purified c-Bid. Cole Haynes (Memorial Sloan Kettering) kindly provided us with advice and reagents. We thank Drs. Allan Levey (Emory University), James Zheng (Emory University), Edward Bampton (University of Leicester, UK), Richard Vallee (Columbia University, NY), and Richard Pagano (Mayo Clinic, MN, USA) for their gifts of plasmids. We thank Drs. Gyorgy Hajnoczky (Thomas Jefferson University, Pennsylvania, USA) and Heidi McBride (McGill University, Montreal, Canada) for their ideas in discussions of this work at various stages. We gratefully acknowledge Drs. Heidi McBride and Larry Boise for careful reading of earlier versions of the manuscript during its preparation and advice during the work. ARL2[K71R] was made by Oskar Laur in the Emory Cloning Core facility. We thank the Integrated Cellular Imaging (ICI) core at Emory University for assistance with obtaining imaging data in this paper.

References

Agrimi, G., M.A. Di Noia, C.M. Marobbio, G. Fiermonte, F.M. Lasorsa, and F. Palmieri. 2004. Identification of the human mitochondrial S-adenosylmethionine transporter: bacterial expression, reconstitution, functional characterization and tissue distribution. Biochem J. 379:183-190.

Alkhaja, A.K., D.C. Jans, M. Nikolov, M. Vukotic, O. Lytovchenko, F. Ludewig, W. Schliebs, D. Riedel, H. Urlaub, S. Jakobs, and M. Deckers. 2012. MINOS1 is a conserved component of mitofilin complexes and required for mitochondrial function and cristae organization. Mol Biol Cell. 23:247-257.

An, J., J. Shi, Q. He, K. Lui, Y. Liu, Y. Huang, and M.S. Sheikh. 2012. CHCM1/CHCHD6, novel mitochondrial protein linked to regulation of mitofilin and mitochondrial cristae morphology. J Biol Chem. 287:7411-7426.

Antoshechkin, I., and M. Han. 2002. The C. elegans evl-20 gene is a homolog of the small GTPase ARL2 and regulates cytoskeleton dynamics during cytokinesis and morphogenesis. Dev Cell. 2:579-591.

Beghin, A., S. Honore, C. Messana, E.L. Matera, J. Aim, S. Burlinchon, D. Braguer, and C. Dumontet. 2007. ADP ribosylation factor like 2 (Arl2) protein influences microtubule dynamics in breast cancer cells. Exp Cell Res. 313:473-485.

Beghin, A., E.L. Matera, S. Brunet-Manquat, and C. Dumontet. 2008. Expression of Arl2 is associated with p53 localization and chemosensitivity in a breast cancer cell line. Cell Cycle. 7:3074-3082.

Beltran-Parrazal, L., H.E. Lopez-Valdes, K.C. Brennan, M. Diaz-Munoz, J. de Vellis, and A.C. Charles. 2006. Mitochondrial transport in processes of cortical neurons is independent of intracellular calcium. Am J Physiol Cell Physiol. 291:C1193-1197.

Bhamidipati, A., S.A. Lewis, and N.J. Cowan. 2000. ADP ribosylation factor-like protein 2 (Arl2) regulates the interaction of tubulin-folding cofactor D with native tubulin. J Cell Biol. 149:1087-1096.

Boldogh, I.R., and L.A. Pon. 2007. Mitochondria on the move. Trends Cell Biol. 17:502-510.

Bollag, G., and F. McCormick. 1991. Regulators and effectors of ras proteins. Annu Rev Cell Biol. 7:601-632.

Bowzard, J.B., D. Cheng, J. Peng, and R.A. Kahn. 2007. ELMOD2 is an Arl2 GTPase-activating protein that also acts on Arfs. J Biol Chem. 282:17568-17580.

Bowzard, J.B., J.D. Sharer, and R.A. Kahn. 2005. Assays used in the analysis of Arl2 and its binding partners. Methods Enzymol. 404:453-467.

Brown, A. 2003. Axonal transport of membranous and nonmembranous cargoes: a unified perspective. J Cell Biol. 160:817-821.

Chan, D.C. 2006. Mitochondrial Fusion and Fission in Mammals. Annu Rev Cell Dev Biol. 22:79-99.

Clark, J., L. Moore, A. Krasinskas, J. Way, J. Battey, J. Tamkun, and R.A. Kahn. 1993. Selective amplification of additional members of the ADP-ribosylation factor (ARF) family: cloning of additional human and Drosophila ARF-like genes. Proc Natl Acad Sci U S A. 90:8952-8956.

Cunningham, L.A., and R.A. Kahn. 2008. Cofactor D functions as a centrosomal protein and is required for the recruitment of the gamma-tubulin ring complex at centrosomes and organization of the mitotic spindle. J Biol Chem. 283:7155-7165.

Darshi, M., V.L. Mendiola, M.R. Mackey, A.N. Murphy, A. Koller, G.A. Perkins, M.H. Ellisman, and S.S. Taylor. 2011. ChChd3, an inner mitochondrial membrane protein, is essential for maintaining crista integrity and mitochondrial function. J Biol Chem. 286:2918-2932.

Donaldson, J.G., and C.L. Jackson. 2011. ARF family G proteins and their regulators: roles in membrane transport, development and disease. Nat Rev Mol Cell Biol. 12:362-375.

Dong, J.H., J.F. Wen, and H.F. Tian. 2007. Homologs of eukaryotic Ras superfamily proteins in prokaryotes and their novel phylogenetic correlation with their eukaryotic analogs. Gene. 396:116-124.

East, M.P., J.B. Bowzard, J.B. Dacks, and R.A. Kahn. 2012. ELMO domains, evolutionary and functional characterization of a novel GTPase-activating protein (GAP) domain for Arf protein family GTPases. J Biol Chem. 287:39538-39553.

East, M.P., and R.A. Kahn. 2011. Models for the functions of Arf GAPs. Semin Cell Dev Biol. 22:3-9.

Fanarraga, M.L., J. Bellido, C. Jaen, J.C. Villegas, and J.C. Zabala. 2010. TBCD links centriologenesis, spindle microtubule dynamics, and midbody abscission in human cells. PLoS One. 5:e8846.

Fehrenbacher, K.L., H.C. Yang, A.C. Gay, T.M. Huckaba, and L.A. Pon. 2004. Live cell imaging of mitochondrial movement along actin cables in budding yeast. Curr Biol. 14:1996-2004.

Feig, L.A. 1999. Tools of the trade: use of dominant-inhibitory mutants of Ras-family GTPases. Nature cell biology. 1:E25-27.

Fiermonte, G., E. Paradies, S. Todisco, C.M. Marobbio, and F. Palmieri. 2009. A novel member of solute carrier family 25 (SLC25A42) is a transporter of coenzyme A and adenosine 3',5'-diphosphate in human mitochondria. J Biol Chem. 284:18152-18159.

Gillingham, A.K., and S. Munro. 2007. The small G proteins of the Arf family and their regulators. Annu Rev Cell Dev Biol. 23:579-611.

Hanzal-Bayer, M., M. Linari, and A. Wittinghofer. 2005. Properties of the interaction of Arf-like protein 2 with PDEdelta. J Mol Biol. 350:1074-1082.

Harner, M., C. Korner, D. Walther, D. Mokranjac, J. Kaesmacher, U. Welsch, J. Griffith, M. Mann, F. Reggiori, and W. Neupert. 2011. The mitochondrial contact site complex, a determinant of mitochondrial architecture. EMBO J. 30:4356-4370.

Hoppins, S., S.R. Collins, A. Cassidy-Stone, E. Hummel, R.M. Devay, L.L. Lackner, B. Westermann, M. Schuldiner, J.S. Weissman, and J. Nunnari. 2011. A mitochondrial-

focused genetic interaction map reveals a scaffold-like complex required for inner membrane organization in mitochondria. J Cell Biol. 195:323-340.

Hoyt, M.A., T. Stearns, and D. Botstein. 1990. Chromosome instability mutants of Saccharomyces cerevisiae that are defective in microtubule-mediated processes. Mol Cell Biol. 10:223-234.

Inoue, H., and P.A. Randazzo. 2007. Arf GAPs and their interacting proteins. Traffic. 8:1465-1475.

Ismail, S.A., Y.X. Chen, M. Miertzschke, I.R. Vetter, C. Koerner, and A. Wittinghofer. 2012. Structural basis for Arl3-specific release of myristoylated ciliary cargo from UNC119. The EMBO Journal. 31:4085-4094.

Ismail, S.A., Y.X. Chen, A. Rusinova, A. Chandra, M. Bierbaum, L. Gremer, G. Triola, H. Waldmann, P.I. Bastiaens, and A. Wittinghofer. 2011. Arl2-GTP and Arl3-GTP regulate a GDI-like transport system for farnesylated cargo. Nat Chem Biol. 7:942-949.

Ivanova, A.A., M.P. East, S.L. Yi, and R.A. Kahn. 2014. Characterization of Recombinant ELMOD Proteins as GTPase Activating Proteins (GAPs) for ARF Family GTPases. J Biol Chem.

Jaworek, T.J., E.M. Richard, A.A. Ivanova, A.P.J. Giese, D.I. Choo, S.N. Khan, R.A. Kahn, and S. Riazuddin. in press. Alteration in ELMOD3, a new Arl2 GTPase-activating protein, causes nonsyndromic hearing impairment. Amer J Hum Gen.

Jeyaraju, D.V., L. Xu, M.C. Letellier, S. Bandaru, R. Zunino, E.A. Berg, H.M. McBride, and L. Pellegrini. 2006. Phosphorylation and cleavage of presenilin-associated rhomboid-like protein (PARL) promotes changes in mitochondrial morphology. Proc Natl Acad Sci U S A. 103:18562-18567.

Johnson, K.R., C.M. Longo-Guess, and L.H. Gagnon. 2012. Mutations of the mouse ELMO domain containing 1 gene (Elmod1) link small GTPase signaling to actin cytoskeleton dynamics in hair cell stereocilia. PLoS One. 7:e36074.

Kahn, R.A. 2009. Toward a model for Arf GTPases as regulators of traffic at the Golgi. FEBS Lett. 583:3872-3879.

Liu, Y., R.A. Kahn, and J.H. Prestegard. 2009. Structure and membrane interaction of myristoylated ARF1. Structure. 17:79-87.

Mabjeesh, N.J., D. Escuin, T.M. LaVallee, V.S. Pribluda, G.M. Swartz, M.S. Johnson, M.T. Willard, H. Zhong, J.W. Simons, and P. Giannakakou. 2003. 2ME2 inhibits tumor growth and angiogenesis by disrupting microtubules and dysregulating HIF. Cancer Cell. 3:363-375.

Madesh, M., B. Antonsson, S.M. Srinivasula, E.S. Alnemri, and G. Hajnoczky. 2002. Rapid kinetics of tBid-induced cytochrome c and Smac/DIABLO release and mitochondrial depolarization. J Biol Chem. 277:5651-5659.

Marobbio, C.M., G. Agrimi, F.M. Lasorsa, and F. Palmieri. 2003. Identification and functional reconstitution of yeast mitochondrial carrier for S-adenosylmethionine. Embo J. 22:5975-5982.

McElver, J., D. Patton, M. Rumbaugh, C. Liu, L.J. Yang, and D. Meinke. 2000. The TITAN5 gene of Arabidopsis encodes a protein related to the ADP ribosylation factor family of GTP binding proteins. Plant Cell. 12:1379-1392.

Miller, K.E., and M.P. Sheetz. 2004. Axonal mitochondrial transport and potential are correlated. J Cell Sci. 117:2791-2804.

Muromoto, R., Y. Sekine, S. Imoto, O. Ikeda, T. Okayama, N. Sato, and T. Matsuda. 2008. BART is essential for nuclear retention of STAT3. Int Immunol. 20:395-403.

Nishi, H., K. Ono, Y. Iwanaga, T. Horie, K. Nagao, G. Takemura, M. Kinoshita, Y. Kuwabara, R.T. Mori, K. Hasegawa, T. Kita, and T. Kimura. 2010. MicroRNA-15b modulates cellular ATP levels and degenerates mitochondria via Arl2 in neonatal rat cardiac myocytes. J Biol Chem. 285:4920-4930.

Otera, H., S. Ohsakaya, Z. Nagaura, N. Ishihara, and K. Mihara. 2005. Export of mitochondrial AIF in response to proapoptotic stimuli depends on processing at the intermembrane space. EMBO J. 24:1375-1386.

Palmieri, F., C. Indiveri, F. Bisaccia, and V. Iacobazzi. 1995. Mitochondrial Metabolite Carrier Proteins: Purification, Reconstitution, and Transport Studies. Methods in Enzymology. 260:349-369.

Palmieri, F., and M. Klingenberg. 1979. Direct methods for measuring metabolite transport and distribution in mitochondria. Methods Enzymol. 56:279-301.

Phillips, D., M.J. Reilley, A.M. Aponte, G. Wang, E. Boja, M. Gucek, and R.S. Balaban. 2010. Stoichiometry of STAT3 and mitochondrial proteins: Implications for the regulation of oxidative phosphorylation by protein-protein interactions. J Biol Chem. 285:23532-23536.

Price, H.P., A. Peltan, M. Stark, and D.F. Smith. 2010. The small GTPase ARL2 is required for cytokinesis in Trypanosoma brucei. Mol Biochem Parasitol. 173:123-131.

Radcliffe, P.A., L. Vardy, and T. Toda. 2000. A conserved small GTP-binding protein Alp41 is essential for the cofactor-dependent biogenesis of microtubules in fission yeast. FEBS Lett. 468:84-88.

Rhee, H.W., P. Zou, N.D. Udeshi, J.D. Martell, V.K. Mootha, S.A. Carr, and A.Y. Ting. 2013. Proteomic mapping of mitochondria in living cells via spatially restricted enzymatic tagging. Science. 339:1328-1331.

Scheffzek, K., M.R. Ahmadian, W. Kabsch, L. Wiesmuller, A. Lautwein, F. Schmitz, and A. Wittinghofer. 1997. The Ras-RasGAP complex: structural basis for GTPase activation and its loss in oncogenic Ras mutants. Science. 277:333-338.

Sharer, J.D. 2005. The adenine nucleotide translocase type 1 (ANT1): a new factor in mitochondrial disease. IUBMB Life. 57:607-614.

Sharer, J.D., and R.A. Kahn. 1999. The ARF-like 2 (ARL2)-binding protein, BART. Purification, cloning, and initial characterization. J Biol Chem. 274:27553-27561.

Sharer, J.D., J.F. Shern, H. Van Valkenburgh, D.C. Wallace, and R.A. Kahn. 2002. ARL2 and BART enter mitochondria and bind the adenine nucleotide transporter. Mol Biol Cell. 13:71-83.

She, H., Q. Yang, K. Shepherd, Y. Smith, G. Miller, C. Testa, and Z. Mao. 2011. Direct regulation of complex I by mitochondrial MEF2D is disrupted in a mouse model of Parkinson disease and in human patients. J Clin Invest. 121:930-940.

Shern, J.F., J.D. Sharer, D.C. Pallas, F. Bartolini, N.J. Cowan, M.S. Reed, J. Pohl, and R.A. Kahn. 2003. Cytosolic Arl2 is complexed with cofactor D and protein phosphatase 2A. J Biol Chem. 278:40829-40836.

Stearns, T., M.A. Hoyt, and D. Botstein. 1990. Yeast mutants sensitive to antimicrotubule drugs define three genes that affect microtubule function. Genetics. 124:251-262.

Studier, F.W. 2005. Protein production by auto-induction in high-density shaking cultures. Protein Expr Purif. 41:207-234.

Tian, G., S. Thomas, and N.J. Cowan. 2010. Effect of TBCD and its regulatory interactor Arl2 on tubulin and microtubule integrity. Cytoskeleton (Hoboken). 67:706-714.

Tsai, P.-C., J.-W. Hsu, Y.-W. Liu, K.-Y. Chen, and F.-J.S. Lee. 2013. Arl1p regulates spatial membrane organization at the trans-Golgi network through interaction with Arf-GEF Gea2p and flippase Drs2p. Proceedings of the National Academy of Sciences. 110:E668-E677.

van der Laan, M., M. Bohnert, N. Wiedemann, and N. Pfanner. 2012. Role of MINOS in mitochondrial membrane architecture and biogenesis. Trends Cell Biol. 22:185-192.

Van Valkenburgh, H., J.F. Shern, J.D. Sharer, X. Zhu, and R.A. Kahn. 2001. ADP-ribosylation factors (ARFs) and ARF-like 1 (ARL1) have both specific and shared effectors: characterizing ARL1-binding proteins. J Biol Chem. 276:22826-22837.

Veltel, S., A. Kravchenko, S. Ismail, and A. Wittinghofer. 2008a. Specificity of Arl2/Arl3 signaling is mediated by a ternary Arl3-effector-GAP complex. FEBS Lett. 582:2501-2507.

Veltel, S., A. Kravchenko, S. Ismail, and A. Wittinghofer. 2008b. Specificity of Arl2/Arl3 signaling is mediated by a ternary Arl3-effector-GAP complex. FEBS Letters. 582:2501-2507.

von der Malsburg, K., J.M. Muller, M. Bohnert, S. Oeljeklaus, P. Kwiatkowska, T. Becker, A. Loniewska-Lwowska, S. Wiese, S. Rao, D. Milenkovic, D.P. Hutu, R.M. Zerbes, A. Schulze-Specking, H.E. Meyer, J.C. Martinou, S. Rospert, P. Rehling, C. Meisinger, M. Veenhuis, B. Warscheid, I.J. van der Klei, N. Pfanner, A. Chacinska, and M. van der Laan. 2011. Dual role of mitofilin in mitochondrial membrane organization and protein biogenesis. Dev Cell. 21:694-707.

Wang, K., P. Li, Y. Dong, X. Cai, D. Hou, J. Guo, Y. Yin, Y. Zhang, J. Li, H. Liang, B. Yu, J. Chen, K. Zen, J. Zhang, C.Y. Zhang, and X. Chen. 2011. A microarray-based approach identifies ADP ribosylation factor-like protein 2 as a target of microRNA-16. J Biol Chem. 286:9468-9476.

Wang, X., and T.L. Schwarz. 2009. The Mechanism of Ca2+-Dependent Regulation of Kinesin-Mediated Mitochondrial Motility. Cell. 136:163-174.

Wegrzyn, J., R. Potla, Y.J. Chwae, N.B. Sepuri, Q. Zhang, T. Koeck, M. Derecka, K. Szczepanek, M. Szelag, A. Gornicka, A. Moh, S. Moghaddas, Q. Chen, S. Bobbili, J. Cichy, J. Dulak, D.P. Baker, A. Wolfman, D. Stuehr, M.O. Hassan, X.Y. Fu, N. Avadhani, J.I. Drake, P. Fawcett, E.J. Lesnefsky, and A.C. Larner. 2009. Function of mitochondrial Stat3 in cellular respiration. Science. 323:793-797.

Young, K.W., L.G. Pinon, E.T. Bampton, and P. Nicotera. 2010. Different pathways lead to mitochondrial fragmentation during apoptotic and excitotoxic cell death in primary neurons. J Biochem Mol Toxicol. 24:335-341.

Zerbes, R.M., I.J. van der Klei, M. Veenhuis, N. Pfanner, M. van der Laan, and M. Bohnert. 2012. Mitofilin complexes: conserved organizers of mitochondrial membrane architecture. Biol Chem. 393:1247-1261.

Zhang, C.J., A.G. Rosenwald, M.C. Willingham, S. Skuntz, J. Clark, and R.A. Kahn. 1994. Expression of a dominant allele of human ARF1 inhibits membrane traffic in vivo. J Cell Biol. 124:289-300.

Zhou, C., L. Cunningham, A.I. Marcus, Y. Li, and R.A. Kahn. 2006. Arl2 and Arl3 regulate different microtubule-dependent processes. Mol Biol Cell. 17:2476-2487.

Zick, M., R. Rabl, and A.S. Reichert. 2009. Cristae formation-linking ultrastructure and function of mitochondria. Biochim Biophys Acta. 1793:5-19.

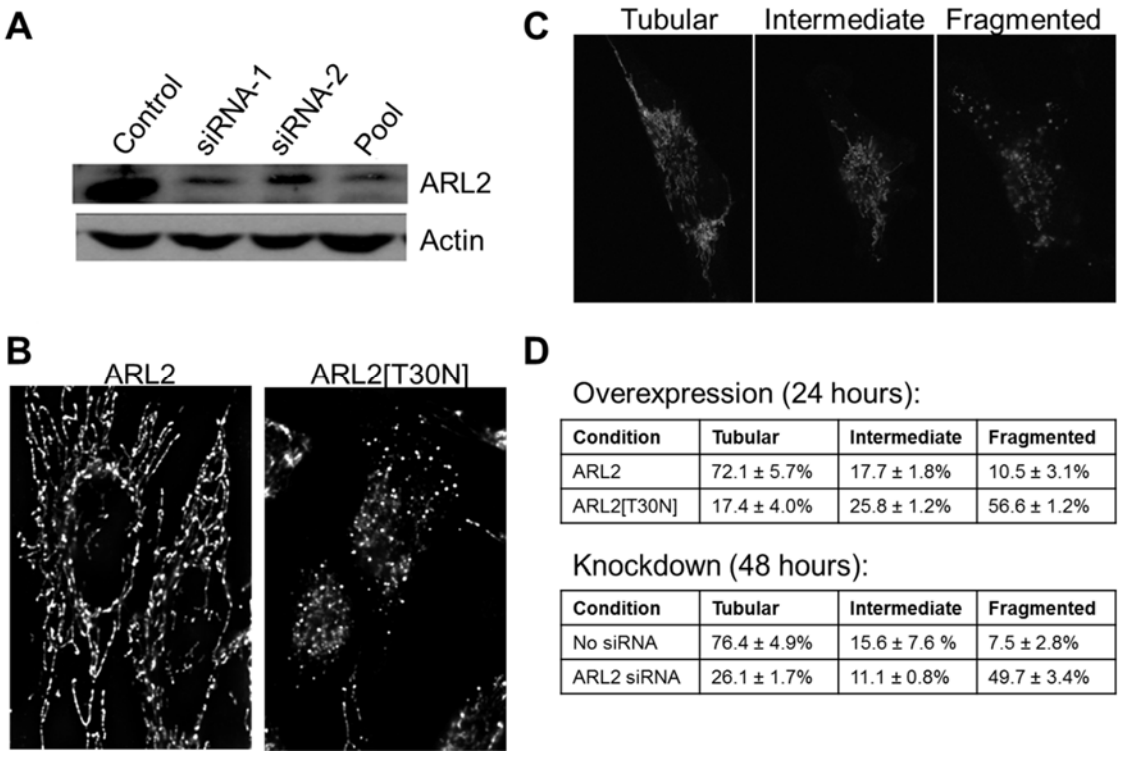

Figure 1. Mitochondria are fragmented in cells where ARL2 activity is compromised. (A) HeLa cells were transfected with either no siRNA (control), each of two individual, sequence-independent siRNAs (siRNA-1 and siRNA-2), or a pool of four siRNAs (siRNA pool) and harvested 48 hours after transfection. Equal amounts (25 μg) of total cellular homogenates were resolved in denaturing polyacrylamide gels. The immunoblot was probed with rabbit polyclonal antibody to ARL2 (upper panel) or actin (lower panel). Only the relevant regions of the gels are shown. **(B)** HeLa cells were transfected with plasmids directing expression of either ARL2 (left), or ARL2[T30N] (right), and stained for cytochrome c, as described under Materials and Methods. Representative widefield images with deconvolution of z-stacks are shown. **(C)** HeLa cells were fixed and stained with an HSP60 antibody and data captured using confocal microscopy. Examples of cells from a mock transfected cell population showing tubular (mostly tubular mitochondria), intermediate (mix of tubular and spherical mitochondria), and fragmented (almost all spherical) mitochondria are shown. **(D)** HeLa cells were co-transfected with mito-GFP and either ARL2 or ARL2[T30N] (for overexpression, scored at 24 hours), or mito-GFP plus ARL2

SmartPool or no siRNA (for knockdown, scored at 48 hours). Mito-GFP expressing cells were scored using the criteria in C, and are expressed as percentages of the transfected cell population. At least 200 cells per condition in three independent experiments were scored. Differences between control and experimental were significant to $p<0.01$ in the tubular and fragmented categories for both ARL2[T30N] and ARL2 siRNA.

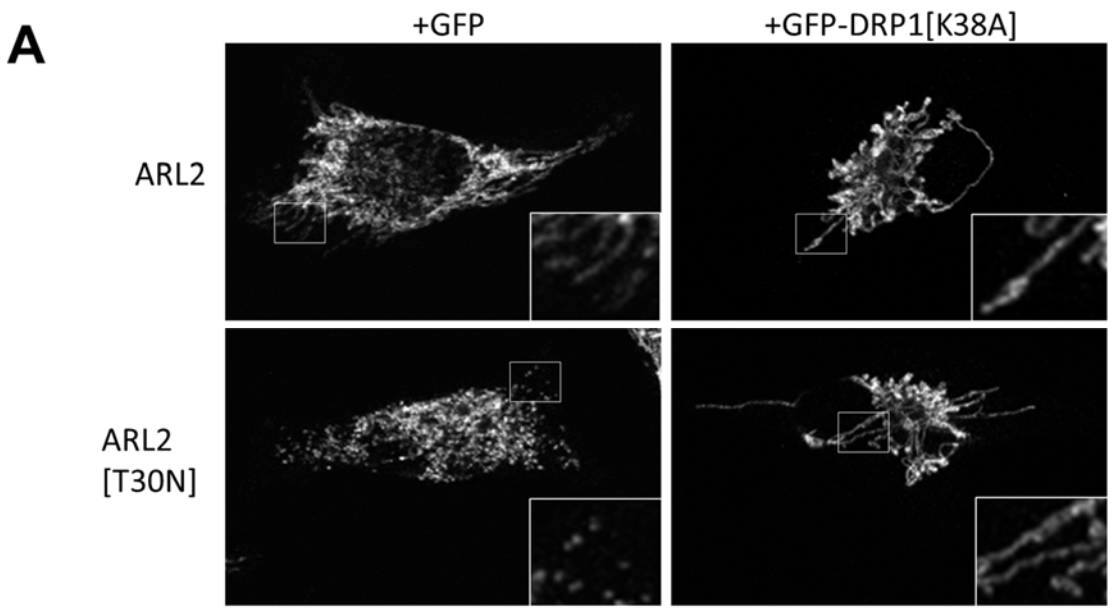

B

Co-expression with DRP1[K38A]

Condition	% Fragmented Mitochondria
Empty Vector	6.2 ± 0.8%
ARL2	5.1 ± 1.8%
ARL2[T30N]	6.5 ± 2.7%

Figure 2. Expression of GFP-DRP1[K38A] reverses fragmentation caused by ARL2[T30N]. HeLa cells were co-transfected with either GFP or GFP-DRP1[K38A] and empty vector, ARL2, or ARL2[T30N]. **(A)** Cells were fixed 24 hours post-transfection and immunostained for HSP60. Representative GFP positive cells are shown. Insets show magnified regions from the cell periphery where the lower densities better highlight mitochondrial morphology. Cells expressing wild type ARL2 have similar mitochondrial morphology to cells transfected with empty vector (not shown). **(B)** Cells expressing GFP-DRP1[K38A] were scored for fragmented mitochondria, using the criteria illustrated in Figure 1D. Cells were quantified from three independent experiments.

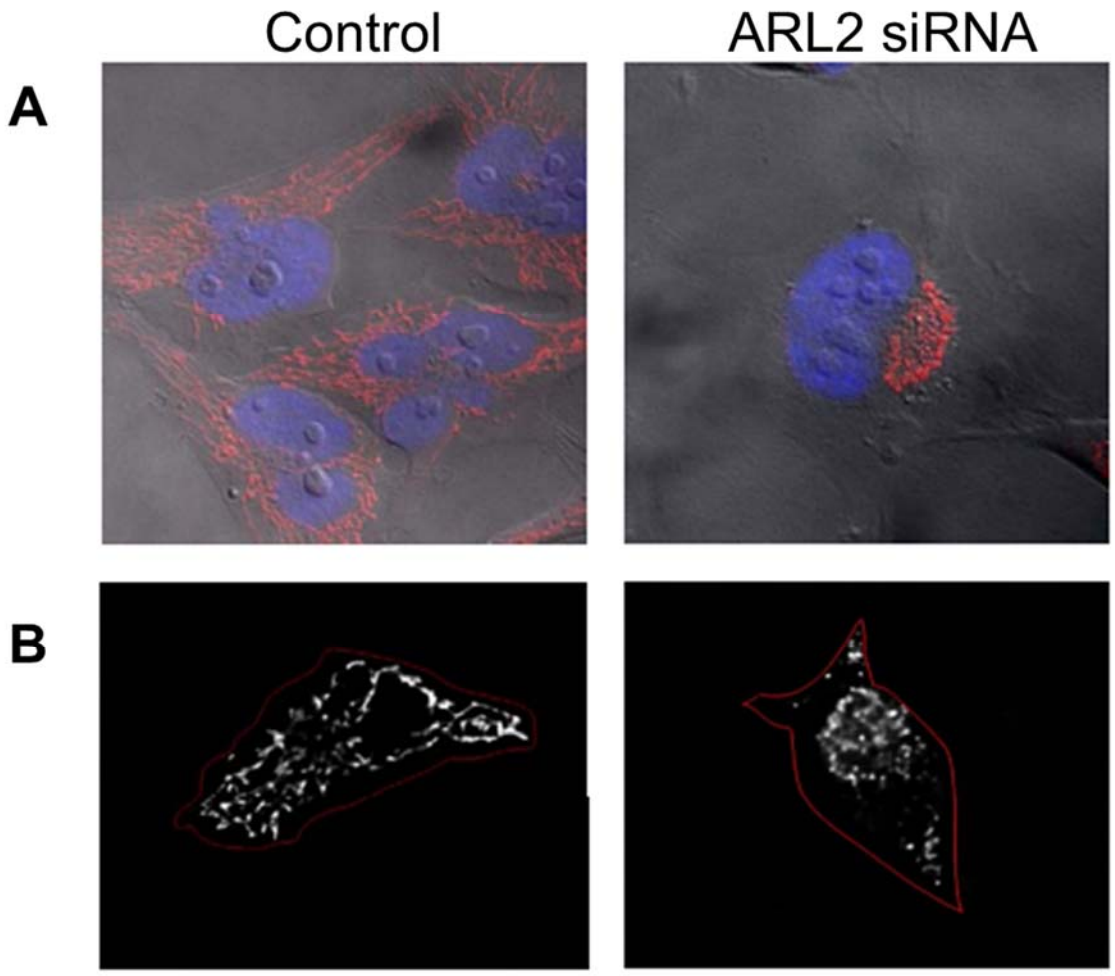

Figure 3. Mitochondria cluster in the perinuclear region in cells depleted of ARL2. (A) HeLa cells were either mock transfected (Control, left panels in A and B), or transfected with the SmartPool of ARL2 siRNAs (right panels in A and B), and the next day were fixed and stained for cytochrome c, as described under Materials and Methods. Cytochrome c staining is shown in red and overlaid onto phase contrast images, along with nuclear (Hoechst) stain, shown in blue. Representative cells are shown. **(B)** Cytochrome c staining is shown in white, with the cell borders outlined in red to highlight the perinuclear clustering in cells lacking ARL2 activity.

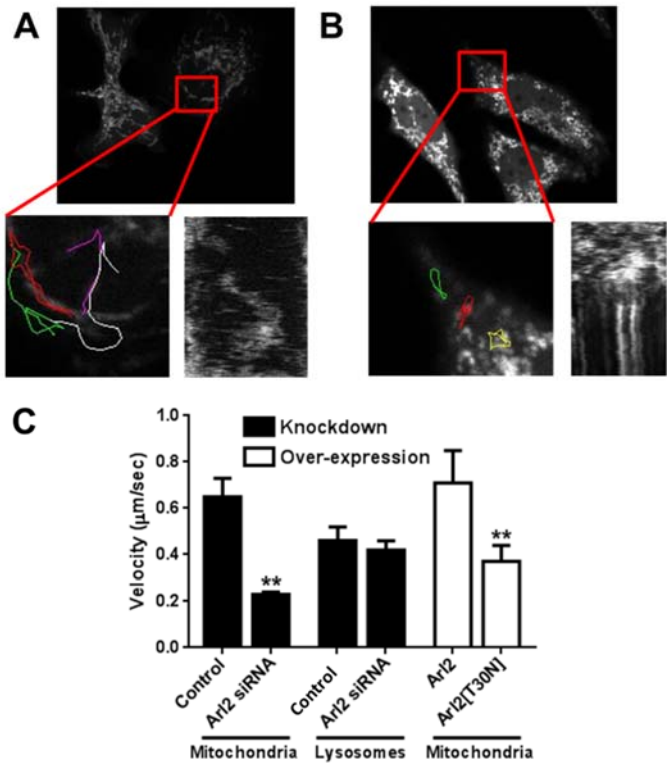

Figure 4. Loss of ARL2 activity compromises mitochondrial motility. HeLa cells were transfected with plasmids directing expression of mito-GFP or mito-GFP plus ARL2 siRNAs. After 24 hours cells displaying normal appearing mitochondria were imaged over time, as described in Materials and Methods. Examples of control **(A)** and knockdown **(B)** cells are shown, with mito-GFP fluorescence in the top panels, blow ups of the boxed areas bottom left, and kymographs from that region shown as a function of time below right. Colored lines showing tracking of individual mitochondria are shown in the bottom left of each panel with different colors indicating different particles tracked. **(C)** Velocities of organelle movements were determined as described under Materials and Methods and averaged over the entire eight hour recording period. HeLa cells were depleted of ARL2 by siRNA (solid bars) or transfected to over-express wild type (ARL2) or the dominant negative mutant (ARL2[T30N] (open bars)). Lysosome movements were recorded with time lapse imaging in control or ARL2 siRNA cells by incubating cells with LysoTracker Red 30 minutes prior to imaging. Double asterisks indicate statistically significant differences ($p<0.01$).

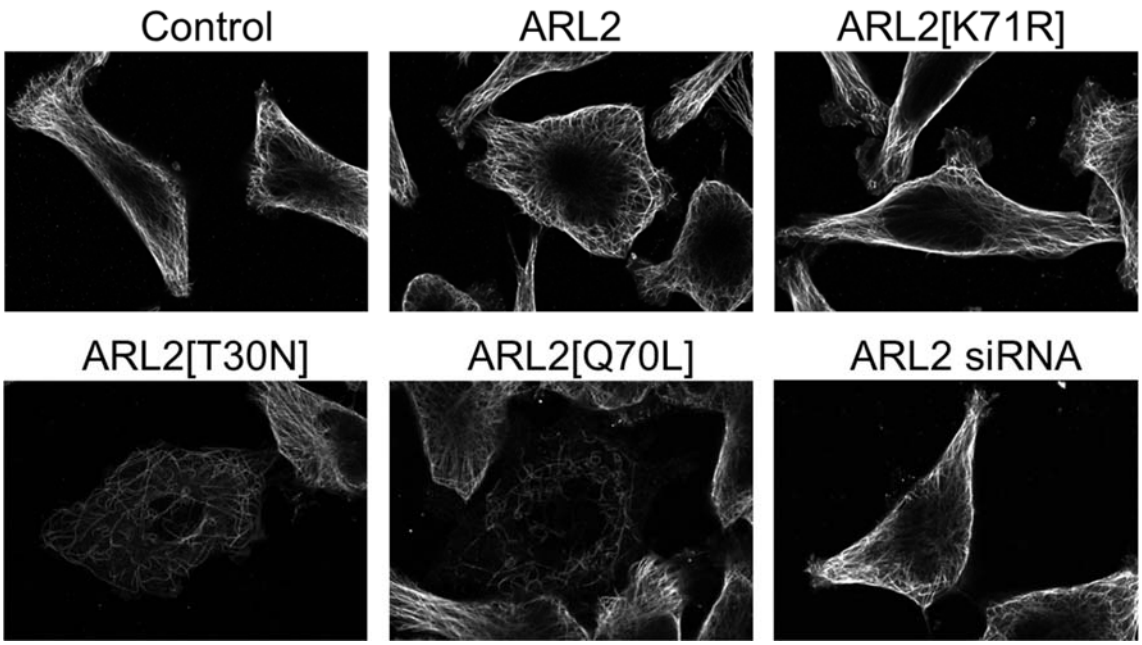

Figure 5. Microtubules are not lost with expression of ARL2[K71R] or ARL2 siRNA. HeLa cells were transfected with plasmids directing expression of ARL2, ARL2[T30N], ARL2[K71R], ARL2[Q70L], or with ARL2 siRNA #1. Cells were fixed 48 hours later and stained for α-tubulin, as described under Materials and Methods. Representative confocal images are shown, though the extent of microtubule density loss with ARL2[T30N] and ARL2[Q70L] vary and is more severe with the latter.

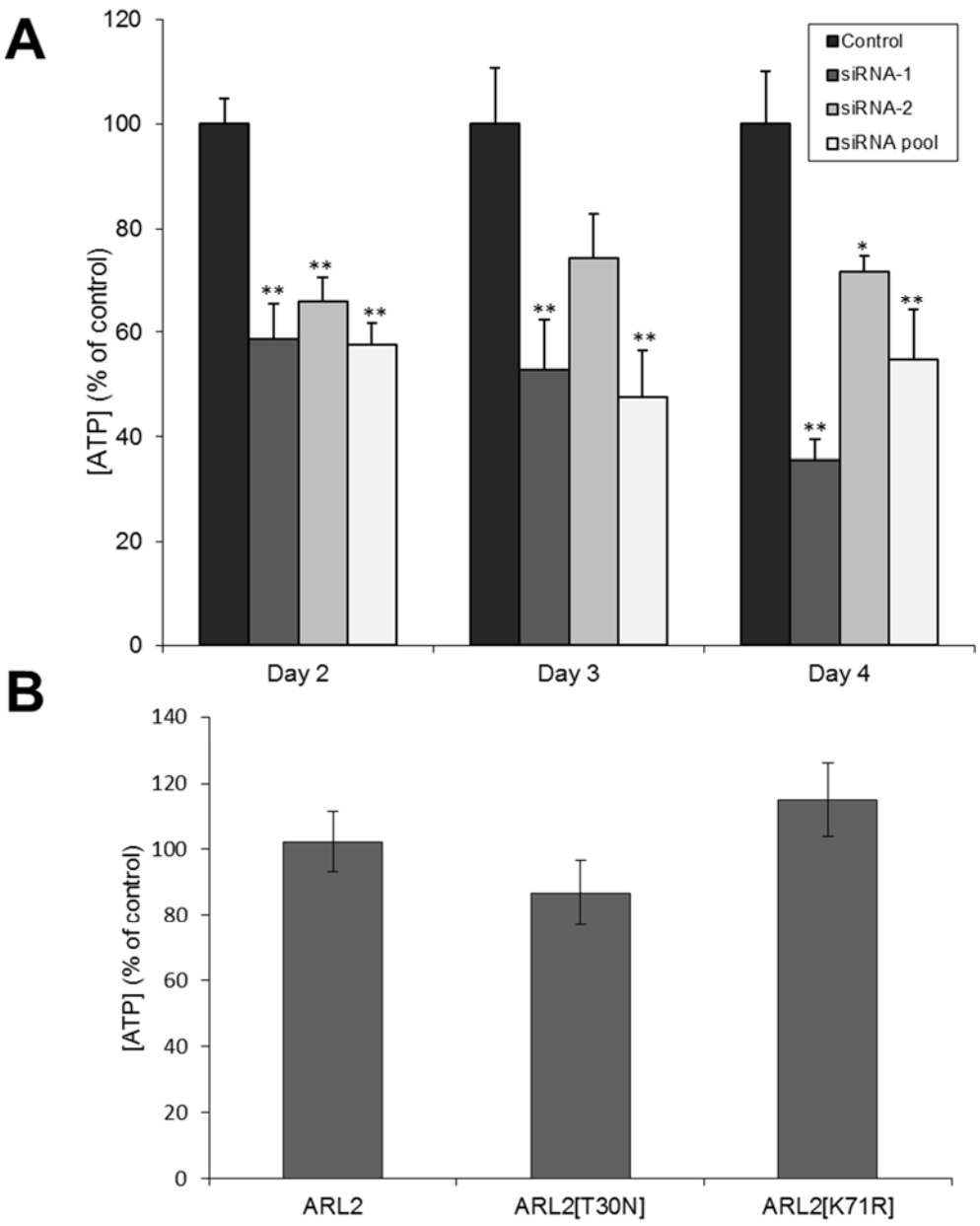

Figure 6. ATP levels are lower in cells depleted of ARL2 by siRNA. (A) HeLa cells were transfected with either no siRNA (control), each of two individual siRNAs (siRNA-1 and siRNA-2), or a pool of four siRNAs (siRNA pool) and collected 48 hours after transfection for ATP determinations, as described under Materials and Methods. A single or double asterisk indicate statistically significant differences at $p<0.05$ and $p<0.01$, respectively. **(B)** HeLa cells were transfected with ARL2, ARL2[T30N], or ARL2[K71R] and assayed for ATP levels as in (A).

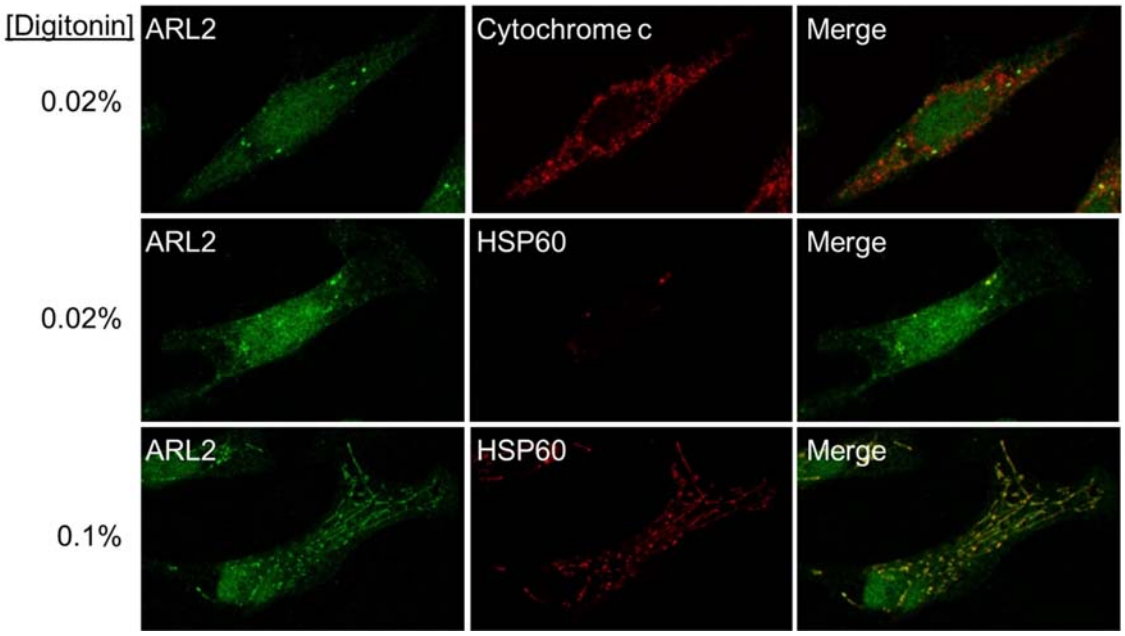

Figure 7. A pool of ARL2 localizes to the mitochondrial matrix. HeLa cells were fixed in 4% paraformaldehyde prior to permeabilization in either 0.02% (two upper rows) or 0.1% w/v digitonin (bottom row) for 10 minutes at room temperature. Cells were then processed for imaging using dual labeling for ARL2 (green, left) and either cytochrome c (top row, middle panel) or HSP60 (lower two rows, middle panels), as markers of the IMS and matrix, respectively. Merged images are shown on the far right in each case.

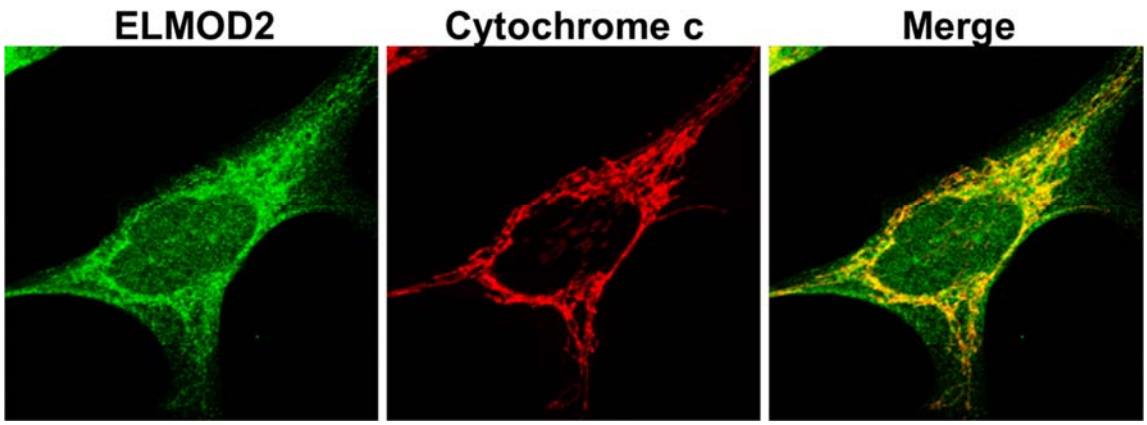

Figure 8. ELMOD2 localizes to mitochondria. HeLa cells were fixed in 4% paraformaldehyde, permeabilized in 0.1% Triton X-100 and stained for ELMOD2 (green, left) and cytochrome c (red, middle). ELMOD2 staining overlaps extensively with that of cytochrome c (Merge, right).

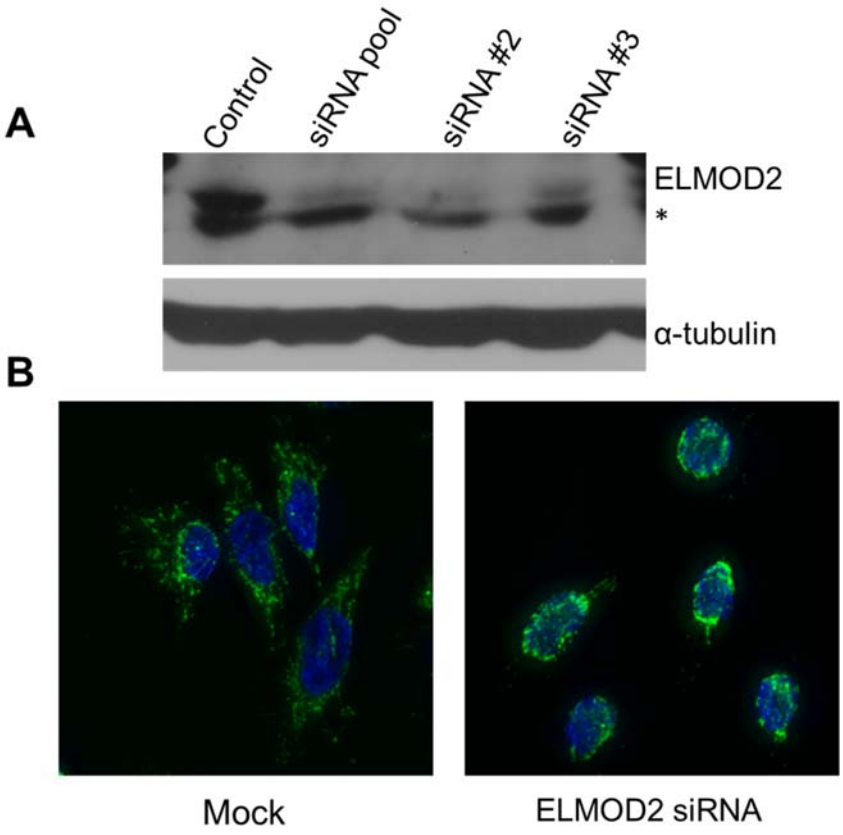

Figure 9. ELMOD2 knockdown alters mitochondrial morphology and distribution. (A) HeLa cells were transfected with a SmartPool or individual siRNAs directed against ELMOD2 and two days later cells were harvested, total protein determined, and equal amounts (40 μg) of total cellular homogenates were resolved in denaturing polyacrylamide gels. Proteins were transferred to nitrocellulose membranes and probed with our rabbit polyclonal antibody to ELMOD2 (upper panel) or α-tubulin (lower panel). Only the relevant regions of the gels are shown. Asterisk indicates a non-specific band, migrating slightly faster than ELMOD2, which is not competable with antigen. **(B)** HeLa cells were transfected with either no siRNA (Mock) or siRNA directed against ELMOD2 and two days later cells were fixed and stained with Mitotracker and Hoechst DNA stain. Representative cells are shown. Note the proximity of mitochondrial staining to the nuclear stain and the lack of peripheral mitochondrial staining in ELMOD2 knockdown cells.

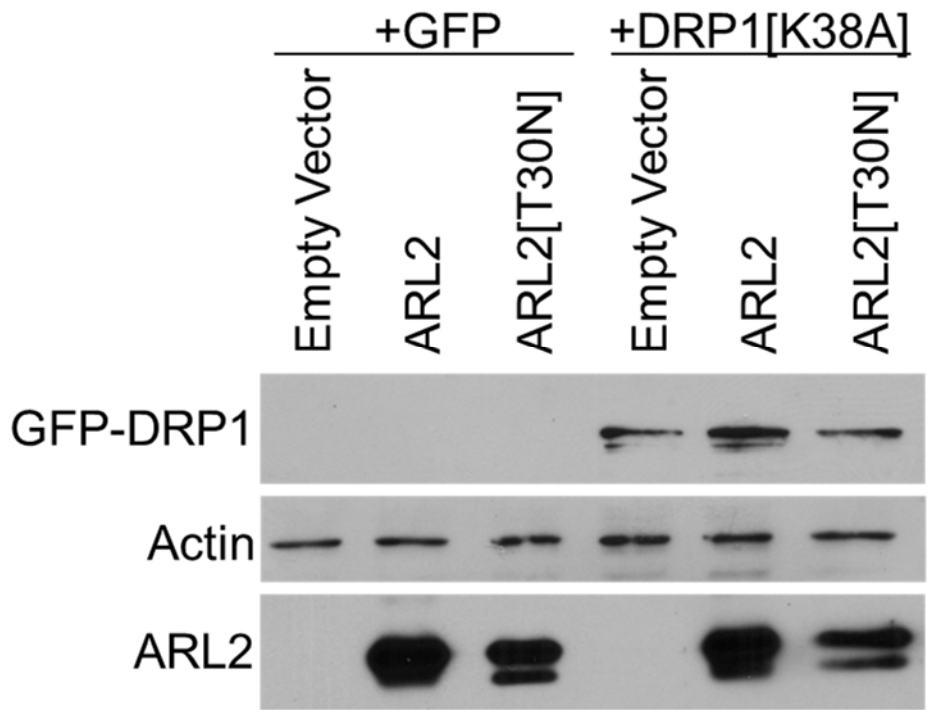

Figure S1. ARL2 and ARL2[T30N] are expressed when co-transfected with GFP-DRP1[K38A]. HeLa cells were co-transfected with either GFP or GFP-DRP1[K38A] and empty vector, ARL2, or ARL2[T30N]. Cells were harvested 24 hours later, lysed, and analyzed by immunoblot. The membrane was cut and probed for ARL2, GFP (for DRP1 expression), and actin (as a loading control).This experiment was done twice with similar results.

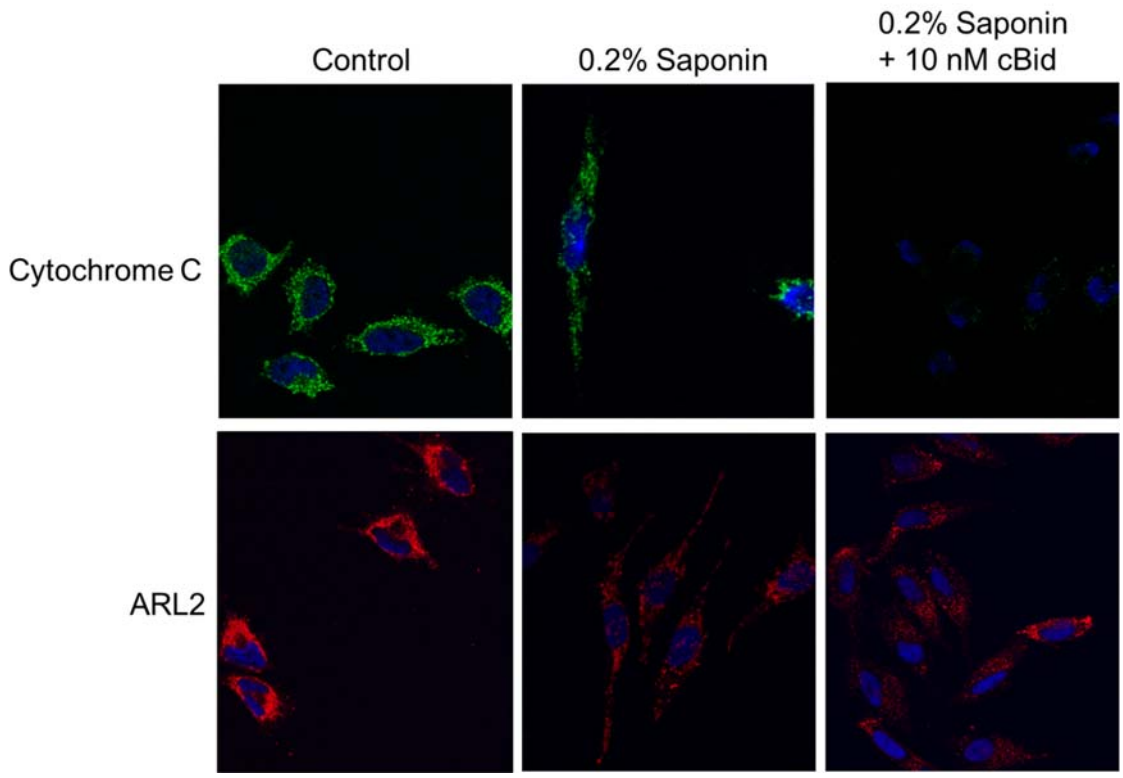

Figure S2. Mitochondrial ARL2 staining is retained after cBid treatment. HeLa cells were incubated in 0.2% saponin for 5 minutes, followed by a 20 minute incubation with 10 nM cBid or vehicle control. Cells were then fixed and immunostained for cytochrome c (top panels) or ARL2 (bottom panels). Cytochrome c staining is clearly lost after treatment with cBid (upper right panel), but ARL2 staining is retained (bottom lower panel).

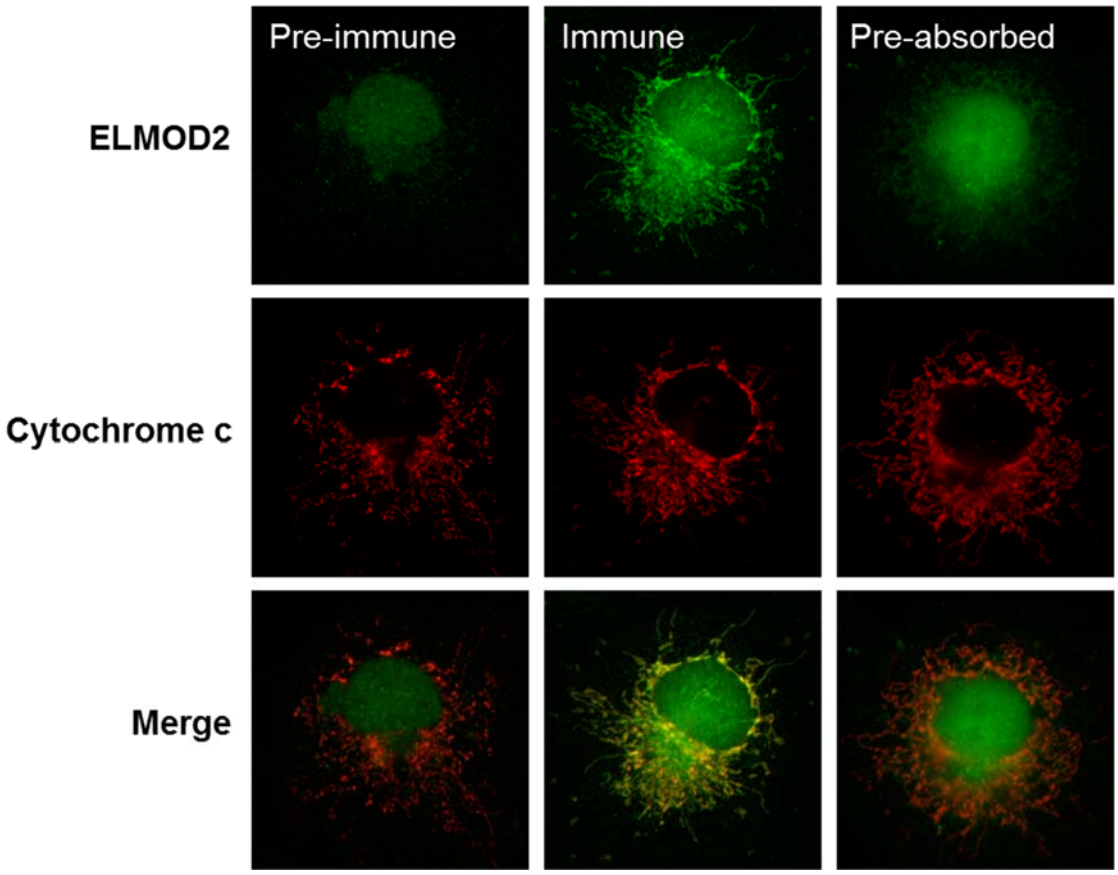

Figure S3. ELMOD2 mitochondrial staining is competed by purified, recombinant ELMOD2. COS7 cells were fixed in 4% paraformaldehyde, permeabilized with 0.1% Triton X-100, and stained with pre-immune serum (left panels), immune serum (middle panels), and immune serum competed with recombinant ELMOD2 (right panels). Cells were also stained for cytochrome c as a mitochondrial marker.

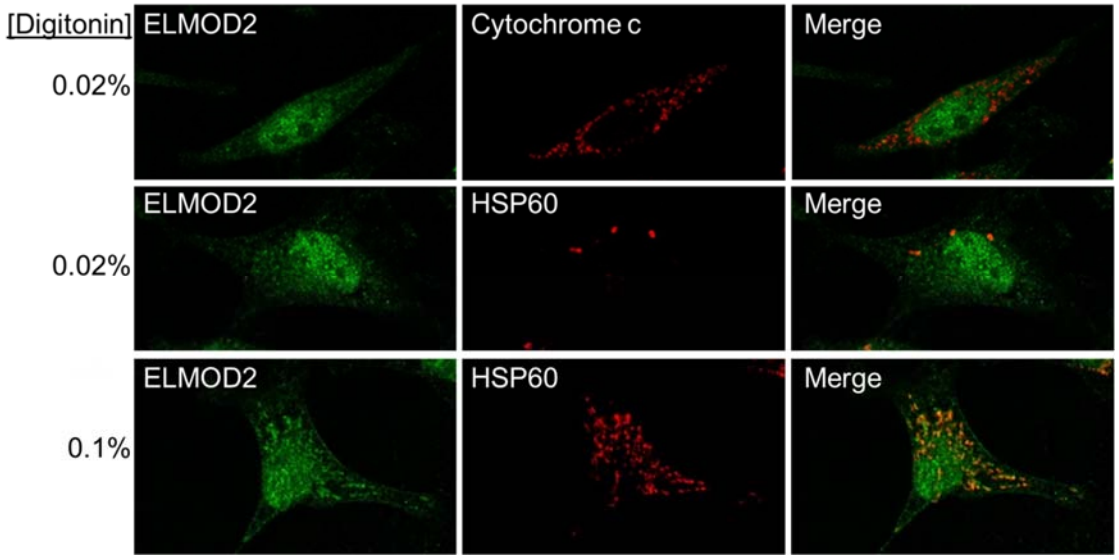

Figure S4. ELMOD2 localizes to the mitochondrial matrix. HeLa cells were fixed in 4% paraformaldehyde prior to permeabilization in either 0.02% (two upper rows) or 0.1% (lowest row) (w/v) digitonin for 10 minutes at room temperature. Cells were then processed for imaging using dual labeling for ELMOD2 (green) and either cytochrome c (top row, middle panel) or HSP60 (lower two rows, middle panels), as markers of the IMS and matrix, respectively.

Chapter 3: Plasmids for variable expression of proteins targeted to the mitochondrial matrix or intermembrane space

This chapter is submitted as:

Laura E. Newman*, Cara Schiavon*, and Richard A. Kahn. Plasmids for variable expression of proteins targeted to the mitochondrial matrix or intermembrane space. Submitted.

*These authors contributed equally

The following figures were generated by Cara Schiavon: Figure 4

The following figures were generated by me, with assistance from Cara Schiavon: 5, 6, 9

Abstract

We describe the construction of a collection of plasmids for varied expression of proteins targeted to the mitochondrial matrix or intermembrane space, using previously defined N-terminal targeting sequences and truncated CMV promoters, to facilitate studies of sites of action within mitochondria, proteomics of mitochondrial compartments, or related studies. The regulated expression, or more commonly over-expression, of proteins in mammalian cells in culture is a mainstay of cell biology research today, which consistently provides invaluable information on protein localization and functions. The interpretation of such data can be compromised by the over-expression itself as a result of saturation of the relevant compartment, resulting in non-physiological localization of the protein under study. This may be particularly important when the protein is targeted to a limited, membrane-bounded compartment where the increase in protein abundance may cause non-specific changes to that compartment. We noted that different proteins display different kinetics of expression and import that should be considered when analyzing results from this approach. Finally, this collection of plasmids has been deposited in the Addgene plasmid repository to facilitate the ready access and use of these tools.

Introduction

Mitochondria are structurally complex, morphologically heterogeneous, and essential organelles best known for their roles in ATP production via respiration and apoptosis. But they are also critical to a number of other essential housekeeping and regulatory processes, including calcium metabolism, signaling via reactive oxygen species, phospholipid metabolism, and more generally in cell metabolism. There are clear links to a host of human diseases that result from defects in mitochondrial proteins and processes (Baloyannis, 2006; Chan, 2006; Dimauro and Davidzon, 2005; Esposito et al., 1999; Graham et al., 1997; Kroemer and Reed, 2000; Mishra and

Chan, 2014; Valentine et al., 2005; Zhao et al., 2001). Depending on cell type and conditions mitochondria can appear as many small, almost spherical puncta, as one highly inter-connected network or anywhere in between these extremes as a result of differences in the net fusion and fission. This morphological diversity and close connection to other structures contribute to the technical difficulties inherent in studies of mitochondrial signaling and functions. A primary source of structural complexity derives from the fact that mitochondria have two membranes; an inner membrane that surrounds the mitochondrial matrix, and an outer membrane that is exposed on one face to cytosol and on the other to the intermembrane space (IMS). The matrix and inner membrane contain the electron transport chain (ETC) complexes that use the proton gradient to synthesize ATP. The IMS houses proteins that may regulate the ETCs or apoptosis, e.g., cytochrome c or Bax (Hung et al., 2014; Vogtle et al., 2012). Though the outer membrane is relatively permeable to small molecules the inner membrane contains a number of channels to carry or exchange metabolites and ions between the IMS/cytosol and matrix. Despite the existence of a mitochondrial genome and protein synthetic machineries, the overwhelming majority of mitochondrial proteins are encoded in the nuclear genome, synthesized on ribosomes in the cytosol, and imported to their sites of action. Specific sub-mitochondrial localization of imported proteins is achieved through the actions of the translocases of the outer and inner membranes, which are distinct, multi-subunit complexes that recognize mitochondria localization sequences (MLS) (Chacinska et al., 2009; Emanuelsson et al., 2001; Neupert and Herrmann, 2007) on target proteins and transport them across their respective membranes. Strong mitochondria localization signals have been identified and shown capable of driving other proteins to specific compartments when fused on their N-termini. A second means of mitochondrial import makes use of disulfide bond formation between the cysteines in a “twin cysteine motif” (C-X3-C or C-X9-C) and Mia40, located in the IMS to aid in targeting to the IMS or matrix (Stojanovski et al., 2008). This mechanism of Mia40-dependent mitochondrial import can be slower than that driven by a strong MLS and rates are sensitive to Mia40 or glutathione

levels (Fischer et al., 2013). Our studies focus on the roles of soluble proteins that localize to the matrix, or IMS, and thus we focus here on the use of MLSs proven to drive fusion proteins to one compartment or the other.

MLSs have low primary sequence conservation, though most form an amphipathic alpha helix. They are most often found near the N-terminus but can also be C-terminal. MLS's are typically cleaved by mitochondrial proteases after import and arrival at their destination and for this reason cleavage or processing of mitochondrial proteins is often used to monitor maturation and targeting (Chacinska et al., 2009; Geissler et al., 2000; Reid and Schatz, 1982). A few MLSs have been extensively studied and shown to be responsible for targeting proteins to the matrix or IMS, with known sites of cleavage by mitochondrial proteases (van Loon et al., 1986). These strong MLSs can also target other proteins to specific compartments when fused at their N-terminus. Among these strong MLSs are the 32 residue N-terminus of human ornithine carbamoyltransferase (OCT) that drives proteins to the mitochondrial matrix (Horwich et al., 1986; Horwich et al., 1985), or the 59 residue leader sequence from human Smac (aka Diablo) that targets the IMS (Burri et al., 2005; Du et al., 2000; Ozawa et al., 2007; Sabharwal et al., 2013; Verhagen et al., 2000). Each of these leaders is cleaved upon arrival at their different destination.

Proteomes of mitochondria, matrix, and IMS have been generated, originally after sub-organelle fractionation of purified mitochondria and more recently using quantitative mass spectrometry, e.g., protein proximity assays (Hung et al., 2014; Lam et al., 2015; Martell et al., 2012). Thus, these proteomes continue to improve but are currently understood to be incomplete datasets. Thus, testing for functional consequences of proteins localizing predominantly to a single compartment within mitochondria is increasingly useful as a test for their functions. There is also a group of proteins that are present and active in other parts of the cell that also contain a (typically smaller) pool inside mitochondria that carry out distinct functions. Included in this list are STAT3 (Gough et al., 2009; Wegrzyn et al., 2009), MEF2D (She et al., 2011), ARL2

(Newman et al., 2014; Nishi et al., 2010; Sharer et al., 2002), ELMOD2 (Newman et al., 2014), and several DNA damage repair proteins (Bauer et al., 2015). Notable about this list of proteins with dual localizations is their importance to cell signaling and regulation. Because these proteins perform two or more functions in distinct cellular locations, they may provide cross talk between those sites of action that could be essential to cell regulation at a higher level, but ways to dissect their actions at distinct locations is important.

It is important to define the sites of action of each protein found to be associated with mitochondria with as much precision as possible. Indirect immunofluorescence or GFP tagging are useful but even the highest resolution fluorescent microscopes in use today are challenged to resolve the compartments or structures within mitochondria. While immunogold labeling and electron microscopy can readily discriminate between the matrix and IMS or inner and outer mitochondrial membranes, these techniques are time consuming, expensive, and require good antibodies to the target. And each of these techniques is challenged further by high "background" non-mitochondrial staining when the target protein is more abundant in cytosol than in mitochondria; e.g., STAT3 and ARL2. We believe the use of targeting vectors that drive exogenous proteins to specific sub-mitochondrial compartments provides a useful complement to high resolution imaging.

We developed a series of plasmids that combines features of previously described mitochondrial targeting leader sequences and expression vectors. We recognized that the matrix and IMS are small, saturable compartments that may be altered non-specifically by excessive protein accumulation. Thus, we sought a system that allows a level of control over the strength of the promoter driving exogenous protein expression and found what we needed in the series of truncated CMV promoters described by Morita, et al. (Morita et al., 2012). We also required strong leader sequences that had been shown previously to efficiently drive protein, both native and exogenous fusions, to the mitochondrial matrix or IMS. The N-termini of SMAC/Diablo and OCT are used to target fusion proteins to the IMS or matrix, respectively. Each of these leader

sequences is cleaved by proteases located in the appropriate compartment, which allows an easy way to monitor the import process over time. We designed into our collection unique restriction sites that allows for ready sub-cloning and the optional use of the HA epitope, if needed for antibody detection. We believe these plasmids will prove useful to researchers involved in studies of mitochondrial protein localization but also in rescue of gene deletions or knockdowns as mutants can be readily screened or tested individually using this system.

Methods

Antibodies & Reagents: The rabbit, polyclonal antibody directed against human ARL2 has been previously described (Sharer et al., 2002; Zhou et al., 2006). Antibodies directed against the following antigens were also used in this study: GFP (Abcam ab290), HSP60 (Enzo Life Sciences ADI-SPA-807), cytochrome C (BD Biosciences 556432), alpha-tubulin (Sigma T9026).

Cloning and Constructs: A plasmid containing the open reading frame of rat OCT, pOCT:GFP, was a gift from Heidi McBride (McGill University) and that of human SMAC/Diablo, SMAC-GFP, a gift from Doug Green (Addgene plasmid #40881), were used as templates in PCR reactions as the sources of the OCT and SMAC leader sequences. The seven plasmids carrying a series of truncations in the CMV promoter, pCMVΔ0 - pCMVΔ6, and resulting in decreasing levels of exogenous protein expression, were described in Morita, et al (Morita et al., 2012) and obtained from DNASU.

Into each of the parental CMVΔ0-6 plasmids we inserted OCT or SMAC leader sequences between the KpnI and BamHI sites, then the HA epitope (YPYDVPDYA) between BamHI and EcoRI sites, and ORFs of interest between EcoRI and XhoI sites (see Figure 1). This allows one to include (or not) the HA epitope. Note that the addition of unique restriction sites and short linkers results in proteins, after cleavage of leader sequences, which are still slightly

larger than the untagged or only HA-tagged proteins. Into these we inserted the open reading frame of eGFP (accession #U55762) or human ARL2 (NP_001658).

The N-terminal leader sequence used for targeting fusion proteins to the mitochondrial matrix is that derived from human ornithine carbamoyltransferase (OCT; aka ornithine trans-carbamylase), as initially described in Horwich, et al (Horwich et al., 1986; Horwich et al., 1985). We used the 96 nt sequence:

ATGCTGTCTAATTTGAGAATCCTGCTCAACAAGGCAGCTCTTAGAAAGGCTCACACT
TCCATGGTTCGAAATTTTCGGTATGGGAAGCCAGTCCAG,

which encodes the 32-residue sequence:

MLSNLRILLNKAALRKAHTSMVRNFRYGKPVQ.

And for the IMS leader sequence we used that described by Ozawa, et al (Ozawa et al., 2007) and Sabharwal, et al (Sabharwal et al., 2013) from human SMAC (aka Diablo), which is 177 nt:

ATGGCGGCTCTGAAGAGTTGGCTGTCGCGCAGCGTAACTTCATTCTTCAGGTACAGA
CAGTGTTTGTGTGTTCCTGTTGTGGCTAACTTTAAGAAGCGGTGTTTCTCAGAATTGA
TAAGACCATGGCACAAAACTGTGACGATTGGCTTTGGAGTAACCCTGTGTGCGGTTC
CTATT,

which encodes the 59 residue leader:

MAALKSWLSRSVTSFFRYRQCLCVPVVANFKKRCFSELIRPWHKTVTIGFGVTLCAVPI.

PCR reactions were designed to amplify each component, using specific primers, and sub-cloned into the parent vectors by standard restriction digestions and ligations. All inserts were verified by DNA sequencing. Note that the pCMVΔ0-6 plasmids are in the pcDNA3.1 backbone and thus contain both AmpR and NeoR selectable markers.

Cell culture: Human cervical carcinoma (HeLa) cells were obtained from ATCC and grown in DMEM medium (supplemented with 10% fetal bovine serum (Invitrogen, Carlsbad, CA) and 2

mM glutamine) at 37°C in the presence of 5% CO2. Cells are screened monthly for mycoplasma and were not cultured for more than 30 passages.

Transfection: Cells at ~90% density were transfected while attached in 6 well plates. Each plasmid (1 µg) was diluted in 250 µl Optimem (Invitrogen). Lipofectamine 2000 (2 µg; Invitrogen) was diluted in a separate tube containing 250 µl Optimem, vortexed briefly, and incubated at room temperature for 5 minutes. The tubes were then mixed and incubated another 20 minutes at room temperature. Following incubation, cell culture medium was changed to 1.5 ml of Optimem, and transfection complexes (500 µl) were added drop wise to the wells. After 4 hours, the medium was changed back to DMEM growth medium. For imaging experiments, cells were split 1:3 after the four hour transfection onto matrigel (BD Biosciences) coated coverslips in a new 6 well plate.

Western blots and data reproducibility: Cells were harvested by rinsing twice with PBS, collected by incubation in 5 mM EDTA in phosphate buffered saline (PBS; 140 mM NaCl, 3 mM KCl, 10 mM Na2HPO4, 2 mM KH2PO4, pH 6.75), and pelleted in a microfuge (14,000 rpm, 4°C). Cells were lysed in 1% CHAPS, 25 mM HEPES pH 7.4, 100 mM NaCl, and protease inhibitors (Sigma #P-2714) on ice for 30 minutes, and the S14 was obtained by clarifying lysates by centrifugation for 30 minutes (14,000 rpm, 4°C). Protein concentrations were determined by Bradford Assay (Bio-Rad) using bovine serum albumin as standard. Protein samples (20 µg/well) were separated on 15% polyacrylamide gels and wet-transferred to nitrocellulose membranes (Bio-Rad #162-0112) at 70V for 2.5 hours. Western blotting procedures were carried out at room temperature. Membranes were blocked in blotto (5% (w/v) dry milk, 50 mM Tris pH 8, 2 mM CaCl2, 80 mM NaCl, 0.2% (v/v) Tween-20, 0.02% sodium azide) for 1 hour. When probing for ARL2, membranes were blocked in an alternate blocking buffer (10% goat serum, 5% Tween-20 in PBS), freshly filtered through a 0.2µm membrane. Membranes were then incubated with primary

antibody in blocking buffer at 4°C overnight. Removal of excess primary antibody was carried out by washing the membranes in PBST (PBS with 0.1% Tween-20) three times for 10 min each. The anti-rabbit 790 secondary antibody (Invitrogen A11374) or anti-mouse 800 secondary antibody (Rockland 610-745-002) was diluted 1:10,000 in PBST and incubated with the membrane for 1 hour at room temperature. The membrane was protected from light from this point on. Excess secondary antibody was removed by washing the membranes in PBST 3 times for 10 min each. Excess Tween-20 was removed by quickly rinsing membranes 3 times in PBS, followed by 2x5 minute washes in PBS. Data were collected using the Odyssey Infrared Imager. For CCCP and ARL2 competition experiments, western blotting was performed as described below, with the exception that HRP-conjugated secondary antibodies were used (GE cat #NA934V, #NA931V), and blots were incubated in luminol containing solution (0.1 mM Tris-HCl pH 8.0, 1.2 mM luminol, 0.2 mM p-coumaric acid, 0.009% hydrogen peroxide) for 1 min prior to exposure to film. The following antibody dilutions were used for western blotting: ARL2 (1:1000), GFP (1:1000), alpha tubulin (1:2500).

Every experiment described herein has been repeated at least twice with similar results. Immunoblotting with antibodies to alpha tubulin was performed in each case as a loading control to confirm equal total protein loaded per lane, in agreement with total protein assays.

Immunofluorescence: Cells were grown on Matrigel (BD Biosciences #356231) coated coverslips. Cells were fixed for 15 minutes in a pre-warmed (37°C) solution of 4% paraformaldehyde in PBS, and then permeabilized with 0.1% (v/v) Triton X-100 in PBS for 10 minutes at room temperature. Alternatively, for differential permeabilization of outer and inner mitochondrial membranes, cells were permeabilized with either 0.02% or 0.1% (w/v) digitonin in PBS for 10 minutes at room temperature. Incubation with primary antibodies was carried out in PBS containing 1% (w/v) BSA, filtered, at 4°C overnight. Secondary antibodies (Alexa fluorophores, Invitrogen) were incubated in the same buffer for 1 hour at room temperature at a

1:500 dilution, following 4 x 5 min washes in PBS. Coverslips were then rinsed twice for 5 minutes each, stained with Hoechst 33342 for 4 min, rinsed twice again for 5 min, and mounted onto slides using Prolong Antifade (Invitrogen). The following antibody dilutions were used: ARL2 (1:1000), HSP60 (1:5000), cytochrome C (1:1000). Images were acquired using an Olympus FV1000 microscope, using 488 and 543 laser excitation and a 100x objective (1.45 NA). Image processing was carried out using ImageJ.

CCCP treatment: The time of CCCP addition to cells following transfection differed based on whether the cells were expressing OCT-GFP or SMAC-GFP because they were found to display different import kinetics. All cells were transfected as described above and were exposed to 10 μM CCCP. OCT-HA-GFP cells were exposed to 4 hours of CCCP treatment 8 hours after transfection, while SMAC-HA-GFP cells were exposed to 2 hours of CCCP treatment 10 hours after transfection. Empty vector and GFP controls were included in each case. Cells were then collected and processed for immunoblotting as described above. Timing was designed to minimize cell toxicity resulting from the drug treatment and maximize drug exposure during the peak of protein expression and potential import.

Results and Discussion

Many proteins include within them linear sequence tags that direct the full-length protein to a specific place or compartment in cells. Many of these targeting sequences also work when added to an unrelated protein and can be invaluable to determining subcellular sites of action. Such tags are typically added to generate fusion proteins that can be transiently expressed in any cell. However, this experimental approach may be compromised when the fusion protein is expressed at substantially higher levels than the endogenous protein under study as a result of saturation of the targeted, biologically relevant location or compartment. This concern may be addressed by minimizing the level of exogenous protein expression; e.g., by using the series of

truncated CMV promoter-containing plasmids described by Morita, et al (Morita et al., 2012) to allow levels of protein expression over a wide range. Concern regarding saturation is particularly important when targeting a small and limited compartment, such as sub-mitochondrial spaces; i.e., the matrix or intermembrane space (IMS).

This paper describes the generation of two series of plasmids, each based upon the original CMV promoter truncation series but into which we have inserted N-terminal leader sequences that direct the fusion proteins to either the mitochondrial matrix or the IMS. The 32-residue, mitochondrial matrix localization tag is that described by Horwich, et al. (Horwich et al., 1986; Horwich et al., 1985) for the human ornithine carbamoyltransferase (OCT, aka ornithine trans-carbamylase) protein. The 59-residue, IMS-directing leader is that derived from the human SMAC/Diablo protein, as previously described (Ozawa et al., 2007; Sabharwal et al., 2013). We also included in our constructs the HA epitope (YPYDVPDYA), between the leader sequences and proteins of interest (see Figure 1), as it allows one to monitor expression of fusion proteins to which one does not have an antibody and because it allows for comparisons of the levels of different proteins expressed by allowing the use of a common antibody that is readily available. The construction of these plasmids is described under Methods and a plasmid map showing key features is shown in Figure 1. Here we describe the use of these series of plasmids, using eGFP as the exogenous protein, to highlight issues surrounding their use in targeting proteins to each compartment. We also generated a series of plasmids, again using CMVΔ0-6 as parental, that includes only GFP with no mitochondrial targeting sequence or HA epitope, resulting in retention of the GFP in cytosol, as control for the others and to assess the effects of mitochondrial import on overall protein expression. No differences from controls were noted in overall mitochondrial morphologies in cells expressing SMAC- or OCT-GFP from even the strongest (CMVΔ0) promoter. Thus, forcing import of GFP (e.g., see Figure 2) to the matrix or IMS alone is not sufficient to alter the overall morphology of mitochondria. It is clear from Figure 2 that GFP lacking a leader sequence is cytosolic and excluded from mitochondria, while that with either

leader is exclusively mitochondrial, as visualized with the marker of the matrix (HSP60, Figure 2) or IMS (cytochrome c, Figure3). In work that will be described in detail elsewhere (Newman, et al; manuscript submitted), we also generated the series of CMVΔ0-6 plasmids to express variable levels of SMAC- or OCT-HA-ARL2, a regulatory GTPase that we are currently studying for its role in mitochondrial biology. We have earlier reported the presence of endogenous ARL2 inside mitochondria, though typically only a small fraction of total cellular ARL2 is imported into mitochondria (Newman et al., 2014; Sharer et al., 2002). The addition of the leader sequences used here allowed us to target each compartment for the vast majority of the exogenously expressed proteins and allowed functional studies of its site of action and mechanisms.

The use of these two N-terminal leader sequences to drive exogenous proteins to the matrix or IMS has been well documented previously but to ensure that they were acting as predicted in this system, we used selective permeabilization of the outer and inner mitochondrial membranes of cultured cells post-fixation, to document specificity in protein import (Figure 3). The SMAC-HA-ARL2 (Figure 3A) or OCT-HA-ARL2 (Figure 3B) proteins were expressed in HeLa cells and one day after transfection the cells on cover slips were fixed in 4% paraformaldehyde and permeabilized with different concentrations of digitonin to selectively permeabilize mitochondrial membranes, as described previously (Jeyaraju et al., 2006; Newman et al., 2014; Otera et al., 2005) and under Methods. At low (0.02%) detergent the outer, but not inner, mitochondrial membrane was permeabilized, allowing staining of IMS but not matrix proteins. This resulted in staining of cytochrome c (Figure 3) or Tom20 (not shown), as positive controls, and SMAC-HA-ARL2 Figure 3A), but not OCT-HA-ARL2 or HSP60, as each of these was in the matrix. In contrast, permeabilization with higher (0.1%) digitonin resulted in staining of either SMAC- or OCT-tagged ARL2 as well as HSP60. These results are completely consistent with previous evidence demonstrating specificity in targeting exogenous proteins to the matrix or IMS using these leader sequences.

Further evidence of import and specific localization within mitochondria was evident by the fact that each of the leader sequences used here was very efficiently cleaved upon import, as seen by the appropriate shifts in electrophoretic mobility in immunoblots and as described previously (Horwich et al., 1986; Horwich et al., 1985; Ozawa et al., 2007). To further confirm that the cleavage observed was dependent upon mitochondrial import, we examined effects of the mitochondrial import inhibitor, carbonyl cyanide m-chlorophenylhydrazone (CCCP) on the processing of the expressed proteins. CCCP is a proton ionophore and thus reduces the proton gradient that is required to drive protein import that is dependent upon leader sequences (Geissler et al., 2000; Reid and Schatz, 1982), though not that driven by the oxidative folding and Mia40 (Bose et al., 2002; Fischer et al., 2013; Gutscher et al., 2008). We compared the processing of expressed OCT-HA-GFP, SMAC-HA-GFP, or untagged GFP in control (untreated) cells and those treated with CCCP, as described under Methods. In untreated cells expressing SMAC-HA-GFP, the majority of SMAC-HA-GFP was cleaved as evidenced by a strong band corresponding to cleaved SMAC-HA-GFP and a significantly weaker band corresponding to the size of uncleaved SMAC-HA-GFP (see below). In cells expressing SMAC-HA-GFP and treated with CCCP, the cleaved band was greatly diminished, with the uncleaved SMAC-HA-GFP band at a similar intensity to the uncleaved band in the untreated SMAC-HA-GFP condition (Figure 4). Therefore, the uncleaved SMAC-HA-GFP band represents a greater fraction of SMAC-HA-GFP in CCCP treated cells, compared to untreated cells. Results were similar for cells expressing OCT-HA-GFP (data not shown). There was no change in band intensity between the CCCP treated and untreated cells expressing leaderless and untagged GFP, as expected (Figure 4). Thus, the efficient import of proteins driven to the IMS or matrix by SMAC or OCT leaders is dependent upon the proton gradient across the inner mitochondrial membrane.

Expression of OCT-HA-GFP actually resulted in the appearance of three bands when lysates were probed in immunoblots, using antibodies directed against GFP (Figure 5A). This was most evident upon over-exposure of immunoblots (Figure 5, middle band). The apparent molecular

weight of the faintest, slowest migrating band is consistent with the uncleaved, full-length protein. The most abundant, middle band is thought to be the cleaved HA-GFP, which migrates slightly slower than does the cytosolic GFP (Figure 5A, lane 2), presumably the result of the HA tag and linker residues. The fastest migrating of the three bands is thought to result from additional protease activity at the N-terminus. While we cannot formally exclude the possibility of some proteolysis occurring at the C-terminus, we found that only the two slower migrating bands were detected in immunoblots using an HA antibody (Figure 5B), consistent with the fastest migrating band having lost some or all of this epitope. We inconsistently observed a minor, fourth band, running just above the major HA-GFP band (e.g., see Fig. 9A). We believe this to be an incompletely processed, imported species, perhaps comparable to that described earlier by Horwich, et al (Horwich et al., 1986; Horwich et al., 1985) that may result from two sites of proteolysis in the leader sequence or even roles for two different proteases. A fourth band, migrating between the unprocessed and fully processed bands was also evident, though again inconsistently, with SMAC-HA-GFP expression (see Fig. 6A, 9B), which we interpret similarly and as reported earlier (Burri et al., 2005).

Figure 5A also shows the results of immunoblots from cells expressing OCT-HA-GFP using the different strength promoters (CMVΔ0-6), at 24 hr post-transfection. The full-length protein, more evident with higher exposure (middle panel) is clearly evident. This upper band decreases with lower overall protein expression (lanes 3-9). Although a minor fraction of the overall protein expressed, the presence of this uncleaved, presumably still cytosolic, protein may complicate certain analyses. Thus, the use of one of the weaker CMV promoters (or later time points, see below) may allow a higher fraction of the exogenous protein to be localized to the matrix. This may be a critical consideration when using these vectors for rescue of specific knockdown related phenotypes or if performing protein proximity assays or protein co-purifications, as incompletely processed proteins are likely to contribute to higher backgrounds in such studies.

The levels of GFP achieved in cytosol (Fig. 5A, lane 2) and of the cleaved OCT-HA-GFP (and thus predominantly HA-GFP; Fig. 5A, lane 3) in the matrix are similar. While this might be expected as a result of the use of the same (CMVΔ0) promoter, this suggests that the imported protein is not rapidly degraded and that one can achieve comparable total cellular levels despite sequestration to a compartment of limited size. Note also the steadily decreasing levels of expression of OCT-HA-GFP in going from CMVΔ0 to CMVΔ6, as described by Morita, et al (Morita et al., 2012) but shown here for a protein that is almost exclusively localized to the matrix.

A completely analogous experiment was conducted to test the SMAC leader sequence, and results are shown in Figure 6A. Again, the total levels of protein expressed were comparable for cytosolic GFP and for SMAC-HA-GFP that targets to the IMS. In this case the uncleaved protein was more prominent and there was a larger difference in size of the cleaved and uncleaved proteins as a result of the fact that the SMAC leader is almost twice as long as the OCT leader. We again observed three bands in the SMAC-HA-GFP expressing lanes with decreasing overall protein expression in moving from CMVΔ0-CMVΔ6. And again, we interpret the three bands to be uncleaved SMAC-HA-GFP, cleaved HA-GFP, and further digested GFP that lacks the HA tag (Figure 6B). Note that in neither case does the proteolysis appear to continue beyond the size of GFP, based upon mobility compared to the cytosolic GFP (lane 2).

Additional testing of this system of varied expression of fusion proteins targeted to mitochondrial compartments revealed variations in the levels of steady state protein expressed and in the rate of import/cleavage. We developed this system to assist in our studies of the ARL2 GTPase pathway inside mitochondria. In contrast to our control, GFP, we found that the levels of HA-ARL2 inside the IMS, driven there by the SMAC (Fig. 7) leader, were substantially lower than ARL2 localizing to cytosol (Fig. 7, compare lanes 2 and 3) despite being driven off the same promoter(s). We believe it is likely that the amount of ARL2 and SMAC-HA-ARL2 proteins expressed were similar but that the half-life of ARL2 is shorter in the IMS than in cytosol. This

conclusion is supported by the observation that the levels of ARL2 and OCT-HA-ARL2, again driven off the same promoters, resulted in very similar levels of recombinant ARL2 proteins (data not shown). Previously published (Sharer et al., 2002) and unpublished data (Newman, Schiavon, and Kahn; unpublished observations) from our lab further suggest that the fraction of total cellular ARL2 imported into mitochondria and/or half-life of mitochondrial ARL2 are likely regulated. Thus, based upon these initial findings we encourage anyone considering using the system described herein to take into account possible effects of targeting on the half-life or stability of your protein.

In contrast to the results with SMAC-HA-GFP, we failed to observe the uncleaved SMAC-HA-ARL2 band (predicted MW ~28.6 kDa; Figure 7, lanes 3-9), indicating that there are also differences in the rate of import/cleavage depending upon the protein fused to the SMAC-HA leader. Note that because of the lower levels of mitochondrial ARL2 achieved from expression of SMAC-HA-ARL2, longer exposure times were needed, resulting in increased appearance of non-specific bands in our immunoblots. Antigen competition (Figure 8) was used to confirm that the bands indicated are indeed ARL2 and those identified in Fig. 7 as non-specific (N.S.) are based upon their presence in all samples, including negative controls (lane 1 and 2).

We further examined the kinetics of fusion protein expression and import/cleavage by comparing effects of different leader sequences and fusion proteins as a function of time after transfection on protein levels with attention to the amounts of full length and processed exogenous proteins. Although it appeared in several instances that expression of the OCT fusion proteins was more evident at the earliest time point (12 hr; Figure 9A, lane 2) than the same proteins fused to the SMAC leader (Figure 9B, lane 2), this is not a large effect and would require extensive quantitation to confirm, so was not pursued further. In contrast, it appears that ARL2 was imported/cleaved more rapidly than was GFP when the two were expressed off the same promoter, with either leader (compare Figure 9C to 9A, 9D to 9B). While the full length OCT-HA-GFP or SMAC-HA-GFP were evident in each case, more so with longer exposures, the full-

length ARL2 fusion proteins were virtually never seen for SMAC-HA-ARL2 and only faintly, and with over-exposure, for OCT-HA-ARL2 (Figure 9C). While a small fraction of total cellular ARL2 has been found inside mitochondria of all cells and tissues examined (Sharer et al., 2002), this is not the case for GFP. Thus, ARL2 is expected to contain its own targeting information that we believe includes its N-terminus (unpublished observations). ARL2 is unique among the ARF family of regulatory GTPases in its ability to localize to mitochondria, and shares with a subset of this family the lack of N-myristoylation at the N-terminus that is important to the biology of the ARFs (Kahn et al., 1988; Randazzo et al., 1995; Weiss et al., 1989).

Finally, when these plasmids were used with a wider range of proteins some larger differences in the apparent half-lives were evident. This difference was much more marked for ELMOD2 (data not shown), an ARL2 GAP, as its level peaked at 24 hr and was essentially undetectable at later time points. Thus, the nature of the protein being examined can clearly influence the apparent kinetics of mitochondrial import as well as stability of the targeted protein and this should be taken into account.

Summary: We describe here a collection of plasmids designed for the variable expression of exogenous proteins targeted to either the mitochondrial matrix or IMS. The combination of the previously described series of CMV promoter truncations (Morita et al., 2012) with the mitochondrial leader sequences, here termed OCT (Horwich et al., 1986; Horwich et al., 1985) and SMAC (Burri et al., 2005; Ozawa et al., 2007; Sabharwal et al., 2013), have provided a powerful means of efficiently targeting exogenous proteins to either compartment. Importantly to the study of the biology of any protein(s) targeted to mitochondria, or any limited cellular compartment, we did not observe any evident changes to mitochondria morphology upon forced import of GFP or ARL2 using this system. Thus, the presence of these proteins alone does not appear to be sufficient to trigger a response that may confound functional studies. This is clearly an important issue that must be addressed for each protein under study however. A number of

uses are envisioned for such tools, including rescue of knockdowns or deletions of specific messages or genes; to examine the mitochondria as the biological site of action. We expect these reagents to be perhaps most useful in analyses of proteins that are incompletely targeted to mitochondria, e.g., ARL2 or STAT3. And as protein proximity assays are becoming increasingly powerful and specific (e.g., see (Hung et al., 2014; Lam et al., 2015; Rhee et al., 2013) it is essential to have tools that allow complete, or nearly so, targeting so as to minimize off-target interactors or background. It was for such studies that we emphasize the need to investigate the kinetics of protein expression and processing as residual cytosolic, full-length protein is expected to confound or complicate such datasets. While the strong MLSs employed here were shown to strongly target the designed compartment we expect residual fusion protein to be in cytosol or in non-targeted compartments. Thus, we expect the optimal use of these reagents in defining a protein's site of action will include targeting multiple compartments, with demonstrated functional specificity to a single compartment. Other uses are likely to be found for these series of plasmids and to assist in such developments we have deposited them in Addgene, to make them more readily available to all researchers.

Acknowledgments

We thank Heidi McBride and Doug Green for the gifts of plasmids. This work was supported in part by grants to R.A.K (R01-GM090158), L.E.N. (American Heart Association pre-doctoral fellowship (14PRE18840040) and NIH pre-doctoral fellowship F31-GM111047) and by the Integrated Cellular Imaging Microscopy Core of the Emory Neuroscience NINDS Core Facilities grant, P30-NS055077.

References

Baloyannis, S.J. 2006. Mitochondrial alterations in Alzheimer's disease. Journal of Alzheimer's disease : JAD. 9:119-126.

Bauer, N.C., A.H. Corbett, and P.W. Doetsch. 2015. The current state of eukaryotic DNA base damage and repair. Nucleic Acids Res. 43:10083-10101.

Bose, H.S., V.R. Lingappa, and W.L. Miller. 2002. The steroidogenic acute regulatory protein, StAR, works only at the outer mitochondrial membrane. Endocrine research. 28:295-308.

Burri, L., Y. Strahm, C.J. Hawkins, I.E. Gentle, M.A. Puryer, A. Verhagen, B. Callus, D. Vaux, and T. Lithgow. 2005. Mature DIABLO/Smac Is Produced by the IMP Protease Complex on the Mitochondrial Inner Membrane. Molecular Biology of the Cell. 16:2926-2933.

Chacinska, A., C.M. Koehler, D. Milenkovic, T. Lithgow, and N. Pfanner. 2009. Importing mitochondrial proteins: machineries and mechanisms. Cell. 138:628-644.

Chan, D.C. 2006. Mitochondria: dynamic organelles in disease, aging, and development. Cell. 125:1241-1252.

Dimauro, S., and G. Davidzon. 2005. Mitochondrial DNA and disease. Ann Med. 37:222-232.

Du, C., M. Fang, Y. Li, L. Li, and X. Wang. 2000. Smac, a Mitochondrial Protein that Promotes Cytochrome c–Dependent Caspase Activation by Eliminating IAP Inhibition. Cell. 102:33-42.

Emanuelsson, O., G. von Heijne, and G. Schneider. 2001. Analysis and prediction of mitochondrial targeting peptides. Methods Cell Biol. 65:175-187.

Esposito, L.A., S. Melov, A. Panov, B.A. Cottrell, and D.C. Wallace. 1999. Mitochondrial disease in mouse results in increased oxidative stress. Proc Natl Acad Sci U S A. 96:4820-4825.

Fischer, M., S. Horn, A. Belkacemi, K. Kojer, C. Petrungaro, M. Habich, M. Ali, V. Kuttner, M. Bien, F. Kauff, J. Dengjel, J.M. Herrmann, and J. Riemer. 2013. Protein import and oxidative folding in the mitochondrial intermembrane space of intact mammalian cells. Mol Biol Cell. 24:2160-2170.

Geissler, A., T. Krimmer, U. Bomer, B. Guiard, J. Rassow, and N. Pfanner. 2000. Membrane potential-driven protein import into mitochondria. The sorting sequence of cytochrome

b(2) modulates the deltapsi-dependence of translocation of the matrix-targeting sequence. Mol Biol Cell. 11:3977-3991.

Gough, D.J., A. Corlett, K. Schlessinger, J. Wegrzyn, A.C. Larner, and D.E. Levy. 2009. Mitochondrial STAT3 supports Ras-dependent oncogenic transformation. Science. 324:1713-1716.

Graham, B.H., K.G. Waymire, B. Cottrell, I.A. Trounce, G.R. MacGregor, and D.C. Wallace. 1997. A mouse model for mitochondrial myopathy and cardiomyopathy resulting from a deficiency in the heart/muscle isoform of the adenine nucleotide translocator. Nat Genet. 16:226-234.

Gutscher, M., A.L. Pauleau, L. Marty, T. Brach, G.H. Wabnitz, Y. Samstag, A.J. Meyer, and T.P. Dick. 2008. Real-time imaging of the intracellular glutathione redox potential. Nat Methods. 5:553-559.

Horwich, A.L., F. Kalousek, W.A. Fenton, R.A. Pollock, and L.E. Rosenberg. 1986. Targeting of pre-ornithine transcarbamylase to mitochondria: definition of critical regions and residues in the leader peptide. Cell. 44:451-459.

Horwich, A.L., F. Kalousek, I. Mellman, and L.E. Rosenberg. 1985. A leader peptide is sufficient to direct mitochondrial import of a chimeric protein. EMBO J. 4:1129-1135.

Hung, V., P. Zou, H.W. Rhee, N.D. Udeshi, V. Cracan, T. Svinkina, S.A. Carr, V.K. Mootha, and A.Y. Ting. 2014. Proteomic mapping of the human mitochondrial intermembrane space in live cells via ratiometric APEX tagging. Mol Cell. 55:332-341.

Jeyaraju, D.V., L. Xu, M.C. Letellier, S. Bandaru, R. Zunino, E.A. Berg, H.M. McBride, and L. Pellegrini. 2006. Phosphorylation and cleavage of presenilin-associated rhomboid-like protein (PARL) promotes changes in mitochondrial morphology. Proc Natl Acad Sci U S A. 103:18562-18567.

Kahn, R.A., C. Goddard, and M. Newkirk. 1988. Chemical and immunological characterization of the 21-kDa ADP-ribosylation factor of adenylate cyclase. J Biol Chem. 263:8282-8287.

Kroemer, G., and J.C. Reed. 2000. Mitochondrial control of cell death. Nat Med. 6:513-519.

Lam, S.S., J.D. Martell, K.J. Kamer, T.J. Deerinck, M.H. Ellisman, V.K. Mootha, and A.Y. Ting. 2015. Directed evolution of APEX2 for electron microscopy and proximity labeling. Nat Methods. 12:51-54.

Martell, J.D., T.J. Deerinck, Y. Sancak, T.L. Poulos, V.K. Mootha, G.E. Sosinsky, M.H. Ellisman, and A.Y. Ting. 2012. Engineered ascorbate peroxidase as a genetically encoded reporter for electron microscopy. Nat Biotechnol. 30:1143-1148.

Mishra, P., and D.C. Chan. 2014. Mitochondrial dynamics and inheritance during cell division, development and disease. Nat Rev Mol Cell Biol. 15:634-646.

Morita, E., J. Arii, D. Christensen, J. Votteler, and W.I. Sundquist. 2012. Attenuated protein expression vectors for use in siRNA rescue experiments. Biotechniques. 0:1-5.

Neupert, W., and J.M. Herrmann. 2007. Translocation of proteins into mitochondria. Annu Rev Biochem. 76:723-749.

Newman, L.E., C.J. Zhou, S. Mudigonda, A.L. Mattheyses, E. Paradies, C.M. Marobbio, and R.A. Kahn. 2014. The ARL2 GTPase is required for mitochondrial morphology, motility, and maintenance of ATP levels. PloS one. 9:e99270.

Nishi, H., K. Ono, Y. Iwanaga, T. Horie, K. Nagao, G. Takemura, M. Kinoshita, Y. Kuwabara, R.T. Mori, K. Hasegawa, T. Kita, and T. Kimura. 2010. MicroRNA-15b modulates cellular ATP levels and degenerates mitochondria via Arl2 in neonatal rat cardiac myocytes. J Biol Chem. 285:4920-4930.

Otera, H., S. Ohsakaya, Z. Nagaura, N. Ishihara, and K. Mihara. 2005. Export of mitochondrial AIF in response to proapoptotic stimuli depends on processing at the intermembrane space. EMBO J. 24:1375-1386.

Ozawa, T., Y. Natori, Y. Sako, H. Kuroiwa, T. Kuroiwa, and Y. Umezawa. 2007. A Minimal Peptide Sequence That Targets Fluorescent and Functional Proteins into the Mitochondrial Intermembrane Space. ACS Chemical Biology. 2:176-186.

Randazzo, P.A., T. Terui, S. Sturch, H.M. Fales, A.G. Ferrige, and R.A. Kahn. 1995. The myristoylated amino terminus of ADP-ribosylation factor 1 is a phospholipid- and GTP-sensitive switch. J Biol Chem. 270:14809-14815.

Reid, G.A., and G. Schatz. 1982. Import of proteins into mitochondria. Yeast cells grown in the presence of carbonyl cyanide m-chlorophenylhydrazone accumulate massive amounts of some mitochondrial precursor polypeptides. J Biol Chem. 257:13056-13061.

Rhee, H.W., P. Zou, N.D. Udeshi, J.D. Martell, V.K. Mootha, S.A. Carr, and A.Y. Ting. 2013. Proteomic mapping of mitochondria in living cells via spatially restricted enzymatic tagging. Science. 339:1328-1331.

Sabharwal, S.S., G.B. Waypa, J.D. Marks, and P.T. Schumacker. 2013. Peroxiredoxin-5 targeted to the mitochondrial intermembrane space attenuates hypoxia-induced reactive oxygen species signalling. Biochem J. 456:337-346.

Sharer, J.D., J.F. Shern, H. Van Valkenburgh, D.C. Wallace, and R.A. Kahn. 2002. ARL2 and BART enter mitochondria and bind the adenine nucleotide transporter. Mol Biol Cell. 13:71-83.

She, H., Q. Yang, K. Shepherd, Y. Smith, G. Miller, C. Testa, and Z. Mao. 2011. Direct regulation of complex I by mitochondrial MEF2D is disrupted in a mouse model of Parkinson disease and in human patients. The Journal of clinical investigation. 121:930-940.

Stojanovski, D., D. Milenkovic, J.M. Muller, K. Gabriel, A. Schulze-Specking, M.J. Baker, M.T. Ryan, B. Guiard, N. Pfanner, and A. Chacinska. 2008. Mitochondrial protein import: precursor oxidation in a ternary complex with disulfide carrier and sulfhydryl oxidase. J Cell Biol. 183:195-202.

Valentine, J.S., P.A. Doucette, and S. Zittin Potter. 2005. Copper-zinc superoxide dismutase and amyotrophic lateral sclerosis. Annu Rev Biochem. 74:563-593.

van Loon, A.P., A.W. Brandli, and G. Schatz. 1986. The presequences of two imported mitochondrial proteins contain information for intracellular and intramitochondrial sorting. Cell. 44:801-812.

Verhagen, A.M., P.G. Ekert, M. Pakusch, J. Silke, L.M. Connolly, G.E. Reid, R.L. Moritz, R.J. Simpson, and D.L. Vaux. 2000. Identification of DIABLO, a Mammalian Protein that Promotes Apoptosis by Binding to and Antagonizing IAP Proteins. Cell. 102:43-53.

Vogtle, F.N., J.M. Burkhart, S. Rao, C. Gerbeth, J. Hinrichs, J.C. Martinou, A. Chacinska, A. Sickmann, R.P. Zahedi, and C. Meisinger. 2012. Intermembrane space proteome of yeast mitochondria. Mol Cell Proteomics. 11:1840-1852.

Wegrzyn, J., R. Potla, Y.J. Chwae, N.B. Sepuri, Q. Zhang, T. Koeck, M. Derecka, K. Szczepanek, M. Szelag, A. Gornicka, A. Moh, S. Moghaddas, Q. Chen, S. Bobbili, J. Cichy, J. Dulak, D.P. Baker, A. Wolfman, D. Stuehr, M.O. Hassan, X.Y. Fu, N. Avadhani, J.I. Drake, P. Fawcett, E.J. Lesnefsky, and A.C. Larner. 2009. Function of mitochondrial Stat3 in cellular respiration. Science. 323:793-797.

Weiss, O., J. Holden, C. Rulka, and R.A. Kahn. 1989. Nucleotide binding and cofactor activities of purified bovine brain and bacterially expressed ADP-ribosylation factor. J Biol Chem. 264:21066-21072.

Zhao, C., J. Takita, Y. Tanaka, M. Setou, T. Nakagawa, S. Takeda, H.W. Yang, S. Terada, T. Nakata, Y. Takei, M. Saito, S. Tsuji, Y. Hayashi, and N. Hirokawa. 2001. Charcot-Marie-Tooth disease type 2A caused by mutation in a microtubule motor KIF1Bbeta. Cell. 105:587-597.

Zhou, C., L. Cunningham, A.I. Marcus, Y. Li, and R.A. Kahn. 2006. Arl2 and Arl3 regulate different microtubule-dependent processes. Mol Biol Cell. 17:2476-2487.

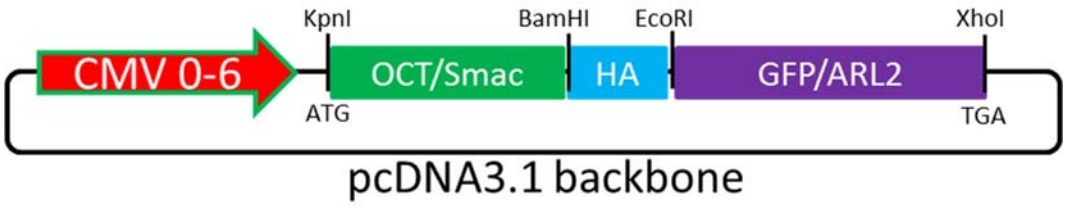

Fig. 1: Schematic of constructs. The parent plasmids are the collection of seven pcDNA3.1-based vectors with decreasing length and strength CMV promoters, going from pCMVΔ0-pCMVΔ6, as described in Morita, et al (Morita et al., 2012). Unique KpnI, BamHI, EcoRI, and XhoI sites were used for insertion of OCT or SMAC leaders, an HA epitope, and GFP or ARL2 open reading frames, as described under Methods.

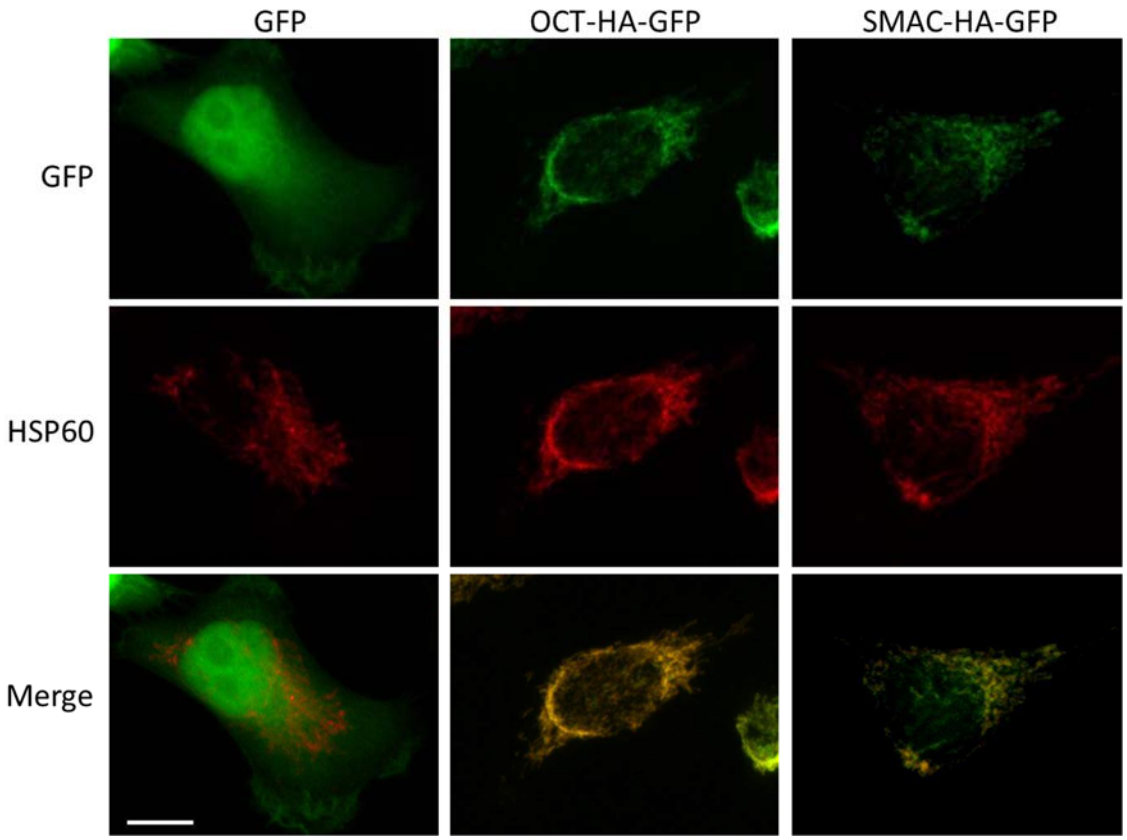

Fig. 2: Neither OCT-HA-GFP nor SMAC-HA-GFP alter mitochondrial morphology. HeLa cells were transfected with GFP, OCT-HA-GFP, or SMAC-HA-GFP, fixed in 4% paraformaldehyde 24 hours later, and stained for HSP60. Z stack projections of representative cells are shown. Scale bar = 10 μm. Similar results were obtained at 48 hours after transfection (data not shown).

3A)

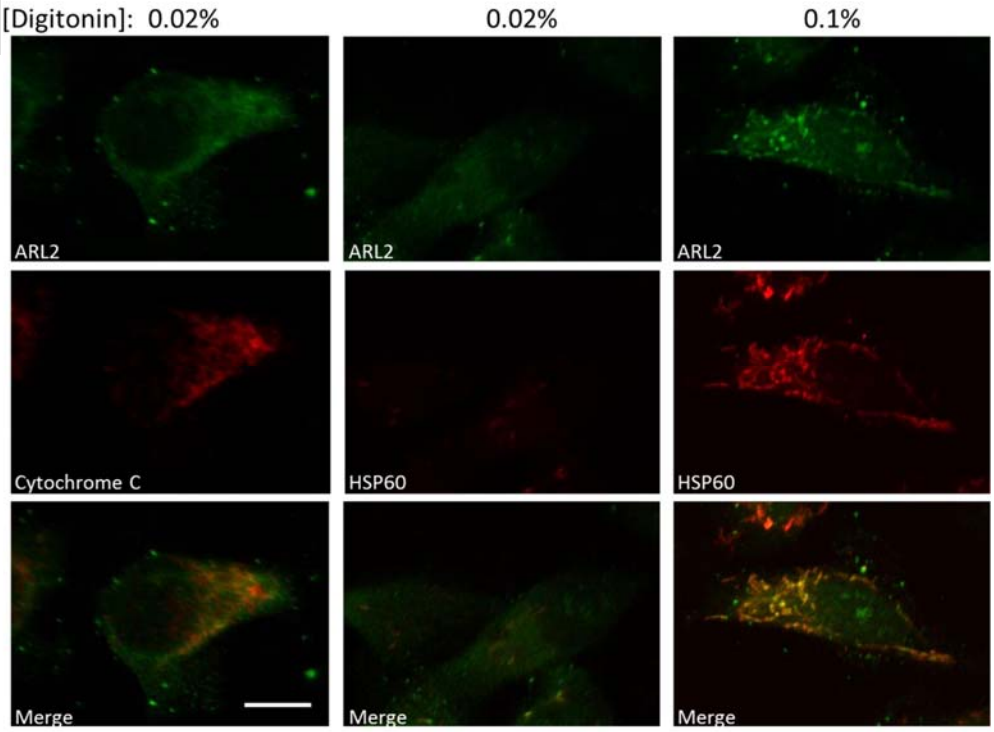
[Digitonin]: 0.02%
0.02%
0.1%
ARL2
ARL2
ARL2
Cytochrome C
HSP60
HSP60
Merge
Merge
Merge

3B)

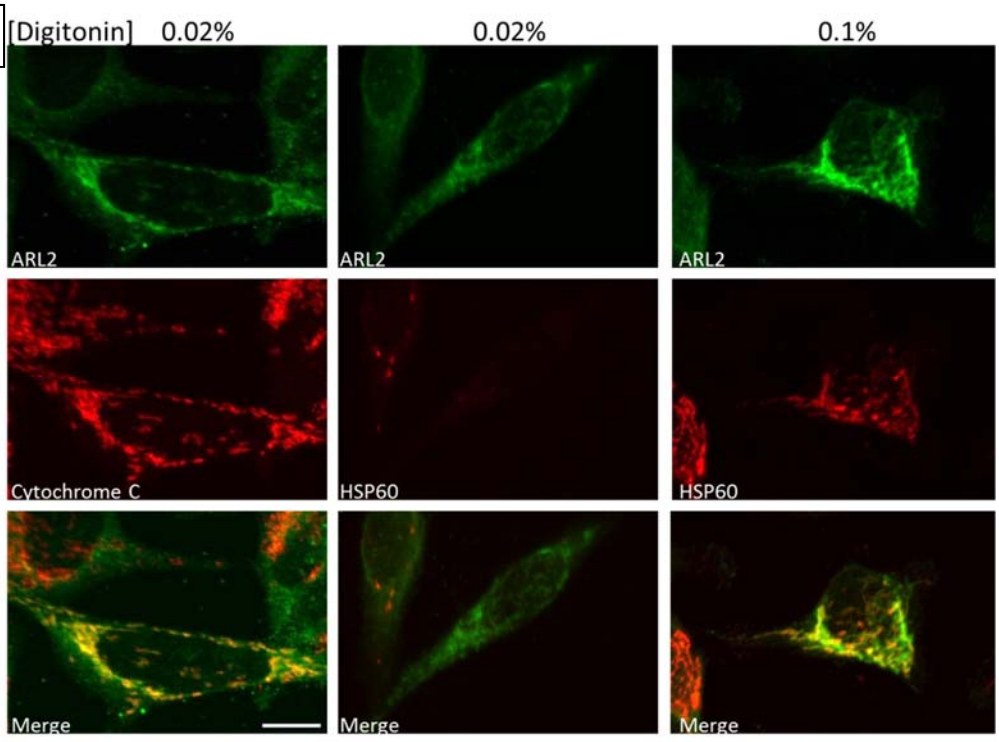
[Digitonin] 0.02%
0.02%
0.1%
ARL2
ARL2
ARL2
Cytochrome C
HSP60
HSP60
Merge
Merge
Merge

Fig. 3: SMAC-HA-ARL2 and OCT-HA-ARL2 are correctly localized to the IMS or matrix, respectively. HeLa cells were transfected with plasmids directing expression of either SMAC-HA-ARL2 (A) or OCT-HA-ARL2 (B) and fixed in 4% paraformaldehyde prior to permeabilization in either 0.02% (left two columns) or 0.1% w/v digitonin (right column) for 10 minutes at room temperature, as described under Methods. Cells were then processed for immunofluorescence using dual labeling for ARL2 (green, top row) and either cytochrome c (middle row, left panel) or HSP60 (middle row, middle and right panels), as markers of the IMS and matrix, respectively. Merged images are shown in the bottom row in each case. Z stack projections are shown. Scale bar = 10 μm.

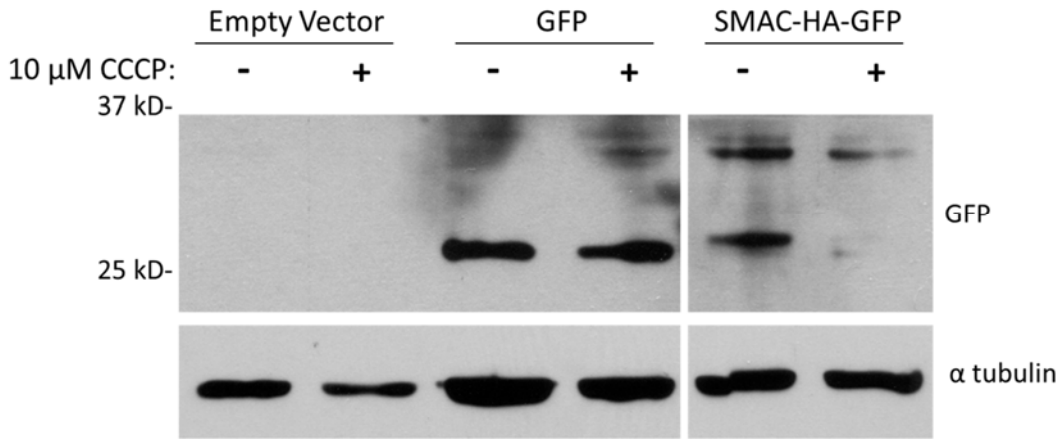

Fig. 4: CCCP treatment prevents the import and cleavage of SMAC-HA-GFP. HeLa cells transfected with 1 µg of either parental plasmid (pcDNA3.1, lanes 1 and 2), or that directing expression of cytosol-localizing, untagged GFP (lane 3 and 4), or IMS-localizing SMAC-HA-GFP (lanes 5 and 6). Ten hours after transfection, 10 µM CCCP (+) or vehicle control (-) was added to the cells, which were then harvested 2 hours later. Total cell lysates were prepared and proteins (20 µg/lane) were resolved in SDS polyacrylamide gels before transfer to nitrocellulose filters and immunoblotted using antibodies directed against GFP (top panel) or α-tubulin (bottom panel), as described under Methods. CCCP treatment had no effect on expression of cytosolic GFP (lanes 3 and 4) but increased the proportion of SMAC-HA-GFP migrating at the expected for the uncleaved protein (~33 kD) compared to the cleaved protein (~26 kD). Nonadjacent lanes from the same blot are shown.

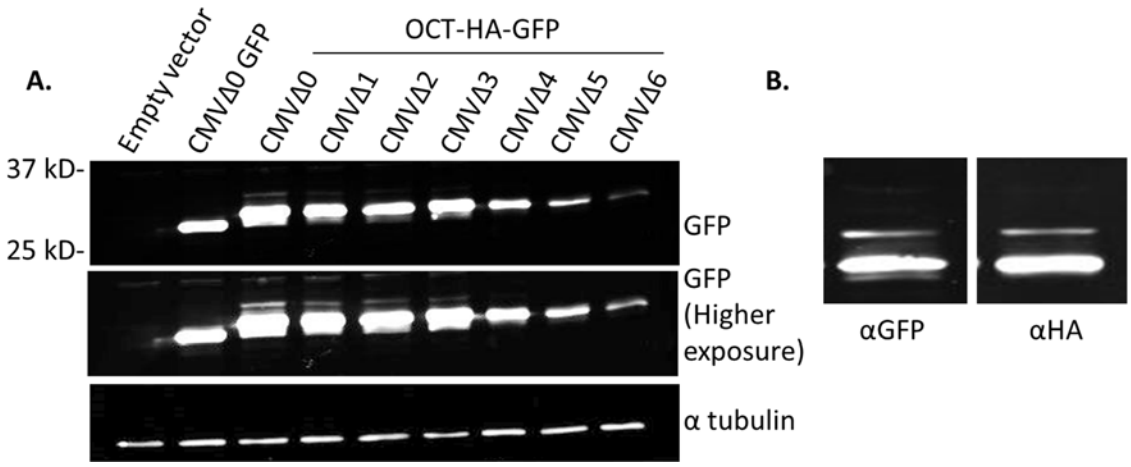

Fig. 5: OCT-HA-GFP is efficiently imported/cleaved and levels of expression decrease with decreasing strength CMV promoters. (A) HeLa cells transfected with 1 μg of either parental plasmid (pcDNA3.1, lane 1), or directing expression of untagged GFP (lane 2), or matrix localizing OCT-HA-GFP under control of CMV promoters CMVΔ0-6 (lanes 3-9) were harvested 24 hr post-transfection. Total cell lysates were prepared and proteins (20 μg/lane) were resolved in SDS polyacrylamide gels before transfer to nitrocellulose filters and immunoblotted using antibodies directed against GFP (top two panels) or α-tubulin (bottom panel), as described under Methods. A single, strong band of immunoreactivity is seen with untagged, presumably cytosolic, GFP (lane 2) while the presence of the HA tag (lanes 3-9) results in a slightly larger protein of similar intensity. The presence of another band of higher apparent molecular weight is seen when the OCT leader is added (lanes 3-9), consistent with the ~3.5 kDa size of this leader. Note that with higher exposures (e.g., middle panel) we also begin to see other bands appear, though these are non-specific as evidenced by their presence in control cells (e.g., lane 1 and 2). Note that higher exposures shown here contain pixel saturation and are unsuitable for quantification. (B) Same as A, except duplicate gels were run, with one gel probed for GFP and the other probed for HA. A single lane from each gel is shown.

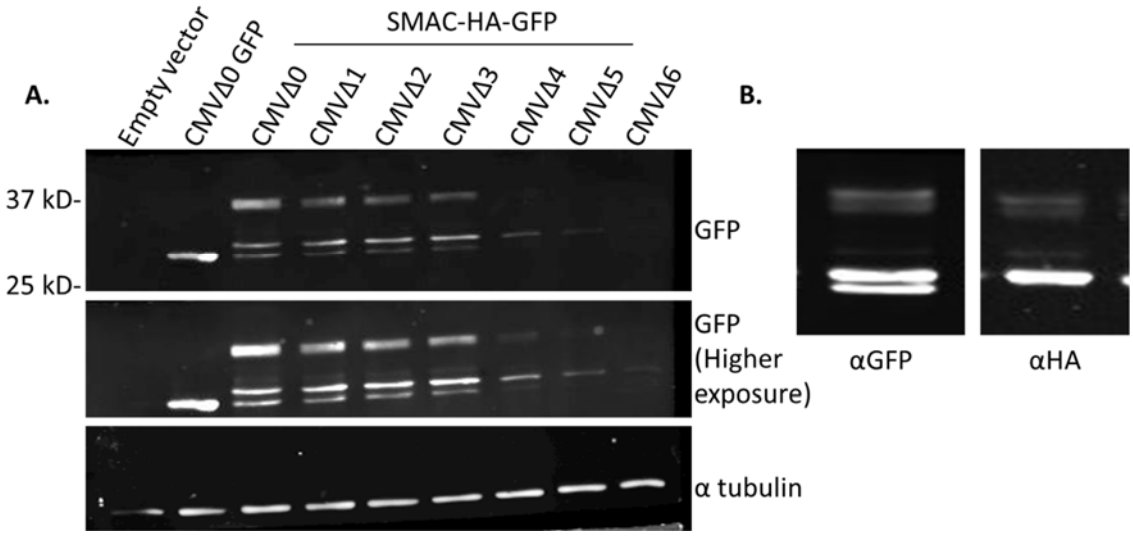

Fig. 6: SMAC-HA-GFP is expressed to similar levels as GFP and processed less completely than OCT-HA-GFP, particularly at higher levels. (A) HeLa cells were transfected with the series of SMAC-HA-GFP expressing plasmids and immunoblotting was performed as described in the legend to Figure 2. Three bands were observed with the slowest migrating one being the most prominent, particularly when expressed off the stronger promoters (e.g., lanes 3-6). This mobility of this upper band is consistent with it being uncleaved (~6.3 kb larger), the middle band is predicted to be cleaved upon import to generate HA-GFP, and the fastest migrating band predicted to be further digested to co-migrate with GFP (lane 2). Note that GFP, OCT-HA-GFP, and SMAC-HA-GFP are each expressed to similar levels and that processing of SMAC-HA-GFP is less complete than is that of OCT-HA-GFP, particularly with higher levels of expression. (B) Same as A, except duplicate gels were run, with one gel probed for GFP and the other probed for HA. A single lane from each gel is shown.

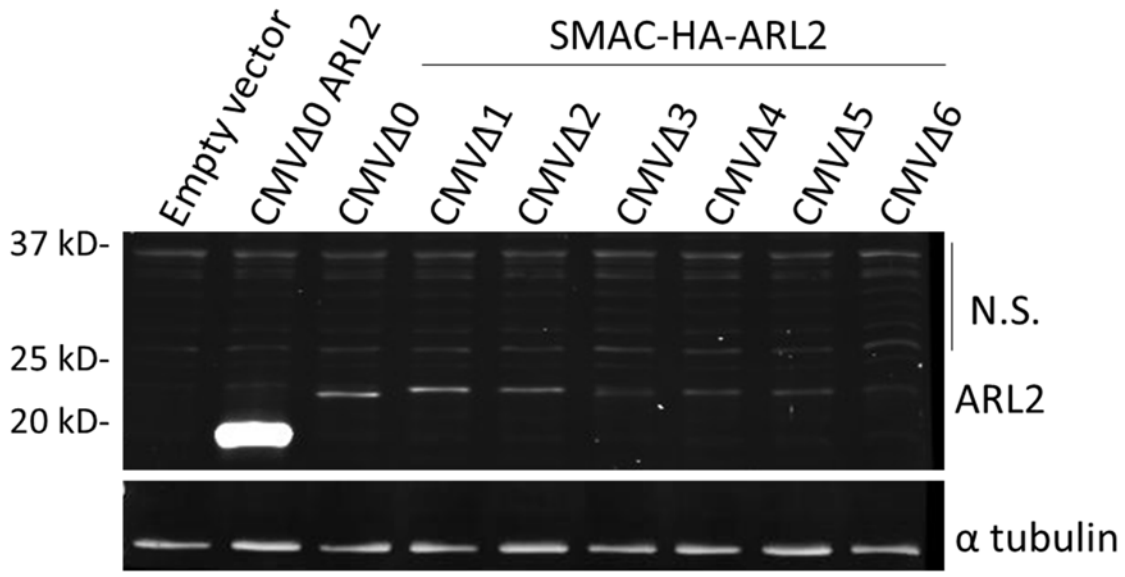

Fig. 7: SMAC-HA-ARL2 is expressed to lower levels than is ARL2 and cleavage appears to be complete at every level of expression. HeLa cells were transfected with the series of 7 different strength CMV promoters to express SMAC-HA-ARL2, as described in the legend to Figure 2 and under Methods, with blotting for either ARL2 or α-tubulin. Empty pcDNA3.1 (lane 1) or expressing untagged ARL2 (lane 2) were included as controls. In contrast to result from SMAC-HA-GFP (see Figure 3), we could detect no evidence of uncleaved SMAC-HA-ARL2, indicating it is very efficiently processed to HA-ARL2, consistent with its mobility in SDS gels. SMAC-HA-ARL2 was also expressed to much lower levels than untagged ARL2, even when each used the same (CMVΔ0) promoter. Note that because of the lower levels of expression it was necessary to use longer exposure times, resulting in the more evident appearance of non-specific bands (N.S.), as seen even in control lanes (1 and 2).

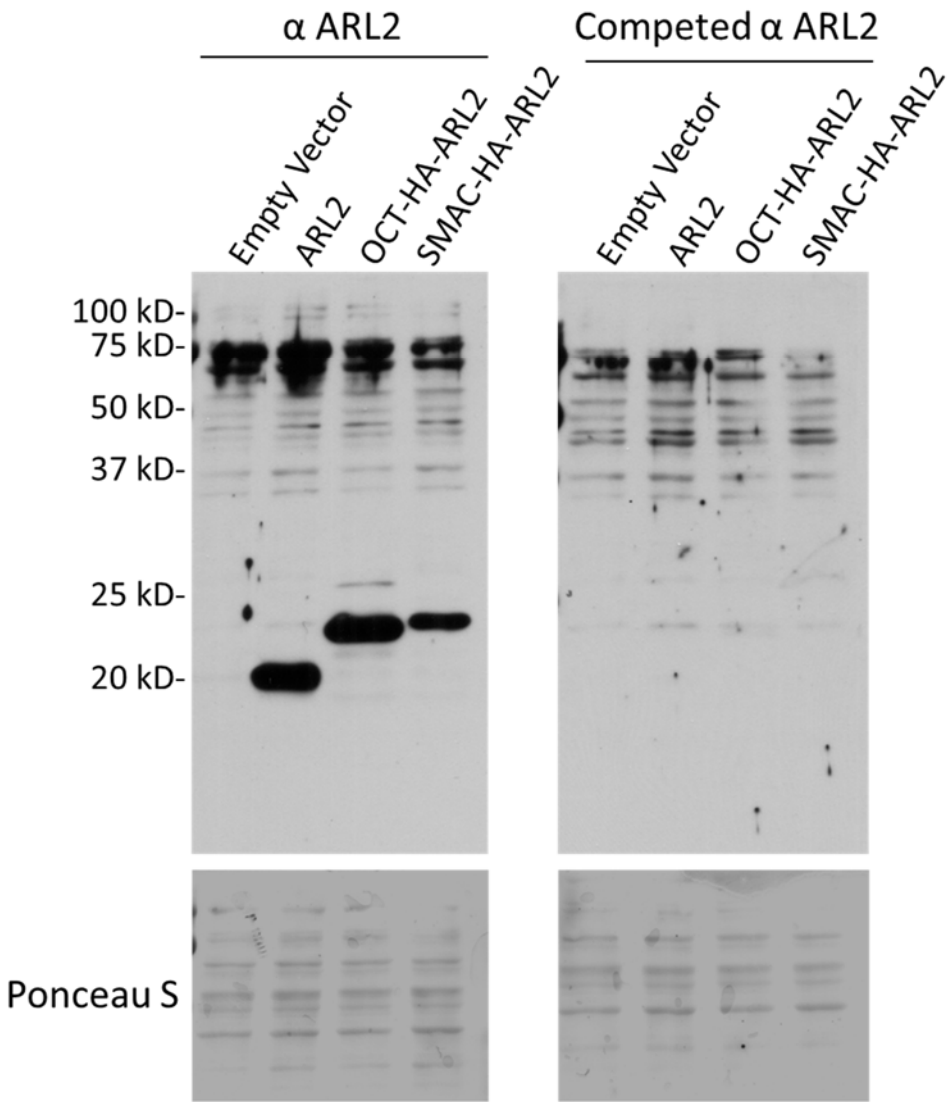

Fig. 8: Antigen competition confirms the identity of ARL2 fusion proteins and specificity of the ARL2 antibody. HeLa cells transfected with 1 μg of either parental plasmid (pcDNA3.1, lane 1), or directing expression of untagged ARL2 (lane 2), OCT-HA-ARL2 (lane 3), or SMAC-HA-ARL2 (lane 4) and were harvested 24 hr post-transfection. Total cell lysates were prepared and two sets of identical samples (5 μg/lane) were resolved in one SDS polyacrylamide gel before transfer to nitrocellulose filters, as described under Methods. The two sets of identical samples were separated and probed with our rabbit polyclonal antibody directed against ARL2 at 1:7,000 dilution, either without (left panel) or with (right panel) prior incubation with 20 μg purified, recombinant ARL2. Bands corresponding to untagged ARL2 (lane 2), uncleaved and cleaved OCT-HA-ARL2 (lane 3), and cleaved SMAC-HA-ARL2 (lane 4) are all absent from the

competition blot. Ponceau S staining of the blots immediately after transfer shows that equal protein was present on both blots.

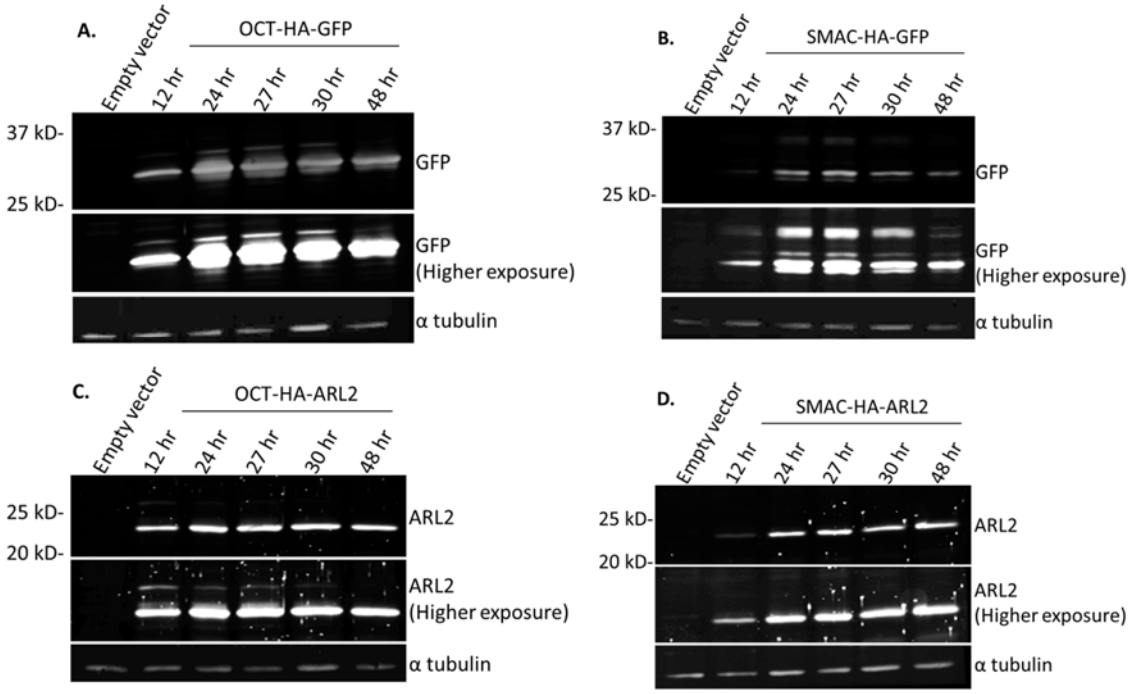

Fig. 9: Different proteins expressed off the same promoters and leader sequences are expressed to different levels and with differing extents or kinetics of import/processing. ALL PANELS: HeLa cells were transfected with 1 μg pCMVΔ0 plasmids directing expression of no exogenous protein (Empty vector), OCT-HA-GFP, SMAC-HA-GFP, OCT-HA-ARL2, or SMAC-HA-ARL2, as described under Methods. Cells were harvested at the indicated times, lysates prepared, and total cellular proteins (20 μg) were resolved in SDS gels. Immunoblotting was performed with antibodies to GFP, ARL2 or α-tubulin (loading control). (A) Processed OCT-HA-GFP is readily apparent within 12 hours after transfection and the level is fairly constant over the 48 hrs of this study. With longer exposure the full length protein is evident though is greatly reduced by 48 hrs, at which point new protein expression is expected to be clearly diminished. Some partially processed or further processed proteins may be seen above or below the major band of HA-GFP, which migrates at the expected 28 kDa. (B) SMAC-HA-GFP expression may be slightly delayed, in comparison to the OCT-HA-GFP, with a larger fraction of the recombinant

protein migrating as the uncleaved ~35 kDa protein. Partially cleaved and further processed proteins are again evident. (C) OCT-HA-ARL2 expression is evident as the imported/cleaved protein is readily observed within 12 hr after transfection and is quite stable over the 48 hr time course. Small amounts of the uncleaved or partially cleaved protein can be seen with over-exposure but these are essentially gone by 48 hrs. (D) SMAC-HA-ARL2 is the most efficiently imported/cleaved protein tested, with difficulty seeing the uncleaved protein at any time point, and is also stable over the 48 hr time course.

Chapter 4: The ARL2 GTPase regulates mitochondrial fusion from the intermembrane space upstream of mitofusins

This chapter is submitted as:

Laura E. Newman, Michael P. East, and Richard A. Kahn. The ARL2 GTPase regulates mitochondrial fusion from the intermembrane space upstream of mitofusins. Submitted.

Abstract

Mitochondria are essential, dynamic organelles, though mechanisms of regulation of their dynamics are poorly understood. We provide evidence that the small GTPase ARL2 regulates mitochondrial fusion upstream of the mitofusins. Expression of dominant activating or dominant negative point mutants of ARL2 causes mitochondrial elongation or fragmentation, respectively, and ARL2 is only active when directed to the mitochondrial intermembrane space. Two independent assays each found that expression of dominant negative ARL2 resulted in the loss of mitochondrial fusion. Further, dominant active ARL2 rescued fragmentation in either *mfn1*$^{-/-}$ or *mfn2*$^{-/-}$ MEFs, but not in *mfn1*$^{-/-}$ *mfn2*$^{-/-}$ or *opa1*$^{-/-}$ MEFs, demonstrating that ARL2 can stimulate fusion through either mitofusin. Finally, we show using structured illumination microscopy that ARL2 and mitofusins co-localize with regular spacing along mitochondria to a novel structure. We propose that ARL2 plays a regulatory role in mitochondrial fusion from the IMS upstream of the mitofusins.

Introduction

Mitochondria are essential organelles that generate ATP through respiration and also play key roles in lipid metabolism, calcium, and in apoptosis. They are morphologically heterogeneous and the regulation of mitochondrial dynamics is an integral part of these crucial cellular functions. Mitochondrial shape is regulated by two cellular processes, fission and fusion, yet our understanding of the mechanisms and regulation of these processes is incomplete. Central players in these processes are the large GTPases DRP1, mitofusins 1 and 2 (MFN1/2), and OPA1. Recruitment of DRP1 from cytosol to the outer membrane is involved in mitochondrial constriction leading to fission (Labrousse et al., 1999; Smirnova et al., 2001). Fusion is mediated

by three large GTPases: the structurally and functionally orthologous MFN1 and MFN2 are transmembrane proteins that promote mitochondrial fusion at the outer membrane, while OPA1 is a transmembrane protein that regulates inner mitochondrial membrane fusion (Chen et al., 2003; Cipolat et al., 2004; Chen et al., 2005; Mishra and Chan, 2014). The importance of fission and fusion is evident by the number of diseases associated with errors in these processes. Mutations in MFN2 cause Charcot-Marie-Tooth Type 2A (Zuchner et al., 2004), while mutations in OPA1 lead to dominant optic atrophy (Alexander et al., 2000; Delettre et al., 2000). Mice lacking MFN1 or MFN2 are embryonic lethal (Chen et al., 2003), and a conditional knockout of MFN2 leads to defective cerebellar development (Chen et al., 2007). In the cell, fusion is important for ATP production, and mitochondria elongate during starvation and stress (Tondera et al., 2009; Gomes et al., 2011; Rambold et al., 2011). Mitochondrial fusion is also thought to be important for mixing of mitochondrial contents (Song et al., 2009; Chan, 2012) and maintenance of mitochondrial DNA (Chen et al., 2007; Chen et al., 2010). Thus, a better understanding of the molecular mechanisms and means of regulation of mitochondrial dynamics is important to our understanding of cell biology and human diseases.

Though essential roles for these three large GTPases have been identified in mitochondrial fusion, we lack information on the other components in the pathway or means of regulation. Perhaps the best understood aspect of regulation is post-translational modifications of the GTPases. OPA1 is cleaved by the proteases OMA1 and YME1L, which regulate its fusion activity (Griparic et al., 2007; Song et al., 2007; Ehses et al., 2009; Head et al., 2009). MFN1 activity is regulated by phosphorylation (Pyakurel et al., 2015) and acetylation (Lee et al., 2014) . Mitofusins act in trans to promote fusion of mitochondria and also form disulfide bonds during oxidative stress, leading to cis-oligomerization and an increase in fusion (Shutt et al., 2012). Mitofusins are also ubiquitinated by Parkin during mitophagy, leading to their degradation and an inhibition in fusion (Tanaka et al., 2010). To date, only a handful of protein regulatory factors

have been shown to regulate mitofusins. Bax stimulates mitochondrial fusion via MFN2 (Hoppins et al., 2011), and MIB can negatively regulate the activity of both mitofusins (Eura et al., 2006). Both Bax and MIB regulate mitofusins from the cytosolic face of the outer membrane. To the best of our knowledge, no regulatory factor has been shown to regulate mitofusins or mitochondrial fusion from inside mitochondria, despite the fact that such a pathway is necessary to communicate between the energetic state inside the organelle and external factors as well as to link inner and outer mitochondrial membrane events.

ARL2 is a small, regulatory GTPase and member of the ARF family of GTPases (Clark et al., 1993). ARL2 is very highly conserved, ubiquitous across eukaryotes, predicted to be present in the last eukaryotic common ancestor (Li et al., 2004), and is essential for at least three model organisms; C. elegans (Antoshechkin and Han, 2002), S. pombe (Radcliffe et al., 2000), and A. thaliana (McElver et al., 2000). An unusual feature of ARL2 is that it localizes to, and has been shown to perform distinct functions at, several different places in the cell. In the cytosol, ARL2 is in a complex with the tubulin folding chaperone cofactor D and is proposed to regulate tubulin folding (Bhamidipati et al., 2000; Shern et al., 2003; Tian et al., 2010). ARL2 and cofactor D are also at centrosomes, with links to recruitment of γ-tubulin ring complex, tubulin polymerization, and mitotic spindle organization (Zhou et al., 2006; Cunningham and Kahn, 2008). ARL2 along with its closest paralog, ARL3, can also regulate traffic of farnesylated proteins (Ismail et al., 2011). In the nucleus, ARL2 and its effector BART are implicated in transcriptional regulation by STAT3 (Muromoto et al., 2008). Finally, we have documented roles for ARL2 in mitochondria (Sharer et al., 2002; Newman et al., 2014b).

We currently model ARL2 as being only partially localized inside mitochondria, though in a regulated fashion, and having at least two distinct functional outcomes or pathways. Based upon our fractionation data we estimate that only about 10% of total cellular ARL2 localizes to mitochondria, in both tissues and cultured cells, along with its effector Binder of

ARL2 (BART)(Sharer et al., 2002). We found that ARL2 complexed with GTP and BART can bind the nucleotide transporter ANT1 (Sharer et al., 2002). While ARL2 expression overall was unchanged, the amount of mitochondrial ARL2 was dramatically increased in the heart and skeletal muscle of ant1-/- mice (Sharer et al., 2002), which exhibit muscle wasting, exercise intolerance, and cardiomyopathy (Graham et al., 1997). Depletion of ARL2 in rat neonatal ventricular cardiomyocytes caused a loss in ATP, supporting a role for mitochondrial ARL2 in heart muscle physiology (Nishi et al., 2010). Later, we found that depletion of ARL2 by siRNA causes three mitochondrial phenotypes: mitochondrial fragmentation, a loss in plus-end directed mitochondrial motility, and a dramatic (~50%) loss in cellular ATP (Newman et al., 2014a). Expression of the dominant negative mutant ARL2[T30N] phenocopied the morphology and motility defects, but not ATP loss, caused by ARL2 siRNA. These observations lead us to propose at least two different pathways involving ARL2 in mitochondria; one affecting ATP levels and the other morphology and motility. We also showed that depletion of the ARL2 GAP, ELMOD2, results in fragmentation and perinuclear clustering, leading us to propose that ELMOD2 is an ARL2 effector for the latter two phenotypes, and supporting at least two sites of action for ARL2 in mitochondria. We extend our previous findings here to document that ARL2 acts from the IMS to regulate mitochondrial fusion upstream of the mitofusins.

Methods

Antibodies & Reagents: Rabbit polyclonal antibody directed against purified human ARL2 has been previously described (Sharer et al., 2002). The following antibodies were purchased: HA (Covance MMS-101P), HSP60 (Enzo Life Sciences ADI-SPA-807), cytochrome C (BD Biosciences 556432), TOM20 (BD Biosciences 61228), alpha tubulin (Sigma T9026), myc (Invitrogen R950-25), OPA1 (BD Biosciences 612606), Complex V subunit alpha (Mitosciences MS502), NDUFA9 (Mitosciences MS111), UQCRC2 (Mitosciences MS304). Mdivi-1 was purchased from Sigma (cat# M0199).

Cloning and Constructs: The following plasmids were generously provided by: MFN1-10xmyc and MFN2-16xmyc in pcDNA3.1 (David Chan, Caltech, (Chen et al., 2003)), OPA1-myc/his in pcDNA3.1 (Heidi McBride, McGill), mito-PAGFP (Richard Youle, NIH, Addgene plasmid #23348, (Karbowski et al., 2004)), mito dsRed (James Zheng, Emory), GFP-MFF (Gia Voeltz, University of Colorado, Addgene plasmid #49153(Friedman et al., 2011)), DRP1-YFP (Alexa Mattheyses, Emory). ARL2, ARL2[T30N], and ARL2[Q70L] in pcDNA3.1 were made in our lab and described previously (Zhou et al., 2006). [F50A] and [L3A] mutations were introduced into ARL2[Q70L] in pcDNA3.1 using QuickChange (Stratagene) and sequence-verified. CMVΔ0 OCT-HA-ARL2 and CMVΔ0 SMAC-HA-ARL2 were also made in our lab as previously described (Newman, Schiavon, and Kahn, manuscript submitted).

Cell culture: Human cervical carcinoma (HeLa), mouse embryonic fibroblast (MEF), and African green monkey kidney (COS7) cells were grown in DMEM supplemented with 10% fetal bovine serum (Invitrogen, Carlsbad, CA) and 2 mM glutamine at 37°C in the presence of 5% CO2. Cells were originally obtained from the ATCC. Wild type and *mfn1*$^{-/-}$, *mfn2*$^{-/-}$, *mfn1*$^{-/-}$*mfn2*$^{-/-}$, *opa1*$^{-/-}$ MEFs were a generous gift from David Chan (California Institute of Technology) (Chen et al., 2003; Koshiba et al., 2004; Chen et al., 2005; Song et al., 2007). Cells were screened for mycoplasma regularly by staining with Hoechst 33342 DNA dye, usually in conjunction with immunofluorescence experiments (described below). Cells were not cultured for more than 30 passages.

Transfection: Cells at 90% density or higher were transfected in 6 well plates using the following protocols. Both the amount of DNA and the ratio of Lipofectamine: DNA were separately optimized for ARL2 expression in HeLa and COS7 cells. A ratio of 2 μg Lipofectamine: 1 μg DNA yielded the highest transfection efficiency. ARL2 plasmids (2 μg) were diluted in 250 μL Opti-MEM (Invitrogen). Lipofectamine 2000 (4 μg; Invitrogen) was diluted in a separate tube containing 250 μL Opti-MEM, vortexed briefly, and incubated at room temperature for 5

minutes. The tubes were mixed and incubated 20 minutes. Cell culture medium was changed to 1.5 ml of Opti-MEM, and transfection complexes (500 µL) were added dropwise to the cells. After 4 hours, cells were trypsinized and replated onto coverslips, typically at a 1:3 split. For time points of 48 hours or longer after transfection, fresh medium (1 mL) was added prior to addition of transfection complexes, and the transfection was allowed to go for 24 hours, after which cells were typically split 1:4 onto coverslips. In both cases, cells were allowed to attach overnight before fixation. This transfection typically resulted in ~70% of cells overexpressing ARL2 and ~50% expressing ARL2[T30N] or ARL2[Q70L] when assayed 48 hours from the start of transfection.

MEFs were transfected using a similar protocol, though we found optimal ARL2 expression was obtained using a 3:1 ratio: 15 µg Lipofectamine 2000 and 5 µg DNA per well. Following transfection, cells were replated 1:4 (*mfn1*$^{-/-}$, *mfn2*$^{-/-}$) or 1:2 (*mfn1*$^{-/-}$*mfn2*$^{-/-}$, *opa1*$^{-/-}$) onto coverslips such that MEFs were at ~90% confluence the next day. This protocol typically resulted in ~40% of MEFs expressing MFN1-myc or MFN2-myc, ~20% expressing ARL2, ~10% expressing ARL2[Q70L], and 1-5% expressing OPA1-myc/his, as determined by immunofluorescence imaging of fixed cells. These differences are likely the result of differences in protein expression and antibody sensitivities rather than plasmid uptake. Slightly lower (~10-20%) transfection efficiencies were observed in *mfn1*$^{-/-}$*mfn2*$^{-/-}$ and *opa1*$^{-/-}$ MEFs, perhaps related to their increased doubling time and increased susceptibility to stress.

Immunofluorescence: Cells were grown on matrigel (BD Biosciences #356231) coated coverslips. Cells were fixed in a pre-warmed (37°C) solution of 4% paraformaldehyde in PBS (140 mM NaCl, 3 mM KCl, 10 mM Na2HPO4, 2 mM KH2PO4, pH 6.75), and permeabilized with 0.1% (v/v) Triton X-100 in PBS for 10 minutes at room temperature. Alternately, cells were permeabilized with either 0.02% or 0.1% (w/v) digitonin in PBS for 10 minutes at room temperature to differentially permeabilized the outer or inner mitochondrial membrane,

respectively, as previously described (Otera et al., 2005; Jeyaraju et al., 2006). Incubation with primary antibodies was carried out in filtered PBS containing 1% (w/v) BSA at 4°C overnight, followed by 4 x 5 minute washes in PBS. Secondary antibodies (1:500, Alexa fluorophores, Invitrogen) were incubated in the same buffer for 1 hour at room temperature, following 4 x 5 minute washes in PBS. Secondary antibody was removed by 2 x 5 minute washes in PBS. DNA was then stained with Hoechst 33342 for 4 minutes, followed by 2 x 5 minutes washes in PBS and mounting onto slides using Prolong Antifade (Invitrogen). Images were acquired using an Olympus FV1000 microscope and Olympus Fluoview v1.7 software, using 488 and 543 laser excitation and a 100x oil objective (1.45 NA). Z-stacks were acquired with a step size of 0.37 μm, which were converted to average image intensity projections using ImageJ where indicated. The following antibody dilutions were used: ARL2 (1:2000), HSP60 (1:5000), myc (1:1000), HA (1:2000), TOM20 (1:5000), cytochrome C (1:1000), alpha tubulin (1:2000), OPA1 (1:100), NDUFA9 [Complex I] (1:100), UQCRC2 [Complex III] (1:100), Complex V subunit alpha (1:100).

Effects of protein expression on mitochondrial morphology were scored by visual inspection of fixed, stained cells. To quantify consequences of protein expression on mitochondrial morphology in MEFs, the following categories were used: 1) Fragmented = mitochondria appear spherical with no long or branched structures evident, 2) short tubes = mitochondria appear shorter than in wild type controls but not spherical and show minimal interconnectivity, 3) tubular = mitochondria appear long and thread-like, with branching. Examples of each of these are shown in Figure 4C. A cell was assigned to a category if an estimated 50% or more of its mitochondria fit one of these descriptions, as described previously (Hoppins et al., 2011). For quantification of elongation in HeLa cells, we used the following categories: 1) elongated = the majority of mitochondria appear interconnected and individual mitochondria are difficult to discern, 2) tubular = individual mitochondria are easily discernable

but the majority are not fragmented, 3) fragmented = a majority of mitochondria appear small and spherical. A cell was excluded from analysis if it appeared to be dying, as defined by cell rounding with membrane blebs and fragmented nuclear staining; these cells typically had the highest levels of expression in the cell population. Only transfected cells were scored, and were identified as follows: 1) ARL2 over-expressing cells were identified by ARL2 staining (ARL2 staining appears obviously brighter than surrounding cells in the field), 2) MFN1/2-myc by detectible mitochondrial myc staining, or 3) GFP-DRP1[K38A] cells by GFP signal (GFP appearing as puncta inside a cell).

Live cell imaging: Cells were transfected with 0.5 µg mito-PAGFP, 0.25 µg mito-dsRed, and 2 µg of either ARL2 WT or ARL2[T30N], and replated onto 35 mm MatTek dishes (#P35GC-1.5-14-C) following 4 hours of transfection, as described above. At least an hour prior to imaging, the medium was changed to DMEM with 25 mM HEPES plus 10% FBS, and without phenol red (Invitrogen #21063). Live cell imaging was performed using a Nikon A1R confocal microscope, enclosed in a temperature control chamber at 37°C, using a 100X (NA 1.49) oil objective. A circular region of interest (4 µm diameter) for photoactivation was selected near the nucleus (Karbowski et al., 2014). Photoactivation was achieved by excitation with 405 nm laser (35% power) for six cycles for a total duration of 2.16 seconds. Images were acquired at 1024 x 1024 pixels at 0.5 frames/second during photoactivation. Images were then acquired every 10 minutes over 40 minutes. GFP and dsRed were sequentially excited with 488 and 561 laser lines. Imaging data were collected using Nikon Elements software. Quantification of the PAGFP mitochondrial fusion assay was performed as previously described (Zunino et al., 2009) using ImageJ. A cell was excluded from analysis if it 1) had less than a 10-fold increase in GFP signal following photoactivation, 2) moved from the field of view during imaging, or 3) was too close to surrounding cells to crop out just one cell. In addition, only cells with fragmented mitochondria

were selected when imaging cells transfected with ARL2[T30N]. Masks for each channel were created, and thresholding was performed using "Otsu dark" in ImageJ. The number of pixels within each mask for both GFP and dsRed was measured, and calculated as a ratio of GFP signal to dsRed signal. The difference in this ratio between 0 min. (immediately after photoactivation) and 40 min. after photoactivation is reported as percent increase in mitochondrial fusion.

For mdivi-1 experiments, COS7 cells were transfected as described above with either ARL2 or ARL2[T30N] (2 µg) along with mito-dsRed (1 µg). We did not perform this experiment in HeLa cells because mdivi-1 did not cause any obvious mitochondrial elongation in that cell line. Cells were imaged using the Nikon A1R as described above. Images were collected every 30 seconds for 2 minutes, at which point imaging was paused and mdivi-1 (50 µM) was added. Imaging was then resumed and cells were imaged for an additional 15 minutes.

Structured Illumination Microscopy (SIM): For SIM experiments, the minimal amount of transfected DNA was determined for each construct for both optimal expression and minimal effects on mitochondrial morphology. COS7 cells were transfected with 0.5 µg MFN1-myc, MFN2-myc, or 2 µg of OPA1-myc/his. A ratio of 2 µg Lipofectamine 2000: 1 µg DNA was used for all constructs. Cells were imaged on a Nikon N-SIM using three dimensional SIM using a 100X (NA 1.49) oil objective. Cells were selected based on an apparently normal mitochondrial morphology, and a range of expression for each construct was examined. Fluorophores were excited by 488 and 561 laser lines. For each cell, a widefield image was obtained in addition to raw SIM data. Reconstruction was achieved using the Nikon Elements software, and reconstruction parameters suggested by the software were adjusted with reference to the widefield image, to avoid previously described artifacts (for examples see http://www.gelifesciences.com/gehcls_images/GELS/Pdf%20documents/2015-05-06-Pellett-Bitesizebio-Seminar.pdf).

Blue native polyacrylamide gel electrophoresis (BN-PAGE): BN-PAGE gels (4-16%) were obtained commercially (Invitrogen) and used according to manufacturer's instructions. Molecular weight standards for native gels were purchased from Invitrogen (cat#LC0725). Western blotting was performed as described below, with the exception that proteins were transferred onto PVDF membranes instead of nitrocellulose, HRP-conjugated secondary antibodies were used (GE cat #NA934V, #NA931V), and blots were incubated in luminol containing solution (0.1 mM Tris-HCl pH 8.0, 1.2 mM luminol, 0.2 mM p-coumaric acid, 0.009% hydrogen peroxide) for 1 min prior to exposure to film.

Partial purification of the ~500 kDa complex: Bovine liver was homogenized in a Potter-Elvehejm teflon on glass homogenizer and a post-nuclear supernatant was obtained after centrifugation at 600xg. A crude mitochondria fraction was generated by taking the pellet from a subsequent centrifugation at 11,000xg. Mitochondrial proteins and complexes were then solubilized in 1% CHAPS and the solution was clarified by centrifugation at 100,000xg, prior to loading onto a 15-35% stepwise sucrose gradient, following the protocol for sucrose gradient fractionation on Mitosciences' website (http://www.mitosciences.com/PDF/sg.pdf), and modified by using 0.05% final concentration of CHAPS throughout the gradient instead of n-dodecyl □-D-maltoside (Hanson et al., 2001). Fractions were analyzed by BN-PAGE (Schagger and von Jagow, 1991; Nijtmans et al., 2002), and those containing the 500 kDa complex were stored at -80°C.

Western blotting: Cells were harvested by rinsing twice with PBS, collected by incubation in 5 mM EDTA in phosphate buffered saline (PBS; 140 mM NaCl, 3 mM KCl, 10 mM Na2HPO4, 2 mM KH2PO4, pH 6.75), and pelleted in a microfuge (14,000 rpm, 4°C). Cells were lysed in 1% CHAPS, 25 mM HEPES pH 7.4, 100 mM NaCl, and protease inhibitors (Sigma #P-2714) on ice for 30 minutes, and the S14 was obtained by clarifying lysates by centrifugation for 30 minutes (14,000 rpm, 4°C). Protein concentrations were determined by Bradford Assay (Bio-Rad) using

bovine serum albumin as standard. Protein samples (20 µg/well) were separated on 15% polyacrylamide gels and wet-transferred to nitrocellulose membranes (Bio-Rad #162-0112) at 70V for 2.5 hours. Western blotting procedures were carried out at room temperature. Membranes were blocked in blotto (5% (w/v) dry milk, 50 mM Tris pH 8, 2 mM CaCl2, 80 mM NaCl, 0.2% (v/v) Tween-20, 0.02% sodium azide) for 1 hour. When probing for ARL2, membranes were blocked in an alternate blocking buffer (10% goat serum, 5% Tween-20 in PBS), freshly filtered through a 0.2 µm membrane. Membranes were then incubated with primary antibody in blocking buffer at 4°C overnight. Removal of excess primary antibody was carried out by washing the membranes in PBST (PBS with 0.1% Tween-20) three times for 10 min each. The anti-rabbit 790 secondary antibody (Invitrogen A11374) or anti-mouse 800 secondary antibody (Rockland 610-745-002) was diluted 1:10,000 in PBST and incubated with the membrane for 1 hour at room temperature. The membrane was protected from light from this point on. Excess secondary antibody was removed by washing the membranes in PBST 3 times for 10 min each. Excess Tween-20 was removed by quickly rinsing membranes 3 times in PBS, followed by 2x5 minute washes in PBS. Data were collected using the Odyssey Infrared Imager. The following antibody dilutions were used for western blotting: ARL2 (1:1000), alpha tubulin (1:2500). Immunoblotting with antibodies to alpha tubulin was performed in each case as a loading control to confirm equal total protein loaded per lane, in agreement with total protein assays.

Reproducibility: Every experiment described has been independently repeated at least twice. For quantification of immunofluorescence experiments, experiments were independently repeated at least three times, and at least 200 cells per condition were analyzed per experiment. Error bars represent one standard deviation.

Summary of supplemental data: Figure S1 shows the presence of an ARL2 immunoreactive band running at approximately 500 kDa in BN-PAGE gels, at the same size as an HSP60 immunoreactive band. Incubation of a partially purified preparation of this complex with 10 mM

ATP causes dissociation of the complex, as previously described (Levy-Rimler et al., 2001) and loss of the ~500 kDa ARL2 band, supporting physical association of ARL2 with the HSP60 heptamer, which is known to be present in the mitochondrial matrix. Figure S2 shows that the import of N-terminal SMAC and OCT fusion proteins are correctly targeting ARL2 to the IMS and matrix, respectively, with subsequent cleavage of each leader sequence, as predicted by their previously demonstrated activities.

Results

Model systems used

For this study, we used cultured cells from three parental lines; HeLa, MEFs, or COS7. HeLa cells were used as we routinely obtain the highest transfection efficiencies (70% or more) and they are relatively flat, making them good for imaging. For high resolution imaging studies of endogenous ARL2, we turned to COS7, as they have stronger endogenous ARL2 staining, particularly in mitochondria, and are even flatter, making them highly suited for imaging endogenous and transfected ARL2 and other proteins. Finally, immortalized MEFs were used due to the availability of immortalized lines depleted of MFN1, MFN2, or OPA1 (Chen et al., 2003; Koshiba et al., 2004; Chen et al., 2005; Song et al., 2007). In experiments that could be readily performed in each of these different cell lines we obtained very similar results; suggesting that there was no obvious cell type specificity to the results obtained, despite the variability in mitochondrial morphology seen between these cell lines.

Dominant activating and inactivating mutants of ARL2 have opposite effects on mitochondrial morphology

We previously reported that loss of ARL2 activity, resulting from ARL2 siRNA or expression of the dominant inactivating ARL2[T30N] mutant, caused mitochondrial fragmentation (Newman et al., 2014a). Importantly, while ARL2 knockdown resulted in dramatically lower cellular ATP levels, expression of ARL2[T30N] had no effect on ATP levels, supporting a role for ARL2 in regulation of mitochondrial morphology independent of changes in cellular ATP levels. The idea that this effect of ARL2[T30N] on mitochondrial morphology is not simply secondary to depletion of ATP is supported by the observation that expression of the dominant activating mutant, ARL2[Q70L], has the opposite effect in that it causes mitochondrial elongation (Figure 1A). Overexpression of wild type ARL2 has no effect on mitochondrial morphology and transfected cells appear indistinguishable from untransfected cells or those receiving empty vector (Newman et al., 2014a). In striking contrast, mitochondria in HeLa cells expressing ARL2[Q70L] displayed obviously longer mitochondria. The mitochondria in these cells also appear to be more interconnected, as more branching and looping structures were apparent, compared to controls. The increased length and interconnectivity made it difficult to locate individual mitochondria in these cells. Using the scoring matrix described under Methods, we found that 19 and 21% of control cells, receiving empty vector or ARL2 respectively, contained elongated mitochondria, compared to 66% of cells expressing ARL2[Q70L] (Figure 1B; “elongated”).

Unlike the mitochondrial fragmentation caused by ARL2[T30N], which was apparent 24 hours after transfection, mitochondrial elongation caused by ARL2[Q70L] was not obvious until later time points, specifically 2-3 days after transfection. We note that in both ARL2 and ARL2[Q70L] expressing cells, ARL2 staining appeared diffuse in the majority of cells the day after transfection, and mitochondrial morphology appeared normal. At later time points, when the mitochondrial elongation phenotype was most apparent in ARL2[Q70L] cells, transfected cells

had obviously stronger mitochondrial ARL2 staining. Though shown here in HeLa cells (Figure 1), ARL2[Q70L] also caused mitochondrial elongation in MEFs (not shown).

In addition to mitochondrial elongation, HeLa cells expressing ARL2[Q70L] appeared larger or more spread out than control cells, as the cells appeared to cover a larger surface area when imaged. When collecting z stacks we noted that these cells also appeared to be thicker, as more z sections were required to capture the entire cell, indicating a larger cell volume and not just a flatter cell. Though we did not pursue this further, the observation that ARL2[Q70L] might lead to an increase in cell size is consistent with previously reported results that cells depleted of ARL2 appear to be smaller (Beghin et al., 2007).

We have previously reported that expression of ARL2[Q70L] also causes microtubule loss (Zhou et al., 2006). To rule out the possibility that mitochondrial elongation may be secondary to changes in microtubules we generated a series of point mutations intended to abrogate binding to a subset of effectors, based on the crystal structures of ARL2 bound to two effectors, BART and PDEδ (Bhamidipati et al., 2000; Hanzal-Bayer et al., 2002; Zhang et al., 2009). We found that combining either [F50A] or [L3A] point mutations with ARL2[Q70L] greatly reduced the ability to cause microtubule loss (Francis et al., manuscript in preparation). In contrast, ARL2[Q70L, F50A] or ARL2[Q70L, L3A] caused a similar degree of mitochondrial elongation (48% and 56%, respectively) as the ARL2[Q70L] mutation alone (66%; Figure 1B). Together, these data suggest that changes in ARL2 activity in cells correlates with mitochondrial morphology, with more activity linked to elongation and less activity linked to fragmentation. Like other members of the ARF family of regulatory GTPases, ARL2 has multiple effectors and sites of action. Our data indicate that effects of ARL2 on mitochondrial morphology are distinct from those on ATP levels or microtubule dynamics. Thus, we explored potentially novel sites and mechanisms of action for its effects on mitochondria.

ARL2 regulates mitochondrial fusion

Mitochondrial morphology results from a balance of fission and fusion. Disruption of either of these processes leads to abnormal mitochondrial morphology, with consequences to functions (Mishra and Chan, 2014). Previously, we reported that co-expression of ARL2[T30N] with DRP1[K38A] reversed the fragmentation caused by ARL2[T30N]. Because DRP1 is required for mitochondrial fission and this mutation acts in a dominant negative fashion, we concluded that ARL2[T30N] was causing an increase in mitochondrial fission (Newman et al., 2014a). However, expression of DRP1[K38A] also reverses fragmentation associated with defects in mitochondrial fusion (Chen et al., 2003). Therefore, we reopened the question as to whether ARL2 acts in the fission or fusion pathways, using two independent approaches.

We monitored mitochondrial fusion in live cells using photoactivatable GFP (PAGFP), as described previously (Karbowski et al., 2004; Karbowski et al., 2014) and under Methods. Briefly, cells were co-transfected with matrix-targeted photoactivatable GFP (mito-PAGFP) and a mitochondrial marker (mito-dsRed). A region of interest (ROI) was then photoactivated, and fluorescence within the entire cell was monitored with time lapse imaging or single images for up to 40 minutes, to determine the speed with which the GFP signal moved away from the ROI. While the mito-dsRed marks all mitochondria at all time points, the matrix localized PAGFP can only spread to mitochondria outside of the ROI by either rapid diffusion within one mitochondria (note the green signal just outside of the ROI even at 0 minutes in Fig. 2A in the ARL2 expressing cell), or after fusion between mitochondria, as documented earlier (Karbowski et al., 2004). Thus, a decrease in the rate of spreading of the green (mito-PAGFP) fluorescence from the ROI into the rest of the cell is interpreted as a defect in the rate of mitochondrial fusion. Cells were co-transfected with mito-PAGFP, mito-dsRed, and either ARL2 or ARL2[T30N]. In cells

overexpressing ARL2, the GFP signal was very clearly reduced within the ROI and spread throughout the cell within the 40 minutes of imaging (Fig. 2B, left panels). In contrast, expression of ARL2[T30N] resulted in the obvious decrease in the rate of spreading of photoactivated mito-PAGFP to the rest of the mitochondrial network under the same conditions and time frame (Figure 2A, right panels). We quantified the rate of spreading of activated mito-PAGFP by determining the percentage of red (mito-dsRed) pixels that were also green (Fig. 2B), as previously described and characterized (Zunino et al., 2009; Anand et al., 2014). The difference in this ratio between 0 minutes (immediately after photoactivation) and 40 minutes after photoactivation is reported as percent increase in mitochondrial fusion (Fig. 2B). We found that cells receiving empty vector had a 30% increase in mitochondrial fusion over the 40 minute imaging window, in agreement with previously reported numbers (Zunino et al., 2009; Anand et al., 2014). Expression of ARL2 had no effect on the rate of mitochondrial fusion (31%). However, we observed a decrease in the rate of fusion in cells expressing ARL2[T30N] to 13% (Figure 2B). We conclude that expression of the dominant negative mutant ARL2 [T30N] results in a block in mitochondrial fusion.

We sought an independent means of assessing effects of ARL2[T30N] on mitochondrial morphology and turned to mdivi-1, a specific inhibitor of DRP1 that causes lengthening and increased branching of mitochondria as a result of ongoing fusion in the absence of fission (52). Though this approach is conceptually similar to expression of DRP1[K38A], which also inhibits DRP1 and blocks fission, mdivi-1 works in a much shorter time frame (<15 minutes) and thus is less prone to artifacts resulting from extended periods of changes in mitochondrial morphologies. If expression of ARL2[T30N] results in an increase in fission, then we predict that mdivi-1 should reverse the fragmentation phenotype observed. In contrast, if the ARL2 mutant blocks fusion we predict no effect on fragmented mitochondria. We tested the effects of mdivi-1 in COS7 cells, where it was previously described (Cassidy-Stone et al., 2008).

Cells were co-transfected with mito-GFP and either ARL2 or ARL2[T30N], and the next day live cells were imaged every 5 min for 15 min after addition of mdivi-1 (50 μM). In untransfected cells or those over-expressing ARL2, addition of mdivi-1 led to mitochondrial lengthening and an increase in branching within the 15 minute imaging window in 11 out of 14 ARL2-expressing cells examined across two independent experiments. In contrast, mdivi-1 is unable to promote mitochondrial lengthening and branching in cells expressing ARL2[T30N] (0 out of 13 cells examined across two independent experiments), suggesting that fusion is impaired in these cells. Together, the results from these two independent assays support the conclusion that expression of ARL2[T30N] results in the loss in mitochondrial fusion.

ARL2 is present in multiple compartment but regulates mitochondrial fusion from the intermembrane space (IMS)

We previously reported that the substantial majority of mitochondria associated ARL2 localizes to the IMS (Sharer et al., 2002), based upon differential solubilization of purified rat brain mitochondria with digitonin, though noted its presence also in a pellet that contained matrix proteins. Later we found additional evidence that some ARL2 is either present in the matrix, using different concentrations of digitonin to solubilize either the outer or inner membrane of fixed cells, followed by immunofluorescence (Newman et al., 2014a). Upon initial analyses of cell and tissue lysates using BN-PAGE, we noted the existence of a band positive for ARL2 in immunoblots migrating slightly above the 480 kDa size marker. Differential centrifugation revealed that this band co-migrated with mitochondrial markers, in contrast to the other major ARL2 immunoreactive band at ~240 kDa that we saw in cytosolic fractions. ARL2 immunoreactivity after BN-PAGE gels, migrating at ~500 kDa, was observed when mouse tissues or several different cultured cell lines were used as starting material so this protein

complex is thought to be present in a wide array of cells. The 500 kDa band was purified starting from a crude preparation of bovine liver mitochondria, solubilized in 1% CHAPS, and fractionated in a 15-35% discontinuous sucrose gradient. Fractions containing the 500 kDa complex were >50% pure and contained only one major contaminant, migrating at ~140 kDa. The band at 500 kDa was excised and analyzed by LC-MS/MS after trypsin digestion, revealing the predominant presence of the mitochondrial matrix protein HSP60. This heat shock protein has previously been shown to localize to the matrix and homo-oligomerize into heptamers (Cheng et al., 1989), reasonably consistent with its mobility in BN-PAGE gels to a size of ~500 kDa. Immunoblotting of crude cell or tissue lysates or enriched preparations consistently showed that ARL2 and HSP60 co-migrated in the native gels (Figure S1A). The HSP60 heptamer has been shown previously to be unstable upon incubation with ATP or at 4 degrees (Levy-Rimler et al., 2001). We found that the bands migrating at ~500 kDa and staining positive for ARL2 or HSP60 were each lost upon incubation of samples with 10 mM ATP at 4°C overnight, prior to resolution in BN-PAGE gels (Figure S1B). We conclude that there is a pool of ARL2 that is bound to HSP60 and that on the basis of this interaction with a well established matrix protein, and our sub-mitochondrial fractionation and immunofluorescence data. Whether this pool represents a folding intermediate for another pool of monomeric ARL2 that resides in the matrix or is exported back to the IMS cannot be resolved at this time, at least in part because these same BN-PAGE immunoblots are quite insensitive at visualizing small, 20 kDa proteins. We believe that the matrix pool or ARL2 is much smaller than that in the IMS, which is much smaller than the cytosolic pool, based upon quantitative immunoblotting. Thus, ARL2 is unusual, though not unique (Zhou et al., 2016), in demonstrating localization to both the IMS and the matrix, not to mention the cytosol, centrosomes, and nucleus. For this reason, we sought a means for identifying the site of action for ARL2 effects on mitochondrial fusion.

To determine ARL2's site of action in regulating mitochondrial fusion, we used strong N-terminal leader sequences to direct wild type or dominant mutant ARL2 specifically to the IMS, matrix, or cytosol (preventing its import into mitochondria) in HeLa cells. Each of the two mitochondrial localization sequences (MLS) used here have been shown previously to direct fusion proteins to the appropriate site and are cleaved following import, allowing a ready means of monitoring import in immunoblots of whole cell lysates. The MLS from ornithine carbamoyltransferase (OCT, residues 1-32) was used to direct ARL2 proteins to the matrix (Horwich et al., 1985; Horwich et al., 1986), and the MLS from SMAC/Diablo (SMAC, residues 1-59) was used to direct them to the IMS (Ozawa et al., 2007; Sabharwal et al., 2013). Each MLS was fused upstream of ARL2, with insertion of an HA epitope tag between the leader and the ARL2 sequences. The vast majority (estimated at >90% by visual inspection) of OCT-HA-ARL2 and SMAC-HA-ARL2 was determined to be imported, based on their cleavage to a faster migrating species in SDS gels by 24 hours after transfection (Figure S2). We further confirmed that OCT-HA-ARL2 and SMAC-HA-ARL2 are each correctly localized to the matrix and IMS, respectively, based upon staining in fixed cells, after differential permeabilization of mitochondrial membranes with increasing concentrations of digitonin (Figure S3).

We found that addition of even a short epitope tag, HA was used here, to the N-terminus of ARL2 was sufficient to prevent its import into mitochondria. Like other members of the ARF family, the N-terminus of ARL2 forms an amphipathic alpha helix (Zhang et al., 2009). While the ARFs are N-myristoylated and their activation is tightly linked to translocation onto a membrane surface, ARL2 is not N-myristoylated (Sharer et al., 2002) and is not membrane associated. Because a small fraction of total cellular ARL2 is found inside mitochondria in a wide range of cultured cells and tissues, we predict that its N-terminus contains a weak MLS that may be blocked by addition of residues at that end. In contrast, addition of the same tag at the C-terminus should not interfere with import. To test this, we co-expressed either HA-ARL2 or

ARL2-HA with mito-GFP in cells. Cells were later briefly (1 minute) permeabilized immediately prior to fixation to wash out cytosolic ARL2 and facilitate visualization of the mitochondrial pool of ARL2. Following washout, HA staining was clearly observed in cells expressing ARL2-HA, and this staining overlapped extensively with that of mito-GFP, indicating mitochondrial localization (Figure 3A; bottom left and top left, respectively). In contrast, no mitochondrial HA staining was observed in cells expressing HA-ARL2 after washout (Figure 3A, bottom right); despite its expression to comparable levels as ARL2-HA or ARL2 (data not shown). Therefore, addition of an HA tag to the N terminus of ARL2 prevents its import into mitochondria. This is consistent with, but does not prove, that the N-terminus of ARL2 contains a mitochondrial import sequence (Sharer et al., 2002).

We next determined whether the different constructs that are restricted in cellular distribution to the cytosol (HA-ARL2[T30N]), matrix (OCT-HA-ARL2[T30N]), or IMS (SMAC-HA-ARL2[T30N]) were capable of causing mitochondrial fragmentation, similar to untagged ARL2[T30N]. We found that only SMAC-HA-ARL2[T30N] retained the ability to fragment mitochondria (Figure 3B). Expression of SMAC-HA-ARL2[T30N] caused mitochondrial fragmentation in 52% of transfected HeLa cells, compared to 58% of cells expressing untagged ARL2[T30N] (Figure 3C). Because SMAC-HA-ARL2[T30N] was still able to cause mitochondrial fragmentation, despite the retention of the N-terminal HA tag after import to the IMS and cleavage of the SMAC leader, we conclude that this N-terminal extension did not interfere with ARL2 functions at that location. Neither HA-ARL2 nor OCT-HA-ARL2 caused mitochondrial fragmentation to the same magnitude as SMAC-HA-ARL2[T30N] (Figure 3C), suggesting that ARL2[T30N] is inactive in regards to fragmentation when sequestered in the cytosol or matrix. Though cells expressing OCT-HA-ARL2[T30N] displayed a slightly elevated level of fragmentation, the degree of fragmentation observed was inconsistent between experiments and never reached the level observed for SMAC-HA-ARL2[T30N]. A clear

preference for IMS localized ARL2[T30N] in causing fragmentation is further supported by the fact that SMAC-HA-ARL2 expressed to much lower levels than OCT-HA-ARL2 or untagged ARL2 (Figure S2). SMAC-HA-ARL2 was inactive in the fragmentation assay (Figure 3C), confirming that the fragmentation was not simply due to saturation of the IMS with exogenous ARL2.

Because the T30N mutation in every context (with or without leader sequences or HA tags) results in lower levels of expression than the wild type or Q70L mutation in comparable contexts (Zhou et al., 2006; Newman et al., 2014a), we were concerned about the potential for artifacts resulting from differences in protein expression. The IMS is a small compartment and saturation of either the IMS or the mitochondrial import system with excess exogenous protein might confound our interpretation of the data shown in Figure 3C. To minimize this possibility, we used a series of variable strength CMV promoters to drive SMAC-HA-ARL2[T30N] into the mitochondrial IMS (Morita et al., 2012) (Newman, Schiavon, and Kahn, manuscript submitted). This is a series of 7 promoters with increasing truncation of the CMV promoter, with the largest truncation (CMVΔ6) resulting in the lowest level of expression (Morita et al., 2012). We found that even the weakest (CMVΔ6) promoter, was sufficient to achieve near maximal levels of fragmentation (Figure 3C). Given the requirement for the dominant negative mutation, the strong preference for IMS targeting and the inactivity in this assay of cytosolic or matrix localized proteins, we conclude that ARL2 regulates mitochondrial fusion from the IMS.

ARL2 acts upstream of the mitofusins

Mitochondrial fusion is mediated by and dependent upon three large, dynamin-related GTPases. Mitofusins 1 and 2 (MFN1, MFN2) have overlapping roles in outer membrane fusion, and OPA1 regulates inner membrane fusion (Mishra and Chan, 2014). From the IMS, ARL2 has

direct access to both mitochondrial membranes so could potentially regulate the mitofusins, OPA1, or some unknown component in the fusion pathway. To begin to address the molecular mechanisms of ARL2 action on mitochondrial fusion, we tested for the dependence of ARL2-mediated elongation on MFN1, MFN2, or OPA1. We used the previously characterized, immortalized MEF lines established from *mfn1*$^{-/-}$, *mfn2*$^{-/-}$, *mfn1*$^{-/-}$*mfn2*$^{-/-}$, and *opa1*$^{-/-}$ mice. Each of these MEF lines displayed fragmented mitochondria due to defective mitochondrial fusion (Chen et al., 2003; Koshiba et al., 2004; Chen et al., 2005; Song et al., 2007). We tested whether expression of the activated mutant, ARL2[Q70L], was able to rescue these morphological defects, resulting from deletion of the other GTPases.

Strikingly, expression of activated ARL2 (ARL2[Q70L]) was sufficient to largely reverse the fragmentation of mitochondria resulting from deletion of MFN1 or MFN2, but not that from OPA1. We first examined the effects of ARL2 or ARL2[Q70L] expression in *mfn2*$^{-/-}$ MEFs. In *mfn2*$^{-/-}$ MEFs receiving empty vector, 26% of cells displayed tubular mitochondria – the remaining cells had mitochondria that were completely fragmented (44%), or displayed short tubes that were distinct from a normal, tubular mitochondrial morphology (30%), using the scoring criteria described under Methods (examples shown in Figure 4C), as previously described (Hoppins et al., 2011). Expression of ARL2[Q70L] restored tubular morphology in 55% of transfected cells (Figure 4A, B). In most cells expressing ARL2[Q70L] we saw obviously longer mitochondria that also contained looping structures, similar to what we observed in HeLa cells (compare Figures 1A and 4A). Somewhat surprisingly, we also observed that cells overexpressing ARL2 also regained tubular morphology, to a similar extent as cells expressing ARL2[Q70L]. However, ARL2 expressing cells only occasionally displayed elongated mitochondria with looping structures, and typically only in the cells displaying the strongest ARL2 expression (compare Figure 4A, middle and right panels). The majority of ARL2 expressing cells had a mitochondrial morphology that was similar to that found in wild type MEFs. Though we note the

differences between elongated and normal morphology, both were scored as tubular mitochondria in our assay. This effect was transient as we observed reversal of fragmentation in *mfn2*$^{-/-}$ MEFs 24 hours after transfection, but the effect was gone by 48 hours.

ARL2[Q70L] was also able to rescue mitochondrial morphology in cells deleted for MFN1, though it did so at later times after expression. We note that cells lacking MFN1 were more fragmented than those lacking MFN2 and had essentially no tubular mitochondria (compare Figures 4A and 5A or quantification in Figures 4B and 5B). We performed a time course and found that the reversal of fragmentation began 2 days after transfection and peaked 51 hours after transfection. At this time point, 16% of ARL2[Q70L] expressing *mfn1*$^{-/-}$ MEFs displayed tubular mitochondria, clearly more than the 0% seen with empty vector or 3% in cells expressing ARL2 (Figure 5A, B). The number of cells displaying the intermediate mitochondrial morphology ("short tubes") was also increased (32%), compared to cells receiving empty vector (11%) or expressing ARL2 (18%). Combining these two categories, ARL2[Q70L] reduced mitochondrial fragmentation in 48% of transfected cells, compared to 11% of cells receiving empty vector or 21% expressing ARL2 (Figure 5B). Thus, ARL2[Q70L] approached the ability of MFN2-myc to reverse the fragmentation of mitochondria seen in MEFs deleted for MFN1 (Figure 5B).

Given that ARL2[Q70L] could rescue the mitochondrial fragmentation present in either *mfn2*$^{-/-}$ or *mfn1*$^{-/-}$ MEFs, we next asked it could do so in the absence of both mitofusins, using the *mfn1*$^{-/-}$*mfn2*$^{-/-}$ MEFs. We obtained lower transfection efficiencies and expression of ARL2 or ARL2[Q70L] in *mfn1*$^{-/-}$ *mfn2*$^{-/-}$ MEFs, so we had to use higher laser power to image these cells, resulting in a higher background of cytosolic ARL2 in our images (Figure 6A). Expression of neither ARL2 nor ARL2[Q70L] reversed the fragmentation at 24 or 48 hours after transfection. In contrast, transient expression of either MFN1-myc or MFN2-myc rescued a large percentage of transfected cells (Figure 6B).

Expression of ARL2[Q70L] was also unable to rescue fragmentation in cells lacking OPA1. We expressed ARL2 or ARL2[Q70L] in opa1-/- MEFs and found no reversal of fragmentation, at either 24 or 48 hours. Similar to *mfn1*$^{-/-}$*mfn2*$^{-/-}$ MEFs, lower expression of ARL2 was observed, so we used higher laser power to image cells (Figure 7A). In contrast, the transient expression of epitope tagged OPA1 restored tubular morphology in 46% of transfected cells and at least partial rescue was seen in 27% of transfected cells (Figure 7B). Thus, reversal of fragmentation by ARL2[Q70L] requires at least one mitofusin and OPA1.

ARL2 forms regularly spaced puncta that align with the mitofusins

In order for increased ARL2 activity in the IMS to reverse the fragmentation phenotype resulting from the loss of either mitofusin, but fail to do so when both are deleted, we posited that ARL2 may regulate the activity of the remaining mitofusin, either directly or indirectly. To begin to explore this model we asked if ARL2 and mitofusins share physical proximity. Wide field, or even confocal, microscopy lack the spatial resolution to determine sub-mitochondrial locations for proteins so we performed structured illumination microscopy (SIM) on cells stained for endogenous ARL2 and mitochondrial markers. COS7 cells were chosen for these experiments because they are large, flat, and have strong endogenous mitochondrial ARL2 staining. We noted earlier that confocal images of endogenous ARL2 in cells showed mitochondrial staining that was more punctate in appearance than expected for a protein freely diffusible in the IMS. Reconstructions of three dimensional SIM images clearly sharpened these differences, making them even more obvious. In our reconstructed images, we observed that ARL2 localizes to discrete puncta along mitochondria (Figure 8) and these puncta often appeared to display regularity in spacing. We used ImageJ to perform line scan analysis through cells, and demonstrate that these puncta often show periodicity, repeating at an interval of ~0.4 μm (Figure

8). These ARL2-positive puncta were also observed in HeLa cells and displayed similar spacing, though in this case cytosolic ARL2 staining obscured the mitochondrial puncta unless it was removed by cell permeabilization prior to fixation (data not shown), due to a weaker signal from mitochondrial ARL2 in that cell line. We also observed these puncta in MEFs, though we found them more difficult to image compared to COS7 because these cells are not as flat. Additionally, we observed ARL2 puncta if we permeabilized with either Triton X100 (0.1%, 10 minutes at room temperature) or methanol (5 minutes at -20), suggesting that these puncta are not artifacts of permeabilization. In attempts to determine how widespread such regularly spaced punctate staining of mitochondrial proteins may be, we performed dual labeling experiments with several mitochondrial markers, including cytochrome C, TOM20, HSP60, a subunit of each of complexes I (NDUFA9), III (UQCRC2), or V (subunit alpha), DRP1, or mic60/mitophilin. None showed staining patterns similar to what we observed for ARL2 (data not shown). We also examined co-localization with ARL2 after expression of MFF-GFP, DRP1-YFP, or SMAC(1-59)-GFP, and again found no evidence of co-staining with ARL2 positive puncta (data not shown). The ARL2 effector BART also localizes to mitochondria (Sharer et al., 2002), and it appeared as diffuse staining along mitochondria and thus not evident in ARL2 puncta.

In marked contrast to the negative data for a large number of mitochondrial proteins, we found that mitofusins do overlap with ARL2 in discrete puncta along mitochondria. We were unable to find an antibody to either MFN1 or MFN2 that was useful in such studies, so we expressed C-terminal myc-tagged MFN1/2, and stained for myc in fixed COS7 cells. Because overexpression of mitofusins can lead to hyperfusion, perinuclear clustering, and even fragmentation at higher levels (Santel and Fuller, 2001; Eura et al., 2003), we chose to transfect a low amount (0.5 μg) of either plasmid, which proved to be optimal for minimizing expression while maintaining a transfection efficiency of ~40-50%. Only cells that had an apparently normal mitochondrial morphology were selected for imaging. We found that MFN1-myc and MFN2-myc

each localize to puncta (Figure 9) along mitochondria and displayed very similar staining patterns to each other and to ARL2. When co-staining for endogenous ARL2 and MFN1/2-myc, we found that the puncta appeared to be adjacent. Further, we noted that the ARL2 signal was often sandwiched in between two mitofusin puncta, and this pattern was true for both MFN1-myc and MFN2-myc. This adjacent and partially-overlapping staining pattern is consistent with the localization of ARL2 to the IMS and mitofusins to the outer membrane, as the C terminal myc tag is predicted to face the cytosol based on predicted mitofusin topology (Rojo et al., 2002). This staining also suggests that both ARL2 and mitofusins are concentrated in loci and may not be freely diffusible in the IMS or outer membrane, respectively. MFN puncta also appeared to display the same periodicity as ARL2 puncta, as they typically were found adjacent to ARL2 puncta. This pattern of MFN-myc localization was consistent across varying levels of MFN-myc expression examined.

We then asked if OPA1 also aligned with ARL2 puncta along mitochondria in COS7 cells. We first examined endogenous OPA1, and found that OPA1 also formed puncta along mitochondria. However, these puncta did not show any consistent spatial correlation with ARL2 puncta; i.e., they appeared next to ARL2 puncta as well as in between ARL2 puncta. OPA1 puncta also appeared to repeat along mitochondria at a different interval from ARL2 puncta that was less uniform. We also expressed OPA1-myc/his in COS7 cells and stained for the myc epitope. OPA1-myc/his expression caused mitochondrial fragmentation in some cells and elongation in others. Despite this we were able to image in each case. Labeling for expressed OPA1-myc in COS7 cells using SIM revealed puncta that appeared similar to endogenous OPA1 staining, in that they displayed no obvious regularity in spacing and were not correlated with those positive for ARL2 (Figure 10).

Thus, we conclude that ARL2 and mitofusins display novel localization along mitochondria that includes a punctate staining pattern with periodicity of ~0.4 μm. These features

were not observed for a number of other mitochondrial proteins including those that should mark cristae (Complex V subunit alpha), the TOM complex, sites of mitochondrial fission, the MICOS complex, the matrix, or the soluble fraction in the IMS. Our high resolution fluorescence imaging is consistent with ARL2 being present in the IMS and the mitofusins in the outer mitochondrial membrane, with the possibility of them being physically linked, either directly or indirectly, in a larger protein complex with clear implications to mitochondrial fusion.

Discussion

In this study, we identify the small GTPase ARL2 as a novel regulator of mitochondrial fusion, acting from the IMS and capable of promoting fusion through a mitofusin-dependent pathway. The findings that dominant mutants with opposite effects on ARL2 activity have opposing effects on mitochondrial morphology strongly support a role for ARL2 in regulation of mitochondrial morphology. Using two independent assays, we show that the dominant negative ARL2[T30N] causes mitochondrial fragmentation as a result of a defect in fusion and that expression of the dominant activating ARL2[Q70L] mutant leads to hyperfusion and elongation of mitochondria. By targeting ARL2[T30N] to different sub-mitochondrial compartments or cytosol we found that its effects on fusion only occur from the IMS. The finding that expression of ARL2[Q70L] is sufficient to restore fusion in MEFs deleted for either MFN1 or MFN2, but not both, is consistent with ARL2 acting as a positive regulator of mitofusin actions but requiring at least one of them to act. Using super resolution microscopy, we discovered that ARL2 localizes to discrete, regularly spaced puncta along mitochondria that align with mitofusins but not with a number of markers of known mitochondrial complexes, including those for electron chain complexes, MICOS, or the TOM importer. Thus, in addition to describing this novel role for ARL2 in mitochondrial fusion we speculate that there exists a novel protein complex that includes at least ARL2 and mitofusins that is involved in the fusion process but that requires additional work to confirm.

Expression of ARL2[T30N] causes mitochondrial fragmentation, as we previously reported (Newman et al., 2014a), and expression of ARL2[Q70L] causes mitochondrial elongation. These observations suggest that increasing or decreasing ARL2 activity regulates mitochondrial shape in opposite ways. These mutations are homologous to those used extensively in ARF family and RAS superfamily research. Mutation of glutamine 70 in ARL2[Q70L] acts as a dominant activating mutation, like ARF1[Q71L](Zhang et al., 1994; Van Valkenburgh et al., 2001) or RAS[Q61L](Vogel et al., 1988; Gideon et al., 1992), as this residue is directly involved in coordinating a water molecule that attacks the β-γ phosphate bond to hydrolyze the bound GTP, leading to persistent activation of the GTPase. In contrast, the ARL2[T30N] is thought to act analogously to ARF1[T31N](Dascher and Balch, 1994) or RAS[S17N](van den Berghe et al., 1999), to decrease affinity for guanine nucleotides, mimic the transition state in the exchange factor-mediated activation process, and thereby prevent activation of the mutant or endogenous GTPases that share a common exchange factor. Thus, our observations that the activating mutant of ARL2 promotes fusion and the inactivating mutant causes fragmentation, as a result of inhibition of fusion, are completely consistent with a model in which ARL2 acts as a classical regulatory GTPase to regulate the fusion process. Such a model is further supported by our findings that the ARL2 GTPase activating protein (GAP), ELMOD2 (Bowzard et al., 2007; East et al., 2012; Ivanova et al., 2014; Newman et al., 2014b), also localizes to mitochondria and its knockdown also causes mitochondrial fragmentation and loss of motility (Newman et al., 2014a). And again, the model that a GAP acts as both an effector and terminator of GTPase signaling (via promotion of GTP hydrolysis) is completely consistent with paradigms for the actions of ARF family GTPases and their interactors (East and Kahn, 2011).

Because inhibition of mitochondrial fission can mimic activation of fusion, and vice versa, it can be difficult to clearly distinguish mechanisms and pathways for novel regulators. We now believe that we misinterpreted our earlier experiments that depended solely upon expression

of a dominant negative mutant of DRP1 (Newman et al., 2014b), so in the current study we used two independent methods to identify which process may be regulated by ARL2. The most rigorous test of mechanism was to monitor the rate at which a matrix localized PAGFP spread throughout the mitochondrial network, as this assay has been well documented and characterized (Karbowski et al., 2004; Zunino et al., 2009; Anand et al., 2014; Karbowski et al., 2014). We found that expression of ARL2[T30N] blocked the spread of photoactivated matrix-localized GFP, which is dependent upon mitochondrial fusion (Figure 2). Thus, we concluded that ARL2 activity in mitochondria is required for fusion. Similarly, fragmentation caused by expression of ARL2[T30N] was not altered by inhibition of fission, using the DRP1 inhibitor mdivi-1. This drug causes elongation and increased branching of mitochondria as a result of ongoing fusion after inhibition of fission (Cassidy-Stone et al., 2008), but this effect was ablated in cells expressing ARL2[T30N], again supporting a role for ARL2 activity in fusion. Together these data strongly implicate increased ARL2 activity with increases in mitochondrial fusion and decreased ARL2 activity with loss of fusion, though we cannot rule out that ARL2 may also influence mitochondrial fission. These data are also consistent with our earlier observation that depletion of ARL2 via siRNA also caused fragmentation of mitochondria (Newman et al., 2014a) and further support our conclusion that ARL2 activity promotes fusion.

There are several other proteins with well-established roles outside of mitochondria, later shown to act on different pathways inside mitochondria; including STAT3 (Gough et al., 2009; Wegrzyn et al., 2009), MEF2D (She et al., 2011), fumarase (Yogev et al., 2011), several DNA repair proteins (Bauer et al., 2015a), and others (Regev-Rudzki et al., 2008; Yogev et al., 2011; Li et al., 2012; Ackema et al., 2014; Petrungaro and Riemer, 2014; Bauer et al., 2015b). Based upon fractionation of cultured cells and mammalian tissues we have estimated that ~5-10% of cellular ARL2 is found in mitochondria, with the vast majority of the rest in cytosol, complexed to the tubulin co-chaperone cofactor D or at centrosomes (Sharer et al., 2002; Shern et

al., 2003; Zhou et al., 2006). This is a rough estimate and likely to vary with cell or tissue type. In contrast to these other proteins with dual localization outside and inside mitochondria, we have found evidence that ARL2 localizes to at least two different compartments in mitochondria; IMS and matrix, though the latter is quite small in percentage of total ARL2 and could represent an intermediate in traffic or degradation. Indeed, this situation might be analogous to the mitochondrial traffic of the STaR protein, which is thought to act at the outer mitochondrial membrane while in transit to the matrix (Bose et al., 2002). Though unusual, at least one other protein, CPS-6, also localizes to both the IMS and matrix (Zhou et al., 2016). Our data support the model that it regulates fusion from the IMS. Whether the pool of matrix ARL2, identified in complex with HSP60, is a folding intermediate, an import intermediate, heading toward degradation, or a specific function in the matrix is unknown. Its presence in multiple compartments has complicated analyses but is also consistent with our model that ARL2 plays at least two distinct roles in mitochondria; regulator of fusion from the IMS and of ATP from a currently undefined site.

We also have found evidence that the fraction of cellular ARL2 inside mitochondria can change in response to stressors, e.g., deletion of ANT1 (Sharer et al., 2002). Based upon our findings that even small epitope tags added to the N-terminus (Figure 3A) or deletion of the N-terminal 9 residues of ARL2 (unpublished observation) prevents its import into mitochondria, we believe it has a MLS at its N-terminus. Such a conclusion is also consistent with the use of N-terminal amphipathic helices (a hallmark of members of the ARF family of regulatory GTPases (80)) serving as import sequences (Hartl and Neupert, 1989; Neupert, 1997; Neupert and Herrmann, 2007), but unlike many we see no evidence that ARL2 is cleaved upon import as the electrophoretic mobility in SDS is unaltered when comparing mitochondrial or cytosolic ARL2. At this point we do not understand the mechanism(s) by which mitochondrial import of ARL2 is regulated, though speculate that changes in localization may provide the cell a means of

communication between different essential processes, e.g., mitotic spindle formation and energy metabolism.

Because ARL2 localizes to multiple sites in all cells we used N-terminal fusions of previously characterized MLSs to drive ARL2 to different compartments and assess consequences to mitochondrial morphology. We show that ARL2[T30N] is most active to cause mitochondrial fragmentation when targeted to the IMS. Only SMAC-HA-ARL2[T30N] was able to cause mitochondrial fragmentation to a similar extent as untagged ARL2[T30N]. The observations that SMAC-HA-ARL2 did not cause fragmentation, and that SMAC-HA-ARL2[T30N] still was able to promote fragmentation when expressed from a greatly weakened CMV promoter, CMV6 (Morita et al., 2012), supports the idea that the mitochondrial fragmentation we observed is not due to saturation of the IMS or mitochondrial import system. This conclusion is further strengthened by the observation that while the wild type and [Q70L] mutant proteins are expressed to comparable levels, ARL2[T30N] is always found at lower levels due to its relative instability, resulting from its decreased affinity for guanine nucleotides. We also interpret our SIM data as supporting evidence that endogenous ARL2 localizes to the IMS (see below). Therefore, we conclude that ARL2 acts from the IMS to regulate mitochondrial fusion.

We show that expression of ARL2[Q70L] reverses the loss of either MFN1 or MFN2, but not both, and interpret these data as evidence that ARL2 can increase the activity of either mitofusin to promote fusion. The kinetics of rescue differed among the different MEF lines, with rescue in *mfn2*$^{-/-}$ MEFs observed at 24 hours after transfection and gone by 48 hours, while reversal of fragmentation in *mfn1*$^{-/-}$ MEFs took 48 hours to appear. Given that the same plasmid is used for rescue of each we believe this difference in kinetics is a reflection of the previously described (Ishihara et al., 2004) differences in fusogenic properties of MFN1 and MFN2. While the two proteins share 60% identity (Santel et al., 2003) and a level of functional redundancy,

they differ in that MFN2 is thought to have additional metabolic roles (Bach et al., 2003; Chen et al., 2005; Pich et al., 2005; Mourier et al., 2015; Schrepfer and Scorrano, 2016) and is proposed to play a role in mitochondria/ER tethering (de Brito and Scorrano, 2008), though this is contested (Cosson et al., 2012; Filadi et al., 2015). The fusion activity in MFN1, still present in the *mfn2*$^{-/-}$ MEFs, is probably higher than that of MFN2 present in *mfn1*$^{-/-}$ MEFs, as evidenced by the higher percentage of cells with tubular morphology in *mfn2*$^{-/-}$ MEFs (26%) compared to *mfn1*$^{-/-}$ MEFs (0%). This is also consistent with the observation that MFN1 has better tethering and fusion activity in vitro (Ishihara et al., 2004). We speculate that the higher fusogenic activity of MFN1 over that of MFN2 in MEFs also explains our result that overexpression of ARL2 was able to rescue *mfn2*$^{-/-}$, but not *mfn1*$^{-/-}$ MEFs.

Importantly, ARL2[Q70L] was unable to reverse fragmentation in *mfn1*$^{-/-}$ *mfn2*$^{-/-}$ MEFs, demonstrating that elongation mediated by ARL2[Q70L] is dependent on the presence of a mitofusin, as previously shown for mitochondrial fusion (Chen et al., 2005). ARL2[Q70L] was also unable to reverse fragmentation in *opa1*$^{-/-}$ MEFs, consistent with the fact that OPA1 is also absolutely required for fusion (Chen et al., 2005). Though we cannot definitively rule out the possibility of an effect on fission, we interpret this as evidence that ARL2 stimulates fusion upstream of mitofusins. To the best of our knowledge, only two other proteins are known to reverse fragmentation when expressed in either *mfn1*$^{-/-}$ or *mfn2*$^{-/-}$ MEFs (besides the mitofusins themselves, and DPR1[K38A], which blocks fission (Chen et al., 2003)). Expression of Bax restores tubular morphology in *mfn1*$^{-/-}$ but not *mfn2*$^{-/-}$ MEFs (Hoppins et al., 2011), and expression of OPA1 causes elongation in *mfn2*$^{-/-}$ but not *mfn1*$^{-/-}$ MEFs (Cipolat et al., 2004). Therefore, ARL2 is unique not only in that it can reverse fragmentation in these MEFs, but that it can do so through either MFN1 or MFN2. Together with our SIM data showing similar staining patterns between ARL2 and MFN1/2, we propose that ARL2 acts upstream of mitofusins and causes an increase in mitofusin-dependent fusion activity.

Using high resolution fluorescence imaging, we showed that ARL2 localizes to puncta along mitochondria. After examining 9 different mitochondrial proteins, including those that localize to the matrix, the IMS, the inner membrane or the outer membrane, only MFN1 and MFN2 were found to localize to discrete puncta with the same regular spacing seen for ARL2. Most proteins examined displayed largely diffuse staining along mitochondria (TOM20, cytochrome C, HSP60, BART, SMAC-GFP), while the proteins that localized to puncta (DRP1, MFF, OPA1) did not show any obvious relationship to ARL2 puncta. Additionally, MICOS puncta previously observed by STED microscopy repeat at a much smaller interval than 0.4 μm (Jans et al., 2013) and were difficult to resolve by SIM. Only the mitofusins showed punctate staining that aligned with ARL2 puncta. Note that the myc tag on the mitofusins is at the C-terminus, which is predicted to project out from the outer mitochondrial membrane into the cytosol (Rojo et al., 2002). When double labeling was performed we observed ARL2 staining typically was present adjacent to and even between mitofusin puncta, consistent with ARL2 localization in the IMS to puncta that were positive for mitofusins stained on the outer side of the outer membrane. The fact that no other mitochondrial proteins, with the exception of the mitofusins, displayed such localization suggests a specific physical relationship between ARL2 and the mitofusins. It has been previously described that MFN2 forms puncta along mitochondria, and mutation of a residue involved in nucleotide binding disrupts this localization (Neuspiel et al., 2005). During apoptosis, MFN2 also forms puncta that co-localize with Bax and DRP1 (Karbowski et al., 2002). These observations support the idea that mitofusins may not be freely diffusible along the outer membrane, and suggest that there may be functional significance to mitofusin (and ARL2) puncta.

To summarize, we provide evidence that ARL2 can regulate mitochondrial fusion from the IMS and that it does so upstream of the mitofusins. To the best of our knowledge, this is the first IMS-acting regulator of mitofusins identified. The only other proteins implicated in

regulating fusion from the IMS are proteases embedded in the inner membrane that cleave OPA1 (Griparic et al., 2007; Song et al., 2007; Ehses et al., 2009; Head et al., 2009). In addition, the little that is known about regulation of mitofusins occurs from the cytosol and outer membrane, not the IMS. MIB binds mitofusins and may directly regulate their activity, while the mechanism for Bax-stimulated MFN2 activity is unknown (Eura et al., 2006; Hoppins et al., 2011). In addition, mitofusin 1 activity is regulated by phosphorylation (Pyakurel et al., 2015) and acetylation (Lee et al., 2014). Our data also provide preliminary support for the existence of a novel structure or protein complex that contains at a minimum ARL2 and mitofusins and that may serve as the site of fusion coordination or nucleation. Therefore, we believe we have uncovered a novel regulator of mitochondrial fusion that is clearly distinct from other previously identified regulators. Further study of ARL2 and this putative protein complex will build upon these observations and help define the molecular mechanisms of mitochondrial fusion and its regulation in health and disease.

Acknowledgements: We thank Drs. David Chan (Caltech), Heidi McBride (McGill), Richard Youle (NIH), James Zheng (Emory), Gia Voeltz (University of Colorado), and Alexa Mattheyses (Emory) for their generous gift of plasmids. We gratefully acknowledge Drs. Heidi McBride, David Chan, and Gerald Shadel for their ideas in discussions of this work at various stages. We thank Dr. Alexa Mattheyses, Laura Fox-Goharioon, and Neil Anthony of the Integrated Cellular Imaging (ICI) core at Emory University for assistance with obtaining and analyzing imaging data in this paper. This research project was supported in part by the Emory University Integrated Cellular Imaging Microscopy Core of the Emory Neuroscience NINDS Core Facilities grant, P30NS055077. This work was supported by grants from the National Institutes of Health 5R01GM090158 to RAK and 1F31GM111047 to LEN, and an American Heart Association pre-doctoral fellowship 14PRE18840040 to LEN.

References

Ackema, K.B., Hench, J., Bockler, S., Wang, S.C., Sauder, U., Mergentaler, H., Westermann, B., Bard, F., Frank, S., and Spang, A. (2014). The small GTPase Arf1 modulates mitochondrial morphology and function. EMBO J 33, 2659-2675.

Alexander, C., Votruba, M., Pesch, U.E., Thiselton, D.L., Mayer, S., Moore, A., Rodriguez, M., Kellner, U., Leo-Kottler, B., Auburger, G., Bhattacharya, S.S., and Wissinger, B. (2000). OPA1, encoding a dynamin-related GTPase, is mutated in autosomal dominant optic atrophy linked to chromosome 3q28. Nat Genet 26, 211-215.

Anand, R., Wai, T., Baker, M.J., Kladt, N., Schauss, A.C., Rugarli, E., and Langer, T. (2014). The i-AAA protease YME1L and OMA1 cleave OPA1 to balance mitochondrial fusion and fission. J Cell Biol 204, 919-929.

Antoshechkin, I., and Han, M. (2002). The C. elegans evl-20 gene is a homolog of the small GTPase ARL2 and regulates cytoskeleton dynamics during cytokinesis and morphogenesis. Dev Cell 2, 579-591.

Bach, D., Pich, S., Soriano, F.X., Vega, N., Baumgartner, B., Oriola, J., Daugaard, J.R., Lloberas, J., Camps, M., Zierath, J.R., Rabasa-Lhoret, R., Wallberg-Henriksson, H., Laville, M., Palacin, M., Vidal, H., Rivera, F., Brand, M., and Zorzano, A. (2003). Mitofusin-2 determines mitochondrial network architecture and mitochondrial metabolism. A novel regulatory mechanism altered in obesity. J Biol Chem 278, 17190-17197.

Bauer, N.C., Corbett, A.H., and Doetsch, P.W. (2015a). The current state of eukaryotic DNA base damage and repair. Nucleic Acids Res 43, 10083-10101.

Bauer, N.C., Doetsch, P.W., and Corbett, A.H. (2015b). Mechanisms Regulating Protein Localization. Traffic 16, 1039-1061.

Beghin, A., Honore, S., Messana, C., Matera, E.L., Aim, J., Burlinchon, S., Braguer, D., and Dumontet, C. (2007). ADP ribosylation factor like 2 (Arl2) protein influences microtubule dynamics in breast cancer cells. Exp Cell Res 313, 473-485.

Bhamidipati, A., Lewis, S.A., and Cowan, N.J. (2000). ADP ribosylation factor-like protein 2 (Arl2) regulates the interaction of tubulin-folding cofactor D with native tubulin. J Cell Biol 149, 1087-1096.

Bose, H.S., Lingappa, V.R., and Miller, W.L. (2002). Rapid regulation of steroidogenesis by mitochondrial protein import. Nature 417, 87-91.

Bowzard, J.B., Cheng, D., Peng, J., and Kahn, R.A. (2007). ELMOD2 is an Arl2 GTPase-activating protein that also acts on Arfs. J Biol Chem 282, 17568-17580.

Cassidy-Stone, A., Chipuk, J.E., Ingerman, E., Song, C., Yoo, C., Kuwana, T., Kurth, M.J., Shaw, J.T., Hinshaw, J.E., Green, D.R., and Nunnari, J. (2008). Chemical inhibition of the mitochondrial division dynamin reveals its role in Bax/Bak-dependent mitochondrial outer membrane permeabilization. Developmental cell 14, 193-204.

Chan, D.C. (2012). Fusion and fission: interlinked processes critical for mitochondrial health. Annu Rev Genet 46, 265-287.

Chen, H., Chomyn, A., and Chan, D.C. (2005). Disruption of fusion results in mitochondrial heterogeneity and dysfunction. J Biol Chem 280, 26185-26192.

Chen, H., Detmer, S.A., Ewald, A.J., Griffin, E.E., Fraser, S.E., and Chan, D.C. (2003). Mitofusins Mfn1 and Mfn2 coordinately regulate mitochondrial fusion and are essential for embryonic development. The Journal of Cell Biology 160, 189-200.

Chen, H., McCaffery, J.M., and Chan, D.C. (2007). Mitochondrial fusion protects against neurodegeneration in the cerebellum. Cell 130, 548-562.

Chen, H., Vermulst, M., Wang, Y.E., Chomyn, A., Prolla, T.A., McCaffery, J.M., and Chan, D.C. (2010). Mitochondrial fusion is required for mtDNA stability in skeletal muscle and tolerance of mtDNA mutations. Cell 141, 280-289.

Cheng, M.Y., Hartl, F.U., Martin, J., Pollock, R.A., Kalousek, F., Neupert, W., Hallberg, E.M., Hallberg, R.L., and Horwich, A.L. (1989). Mitochondrial heat-shock protein hsp60 is essential for assembly of proteins imported into yeast mitochondria. Nature 337, 620-625.

Cipolat, S., de Brito, O.M., Dal Zilio, B., and Scorrano, L. (2004). OPA1 requires mitofusin 1 to promote mitochondrial fusion. Proceedings of the National Academy of Sciences of the United States of America 101, 15927-15932.

Clark, J., Moore, L., Krasinskas, A., Way, J., Battey, J., Tamkun, J., and Kahn, R.A. (1993). Selective amplification of additional members of the ADP-ribosylation factor (ARF) family: cloning of additional human and Drosophila ARF-like genes. Proc Natl Acad Sci U S A 90, 8952-8956.

Cosson, P., Marchetti, A., Ravazzola, M., and Orci, L. (2012). Mitofusin-2 independent juxtaposition of endoplasmic reticulum and mitochondria: an ultrastructural study. PLoS One 7, e46293.

Cunningham, L.A., and Kahn, R.A. (2008). Cofactor D functions as a centrosomal protein and is required for the recruitment of the gamma-tubulin ring complex at centrosomes and organization of the mitotic spindle. J Biol Chem 283, 7155-7165.

Dascher, C., and Balch, W.E. (1994). Dominant inhibitory mutants of ARF1 block endoplasmic reticulum to Golgi transport and trigger disassembly of the Golgi apparatus. J Biol Chem 269, 1437-1448.

de Brito, O.M., and Scorrano, L. (2008). Mitofusin 2 tethers endoplasmic reticulum to mitochondria. Nature 456, 605-610.

Delettre, C., Lenaers, G., Griffoin, J.M., Gigarel, N., Lorenzo, C., Belenguer, P., Pelloquin, L., Grosgeorge, J., Turc-Carel, C., Perret, E., Astarie-Dequeker, C., Lasquellec, L., Arnaud, B., Ducommun, B., Kaplan, J., and Hamel, C.P. (2000). Nuclear gene OPA1, encoding a mitochondrial dynamin-related protein, is mutated in dominant optic atrophy. Nat Genet 26, 207-210.

East, M.P., Bowzard, J.B., Dacks, J.B., and Kahn, R.A. (2012). ELMO domains, evolutionary and functional characterization of a novel GTPase-activating protein (GAP) domain for Arf protein family GTPases. J Biol Chem 287, 39538-39553.

East, M.P., and Kahn, R.A. (2011). Models for the functions of Arf GAPs. Semin Cell Dev Biol 22, 3-9.

Ehses, S., Raschke, I., Mancuso, G., Bernacchia, A., Geimer, S., Tondera, D., Martinou, J.C., Westermann, B., Rugarli, E.I., and Langer, T. (2009). Regulation of OPA1 processing and mitochondrial fusion by m-AAA protease isoenzymes and OMA1. J Cell Biol 187, 1023-1036.

Eura, Y., Ishihara, N., Oka, T., and Mihara, K. (2006). Identification of a novel protein that regulates mitochondrial fusion by modulating mitofusin (Mfn) protein function. Journal of Cell Science 119, 4913-4925.

Eura, Y., Ishihara, N., Yokota, S., and Mihara, K. (2003). Two mitofusin proteins, mammalian homologues of FZO, with distinct functions are both required for mitochondrial fusion. J Biochem 134, 333-344.

Filadi, R., Greotti, E., Turacchio, G., Luini, A., Pozzan, T., and Pizzo, P. (2015). Mitofusin 2 ablation increases endoplasmic reticulum-mitochondria coupling. Proc Natl Acad Sci U S A 112, E2174-2181.

Friedman, J.R., Lackner, L.L., West, M., DiBenedetto, J.R., Nunnari, J., and Voeltz, G.K. (2011). ER Tubules Mark Sites of Mitochondrial Division. Science 334, 358-362.

Gideon, P., John, J., Frech, M., Lautwein, A., Clark, R., Scheffler, J.E., and Wittinghofer, A. (1992). Mutational and kinetic analyses of the GTPase-activating protein (GAP)-p21 interaction: the C-terminal domain of GAP is not sufficient for full activity. Mol Cell Biol 12, 2050-2056.

Gomes, L.C., Di Benedetto, G., and Scorrano, L. (2011). During autophagy mitochondria elongate, are spared from degradation and sustain cell viability. Nature cell biology 13, 589-598.

Gough, D.J., Corlett, A., Schlessinger, K., Wegrzyn, J., Larner, A.C., and Levy, D.E. (2009). Mitochondrial STAT3 supports Ras-dependent oncogenic transformation. Science 324, 1713-1716.

Graham, B.H., Waymire, K.G., Cottrell, B., Trounce, I.A., MacGregor, G.R., and Wallace, D.C. (1997). A mouse model for mitochondrial myopathy and cardiomyopathy resulting from a deficiency in the heart/muscle isoform of the adenine nucleotide translocator. Nat Genet 16, 226-234.

Griparic, L., Kanazawa, T., and van der Bliek, A.M. (2007). Regulation of the mitochondrial dynamin-like protein Opa1 by proteolytic cleavage. J Cell Biol 178, 757-764.

Hanson, B.J., Schulenberg, B., Patton, W.F., and Capaldi, R.A. (2001). A novel subfractionation approach for mitochondrial proteins: a three-dimensional mitochondrial proteome map. Electrophoresis 22, 950-959.

Hanzal-Bayer, M., Renault, L., Roversi, P., Wittinghofer, A., and Hillig, R.C. (2002). The complex of Arl2-GTP and PDE delta: from structure to function. EMBO J 21, 2095-2106.

Hartl, F.U., and Neupert, W. (1989). Import of proteins into the various submitochondrial compartments. J Cell Sci Suppl 11, 187-198.

Head, B., Griparic, L., Amiri, M., Gandre-Babbe, S., and van der Bliek, A.M. (2009). Inducible proteolytic inactivation of OPA1 mediated by the OMA1 protease in mammalian cells. J Cell Biol 187, 959-966.

Hoppins, S., Edlich, F., Cleland, M.M., Banerjee, S., McCaffery, J.M., Youle, R.J., and Nunnari, J. (2011). The soluble form of Bax regulates mitochondrial fusion via MFN2 homotypic complexes. Mol Cell 41, 150-160.

Horwich, A.L., Kalousek, F., Fenton, W.A., Pollock, R.A., and Rosenberg, L.E. (1986). Targeting of pre-ornithine transcarbamylase to mitochondria: Definition of critical regions and residues in the leader peptide. Cell 44, 451-459.

Horwich, A.L., Kalousek, F., Mellman, I., and Rosenberg, L.E. (1985). A Leader Peptide Is Sufficient to Direct Mitochondrial Import of a Chimeric Protein. Embo Journal 4, 1129-1135.

Ishihara, N., Eura, Y., and Mihara, K. (2004). Mitofusin 1 and 2 play distinct roles in mitochondrial fusion reactions via GTPase activity. J Cell Sci 117, 6535-6546.

Ismail, S.A., Chen, Y.-X., Rusinova, A., Chandra, A., Bierbaum, M., Gremer, L., Triola, G., Waldmann, H., Bastiaens, P.I.H., and Wittinghofer, A. (2011). Arl2-GTP and Arl3-GTP regulate a GDI-like transport system for farnesylated cargo. Nat Chem Biol 7, 942-949.

Ivanova, A.A., East, M.P., Yi, S.L., and Kahn, R.A. (2014). Characterization of recombinant ELMOD (cell engulfment and motility domain) proteins as GTPase-activating proteins (GAPs) for ARF family GTPases. J Biol Chem 289, 11111-11121.

Jans, D.C., Wurm, C.A., Riedel, D., Wenzel, D., Stagge, F., Deckers, M., Rehling, P., and Jakobs, S. (2013). STED super-resolution microscopy reveals an array of MINOS clusters along human mitochondria. Proc Natl Acad Sci U S A 110, 8936-8941.

Jeyaraju, D.V., Xu, L., Letellier, M.C., Bandaru, S., Zunino, R., Berg, E.A., McBride, H.M., and Pellegrini, L. (2006). Phosphorylation and cleavage of presenilin-associated rhomboid-like protein (PARL) promotes changes in mitochondrial morphology. Proc Natl Acad Sci U S A 103, 18562-18567.

Karbowski, M., Arnoult, D., Chen, H., Chan, D.C., Smith, C.L., and Youle, R.J. (2004). Quantitation of mitochondrial dynamics by photolabeling of individual organelles shows that mitochondrial fusion is blocked during the Bax activation phase of apoptosis. The Journal of Cell Biology 164, 493-499.

Karbowski, M., Cleland, M.M., and Roelofs, B.A. (2014). Chapter Four - Photoactivatable Green Fluorescent Protein-Based Visualization and Quantification of Mitochondrial Fusion and Mitochondrial Network Complexity in Living Cells. In: Methods in Enzymology, vol. Volume 547, eds. N.M. Anne and C.C. David: Academic Press, 57-73.

Karbowski, M., Lee, Y.J., Gaume, B., Jeong, S.Y., Frank, S., Nechushtan, A., Santel, A., Fuller, M., Smith, C.L., and Youle, R.J. (2002). Spatial and temporal association of Bax with mitochondrial fission sites, Drp1, and Mfn2 during apoptosis. J Cell Biol 159, 931-938.

Koshiba, T., Detmer, S.A., Kaiser, J.T., Chen, H., McCaffery, J.M., and Chan, D.C. (2004). Structural basis of mitochondrial tethering by mitofusin complexes. Science 305, 858-862.

Labrousse, A.M., Zappaterra, M.D., Rube, D.A., and van der Bliek, A.M. (1999). C. elegans dynamin-related protein DRP-1 controls severing of the mitochondrial outer membrane. Mol Cell 4, 815-826.

Lee, J.-Y., Kapur, M., Li, M., Choi, M.-C., Choi, S., Kim, H.-J., Kim, I., Lee, E., Taylor, J.P., and Yao, T.-P. (2014). MFN1 deacetylation activates adaptive mitochondrial fusion and protects metabolically challenged mitochondria. Journal of Cell Science.

Levy-Rimler, G., Viitanen, P., Weiss, C., Sharkia, R., Greenberg, A., Niv, A., Lustig, A., Delarea, Y., and Azem, A. (2001). The effect of nucleotides and mitochondrial chaperonin 10 on the structure and chaperone activity of mitochondrial chaperonin 60. Eur J Biochem 268, 3465-3472.

Li, C.C., Wu, T.S., Huang, C.F., Jang, L.T., Liu, Y.T., You, S.T., Liou, G.G., and Lee, F.J. (2012). GTP-binding-defective ARL4D alters mitochondrial morphology and membrane potential. PLoS One 7, e43552.

Li, Y., Kelly, W.G., Logsdon, J.M., Jr., Schurko, A.M., Harfe, B.D., Hill-Harfe, K.L., and Kahn, R.A. (2004). Functional genomic analysis of the ADP-ribosylation factor family of GTPases: phylogeny among diverse eukaryotes and function in C. elegans. FASEB J 18, 1834-1850.

McElver, J., Patton, D., Rumbaugh, M., Liu, C., Yang, L.J., and Meinke, D. (2000). The TITAN5 gene of Arabidopsis encodes a protein related to the ADP ribosylation factor family of GTP binding proteins. Plant Cell 12, 1379-1392.

Mishra, P., and Chan, D.C. (2014). Mitochondrial dynamics and inheritance during cell division, development and disease. Nat Rev Mol Cell Biol 15, 634-646.

Morita, E., Arii, J., Christensen, D., Votteler, J., and Sundquist, W.I. (2012). Attenuated protein expression vectors for use in siRNA rescue experiments. Biotechniques 0, 1-5.

Mourier, A., Motori, E., Brandt, T., Lagouge, M., Atanassov, I., Galinier, A., Rappl, G., Brodesser, S., Hultenby, K., Dieterich, C., and Larsson, N.G. (2015). Mitofusin 2 is required to maintain mitochondrial coenzyme Q levels. J Cell Biol 208, 429-442.

Muromoto, R., Sekine, Y., Imoto, S., Ikeda, O., Okayama, T., Sato, N., and Matsuda, T. (2008). BART is essential for nuclear retention of STAT3. International Immunology 20, 395-403.

Neupert, W. (1997). Protein import into mitochondria. Annu Rev Biochem 66, 863-917.

Neupert, W., and Herrmann, J.M. (2007). Translocation of proteins into mitochondria. Annu Rev Biochem 76, 723-749.

Neuspiel, M., Zunino, R., Gangaraju, S., Rippstein, P., and McBride, H. (2005). Activated mitofusin 2 signals mitochondrial fusion, interferes with Bax activation, and reduces susceptibility to radical induced depolarization. J Biol Chem 280, 25060-25070.

Newman, L.E., Zhou, C.-j., Mudigonda, S., Mattheyses, A.L., Paradies, E., Marobbio, C.M.T., and Kahn, R.A. (2014a). The ARL2 GTPase Is Required for Mitochondrial Morphology, Motility, and Maintenance of ATP Levels. PLoS One 9, e99270.

Newman, L.E., Zhou, C.J., Mudigonda, S., Mattheyses, A.L., Paradies, E., Marobbio, C.M., and Kahn, R.A. (2014b). The ARL2 GTPase is required for mitochondrial morphology, motility, and maintenance of ATP levels. PloS one 9, e99270.

Nijtmans, L.G.J., Henderson, N.S., and Holt, I.J. (2002). Blue Native electrophoresis to study mitochondrial and other protein complexes. Methods 26, 327-334.

Nishi, H., Ono, K., Iwanaga, Y., Horie, T., Nagao, K., Takemura, G., Kinoshita, M., Kuwabara, Y., Mori, R.T., Hasegawa, K., Kita, T., and Kimura, T. (2010). MicroRNA-15b modulates cellular ATP levels and degenerates mitochondria via Arl2 in neonatal rat cardiac myocytes. J Biol Chem 285, 4920-4930.

Otera, H., Ohsakaya, S., Nagaura, Z., Ishihara, N., and Mihara, K. (2005). Export of mitochondrial AIF in response to proapoptotic stimuli depends on processing at the intermembrane space. EMBO J 24, 1375-1386.

Ozawa, T., Natori, Y., Sako, Y., Kuroiwa, H., Kuroiwa, T., and Umezawa, Y. (2007). A Minimal Peptide Sequence That Targets Fluorescent and Functional Proteins into the Mitochondrial Intermembrane Space. ACS Chemical Biology 2, 176-186.

Petrungaro, C., and Riemer, J. (2014). Mechanisms and physiological impact of the dual localization of mitochondrial intermembrane space proteins. Biochem Soc Trans 42, 952-958.

Pich, S., Bach, D., Briones, P., Liesa, M., Camps, M., Testar, X., Palacin, M., and Zorzano, A. (2005). The Charcot-Marie-Tooth type 2A gene product, Mfn2, up-regulates fuel oxidation through expression of OXPHOS system. Hum Mol Genet 14, 1405-1415.

Pyakurel, A., Savoia, C., Hess, D., and Scorrano, L. (2015). Extracellular Regulated Kinase Phosphorylates Mitofusin 1 to Control Mitochondrial Morphology and Apoptosis. Molecular Cell 58, 244-254.

Radcliffe, P.A., Vardy, L., and Toda, T. (2000). A conserved small GTP-binding protein Alp41 is essential for the cofactor-dependent biogenesis of microtubules in fission yeast. FEBS Lett 468, 84-88.

Rambold, A.S., Kostelecky, B., Elia, N., and Lippincott-Schwartz, J. (2011). Tubular network formation protects mitochondria from autophagosomal degradation during nutrient starvation. Proceedings of the National Academy of Sciences of the United States of America 108, 10190-10195.

Regev-Rudzki, N., Yogev, O., and Pines, O. (2008). The mitochondrial targeting sequence tilts the balance between mitochondrial and cytosolic dual localization. J Cell Sci 121, 2423-2431.

Rojo, M., Legros, F., Chateau, D., and Lombès, A. (2002). Membrane topology and mitochondrial targeting of mitofusins, ubiquitous mammalian homologs of the transmembrane GTPase Fzo. Journal of Cell Science 115, 1663-1674.

Sabharwal, S.S., Waypa, G.B., Marks, J.D., and Schumacker, P.T. (2013). Peroxiredoxin-5 targeted to the mitochondrial intermembrane space attenuates hypoxia-induced reactive oxygen species signalling. Biochem J 456, 337-346.

Santel, A., Frank, S., Gaume, B., Herrler, M., Youle, R.J., and Fuller, M.T. (2003). Mitofusin-1 protein is a generally expressed mediator of mitochondrial fusion in mammalian cells. J Cell Sci 116, 2763-2774.

Santel, A., and Fuller, M.T. (2001). Control of mitochondrial morphology by a human mitofusin. J Cell Sci 114, 867-874.

Schagger, H., and von Jagow, G. (1991). Blue native electrophoresis for isolation of membrane protein complexes in enzymatically active form. Analytical biochemistry 199, 223-231.

Schrepfer, E., and Scorrano, L. (2016). Mitofusins, from Mitochondria to Metabolism. Mol Cell 61, 683-694.

Sharer, J.D., Shern, J.F., Van Valkenburgh, H., Wallace, D.C., and Kahn, R.A. (2002). ARL2 and BART enter mitochondria and bind the adenine nucleotide transporter. Mol Biol Cell 13, 71-83.

She, H., Yang, Q., Shepherd, K., Smith, Y., Miller, G., Testa, C., and Mao, Z. (2011). Direct regulation of complex I by mitochondrial MEF2D is disrupted in a mouse model of Parkinson disease and in human patients. J Clin Invest 121, 930-940.

Shern, J.F., Sharer, J.D., Pallas, D.C., Bartolini, F., Cowan, N.J., Reed, M.S., Pohl, J., and Kahn, R.A. (2003). Cytosolic Arl2 is complexed with cofactor D and protein phosphatase 2A. J Biol Chem 278, 40829-40836.

Shutt, T., Geoffrion, M., Milne, R., and McBride, H.M. (2012). The intracellular redox state is a core determinant of mitochondrial fusion. Embo Rep 13, 909-915.

Smirnova, E., Griparic, L., Shurland, D.L., and van der Bliek, A.M. (2001). Dynamin-related protein Drp1 is required for mitochondrial division in mammalian cells. Mol Biol Cell 12, 2245-2256.

Song, Z., Chen, H., Fiket, M., Alexander, C., and Chan, D.C. (2007). OPA1 processing controls mitochondrial fusion and is regulated by mRNA splicing, membrane potential, and Yme1L. J Cell Biol 178, 749-755.

Song, Z., Ghochani, M., McCaffery, J.M., Frey, T.G., and Chan, D.C. (2009). Mitofusins and OPA1 mediate sequential steps in mitochondrial membrane fusion. Mol Biol Cell 20, 3525-3532.

Tanaka, A., Cleland, M.M., Xu, S., Narendra, D.P., Suen, D.F., Karbowski, M., and Youle, R.J. (2010). Proteasome and p97 mediate mitophagy and degradation of mitofusins induced by Parkin. J Cell Biol 191, 1367-1380.

Tian, G., Thomas, S., and Cowan, N.J. (2010). Effect of TBCD and its regulatory interactor Arl2 on tubulin and microtubule integrity. Cytoskeleton (Hoboken) 67, 706-714.

Tondera, D., Grandemange, S., Jourdain, A., Karbowski, M., Mattenberger, Y., Herzig, S., Da Cruz, S., Clerc, P., Raschke, I., Merkwirth, C., Ehses, S., Krause, F., Chan, D.C., Alexander, C., Bauer, C., Youle, R., Langer, T., and Martinou, J.C. (2009). SLP-2 is required for stress-induced mitochondrial hyperfusion. EMBO J 28, 1589-1600.

van den Berghe, N., Cool, R.H., and Wittinghofer, A. (1999). Discriminatory residues in Ras and Rap for guanine nucleotide exchange factor recognition. J Biol Chem 274, 11078-11085.

Van Valkenburgh, H., Shern, J.F., Sharer, J.D., Zhu, X., and Kahn, R.A. (2001). ADP-ribosylation factors (ARFs) and ARF-like 1 (ARL1) have both specific and shared effectors: characterizing ARL1-binding proteins. J Biol Chem 276, 22826-22837.

Vogel, U.S., Dixon, R.A., Schaber, M.D., Diehl, R.E., Marshall, M.S., Scolnick, E.M., Sigal, I.S., and Gibbs, J.B. (1988). Cloning of bovine GAP and its interaction with oncogenic ras p21. Nature 335, 90-93.

Wegrzyn, J., Potla, R., Chwae, Y.J., Sepuri, N.B., Zhang, Q., Koeck, T., Derecka, M., Szczepanek, K., Szelag, M., Gornicka, A., Moh, A., Moghaddas, S., Chen, Q., Bobbili, S., Cichy, J., Dulak, J., Baker, D.P., Wolfman, A., Stuehr, D., Hassan, M.O., Fu, X.Y., Avadhani, N., Drake, J.I., Fawcett, P., Lesnefsky, E.J., and Larner, A.C. (2009). Function of mitochondrial Stat3 in cellular respiration. Science 323, 793-797.

Yogev, O., Naamati, A., and Pines, O. (2011). Fumarase: a paradigm of dual targeting and dual localized functions. FEBS J 278, 4230-4242.

Zhang, C.J., Rosenwald, A.G., Willingham, M.C., Skuntz, S., Clark, J., and Kahn, R.A. (1994). Expression of a dominant allele of human ARF1 inhibits membrane traffic in vivo. J Cell Biol 124, 289-300.

Zhang, T., Li, S., Zhang, Y., Zhong, C., Lai, Z., and Ding, J. (2009). Crystal structure of the ARL2-GTP-BART complex reveals a novel recognition and binding mode of small GTPase with effector. Structure 17, 602-610.

Zhou, C., Cunningham, L., Marcus, A.I., Li, Y., and Kahn, R.A. (2006). Arl2 and Arl3 regulate different microtubule-dependent processes. Mol Biol Cell 17, 2476-2487.

Zhou, Q., Li, H., Li, H., Nakagawa, A., Lin, J.L.J., Lee, E.-S., Harry, B.L., Skeen-Gaar, R.R., Suehiro, Y., William, D., Mitani, S., Yuan, H.S., Kang, B.-H., and Xue, D. (2016). Mitochondrial endonuclease G mediates breakdown of paternal mitochondria upon fertilization. Science 353, 394-399.

Zuchner, S., Mersiyanova, I.V., Muglia, M., Bissar-Tadmouri, N., Rochelle, J., Dadali, E.L., Zappia, M., Nelis, E., Patitucci, A., Senderek, J., Parman, Y., Evgrafov, O., Jonghe, P.D., Takahashi, Y., Tsuji, S., Pericak-Vance, M.A., Quattrone, A., Battaloglu, E., Polyakov, A.V., Timmerman, V., Schroder, J.M., and Vance, J.M. (2004). Mutations in the mitochondrial GTPase mitofusin 2 cause Charcot-Marie-Tooth neuropathy type 2A. Nat Genet 36, 449-451.

Zunino, R., Braschi, E., Xu, L., and McBride, H.M. (2009). Translocation of SenP5 from the Nucleoli to the Mitochondria Modulates DRP1-dependent Fission during Mitosis. Journal of Biological Chemistry 284, 17783-17795.

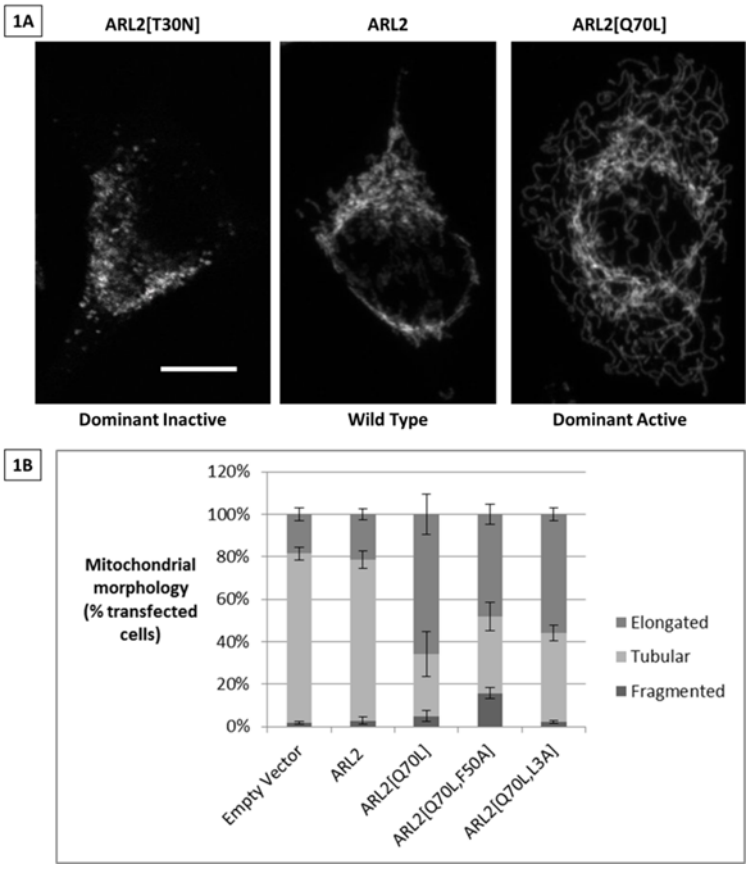

Figure 1: Activating and inactivating mutants of ARL2 have opposing effects on mitochondrial morphology. (A) HeLa cells were transiently transfected with plasmids directing expression of ARL2, ARL2[T30N] (dominant inactivating), or ARL2[Q70L] (dominant activating). Cells were fixed 1 day after transfection (ARL2[T30N]) or 3 days after transfection (ARL2 and ARL2[Q70L]). Cells were stained for ARL2 (not shown) and HSP60. Untransfected cells (not shown) were indistinguishable from ARL2 over-expressing cells (See also Newman et al., 2014). 2D projections of z stacks acquired by confocal microscopy are shown in the middle and right panels, and a single z section on the left. Scale bar = 10 μm. (B) HeLa cells were transiently transfected with ARL2 plasmids, fixed 2 days later, and stained for ARL2 and HSP60. Cells were scored for mitochondrial elongation as described under Methods. Error bars represent standard deviation, and the average of 3 independent experiments is shown. N = 625 for empty vector, 606 for ARL2-expressing cells, 601 for ARL2[Q70L], 601 for ARL2[Q70L, F50A], and 600 for ARL2[Q70L, L3A].

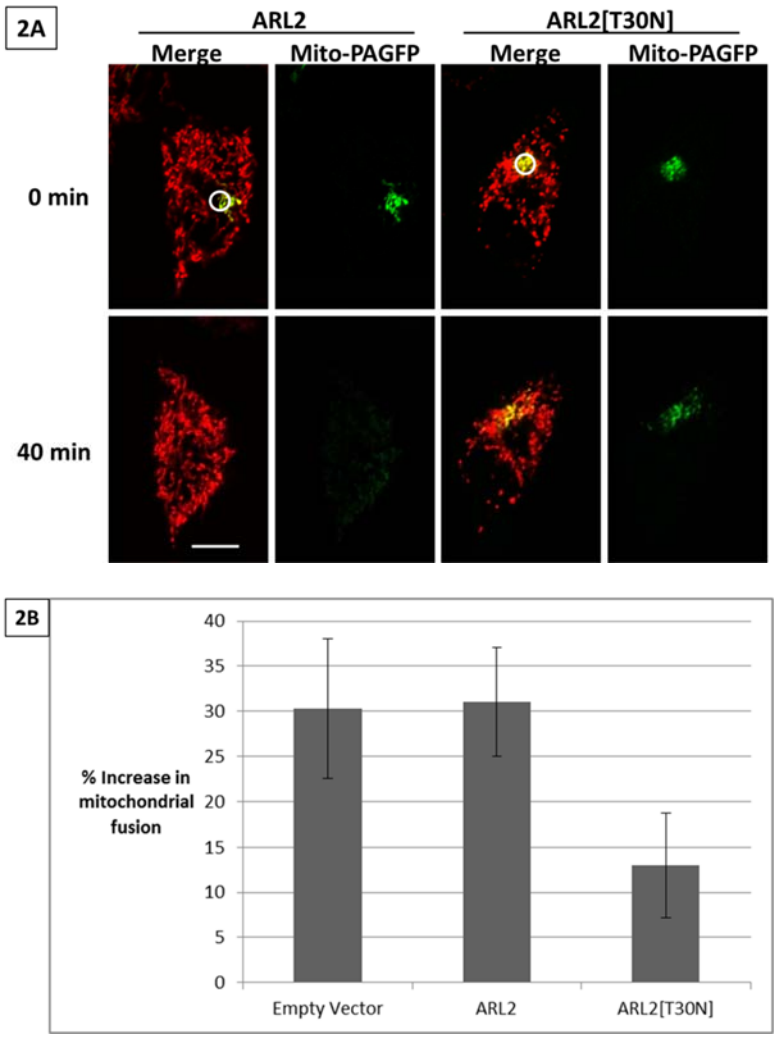

Figure 2: Mitochondrial fusion is impaired in cells expressing ARL2[T30N]. (A) HeLa cells expressing mito-photoactivatable GFP (mito-PAGFP), mito-dsRed, and either ARL2 (left) or ARL2[T30N] (right) were photoactivated in the small region of interest (white circle; 0 min, top panels) shown, as described under Methods, and cells were imaged for up to 40 min (bottom). Over the imaging window, PAGFP signal spread from the region of interest in cells expressing ARL2, but was clearly retarded in cells co-expressing ARL2[T30N] (right). A single z plane is shown in each case. Scale bar = 10 µm. Merged images of GFP and dsRed are shown on the left for both conditions, while the GFP channel only is shown on the right. (B) The mitochondrial fusion assay was quantified by determining the percentage of pixels within a cell that were positive for both green (activated mito-PAGFP) and red (mito-dsRed) signals. The difference in

this ratio between 0 min (immediately after photoactivation) and 40 min is shown as the percent increase in mitochondrial fusion. N = 15 cells for empty vector, 14 for ARL2-expressing cells, and 14 for ARL2[T30N]-expressing cells. Error bars represent standard deviation.

3A

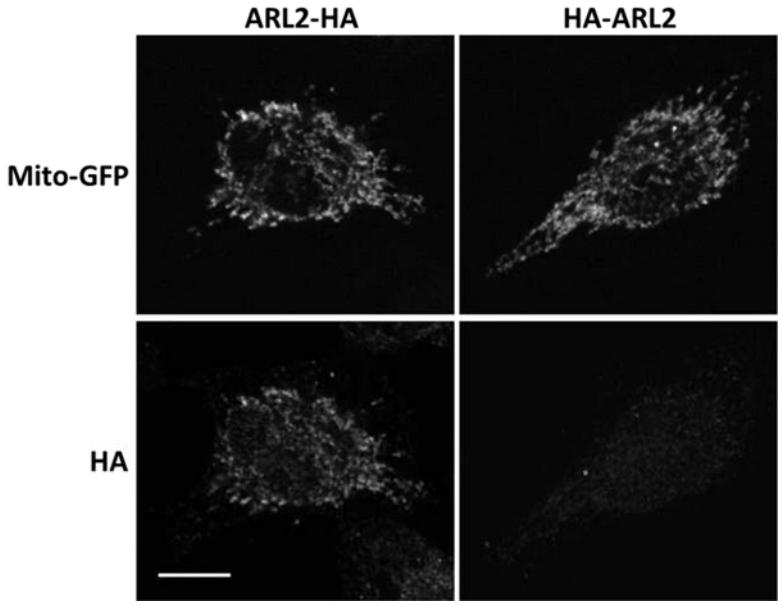
ARL2-HA
HA-ARL2
Mito-GFP
HA

3B

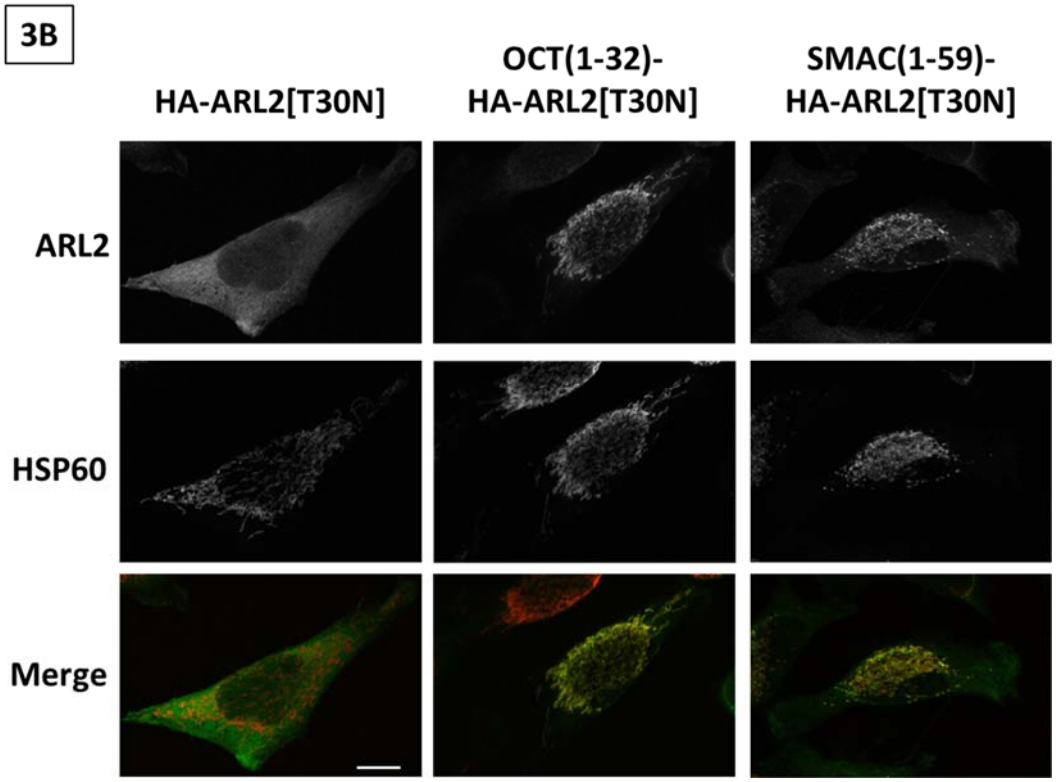
HA-ARL2[T30N]
OCT(1-32)-
HA-ARL2[T30N]
SMAC(1-59)-
HA-ARL2[T30N]
ARL2
HSP60
Merge

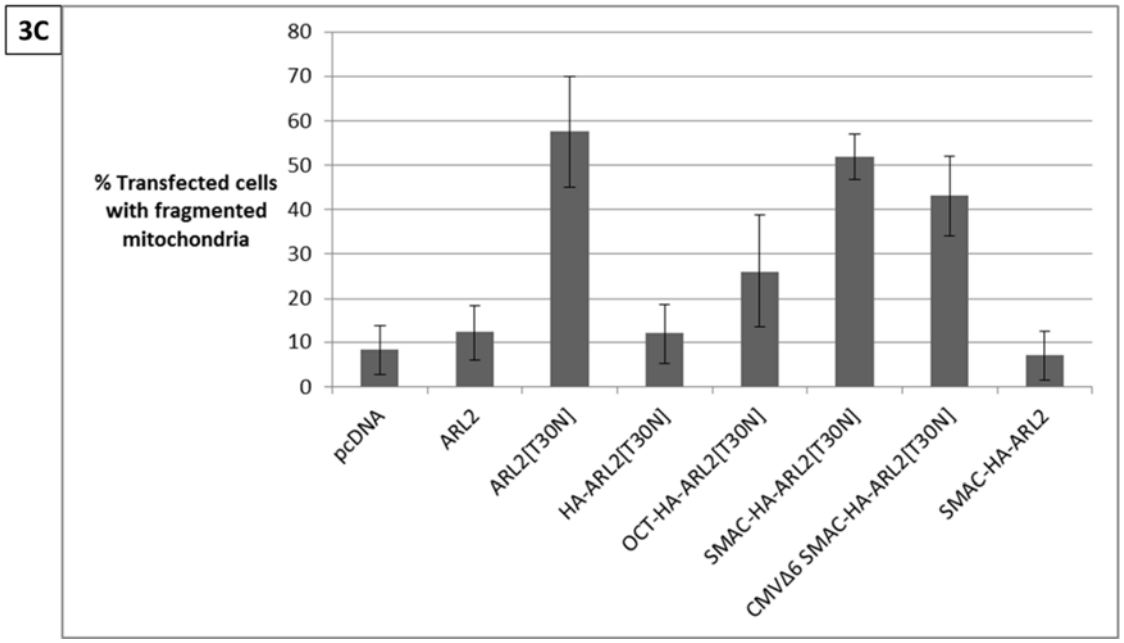

Figure 3: ARL2[T30N] acts from the IMS to fragment mitochondria. (A) HeLa cells were co-transfected with mito-GFP and either ARL2-HA or HA-ARL2. Cytosolic staining of ARL2 was reduced by permeabilizing cells with 0.05% saponin in PBS for one minute immediately prior to fixation. Cells were then stained for the HA epitope. Single planes of representative cells are shown and reveal the near complete absence of import of HA-ARL2 into mitochondria (lower right panel). (B) HeLa cells were transfected with the indicated plasmid, shown along the top, fixed one day after transfection and stained for ARL2 and HSP60. Single planes of representative cells are shown. (C) Cells treated as described in part B were quantified for mitochondrial fragmentation. Error bars represent standard deviation, and the average of five independent experiments is shown. Scale bar = 10 μm. N = 1035 cells for empty vector, 1005 for ARL2-expressing cells, 1214 for ARL2[T30N], 1023 for OCT(1-32)-HA-ARL2[T30N], 1020 for SMAC(1-59)-HA-ARL2[T30N], 1023 for HA-ARL2[T30N], 1008 for SMAC(1-59)-HA-ARL2, and 1001 for CMV6 SMAC(1-59)-HA-ARL2[T30N]. Error bars represent standard deviation.

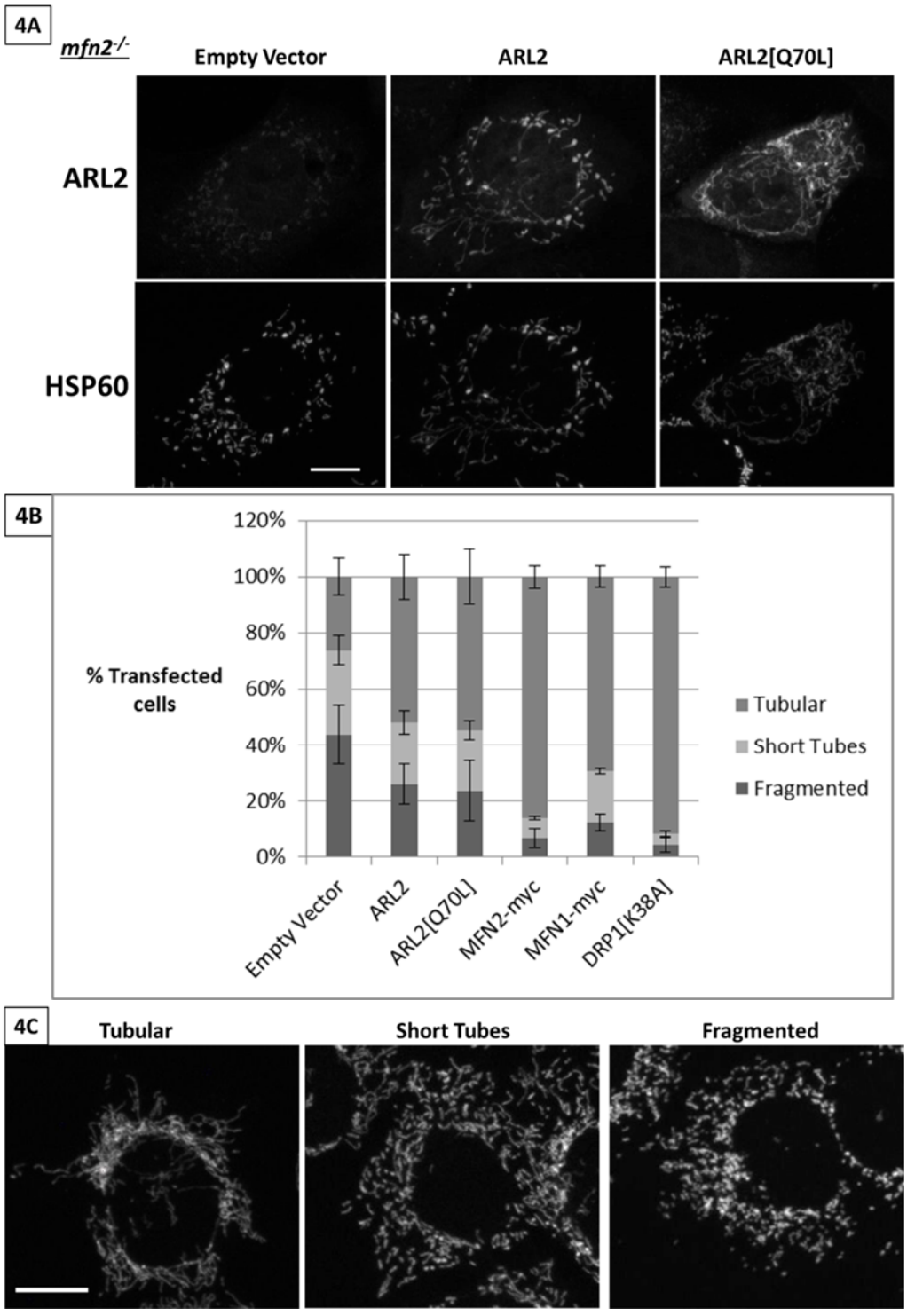

Figure 4: ARL2 or ARL2[Q70L] expression reverses fragmentation in *mfn2*$^{-/-}$ MEFs. (A) *mfn2*$^{-/-}$ MEFs were transfected with empty vector, ARL2 or ARL2[Q70L], fixed 24 hours later,

and stained for ARL2 and HSP60. Z stack projections are shown. Scale bar = 10 μm. (B) Cells treated as described in part A were scored for mitochondrial morphology, as described under Methods. Error bars represent standard deviation, and the average of 3 independent experiments is shown. N= 612 for empty vector, 602 for ARL2 expressing cells, 600 for ARL2[Q70L], 602 for MFN2-myc, 604 for MFN1-myc, and 600 for GFP-DRP1[K38A]. (C) Representative cells from the categories used to score mitochondrial morphology in MEFs are shown. Left two images are wild type MEFs, right image is an *mfn1*$^{-/-}$ MEF. Z stack projections are shown. Scale bar = 10 μm.

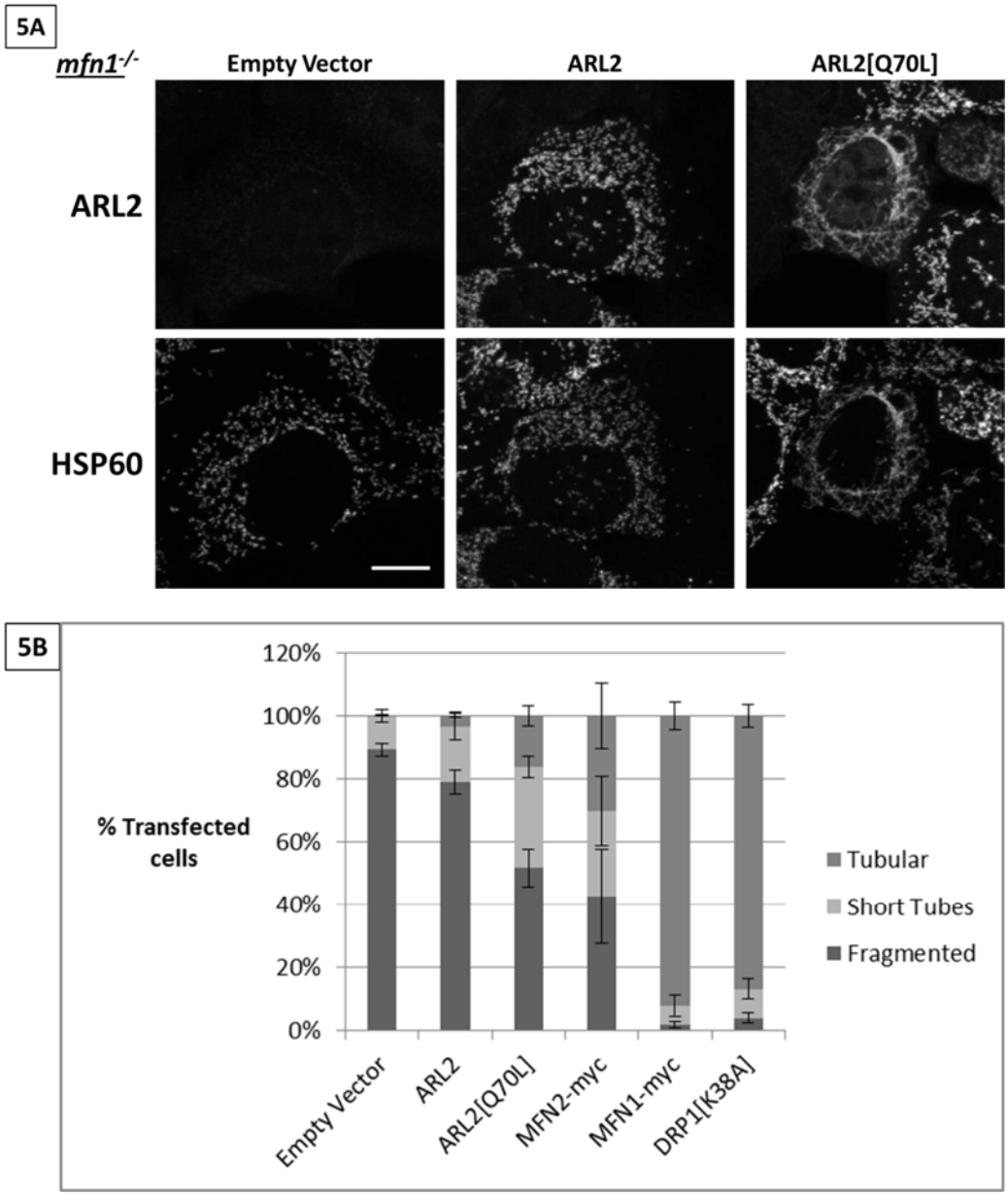

Figure 5: ARL2[Q70L] expression reverses fragmentation in *mfn1*$^{-/-}$ MEFs. (A) *mfn1*$^{-/-}$ MEFs were transfected with pcDNA3.1, ARL2 or ARL2[Q70L] for 24 hours, fixed 51 hours later, and stained for ARL2 and HSP60. 2D projections of z stacks acquired by confocal microscopy are shown. Scale bar = 10 µm. **(B)** MEFs were transfected, fixed, and stained as in **A**, and scored for mitochondrial morphology. Error bars represent standard deviation, and the average of 3 independent experiments is shown, N = 622 for empty vector, 614 for ARL2-expressing cells, 607 for ARL2[Q70L], 612 for MFN2-myc, 606 for MFN1-myc, and 611 for GFP-DRP1[K38A].

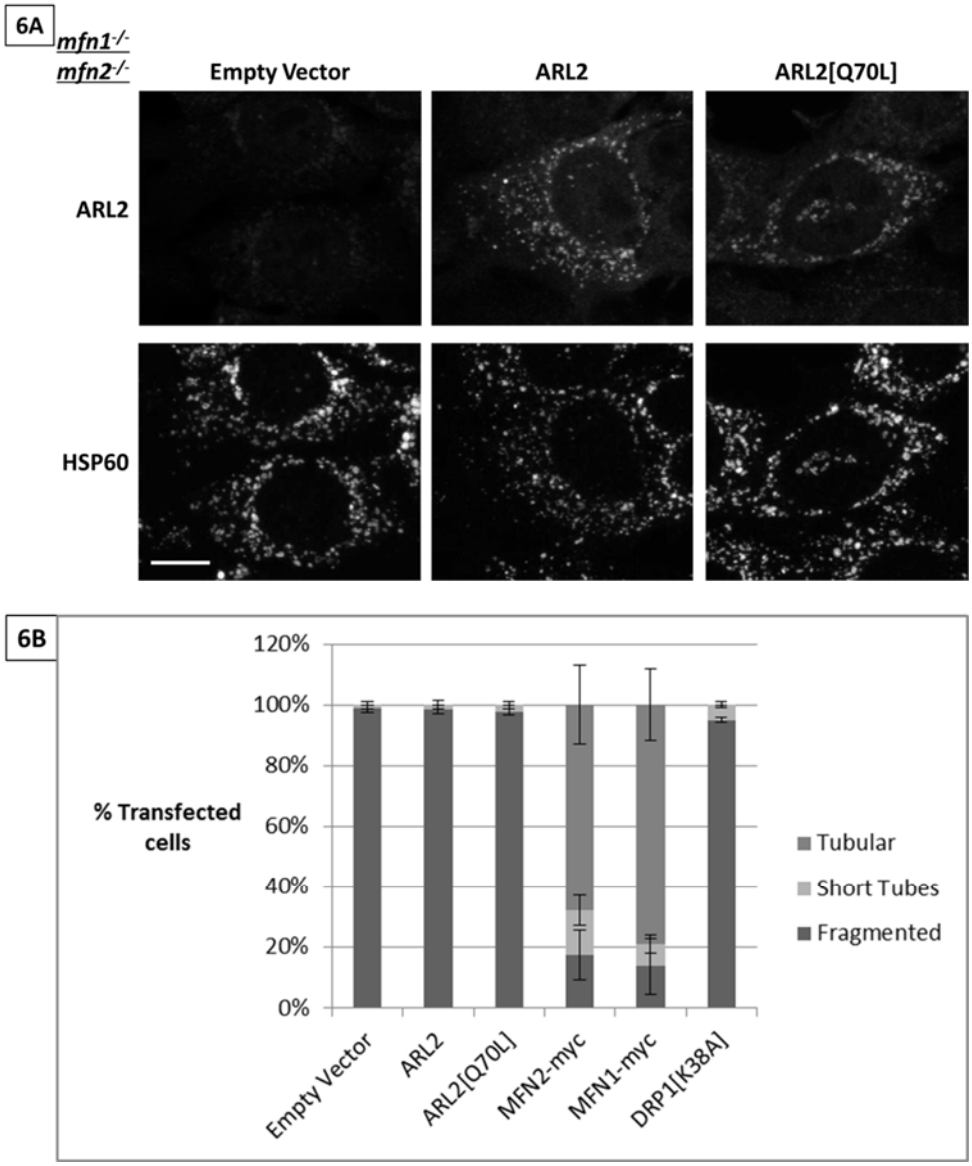

Figure 6: ARL2 or ARL2[Q70L] expression does not reverse fragmentation in MEFs deleted for both MFNs. (A) *mfn1*$^{-/-}$ *mfn2*$^{-/-}$ MEFs were treated as described in Figure 5. Z stack projections are shown. Lower expression of ARL2 and ARL2[Q70L] was observed, so higher laser power was used to capture these images compared to figures 4 and 5. Scale bar = 10 μm. **(B)** Results from part A were quantified for mitochondrial morphology as described. Error bars represent standard deviation, and the average of 3 independent experiments is shown. N = 611 for empty vector, 602 for ARL2-expressing cells, 603 for ARL2[Q70L], 609 for MFN2-myc, 605 for MFN1-myc, and 605 for GFP-DRP1[K38A].

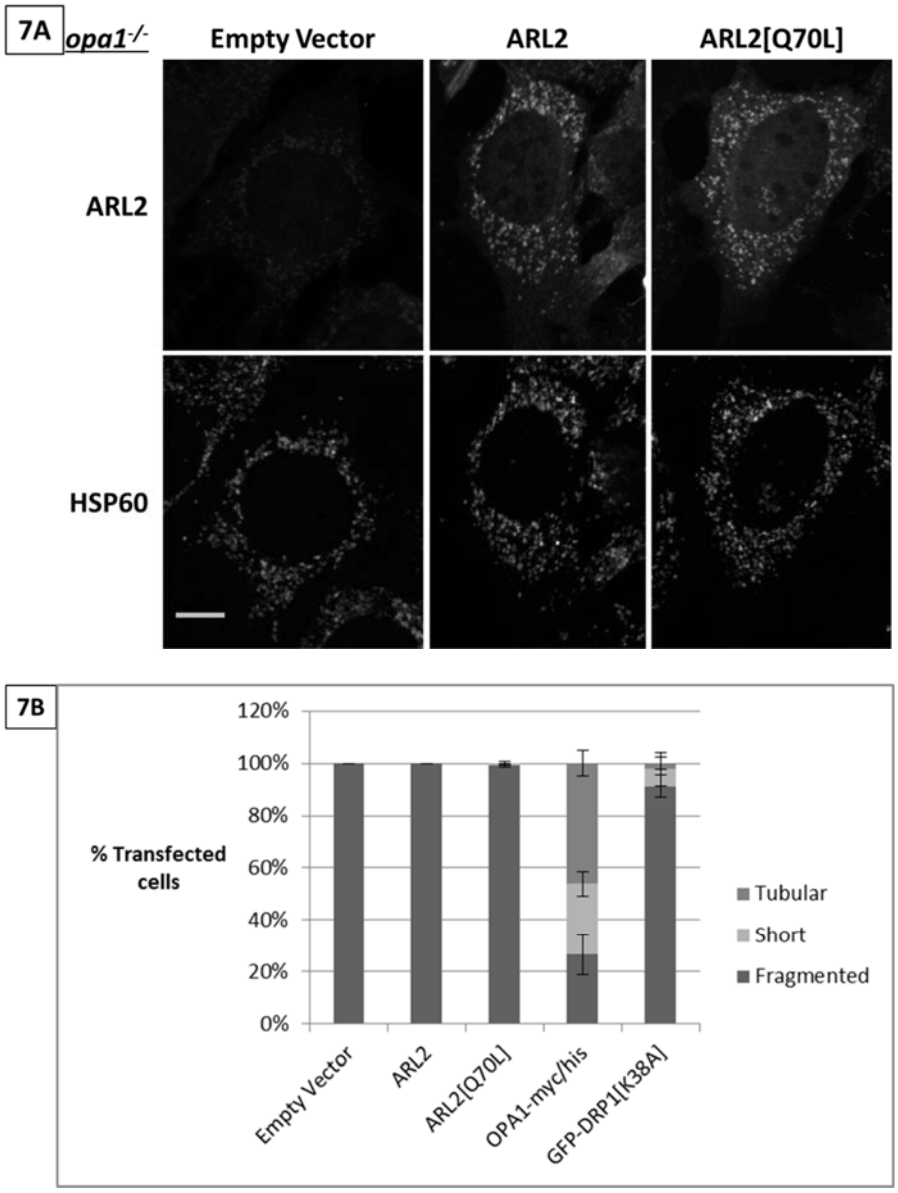

Figure 7: ARL2 or ARL2[Q70L] expression does not reverse fragmentation in MEFs deleted for OPA1. (A) *opa1*$^{-/-}$ MEFs were treated as described in Figures 4 and 5. Z stack projections are shown. Scale bar = 10 µm. Lower expression of ARL2 and ARL2[Q70L] was observed, so higher laser power was used to capture these images compared to Figures 4 and 5. **(B)** Results from part A were quantified for mitochondrial morphology. Error bars represent standard deviation, and the average of 3 independent experiments is shown. N = 620 for empty vector, 606 for ARL2-expressing cells, 603 for ARL2[Q70L], 605 for OPA1-myc/his, and 605 for GFP-DRP1[K38A].

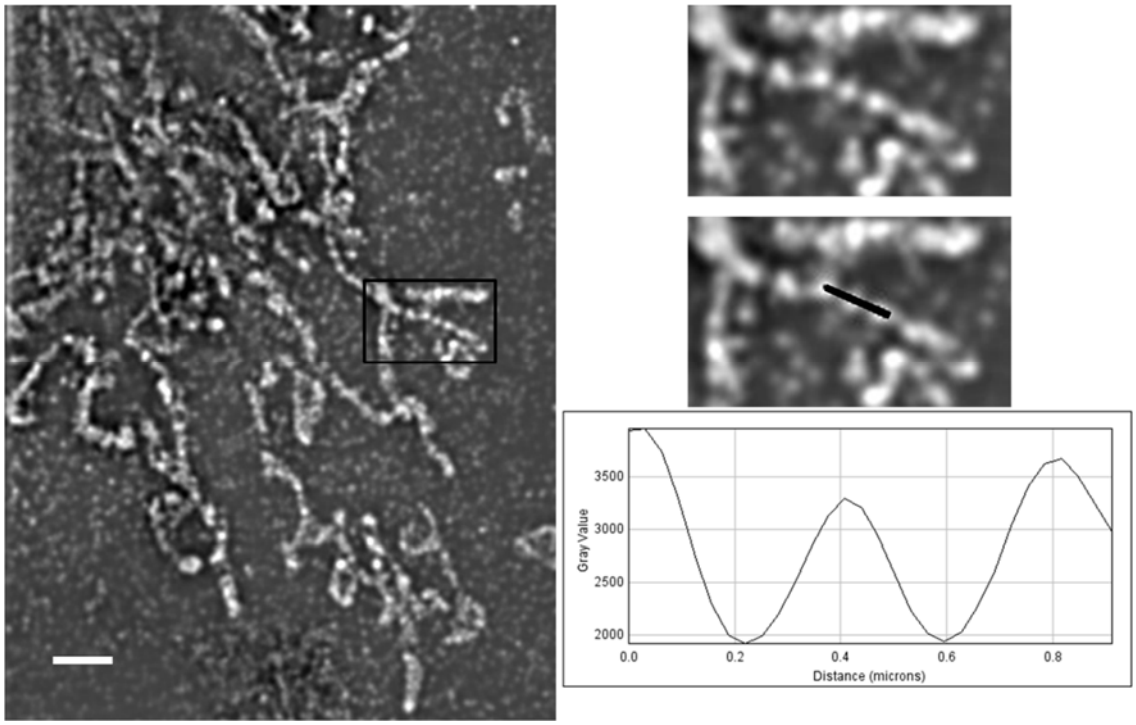

Figure 8: ARL2 localizes to puncta within mitochondria that display regularity in spacing. COS7 were stained for ARL2 and imaged using three-dimensional SIM. A representative cell is shown, with a blowup of the boxed region shown on the right. Line scan analysis reveals that ARL2 puncta repeat at a regular interval of ~0.4 μm. Blowups are 2.5x the size of the larger image shown. Scale bar = 2 μm.

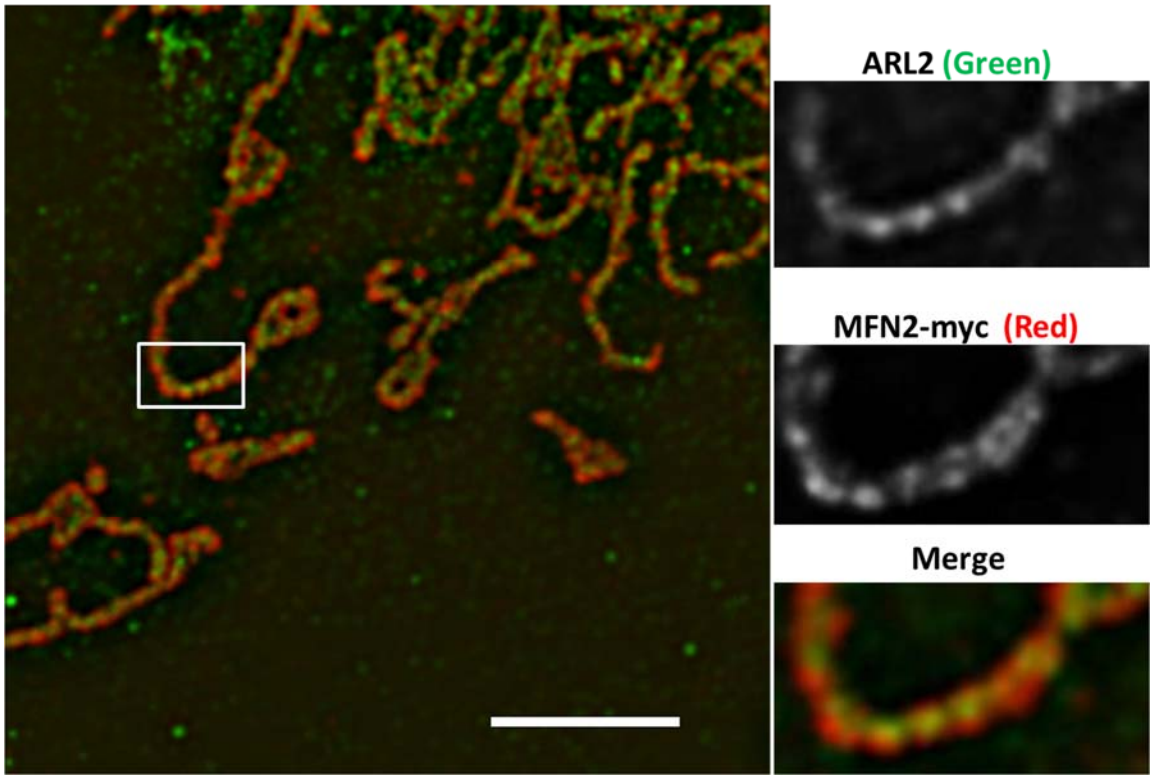

Figure 9: Mitofusins localize to puncta that align with ARL2 puncta. COS7 cells were transfected with MFN2-myc, stained for ARL2 and myc, and imaged using three-dimensional SIM. Myc staining (red) localizes to puncta along the outer membrane that align with endogenous ARL2 puncta, consistent with its proposed localization in the IMS. Similar results were obtained for MFN1-myc (not shown). Blowups are 2.5x the size of the larger image shown. Scale bar = 5 µm.

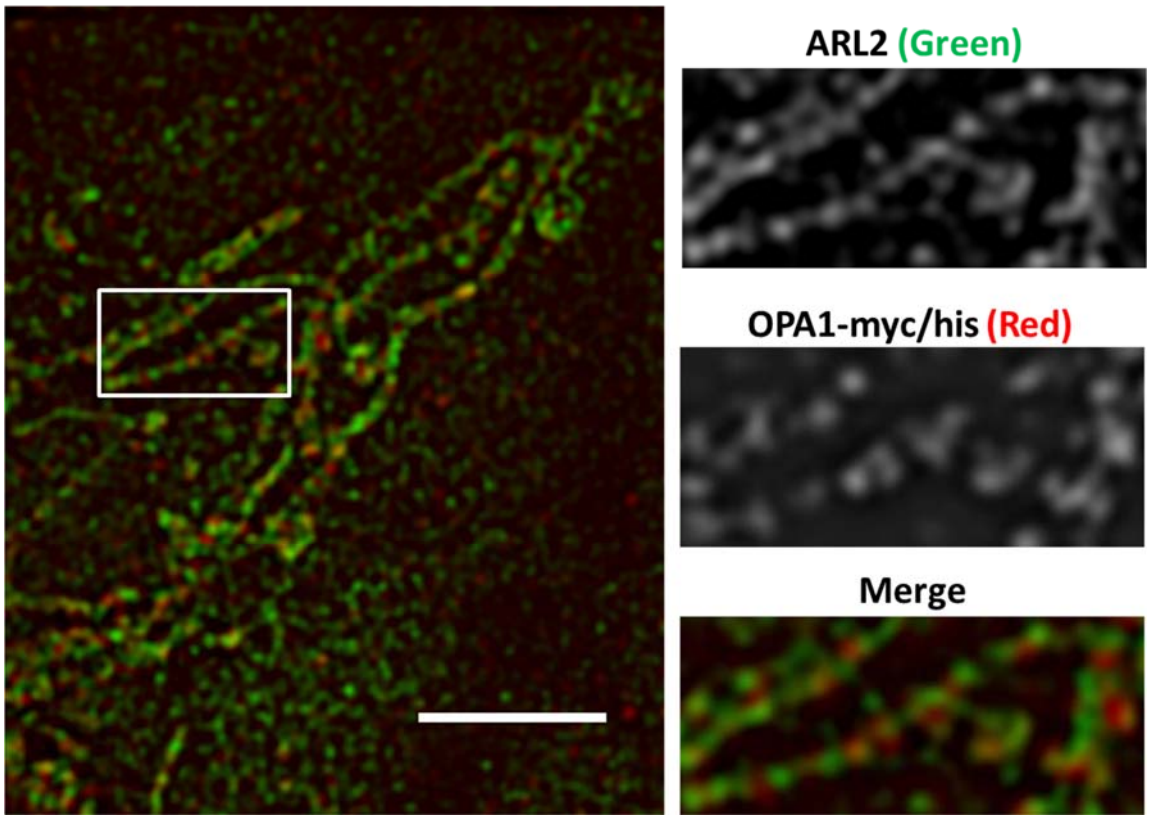

Figure 10: OPA1 shows no clear association with ARL2 puncta. COS7 cells were transfected with OPA1-myc/his, stained for ARL2 and myc, and imaged using three-dimensional SIM. Myc staining (red) localizes to puncta, however, these puncta appear to repeat at a different interval from ARL2 puncta. Additionally, puncta appear both next to ARL2 puncta and in between ARL2 puncta, showing no obvious relationship, in clear contrast to the mitofusins. Blowups are 2x the size of the larger image shown. Scale bar = 5 μm.

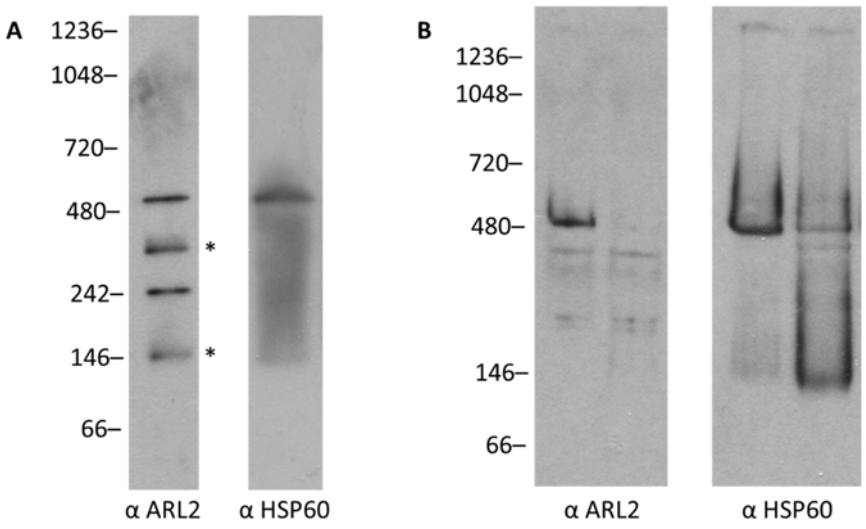

Figure S1: ARL2 is present in a complex with HSP60. (A) HeLa cells were lysed in 1% CHAPS, 25 mM HEPES, pH 7.4, and 100 mM NaCl, and lysate (20 ug) was resolved a blue native gel. The gel was transferred to PVDF membranes and probed with antibodies against ARL2 or HSP60, as described under Methods. The entire lane of the gel is shown. Asterisks (*) indicate bands that are not competable with purified, recombinant ARL2. The band at 242 kD is the ARL2/Cofactor D complex (Francis et al., manuscript in preparation). (**B**) The ARL2/HSP60 complex was partially purified from bovine liver (described under Methods) and incubated with 10 mM ATP on ice overnight. The HSP60 complex dissociated as previously described (Levy-Rimler et al., 2001). The ARL2 band was also lost with ATP incubation, confirming its presence in the HSP60 complex.

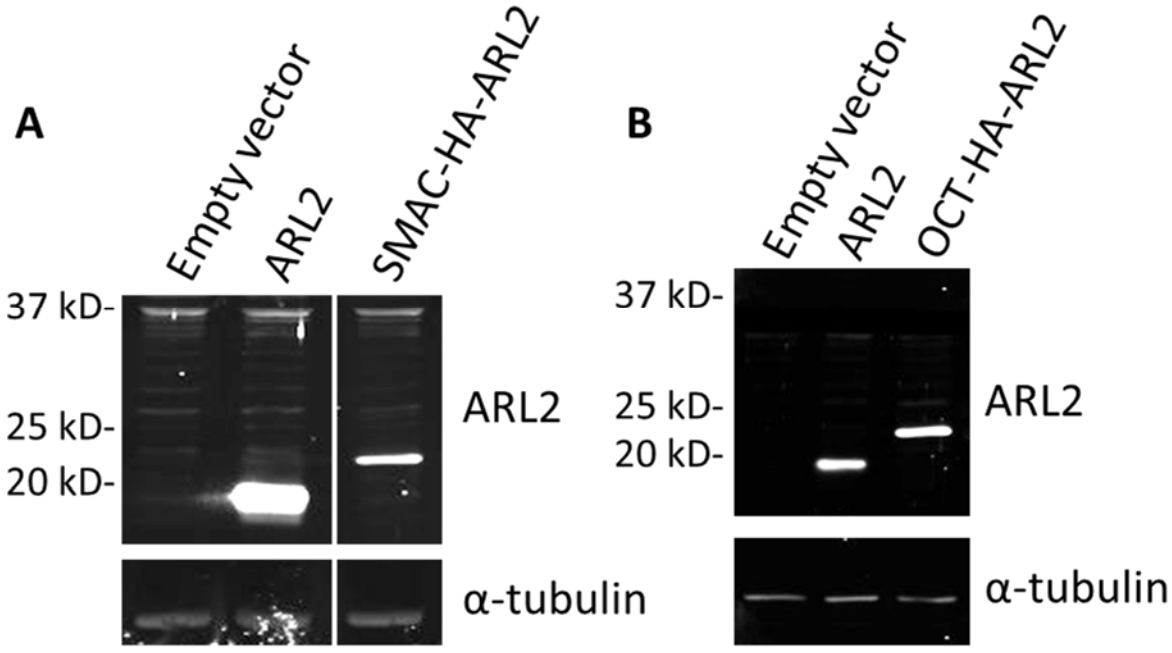

Figure S2: SMAC-HA-ARL2 and OCT-HA-ARL2 are imported into mitochondria and cleaved. (**A**) HeLa cells were transfected with empty vector, ARL2, or SMAC-HA-ARL2 and lysed 24 hours later in 1% CHAPS, 25 mM HEPES pH 7.4, and 100 mM NaCl. Lysate (20 µg) was resolved by SDS-PAGE, transferred to nitrocellulose, and probed for ARL2 and alpha tubulin, as loading control. Blots were developed using the Odyssey system. Nonadjacent lanes from the same blot are shown. (**B**) Same as A, except OCT-HA-ARL2 was expressed.

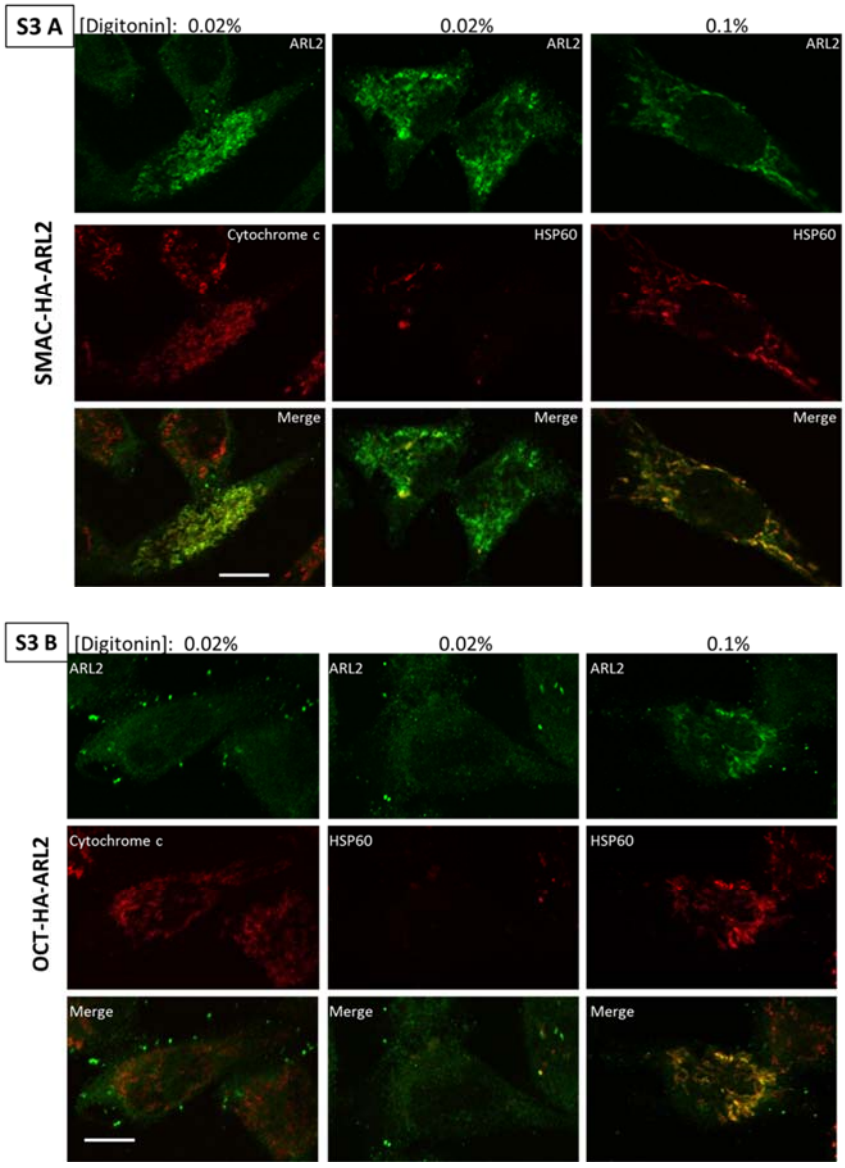

Figure S3: SMAC-HA-ARL2 and OCT-HA-ARL2 are targeted to the appropriate compartments. (**A**) HeLa cells were transfected with SMAC-HA-ARL2 and 24 hours later fixed in 4% paraformaldehyde prior to permeabilization in either 0.02% (left two columns) or 0.1% w/v digitonin (right column) for 10 minutes at room temperature. Cells were then processed for imaging using dual labeling for ARL2 (green, top row) and either cytochrome c (middle row, left and middle panels) or HSP60 (middle row, middle and right panels), as markers of the IMS and matrix, respectively. Merged images are shown in the bottom row in each case. (**B**) Same as A, except cells were expressing and analyzed for OCT-HA-ARL2. Scale bar = 10 μm.

Chapter 5: Recruitment of the ARL2 GTPase and its GAP, ELMOD2, to mitochondria is modulated by the fusogenic activity of mitofusins

This chapter is submitted as:

Laura E. Newman*, Cara R. Schiavon*, Chengjing Zhou, and Richard A. Kahn. Recruitment of the ARL2 GTPase and its GAP, ELMOD2, to Mitochondria is Modulated by the Fusogenic Activity of Mitofusins. Submitted.

*These authors contributed equally

The following figures were generated by Cara Schiavon: 6, 7, 8, 9

For the following figures, Cara Schiavon performed the experiment and I peformed imaging and generated the figure: 2A, 10

Abstract

Mitochondria are essential, dynamic organelles that respond to a number of stressors with changes in morphology that are linked to several mitochondrial functions, though the mechanisms involved are poorly understood. We show that the levels of the regulatory GTPase ARL2 and its GAP, ELMOD2, are specifically increased in mitochondria in immortalized mouse embryo fibroblasts deleted for Mitofusin 2 (MFN2), but not MFN1. Elevated ARL2 and ELMOD2 in MEFs deleted for MFN2 could be reversed by re-introduction of MFN2, but only when the mitochondrial fragmentation in these MEFs was also reversed, demonstrating that reversal of elevated ARL2 and ELMOD2 requires fusogenic activity of MFN2. Other stressors with links to mitochondrial morphology were investigated and several, including glucose or serum deprivation also causing increases in ARL2 and ELMOD2. In contrast, a number of pharmacological inhibitors of energy metabolism caused increases in ARL2 without affecting ELMOD2 levels. Together we interpret these data as evidence of two ARL2-sensitive pathways in mitochondria, one affecting ATP levels that is independent of ELMOD2 and the other leading to mitochondrial fusion involving MFN2 that does involve ELMOD2.

Introduction

Mitochondria are essential organelles that are hubs for several important cellular functions, including ATP production, lipid metabolism, calcium regulation, and apoptosis. This diversity of essential functions is accompanied by diversity in morphology as mitochondria are highly dynamic organelles that can range in size and shape from many small spheres to one large inter-connected network. Previous studies have documented the linkages between form and function and that morphology must be sensitive to cues coming from other parts of the cell (Sauvanet et al.; Karbowski and Youle, 2003; Chan, 2006). Mitochondrial morphology is the result of a balance between fission and fusion, which are mediated by four large dynamin-related

GTPases. Mitochondrial fission is mediated by DRP1 (Labrousse et al., 1999; Smirnova et al., 2001), while fusion is controlled by three GTPases: MFN1 and MFN2 regulate outer membrane fusion (Chen et al., 2003; Chen et al., 2005), and OPA1 promotes inner membrane fusion (Cipolat et al., 2004). Mitochondria elongate during several types of stress as a result of increased fusion (Tondera et al., 2009; Mishra et al., 2014) and also elongate during starvation, protecting them from autophagy (Gomes et al., 2011; Rambold et al., 2011). To date, only a handful of proteins have been shown to regulate either mitofusins or OPA1, and how these regulators promote fusion under stress is an area of ongoing research.

We recently discovered that ARL2 plays a role in the regulation of mitochondrial fusion (Newman et al., manuscript submitted). ARL2, a ~20 kDa member of the ARF family of regulatory GTPases, is very highly conserved throughout eukaryotic evolution, ubiquitously expressed, predicted to be present in the last eukaryotic common ancestor (Li et al., 2004), and is essential for at least three model organisms (McElver et al., 2000; Radcliffe et al., 2000; Antoshechkin and Han, 2002). ARL2 plays essential roles in the biogenesis of tubulin and in microtubule dynamics and only later was found to also localize specifically to mitochondria where it also plays essential roles. We showed that depletion of ARL2 by siRNA causes mitochondrial fragmentation, a loss in plus-end directed mitochondrial motility, and a dramatic (~50%) loss in cellular ATP (Newman et al., 2014). More recently, we showed that ARL2 regulates mitochondrial fusion, that it does so from the IMS, and that it can stimulate fusion via either MFN1 or MFN2 (Newman, et al., manuscript submitted).

We also identified and purified the ARL2 GAP, ELMOD2, and found that it too localizes to mitochondria (Bowzard et al., 2007). Like ARL2 siRNA, depletion of ELMOD2 results in fragmentation and perinuclear clustering but has no effect on ATP levels. As a result, we currently model ARL2 as having at least two distinguishable actions in mitochondria: one

leading to regulation of ATP production and a separate one that involves ELMOD2 and impacts fusion and motility.

Because mitochondria play such crucial roles in several essential cellular processes and must be sensitive to inputs from different parts of the cell to maintain homeostasis or respond to a changing environment it should not be surprising that regulatory processes are critical, yet little is known about such systems. With the identification of a regulatory GTPase and an effector/GAP implicated as regulators of fusion and motility, we sought to examine whether they may be responsive to stressors that are known to impact mitochondrial morphology and functions. Here, we show that the levels of mitochondrial ARL2 and ELMOD2 are highly sensitive to mitochondrial stress and changes in the levels of MFN2. These results further the model that ARL2 and ELMOD2 are components in a system of communication between mitochondria and other parts of the cell.

Materials and Methods

Antibodies & Reagents: Rabbit polyclonal antibodies directed against human ARL2 and ELMOD2 were generated in our lab and have been described previously (Sharer et al., 2002; Newman et al., 2014). Characterization of the specificity of these reagents has included comparisons to pre-immune serum and antigen competition in both immunoblots and indirect immunofluorescence. Each of these methods have been optimized for specificity and sensitivity of these antibodies. The following antibodies were obtained from commercial sources: HA (Covance MMS-101P), HSP60 (Enzo Life Sciences ADI-SPA-807), cytochrome c (BD Biosciences 556432), myc (Invitrogen R950-25), TOM20 (BD Biosciences 61228), OPA1 (BD Biosciences 612606), Complex V subunit alpha (Mitosciences MS502), NDUFA9 (Mitosciences MS111), UQCRC2 (Mitosciences MS304). The following antibody dilutions were used in our studies for immunofluorescence: ARL2 (1:2000), ELMOD2 (1:500), HSP60 (1:5000), myc

(1:1000), HA (1:2000), cytochrome c (1:2000), TOM20 (1:5000), OPA1 (1:100), Complex V subunit alpha (1:200), NDUFA9 (1:200), UQCRC2 (1:2000).

Cloning and Constructs: The following plasmids were generously provided by David Chan: MFN1-10xmyc and MFN2-16xmyc in pcDNA3.1, and MFN2 CMT2A mutations [V69F], [L76P], [R94Q], and [R274Q] in MFN2-7xmyc in pcDNA3.1 (Chen et al., 2003; Detmer and Chan, 2007). The MFN2[K109A]-16xmyc plasmid (in pcDNA3.1) was generated in the lab of David Chan and obtained through Addgene (plasmid 26051). CMVΔ6 SMAC-HA-ARL2 and OCT-HA-ARL2 have been described and characterized previously (Newman, Schiavon, and Kahn, manuscript submitted).

Cell culture: Human cervical carcinoma (HeLa), mouse embryonic fibroblast (MEF) and African green monkey kidney (COS7) cell lines were used in our studies to allow comparisons between them, ensure against a phenomenon that may be unique to one line, and to allow comparisons between cells displaying different mitochondrial morphologies. All were used as they are relatively flat, making them good for imaging. Additionally, we routinely obtain high transfection efficiencies (50-90%) and can readily detect endogenous ARL2 and ELMOD2 in HeLa and COS7 cell lines. Most experiments described here were performed in each of the different cell lines and we obtained very similar results. Cells were grown in DMEM medium, supplemented with 10% fetal bovine serum (FBS; cat# 11965-092, Invitrogen, Carlsbad, CA) and 2 mM glutamine at 37°C in the presence of 5% CO2. For imaging, cells were grown on matrigel (BD Biosciences #356231) coated coverslips. HeLa and COS7 cells were originally obtained from the ATCC. Immortalized MEFs from wild type, *mfn1*$^{-/-}$, *mfn2*$^{-/-}$, or *mfn1*$^{-/-}$*mfn2*$^{-/-}$, mice were a generous gift from Dr. David Chan (Chen et al., 2003; Koshiba et al., 2004; Chen et al., 2005; Song et al., 2007). Cells were screened for mycoplasma regularly by staining with Hoechst 33342 DNA dye, usually in conjunction with immunofluorescence experiments (described below). Cells were not cultured for more than 30 passages.

Treatment with metabolic stressors: Prior to exposure to stressors, cells were plated on matrigel-coated coverslips and allowed to attach for at least four hours in standard DMEM medium. For growth in medium containing different carbon sources, the medium was exchanged after cells had attached. Cells were then fixed 24 or 48 hours later. Our normal DMEM medium contains 25 mM glucose supplemented with 10% FBS. No glucose medium is DMEM with no added glucose (cat# 11966-025, Invitrogen) supplemented with 10% FBS. Low serum medium is DMEM (25 mM glucose) supplemented with 2% FBS. Galactose medium was previously described (Benard et al., 2007) and was made with DMEM containing no glucose but with 10 mM galactose, 10 mM HEPES pH 7.4, and 10% FBS.

For other treatments, cells were plated and maintained in standard (25 mM glucose) DMEM with 10% FBS. One day after plating, cells were treated with the following drugs for the following times: 25mM 2-deoxyglucose (Sigma cat#D8375, 16 hours), 10 μM oligomycin (Seahorse cat#101706-100, 16 hours), 10 μM antimycin A (Seahorse cat#101706-100, 16 hours), 10 μM rotenone (Seahorse cat#101706-100, 16 hours).

Mitochondrial fractionation: Mitochondria were fractionated using a previously published protocol (Tapper et al., 1983). Cells were washed twice in PBS, incubated for 10 minutes in 5 mM EDTA in PBS, and collected. Cells were pelleted and washed in TD buffer (25 mM Tris-HCl, pH 7.4, 0.7 mM Na_2HPO_4, 133 mM NaCl, 5 mM KCl). Cells were resuspended in RSB buffer (10 mM Tris-HCl pH 7.4, 10 mM NaCl, 1.5 mM $CaCl_2$, protease inhibitors (Sigma #P-2714)), to a final volume of about 10x the volume of the cell pellet, and incubated on ice for 20 minutes prior to homogenization with a Dounce glass/glass tight homogenizer (30 strokes). Lysis of cells was verified using trypan blue. MS buffer, prepared as a 2.5X stock, was added to yield a final concentration of 1x MS (5 mM Tris-HCl pH 7.4, 210 mM mannitol, 70 mM sucrose, 5 mM EDTA pH 8). Unbroken cells and nuclei were removed by centrifugation (10 min., 1000xg), after which mitochondria were pelleted from the post-nuclear supernatant (20 min., 14,000xg).

Mitochondria were then solubilized for 30 minutes on ice in 1% CHAPS, 25 mM HEPES pH 7.4, 100 mM NaCl, protease inhibitors.

Western blotting: Cells were harvested by rinsing twice with PBS, collected by incubation in 5 mM EDTA in phosphate buffered saline (PBS; 140 mM NaCl, 3 mM KCl, 10 mM Na_2HPO_4, 2 mM KH_2PO_4, pH 6.75), and pelleted in a microfuge (14,000 rpm, 4°C). Cells were lysed in 1% CHAPS, 25 mM HEPES pH 7.4, 100 mM NaCl, and protease inhibitors (Sigma #P-2714) on ice for 30 minutes, and the S14 was obtained by clarifying lysates by centrifugation for 30 minutes (14,000 rpm, 4°C). Protein concentrations were determined by Bradford Assay (Bio-Rad) using bovine serum albumin as standard. Samples were separated on 13% polyacrylamide gels and wet-transferred to nitrocellulose membranes (Bio-Rad #162-0112) at 70V for 2.5 hours. Western blotting procedures were carried out at room temperature. Membranes were blocked in blotto (5% (w/v) dry milk, 50 mM Tris pH 8, 2 mM $CaCl_2$, 80 mM NaCl, 0.2% (v/v) Tween-20, 0.02% sodium azide) for 1 hour. When probing for ARL2 (1:1000 dilution), membranes were blocked in an alternate blocking buffer (10% goat serum, 5% Tween-20 in PBS), freshly filtered through a 0.2 μm membrane. Membranes were then incubated with primary antibody in blocking buffer at 4°C overnight. Removal of excess primary antibody was carried out by washing the membranes in PBST (PBS with 0.1% Tween-20) three times for 10 min each. HRP-conjugated secondary antibodies (GE cat #NA934V, #NA931V) were diluted 1:5,000 in PBST and incubated with the membrane for 1 hour at room temperature. Excess secondary antibody was removed by washing the membranes in PBST 3 times for 10 min each, then incubated in luminol containing solution (0.1 mM Tris-HCl pH 8.0, 1.2 mM luminol, 0.2 mM p-coumaric acid, 0.009% hydrogen peroxide) for 1 min prior to exposure to film.

Transfections: Cells at 90% density or higher were transfected in 6 well plates using the following protocols. Both the amount of DNA and the ratio of Lipofectamine: DNA were separately optimized for ARL2 expression in HeLa and COS7 cells. A ratio of 2 μg

Lipofectamine: 1 µg DNA yielded the highest transfection efficiency. ARL2 plasmids (2 µg) were diluted in 250 µL Optimem (Invitrogen). Lipofectamine 2000 (4 µg; Invitrogen) was diluted in a separate tube containing 250 µL Optimem, vortexed briefly, and incubated at room temperature for 5 minutes. The tubes were mixed and incubated 20 minutes. Cell culture medium was changed to 1.5 ml of Optimem, and transfection complexes (500 µL) were added dropwise to the cells. After 4 hours, cells were trypsinized and replated onto coverslips, typically at a 1:3 (24 hour time point) or 1:4 (48 hour time point) split. This transfection typically resulted in at least 70% of cells overexpressing ARL2.

MEFs were transfected using a similar protocol. Both the amount of DNA and the ratio of Lipofectamine: DNA were optimized for expression in MEFs. A ratio of 3 µg Lipofectamine: 1 µg DNA yielded the highest percentage of transfected cells, based upon immunofluorescent staining. Plasmids (5 µg) and Lipofectamine 2000 (15 µg; Invitrogen) were diluted in separate tubes, each containing 250 µL Optimem. The tube containing Lipofectamine was vortexed briefly, and incubated at room temperature for 5 minutes. The tubes were then mixed and incubated 20 minutes at room temperature. Cell culture medium was changed to 1.5 ml of Optimem, and transfection complexes (500 µL) were added dropwise to the cells. After 4 hours, cells were trypsinized and replated onto matrigel-coated coverslips, typically at a 1:4 split, and allowed to attach overnight. This transfection protocol typically resulted in ~40% of MEFs expressing MFN1-myc or MFN2-myc.

Immunofluorescence: Cells grown on matrigel-coated coverslips were fixed in a pre-warmed (37°C) solution of 4% paraformaldehyde in PBS (10 mM Na_2HPO_4, 2 mM KH_2PO_4, pH 6.75, 140 mM NaCl, 3 mM KCl) for 15 minutes at room temperature, and then permeabilized with 0.1% (v/v) Triton X-100 in PBS for 10 minutes at room temperature. Incubation with primary antibodies was carried out in filtered PBS containing 1% (w/v) BSA at 4°C overnight, followed by 4 x 5 minute washes in PBS. Secondary antibodies (1:500, Alexa fluorophores, Invitrogen)

were incubated in PBS containing 1% BSA for 1 hour at room temperature. Secondary antibody was removed by 2 x 5 minute washes in PBS. DNA was then stained with Hoechst 33342 (1 μM) for 4 minutes, followed by 2 x 5 minute washes in PBS. Coverslips were then mounted onto slides using Prolong Antifade (Invitrogen). To perform pre-permeabilization fixation, cells were treated with ice-cold 0.5% saponin in PBS for 1 minute on ice and immediately fixed with ice cold 4% PFA. Staining was then performed as described above.

Imaging: Images were acquired using an Olympus FV1000 microscope and Olympus Fluoview v1.7 software, using 488 and 543 laser excitation and a 100x oil objective (1.45 NA). Images were acquired with a resolution of 1024x1024 pixels. Z-stacks were acquired with a step size of 0.37 μm, which were converted to average image intensity projections using ImageJ, where indicated. Whenever ARL2 or ELMOD2 staining was compared between different experimental conditions, imaging settings were held constant between slides and conditions. Cells were plated using coverslips from the same batch, fixed the same day, stained with the same dilution of antibody at the same time, and imaged the same day using the same parameters (laser power, gain, pinhole, and offset). No adjustments to ARL2/ELMOD2 staining were made post-acquisition (other than increasing brightness and contrast of images for easier visualization, which was applied uniformly to all images in any comparison), and post-imaging processing of ARL2 and ELMOD2 staining was limited to generation of z-stack projections. We noted that z-stack projections of ELMOD2 stained cells resulted in higher quality images, so are used for ELMOD2 images. No such improvement was noted with z stack projections of ARL2 stained cells, so single focal planes are shown in order to minimize image processing. Focal planes chosen for presentation were chosen with regard to bringing the most mitochondria in focus.

Results

Mitochondrial ARL2 staining is sensitive to re-plating and cell density

Studies of ARL2 began in the 1990's with a focus on its role in microtubules as a result of data from genetic studies in several model organisms (Hoyt et al., 1990; Stearns et al., 1990; Liu and Meinke, 1998; McElver et al., 2000; Radcliffe et al., 2000; Antoshechkin and Han, 2002). In contrast, studies in our lab during and since that period have consistently pointed to mitochondria as an important site of action for ARL2 (Sharer and Kahn, 1999; Sharer et al., 2002; Newman et al., 2014). Characterization of our specific rabbit polyclonal antibody directed against ARL2 allowed immunofluorescent and immunoblotting evidence of the existence of a mitochondrial pool of ARL2, estimated at ~5-10% of total cellular ARL2 (Sharer et al., 2002). Throughout our studies we have noted that the intensity of mitochondrial staining of ARL2 varied between experiments and cell lines. With our long term goal of understanding the mechanisms of both ARL2 regulation of mitochondrial fusion (Newman et al., manuscript submitted) and its connection to actions in other parts of the cell, we sought to better understand the sources of variation in staining profiles of mitochondrial ARL2. Systematic and careful analysis of imaging data allowed us to identify a number of conditions that contribute to variations in the intensity of imaging data for ARL2 in mitochondria. These are described below and we believe provide further support for our conclusion that ARL2 and its GAP, ELMOD2, regulate mitofusins and mitochondrial fusion and are themselves regulated in abundance inside mitochondria.

The first variable identified was the length of time between plating of cells and fixation prior to imaging. When HeLa cells were fixed and stained within 24 hours of plating, the ARL2 staining profiles were diffuse and only weakly reminiscent of mitochondria, though double labeling with mitochondrial markers confirmed that some ARL2 was indeed overlapping with markers of mitochondria and represented mitochondrial ARL2 (Figure 1). A time course showed that ARL2 staining became stronger and as a result more clearly overlapping with that of the matrix marker HSP60 (Figure 1B) or the intermembrane space (IMS) marker cytochrome c (data not shown) after two days and even more so by the third day. This does not appear to be the result

of depletion of nutrients from culture medium as more frequent feeding with fresh medium did not alter this time course. By the fourth day after plating (data not shown) or if the initial plating was done at higher density (Fig. 1B), cells were typically near confluence and we found that mitochondrial staining of ARL2 was clearly decreased. When the time after plating was held constant but the cell density was varied it was quite clear that higher cell density resulted in decreased mitochondrial staining; typically, this was evident as cells approached ~90% confluence. Note that the effects of time after plating and cell density are quite obvious by visual inspection and consistent throughout the cell population, as seen in the view shown in Figure 1A, but are more evident as mitochondrial-specific in the enlarged view of single cells, shown in Figure 1B and later figures. The effects of days after plating on ARL2 staining at mitochondria was evident in HeLa and MEFs but not COS7 cells, although the effects of cell density on ARL2 was observed in all three cell lines. We also observed that mitochondrial staining of ELMOD2, an ARL2 GAP, diminished with confluence (Figure 2A) but was unchanged with days after plating (Figure 2B). While consistent and highly reproducible, the effects of time after plating and cell density on ARL2 staining were weaker than other effects on ARL2 staining, described below. Note that all immunofluorescence data described used fixation with 4% paraformaldehyde and permeabilization with 1% Triton X-100. These conditions were chosen as optimal for visualization of mitochondrial proteins, particularly ARL2 as its larger cytosolic pool is expected to be incompletely fixed and appear as diffuse staining throughout the cell. However, it is also quite apparent that under these conditions our rabbit, polyclonal antibody raised against ELMOD2 yields a strong signal in the nucleus (Figures 2 and others). This nuclear staining is present in the pre-immune serum and is not competed by prior incubation of the primary antibody with antigen (purified, recombinant ELMOD2) and thus is non-specific. This is in contrast to the signal from this same antibody that overlaps with mitochondria markers, e.g., HSP60 (e.g., Figures 2, 3D, 4B). As a result of these initial data, all comparisons in staining intensities are controlled for time after plating and for cell densities.

Deletion of MFN2 increases mitochondrial staining of ARL2 and ELMOD2

We recently reported that ARL2 regulates mitochondrial fusion upstream of the mitofusins (Newman, et al., manuscript submitted). Using immortalized MEFs deleted for MFN1, MFN2, or both mitofusins (Chen et al., 2003; Koshiba et al., 2004; Chen et al., 2005; Song et al., 2007), we found that expression of the dominant active point mutant, ARL2[Q70L], reversed mitochondrial fragmentation associated with the loss of either MFN1 or MFN2, but not the loss of both. When we stained wild type, *mfn1*$^{-/-}$, *mfn2*$^{-/-}$, or *mfn1*$^{-/-}$*mfn2*$^{-/-}$ MEFs, grown under the same conditions (DMEM medium, 25 mM glucose, 10% FBS), we found strong differences in the levels of endogenous mitochondrial ARL2 staining. MEFs were plated at the same density, and fixed, stained, and imaged in parallel, to control for other factors that may influence the results, as described above. While we observed mitochondrial staining of ARL2 in wild type MEFs, it was clearly stronger in *mfn2*$^{-/-}$ MEFs, and even stronger in the double null (*mfn1*$^{-/-}$*mfn2*$^{-/-}$) MEFs (Figure 3). Though most *mfn1*$^{-/-}$*mfn2*$^{-/-}$ MEFs had clearly stronger mitochondrial staining of ARL2, compared to *mfn2*$^{-/-}$ or wild type MEFs, we noted an increase in heterogeneity in mitochondrial staining of ARL2, compared to the other two MEF lines, possibly due to the previously documented heterogeneity among mitochondria within these cells due to the complete loss of fusion (Chen et al., 2005). Because of this greater heterogeneity we show both a field of cells as well as an enlarged view of 1-2 cells in Figures 3A and B, respectively, with the latter showing double labeling with the matrix marker HSP60. We obtained the same results when ARL2 was visualized with a mouse monoclonal antibody, detecting the increases in staining of mitochondrial ARL2 in *mfn2*$^{-/-}$ and *mfn1*$^{-/-}$*mfn2*$^{-/-}$ MEFs (data not shown). In striking contrast, mitochondrial ARL2 staining in *mfn1*$^{-/-}$ MEFs was clearly diminished, compared to wild type MEFs, with the majority of cells in the population showing no discernable mitochondrial ARL2 signal (Figure 3A, B). Figure 3 also shows, particularly when viewing HSP60 staining, the

fragmentation of mitochondria that results from the loss of MFNs, as described previously (Chen et al., 2003; Chen et al., 2005). Because mitochondrial staining was increased in *mfn2*$^{-/-}$ and *mfn1*$^{-/-}$*mfn2*$^{-/-}$ MEFs, but decreased in *mfn1*$^{-/-}$ MEFs, the increase in mitochondrial signal was clearly not simply an indirect result of mitochondrial fragmentation and was linked to MFN2.

ELMOD2 was first identified as an ARL2 binding partner based upon its GTPase activating protein (GAP) activity (Bowzard et al., 2007) and later evidence pointed to it acting as an ARL2 effector in mitochondria (Newman et al., 2014). Thus, we asked if mitochondrial ELMOD2 staining is also sensitive to MFN2 deletion, and found that it too is elevated in MEFs deleted for MFN2 over that seen in wild type cells (Figure 3C, D). The double null *mfn1*$^{-/-}$*mfn2*$^{-/-}$ cells also displayed higher staining than seen in the wild type MEFs, though this was not clearly or consistently higher than that seen in *mfn2*$^{-/-}$ cells. The ELMOD2 signal was not obviously weaker in the *mfn1*$^{-/-}$ cells than in wild type, perhaps due to the overall weak mitochondrial staining of ELMOD2 in wild type MEFs (Figure 3C, D). Thus, ARL2 and ELMOD2 staining in mitochondria are each specifically increased in cells deleted for MFN2, though only ARL2 is clearly decreased in cells deleted only for MFN1. We observed no evident changes in HSP60 (Figure 3B) or cytochrome c (not shown) signals between these MEF lines, supporting the conclusion that the changes in staining were specific to ARL2 and ELMOD2 in these different MEF populations. Immunoblots of total cell lysates from wild type, *mfn1*$^{-/-}$, *mfn2*$^{-/-}$, or *mfn1*$^{-/-}$ *mfn2*$^{-/-}$ MEFs showed no differences in the levels of endogenous ARL2 or ELMOD2 between these different cell lines (data not shown), supporting our conclusion that the mitochondrial pool of ARL2 and ELMOD2 was specifically altered.

Increased mitochondrial staining of ARL2 and ELMOD2 in mfn1$^{-/-}$*mfn2*$^{-/-}$ *MEFs is reversed upon expression of MFN2 and restoration of tubular morphology*

As a further test of specificity of the effects of MFN2 deletion, we performed rescue experiments. Transfection of *mfn1*$^{-/-}$*mfn2*$^{-/-}$ MEFs with pcDNA3.1 (empty vector) resulted in no changes in either mitochondrial morphology or ARL2 staining (Figure 4A, left). Expression of MFN2-myc in these cells restored tubular mitochondrial morphology, as previously reported (Detmer and Chan, 2007). MFN2-myc also reversed the increased ARL2 staining of mitochondria (Figure 4A). The differences between the mitochondrial staining of ARL2 in *mfn1*$^{-/-}$*mfn2*$^{-/-}$ cells expressing MFN2-myc, compared to empty vector control, is perhaps the strongest change in staining of ARL2 that we observed in this study. Because transient transfection yields a mixed population in terms of transfected cells and in levels of protein expression, it was quite apparent that there was a strong correlation between the ability of MFN2-myc expression to reverse mitochondrial fragmentation and elevated mitochondrial staining of ARL2. In most cells with tubular morphology, ARL2 staining was reduced to the point where it was barely detectible and lower even than ARL2 staining in wild type MEFs (Figure 3A). As mitochondrial staining of ARL2 is reduced, the cytosolic staining becomes more evident (e.g., see Figure 4A, top MFN2-myc panel), thus the loss in mitochondrial ARL2 signal is perhaps best seen in the merged image, revealing the clear loss in overlap with HSP60, the mitochondrial marker. Though a minority of MFN2-myc expressing cells with tubular mitochondrial morphology still displayed mitochondrial staining of ARL2, this staining was clearly diminished compared to untransfected cells or cells receiving empty vector. In MFN2-myc positive cells with fragmented mitochondria, ARL2 staining remained high, suggesting that the effect was correlated with reversal of fragmentation.

We performed the same experiments to investigate effects of MFN2 expression on reversal of increased mitochondrial staining of ELMOD2, and found that MFN2-myc could also reverse the increase (Figure 4B). MEFs deleted for both MFNs displayed strong ELMOD2 staining that overlapped extensively with that of HSP60 (Figure 4B, left panels). In contrast, the double MFN null cells expressing MFN2-myc had clearly reduced staining of mitochondrial

ELMOD2, as evidenced by the lack of overlap between the ELMOD2 and myc staining (Figure 4B). And as was true for ARL2, we observed a strong correlation between rescue of fragmentation by MFN2 and the loss of mitochondrial staining of ELMOD2. Similarly, the small percentage of *mfn1*$^{-/-}$*mfn2*$^{-/-}$ MEFs that expressed low levels of MFN2-myc and retained fragmented mitochondria displayed high levels of mitochondrial ELMOD2 staining that was comparable to cells receiving empty vector. Similar results were obtained when cells were examined 24 or 48 hours after transfection.

Because the reversal of increased mitochondrial ARL2/ELMOD2 staining in *mfn1*$^{-/-}$ *mfn2*$^{-/-}$ MEFs by MFN2-myc was correlated with restoration of tubular morphology, we asked if the reversal depended on the fusogenic activity of the expressed MFN2. A mutation in the GTPase domain of MFN2, [K109A], abolishes its fusogenic activity. We confirmed the failure of MFN2[K109A]-myc to reverse the fragmentation phenotype in *mfn1*$^{-/-}$*mfn2*$^{-/-}$ MEFs (Detmer and Chan, 2007) (Figure 4). No changes in the staining of ARL2 and ELMOD2 were observed in cells expressing MFN2[K109A]-myc, compared to empty vector controls. Staining of ARL2 and ELMOD2 remained mitochondrial, indistinguishable in intensity from controls, and co-localized with myc staining (Figure 4). Results were the same when cells were fixed 24 or 48 hours after transfection. Therefore, we consistently observed close correlations between staining intensities of ARL2 and ELMOD2 at mitochondria and fusion activity of MFN2; e.g., the ability of MFN2 to reverse the increased ARL2/ELMOD2 mitochondrial signal requires its fusogenic activity.

Expression of MFN1-myc also reversed fragmentation in *mfn1*$^{-/-}$*mfn2*$^{-/-}$ MEFs, as previously reported (Detmer and Chan, 2007). But in marked contrast to MFN2-myc, MFN1-myc did not reverse the increased staining of mitochondrial ARL2 (Figure 4A) or ELMOD2 (Figure 4B). Thus, the reversal of elevated ARL2 staining seen with MFN2-myc expression was not due simply to restoration of tubular morphology but was specific to, and perhaps dependent upon, MFN2-mediated fusion. Similar results were obtained 24 and 48 hours after transfection.

In order to ensure that the changes in mitochondrial ARL2 and ELMOD2 were not simply due to differences in expression levels between MFN2-myc, MFN2[K109A]-myc, and MFN1-myc, we performed immunoblots, probing for the myc epitope on the recombinant proteins, of *mfn1*$^{-/-}$*mfn2*$^{-/-}$ MEFs after expressing each construct. These immunoblots showed no differences in the levels of expression between MFN2-myc and MFN2[K109A]-myc (Figure 4C). The signal detected for MFN1-myc was lower than that seen for MFN2-myc, but the MFN1 fusion protein contains 10 myc tags on its C terminus, while each of the MFN2 proteins carries 16 myc tags. The increase in number of epitope tags is expected to increase the sensitivity in immunoblots using the myc antibody and also likely explains the slightly faster mobility of MFN1-myc in these gets (Figure 4C). Thus, it is likely that MFN1-myc and MFN2-myc fusions proteins are expressed to comparable levels as the same vector was used and they each rescue the mitochondrial morphology defects observed in the deletion strains.

Finally, we attempted to dissociate MFN2-mediated fusion from changes in ARL2 and ELMOD2 signal at mitochondria. Mutations in MFN2 cause Charcot Marie Tooth Type 2A, a peripheral neuropathy (Zuchner et al., 2004). Though most disease-associated mutations (such as [R94Q]) interfere with the fusogenic activity of MFN2, a subset (e.g., [V69F], [L76P], [R274]) are still capable of fusion (Detmer and Chan, 2007). We asked if these MFN2 mutants, which are still capable of fusion, have differential effects on ARL2 or ELMOD2 staining at mitochondria, compared to MFN2-myc. We expressed myc-tagged MFN2 harboring [V69F], [L76P] or [R274] mutations in *mfn1*$^{-/-}$*mfn2*$^{-/-}$ MEFs and found that each MFN2 mutant restored tubular morphology, as previously described (Detmer and Chan, 2007). Furthermore, each mutant also reversed the increased ARL2 or ELMOD2 staining at mitochondria, similar to wild type MFN2-myc, at both 24 and 48 hours after transfection. In contrast, MFN2[R94Q]-myc failed to rescue fragmentation, consistent with previously published data (Detmer and Chan, 2007), and did not reverse the elevated ARL2 and ELMOD2 staining in *mfn1*$^{-/-}$*mfn2*$^{-/-}$ MEFs. These data further support our

conclusion that changes in ARL2 and ELMOD2 staining at mitochondria are linked to MFN2-mediated fusion.

Increased mitochondrial staining of ARL2 and ELMOD2 in mfn2$^{-/-}$ MEFs is also reversed upon expression of MFN2 and restoration of tubular morphology

With the result that MFN2-myc could reverse the increased mitochondrial ARL2/ELMOD2 observed in *mfn1$^{-/-}$mfn2$^{-/-}$* MEFs, we asked if MFN2-myc could also reverse the increased staining in *mfn2$^{-/-}$* MEFs. Introduction of MFN2-myc in *mfn2$^{-/-}$* MEFs led to restoration of tubular mitochondria, as well as a decrease in mitochondrial ARL2/ELMOD2 (Figure 5A, B), similar to our results in *mfn1$^{-/-}$mfn2$^{-/-}$* MEFs. Next, we tested if MFN2[K109A]-myc failed to reverse staining of ARL2/ELMOD2, as in *mfn1$^{-/-}$mfn2$^{-/-}$* MEFs. Expression of MFN2[K109A]-myc in *mfn2-/-* MEFs restored tubular mitochondrial morphology in ~50% of transfected cells, consistent with previously reported data (Chen et al., 2003). The partial rescue by MFN2[K109A]-myc in *mfn2$^{-/-}$* MEFs, compared to the lack of any rescue of fragmentation in *mfn1$^{-/-}$mfn2$^{-/-}$* MEFs, is likely due to the presence of endogenous MFN1 in *mfn2$^{-/-}$* MEFs, as MFN1 and MFN2 can hetero-oligomerize to promote fusion (Chen et al., 2003; Eura et al., 2003; Chen et al., 2005). In MEFs expressing MFN2[K109A]-myc and displaying tubular morphology, we observed a decrease in ARL2 and ELMOD2 mitochondrial signal, comparable to expression of MFN2-myc (Figure 5A, B). However, in the remaining cells expressing MFN2[K109A]-myc that retained fragmented mitochondria, mitochondrial staining of ARL2/ELMOD2 remained high and overlapped with mitochondrial myc staining (Figure 5A, B right most panels). Cells expressing MFN2[K109A]-myc with fragmented mitochondria generally appeared to have lower levels of myc expression (Figure 5A, B), possibly explaining the lack of rescue in those cells. Altogether, we conclude that the increase in mitochondrial staining of ARL2 and ELMOD2 that

is so evident in cells deleted for MFN2, alone or in combination with MFN1, is dependent on the ability of MFN2 to support fusion in MEFs.

Expression of MFN2-myc in wild type MEFs does not alter mitochondrial staining of ARL2 or ELMOD2

As re-introduction of MFN2 in *mfn1*$^{-/-}$*mfn2*$^{-/-}$ MEFs caused a decrease in mitochondrial staining of ARL2, we tested if MFN2-myc could also decrease endogenous mitochondrial ARL2 or ELMOD2 in wild type MEFs. Empty vector, MFN1-myc, or MFN2-myc were expressed in wild type MEFs, which were fixed and stained for HSP60 and either ARL2 or ELMOD2 24 or 48 hours later. Wild type MEFs receiving empty vector displayed tubular mitochondrial morphology, whereas MFN1-myc and MFN2-myc led to elongation of mitochondria. Neither empty vector, MFN1-myc, nor MFN2-myc had any obvious effect on mitochondrial staining of ARL2 or ELMOD2 in wild type cells, which remained weakly mitochondrial (appearing similar to Figure 3) (data not shown). Thus, there may exist minimal levels of ARL2 and ELMOD2 which are not subject to regulation by the levels of MFN2.

Mitochondrial ARL2 and ELMOD2 staining increases in response to cellular stressors that cause mitochondrial elongation

Mitochondrial elongation occurs in response to cellular stressors, such as glucose deprivation, as a result of increased fusion and decreased fission (Gomes and Scorrano, 2011; Rambold et al., 2011; Lee et al., 2014; Mishra et al., 2014). Therefore, we asked if mitochondrial staining of ARL2 or ELMOD2 changed in response to different culture conditions, and if these effects were correlated with changes to mitochondrial morphology. We found that the intensity of

ARL2 staining at mitochondria, as visualized by immunofluorescence, was markedly increased under a number of conditions. Two of the conditions that yielded among the most striking changes were growth of COS7 cells in the absence of glucose (0 glucose), or in low (2%) serum (Figure 6). Our cells are routinely maintained in DMEM that contains 25 mM glucose supplemented with 10% fetal bovine serum (FBS). These effects were evident one day after changing the medium to 0 glucose or 2% FBS and were further increased two days after the medium change. In contrast to the marked differences seen in ARL2 staining, no changes in intensity were observed with several other mitochondrial markers, including HSP60 (mitochondrial matrix protein), cytochrome c (mitochondrial IMS protein), TOM20 (outer membrane), Complex I subunit NDUFA9 (inner membrane), Complex III subunit UQCRC2, and Complex V subunit alpha. Similar, though somewhat less striking effects on ARL2 staining, but not those of mitochondrial markers, were observed when cells were cultured for 48 hours in 10 mM galactose with 0 glucose, which makes cells more dependent upon respiration instead of glycolysis (data not shown) (Benard et al., 2007).

We found that mitochondrial staining of ELMOD2 was also increased when cells were grown in the absence of glucose or in low (2%) serum (Figure 7). The kinetics of these effects were similar to those seen for ARL2, with ELMOD2 staining increased after 24 hours, and more so after 48 hours in all three cell lines. Also like ARL2, when cells were grown in galactose containing medium (10 mM, with 0 glucose), we found that ELMOD2 staining was increased within 24 hours and further increased after 48 hours (data not shown). The increase in ELMOD2 staining seen in galactose was less prominent than the effect with 0 glucose or low serum, again similar to ARL2.

In addition to the increased staining of ARL2 and ELMOD2 under the conditions described above, we also observed changes in mitochondrial morphology resulting from the treatments used. Growth in 0 glucose, 2% serum, or 10 mM galactose each resulted in an increase

in mitochondrial elongation, branching, and looping structures, compared to controls (Figures 6,7). This effect was most obvious with 0 glucose or in galactose medium, and was observed in COS7, HeLa, and MEFs, though was most obvious in MEFs, due to mitochondria appearing more elongated in untreated COS7 and HeLa cells. These changes in mitochondrial morphology are consistent with previously published data in regards to cellular starvation (Tondera et al., 2009; Gomes et al., 2011; Rambold et al., 2011; Lee et al., 2014; Mishra et al., 2014; Toyama et al., 2016).

ARL2 and ELMOD2 mitochondrial staining is further increased in stressed mfn2$^{-/-}$ and mfn1$^{-/-}$ mfn2$^{-/-}$ MEFs, but not mfn1$^{-/-}$ MEFs

Given that deletion of MFN2 or starving cells for serum or glucose each increase ARL2 staining in mitochondria, we asked if these effects were additive. We grew wild type, *mfn1*$^{-/-}$, *mfn2*$^{-/-}$, or *mfn1*$^{-/-}$*mfn2*$^{-/-}$ MEFs in normal, 0 glucose, or low serum media for two days before fixing and processing. The wild type MEFs grown in either 0 glucose or low serum had increased ARL2 and ELMOD2 mitochondrial signal compared to those grown in normal medium (Figure 8A, B), and displayed elongated mitochondria, as described above in COS7 and HeLa cells. MEFs deleted for MFN2 cultured in 0 glucose or low serum media had increased ARL2 or ELMOD2 mitochondrial staining compared to the same cells grown in normal medium (Figure 8A). Similarly, *mfn1*$^{-/-}$*mfn2*$^{-/-}$ MEFs grown in 0 glucose or low serum media also had stronger ARL2 (Figure 8A) and ELMOD2 (Figure 8B) mitochondrial staining over that seen in normal medium. For each of the MEF cell lines, the 0 glucose condition resulted in the strongest increase in ARL2 staining, while it was growth in low serum that resulted in the strongest increase in ELMOD2 staining. In contrast, there was little to no increase in ARL2 or ELMOD2 staining in

mfn1$^{-/-}$ MEFs grown in no glucose or low serum medium for 48 hours, compared to mfn1-/- MEFs grown in normal medium (Figure 8).

We also observed striking differences in mitochondrial morphology in response to stress between the MEF lines. MEFs deleted for MFN2 that were cultured in normal medium had fragmented mitochondria, compared to wild type cells, but growth of *mfn2*$^{-/-}$ MEFs in 0 glucose or low serum resulted in a partial reversal in mitochondrial morphology, displaying an intermediate, rod-shaped morphology, with some cells displaying a tubular morphology (Figure 8). In contrast, *mfn1*$^{-/-}$ MEFs show no evidence of even partial rescue of the fragmentation resulting from the absence of MFN1 when grown in 0 glucose or low serum. Finally, *mfn1*$^{-/-}$*mfn2*$^{-/-}$ MEFs cultured in 0 glucose or low serum also displayed no differences in mitochondrial morphology compared to cells grown in normal medium, consistent with their inability to undergo fusion (Chen et al., 2005).

Metabolic inhibitors increase mitochondrial staining of ARL2 but not ELMOD2

Mitochondrial fusion is linked to the activity of the electron transport chain (Mishra et al., 2014). Therefore, we also tested other metabolic stressors to determine the variety of both the conditions and the time courses that influence mitochondrial ARL2 staining intensities. We found that every metabolic poison acting on ATP generation that we tested resulted in increased mitochondrial staining of ARL2. The strongest effect was observed after an overnight (16 hr) treatment with 2-deoxyglucose (25 mM), an inhibitor of glycolysis (Wick et al., 1957) (Figure 9). Similar effects were also observed when cells were treated with specific inhibitors of the electron transport chain; oligomycin (10 μM, complex V inhibitor), rotenone (10 μM, complex I inhibitor), or antimycin A (10 μM, complex III inhibitor) (data not shown). Time courses were performed to determine the maximal effects of 2-deoxyglucose, oligomycin, or antimycin A. We

found that increased ARL2 staining was evident as soon as 3 hours after addition of each drug and continued to increase, peaking 16 hours after drug addition. Cells treated with rotenone did not show any obvious increase until overnight (16 hr) treatment. We also observed an increase in ARL2 staining with 1 hour of menadione treatment, which increases mitochondrial ROS (Castro et al., 2008). These effects were observed in all three cell lines examined – COS7, HeLa, and MEFs (Table 1).

In marked contrast to ARL2, we found that ELMOD2 staining was not altered in response to the same drugs that caused mitochondrial ARL2 staining to increase. Overnight treatment of cells with 2-deoxyglucose (Figure 10), oligomycin, antimycin A, rotenone, or menadione (data not shown) had no effect on ELMOD2 staining (summarized in Table I). Unlike the 0 glucose and low serum treatments described above, which led to obvious mitochondrial elongation, none of the drugs caused mitochondrial elongation. Oligomycin, antimycin A, and rotenone caused mitochondrial fragmentation, while 2-deoxyglucose and menadione had minimal effects on mitochondrial morphology. Therefore, mitochondrial staining of ARL2 responds to metabolic stress, but staining of ELMOD2 only changes when mitochondrial elongation is observed.

Staining of ARL2 at mitochondria is not altered by stressors when the recombinant protein is directed to mitochondria

Western blots of whole cell lysates, comparing controls to the same cells after several of the treatments described, failed to detect any changes in the total cellular ARL2 expressed in any of the three cell lines tested (data not shown). Similarly, when mitochondria were enriched by differential centrifugation, pelleting mitochondria at 14,000 x g from a post-nuclear supernatant, we also could detect no changes in mitochondria-associated ARL2 or ELMOD2. HeLa cells

treated with 2-deoxyglucose, antimycin A, or oligomycin showed no increase in ARL2 in the P14. Similarly, no increases in ARL2 or ELMOD2 were observed between the crude mitochondria fractions from wild type, *mfn1*$^{-/-}$, *mfn2*$^{-/-}$, or *mfn1*$^{-/-}$*mfn2*$^{-/-}$ MEFs.

The finding that immunoblots of the crude mitochondria fraction from cells that display increased staining of ARL2 and ELMOD2 did not show correlated increases in the protein fractionating with mitochondria is difficult to interpret for a number of reasons. Our initial finding that simply detaching cells from the culture dish, the first step in both re-plating cells and for cell fractionation, may be sufficient to reverse any increases in staining at mitochondria (Figure 1) resulting from the treatments used, suggests that a reversible process is involved. As a result, rapid degradation or export of ARL2 and ELMOD2 from mitochondria in response to cell detachment may confound our fractionation results. In addition, we have previously documented that ARL2 localizes to both the matrix (based upon its binding to HSP60, sub-mitochondrial fractionation, and differential permeabilization of fixed cells; (Newman et al., 2014)(Newman, et al., manuscript submitted) and the IMS, based upon sub-mitochondrial fractionation (Sharer et al., 2002) and demonstrated activity in rescue fragmentation in MEFs deleted for MFNs (Newman et al., manuscript submitted); so the pool of ARL2 that is responding to stress may be a subset of the total mitochondrial ARL2. While we believe that the increased import of ARL2 into mitochondria explains the increased ARL2 staining, there exist other possibilities that we sought to test. For example, a time-dependent incorporation of ARL2/ELMOD2 into a macromolecular complex or change in tertiary structure, resulting in altered access of antibodies to specific epitopes upon fixation, could yield the changes in staining intensities identified above.

To ask if changes in antibody recognition of the epitope were involved, we expressed ARL2 carrying a small epitope tag at its C-terminus, ARL2-HA, in HeLa cells and examined changes in HA staining in cells in response to stressors that increase ARL2 staining. The C-termini of ARF family proteins are not involved directly in protein-protein interactions and thus

the access of antibodies to the HA epitope at that location is predicted to be unaltered by ARL2 binding to partners. Like untagged ARL2, ARL2-HA was partially imported into mitochondria, and a brief permeabilization of cells immediately prior to fixation (0.5% saponin for 1 minute) removed cytosolic ARL2 and allowed for better visualization of the mitochondrial pool (Newman, et al., manuscript submitted). Note that this pre-fixation permeabilization process results in changes in mitochondrial morphologies as they appear smaller and more fragmented than the same cells fixed prior to permeabilization. In addition, cells were imaged using higher laser power, due to loss of signal, so Z stack projections are shown as they average the increase in noise to yield the optimal signal to noise. ARL2-HA was expressed in cells, which were replated onto coverslips and grown in low serum. After two days, cells were permeabilized prior to fixation, and stained for ARL2 and HA. As expected, the low serum treatment increased endogenous mitochondrial ARL2 staining in cells receiving empty vector and also increased mitochondrial HA and ARL2 staining in cells expressing ARL2-HA (Figure 10). We were unable to perform a similar experiment for ELMOD2 as we found that epitope tagging at either the N or C terminus interfered with its localization to mitochondria. These results are consistent with the low serum treatment causing an increase in the abundance of ARL2-HA in mitochondria and suggest that increased ARL2 staining at mitochondria reflects increased mitochondrial import or half-life of the imported ARL2 rather than a change in antibody access to the fixed ARL2.

To further test the idea that the increased staining of ARL2 observed in mitochondria in response to stressors is the result of increased protein import, we generated a different epitope tagged construct for ARL2 that is targeted to the IMS, which we recently demonstrated is its site of action in regulating mitochondrial fusion (Newman et al., manuscript submitted). The SMAC-derived N-terminal leader sequence strongly targets the fusion protein (SMAC-HA-ARL2) to the IMS, where the leader sequence is cleaved and results in the strong localization of HA-ARL2 to the IMS. We have previously demonstrated that this construct is appropriately and efficiently

targeted to the IMS, with rapid cleavage of the SMAC leader and retention of the HA-tag in the IMS. We also showed that SMAC-HA-ARL2[T30N] retains the ability of ARL2[T30N] to fragment mitochondria (Newman et al., manuscript submitted), while the construct used here, SMAC-HA-ARL2, does not alter mitochondrial morphology. SMAC-HA-ARL2 was expressed in HeLa cells, which were replated onto coverslips and allowed to attach for four hours before changing to low serum medium. Two days later, cells were fixed and stained for ARL2 and HA. When ARL2 was imaged in cells receiving empty vector, we see the expected increase in endogenous ARL2 staining that co-localizes with mitochondrial markers, in response to growth of cells in low serum medium (data not shown). In contrast, in cells expressing SMAC-HA-ARL2, there was already a strong signal for HA or ARL2 from mitochondria and this was not further increased in response to growth in low serum (Figure 11). Similar results were obtained with OCT-HA-ARL2, which targets ARL2 to the matrix (data not shown). Taken together, these results suggest that the increased staining of ARL2 at mitochondria reflects increased levels of the protein, resulting from either increased import or decreased loss (degradation or export).

Discussion

ARL2 plays essential cellular roles both inside mitochondria, where it regulates energy metabolism and fusion (Sharer et al., 2002; Newman et al., 2014)(Newman et al., manuscript submitted), and in cytosol, where together with TBCD it regulates tubulin biogenesis, microtubules, and has links to cell division (Bhamidipati et al., 2000; Zhou et al., 2006; Tian et al., 2010). Because only a small minority of total cellular ARL2 is found inside mitochondria and the clear majority is tightly bound to TBCD in cytosol there is predicted to be a mechanism for regulating import into mitochondria, though such a mechanism remains elusive. Here, we describe changes in mitochondrial pools of ARL2 in response to a number of environmental changes; including changes in fusogenic activity resulting from deletion of mitofusins (particularly MFN2), time after cell attachment, cell density, and pharmacological stressors that

target energy metabolism. Many, but not all, of the changes observed in mitochondrial pools of ARL2 were also seen for the ARL2 GAP, ELMOD2. Once we were able to control for effects of time on a culture dish and cell density, the changes in ARL2 and ELMOD2 intensities became very clear and consistent in each of the three cell lines used in our studies (see Tables I and II for summaries). We discuss the interpretation of these results within the context of the existing literature and recent data from our lab that we believe demonstrate a role for ARL2, acting from the IMS, to regulate mitochondrial fusion (Newman et al., manuscript submitted).

What is responsible for the increases in staining of ARL2/ELMOD2 at mitochondria described here? Previously, we showed that mitochondrial ARL2 is increased in abundance several fold, only in the affected tissues, heart and skeletal muscle, of *ant1*$^{-/-}$ mice (Sharer et al., 2002), which display muscle wasting and cardiomyopathy (Graham et al., 1997). This observation was interpreted as evidence supporting the existence of a regulated mitochondrial import pathway and led us to study changes to ARL2 in response to stressors in cell culture. Our more recent studies of the effects of dominant mutants of ARL2 on mitochondrial morphology and motility, upstream of mitofusins (Newman et al., manuscript submitted), led us to investigate effects of changes in MFN levels on mitochondrial ARL2 and ELMOD2. While we see quite strong and uniform increases in ARL2 staining at mitochondria, no changes in ARL2 or ELMOD2 were detected in crude mitochondrial fractions by immunoblotting. However, our observation that simply trypsinizing and replating cells diminished ARL2 staining at mitochondria confounds interpretation of these results. We considered changes in availability of epitopes as an alternative explanation for the changes in fluorescence intensity. To control for this, we tested whether stress induced increases were evident in cells expressing C-terminal HA tagged ARL2 and found that they were. Because HA imaging used an unrelated antibody and is directed to a tag that is not present in endogenous ARL2, and thus not likely to be directly involved in protein-protein interactions, we interpret this as strongly supporting our conclusion

that the increased immunofluorescence signal is the result of increases in the amount of protein at mitochondria. This conclusion was further supported by the observation that another recombinant protein, SMAC-HA-ARL2, that is strongly driven to the IMS by the 52-residue SMAC leader sequence prior to its cleavage, did not display any changes in HA staining intensity in response to growth in low serum. Thus, it is not a change in the quaternary structure of the ARL2 inside mitochondria that occurs in response to stress but rather a change in the amount of ARL2 in that compartment. We performed a few experiments using a mouse monoclonal antibody to ARL2, in contrast to the widespread use of our rabbit polyclonal antibody, and found that they both yielded the same results. The epitopes are not known for either of these antibodies but as they were independently derived they further strengthen our conclusions. Finally, we believe the increases in ARL2 are inside mitochondria and not on the outer membrane for two reasons: (1) we have recently shown that ARL2 acts from the IMS to regulate fusion (Newman et al., manuscript submitted), and (2) the increased staining in response to 2-deoxyglucose seen in HeLa cells resulted in an increased signal in ARL2 puncta localized inside mitochondria when visualized by structured illumination microscopy (data not shown). Taken together, these results suggest that changes in ARL2, and by extension ELMOD2, staining is the result of changes in protein abundance specifically at this one organelle. These results cannot distinguish between an increase in protein abundance in mitochondria resulting from increased import vs decreased export or degradation, though we currently favor the former interpretation.

ARL2 and ELMOD2 levels in mitochondria were found to be sensitive to the presence of fusion-competent MFN2. MEFs deleted for MFN2 showed increased ARL2 and ELMOD2 staining at mitochondria, compared to controls. This increased staining was not due to the fragmentation observed in these MEFs, as *mfn1*$^{-/-}$ MEFs did not show increased ARL2/ELMOD2 staining. Though MFN1 and MFN2 share ~60% identity (Santel et al., 2003) and a level of functional redundancy regarding fusion, MFN2 is proposed to have additional metabolic roles

(Bach et al., 2003; Chen et al., 2005; Pich et al., 2005; Mourier et al., 2015; Schrepfer and Scorrano, 2016) and may play a role in mitochondria/ER tethering (de Brito and Scorrano, 2008), though this is contested (Cosson et al., 2012; Filadi et al., 2015). Increased levels of ARL2 and ELMOD2, along with mitochondrial fragmentation, could be reversed by expression of MFN2-myc in either *mfn2*$^{-/-}$ or *mfn1*$^{-/-}$*mfn2*$^{-/-}$ MEFs. Importantly, expression of MFN1-myc could reverse the fragmentation but not the elevation in ARL2 and ELMOD2 levels. This demonstrates that these changes in protein levels were not strictly correlated with the loss of fusion, per se, but more linked to the function(s) of MFN2. A fusion dead mutant (MFN2[K109A]), which cannot reverse fragmentation in *mfn1*$^{-/-}$*mfn2*$^{-/-}$ MEFs (Detmer and Chan, 2007), failed to decrease ARL2/ELMOD2 levels in these cells. Perhaps the most telling linkage between ARL2/ELMOD2 levels and MFN2 fusogenic activity was found when MFN2[K109A] was expressed in *mfn2*$^{-/-}$ MEFs. In this case fragmentation was partially reversed, presumably a result of the presence of MFN1 that can heterodimerize with the mutant MFN1 (Chen et al., 2003), as were the elevation in ARL2 and ELMOD2 at mitochondria. But there was a correlation evident between cells in which fusion had been restored and staining had been reversed.

Results described here further support our earlier conclusion that ARL2 acts in at least two distinct pathways in mitochondria, one affecting ATP levels that is independent of ELMOD2 and another that does involve ELMOD2 and regulates mitochondrial fusion and motility. ARL2 siRNA results in ~50% loss in cellular ATP, while ELMOD2 knockdown had no effect on ATP levels (Newman et al., 2014). Yet knockdown of either protein caused mitochondrial fragmentation and perinuclear clustering, from the loss of plus end directed motility. Despite its discovery as an ARL2 GAP, we view ELMOD2 as most likely acting in mitochondria as an effector, i.e., binding directly to the activated (GTP-bound) form of the GTPase and mediating its biological response, in this case fusion and motility. This is consistent with every other known ARF family GAP, each of which have been found to have effector properties (Zhang et al., 1998;

Zhang et al., 2003; East and Kahn, 2011; East et al., 2012). Note that ARL2 and ELMOD2 behave the same in response to the loss of MFNs in MEFs (summarized in Table II), in which mitochondrial fusion is altered. Yet the stressors of energy metabolism yield clear differences in responses of ARL2 and ELMOD2 (summarized in Table I). Treatments that lower cellular ATP (2-deoxyglucose, oligomycin, antimycin A, etc.) do not alter ELMOD2 mitochondrial staining, consistent with ELMOD2 not playing a role in regulation of ATP. However, a subset of conditions (0 glucose, low serum, and galactose) that increase ARL2 mitochondrial staining also increase ELMOD2 mitochondrial staining. These stressors led to mitochondrial elongation, consistent with changes in ARL2 and ELMOD2 being linked to mitochondrial fusion.

The simple observations that the amounts of ARL2 and ELMOD2 in mitochondria are sensitive to cell attachment and density suggest that a signaling pathway exists to communicate information from the cell surface to mitochondria. A precedent might be seen in STAT3, best known for its role in conveying signals from the cell surface to the nucleus but more recently shown to also act inside mitochondria (Gough et al., 2009; Wegrzyn et al., 2009b; Tammineni et al., 2013). Though we lack details of our signaling pathway, we have identified a number of conditions and reagents that activate it and thus provide the tools and assays required to further explore mechanisms.

To summarize, we conclude that ARL2 and ELMOD2 are increased in mitochondria in response to several types of cellular stress, and that this increase is most often correlated with MFN2 activity and mitochondrial fusion. These data are highly supportive of other studies from our lab (Newman, et al., manuscript submitted) in which we conclude that ARL2 acts from the IMS to regulate mitochondrial fusion upstream of the MFNs. They are also consistent with previous data from the ANT1 mouse knockout model which showed that ARL2 levels in mitochondria are subject to environmental changes that may be tissue specific as they were dramatically increased only in affected tissues, skeletal muscle and heart (Sharer et al., 2002).

Together they support the model that ARL2 and ELMOD2 levels in mitochondria are regulated and responsive to stressors and changes in MFN2-related fusogenic potential. The model that a regulatory GTPase that is predicted to have been present in the last eukaryotic common ancestor, ubiquitous in eukaryotes, and very highly conserved throughout eukaryotic evolution regulates essential aspects of mitochondrial functions, morphology, and motility has broad significance and potential impact to our understanding of the basic cell biology of this organelle and its roles in human disease.

Acknowledgements

We thank David Chan (Caltech) for the generous gift of plasmids and *mfn1*$^{-/-}$, *mfn2*$^{-/-}$, and *mfn1*$^{-/-}$*mfn2*$^{-/-}$ MEFs. We gratefully acknowledge Drs. Heidi McBride, David Chan, Victor Faundez, Elizabeth Sztul, and Gerald Shadel for their ideas and suggestions in discussions of this work at various stages. This research project was supported in part by the Emory University Integrated Cellular Imaging Microscopy Core of the Emory Neuroscience NINDS Core Facilities grant, P30NS055077. This work was supported by grants from the National Institutes of Health 5R01GM090158 to RAK and 1F31GM111047 to LEN, and an American Heart Association pre-doctoral fellowship 14PRE18840040 to LEN.

References

Antoshechkin, I., and Han, M. (2002). The C. elegans evl-20 gene is a homolog of the small GTPase ARL2 and regulates cytoskeleton dynamics during cytokinesis and morphogenesis. Dev Cell 2, 579-591.

Bach, D., Pich, S., Soriano, F.X., Vega, N., Baumgartner, B., Oriola, J., Daugaard, J.R., Lloberas, J., Camps, M., Zierath, J.R., Rabasa-Lhoret, R., Wallberg-Henriksson, H., Laville, M., Palacin, M., Vidal, H., Rivera, F., Brand, M., and Zorzano, A. (2003). Mitofusin-2 determines

mitochondrial network architecture and mitochondrial metabolism. A novel regulatory mechanism altered in obesity. J Biol Chem 278, 17190-17197.

Benard, G., Bellance, N., James, D., Parrone, P., Fernandez, H., Letellier, T., and Rossignol, R. (2007). Mitochondrial bioenergetics and structural network organization. J Cell Sci 120, 838-848.

Bhamidipati, A., Lewis, S.A., and Cowan, N.J. (2000). ADP ribosylation factor-like protein 2 (Arl2) regulates the interaction of tubulin-folding cofactor D with native tubulin. J Cell Biol 149, 1087-1096.

Bowzard, J.B., Cheng, D., Peng, J., and Kahn, R.A. (2007). ELMOD2 is an Arl2 GTPase-activating protein that also acts on Arfs. J Biol Chem 282, 17568-17580.

Castro, F.A., Mariani, D., Panek, A.D., Eleutherio, E.C., and Pereira, M.D. (2008). Cytotoxicity mechanism of two naphthoquinones (menadione and plumbagin) in Saccharomyces cerevisiae. PLoS One 3, e3999.

Chan, D.C. (2006). Mitochondrial Fusion and Fission in Mammals. Annu Rev Cell Dev Biol 22, 79-99.

Chen, H., Chomyn, A., and Chan, D.C. (2005). Disruption of fusion results in mitochondrial heterogeneity and dysfunction. J Biol Chem 280, 26185-26192.

Chen, H., Detmer, S.A., Ewald, A.J., Griffin, E.E., Fraser, S.E., and Chan, D.C. (2003). Mitofusins Mfn1 and Mfn2 coordinately regulate mitochondrial fusion and are essential for embryonic development. J Cell Biol 160, 189-200.

Cipolat, S., de Brito, O.M., Dal Zilio, B., and Scorrano, L. (2004). OPA1 requires mitofusin 1 to promote mitochondrial fusion. Proc Natl Acad Sci U S A 101, 15927-15932.

Cosson, P., Marchetti, A., Ravazzola, M., and Orci, L. (2012). Mitofusin-2 independent juxtaposition of endoplasmic reticulum and mitochondria: an ultrastructural study. PLoS One 7, e46293.

de Brito, O.M., and Scorrano, L. (2008). Mitofusin 2 tethers endoplasmic reticulum to mitochondria. Nature 456, 605-610.

Detmer, S.A., and Chan, D.C. (2007). Complementation between mouse Mfn1 and Mfn2 protects mitochondrial fusion defects caused by CMT2A disease mutations. J Cell Biol 176, 405-414.

East, M.P., Bowzard, J.B., Dacks, J.B., and Kahn, R.A. (2012). ELMO domains, evolutionary and functional characterization of a novel GTPase-activating protein (GAP) domain for Arf protein family GTPases. J Biol Chem 287, 39538-39553.

East, M.P., and Kahn, R.A. (2011). Models for the functions of Arf GAPs. Semin Cell Dev Biol 22, 3-9.

Eura, Y., Ishihara, N., Yokota, S., and Mihara, K. (2003). Two mitofusin proteins, mammalian homologues of FZO, with distinct functions are both required for mitochondrial fusion. J Biochem 134, 333-344.

Filadi, R., Greotti, E., Turacchio, G., Luini, A., Pozzan, T., and Pizzo, P. (2015). Mitofusin 2 ablation increases endoplasmic reticulum-mitochondria coupling. Proc Natl Acad Sci U S A 112, E2174-2181.

Gomes, L.C., Di Benedetto, G., and Scorrano, L. (2011). During autophagy mitochondria elongate, are spared from degradation and sustain cell viability. Nature cell biology 13, 589-598.

Gomes, L.C., and Scorrano, L. (2011). Mitochondrial elongation during autophagy: a stereotypical response to survive in difficult times. Autophagy 7, 1251-1253.

Gough, D.J., Corlett, A., Schlessinger, K., Wegrzyn, J., Larner, A.C., and Levy, D.E. (2009). Mitochondrial STAT3 supports Ras-dependent oncogenic transformation. Science 324, 1713-1716.

Graham, B.H., Waymire, K.G., Cottrell, B., Trounce, I.A., MacGregor, G.R., and Wallace, D.C. (1997). A mouse model for mitochondrial myopathy and cardiomyopathy resulting from a deficiency in the heart/muscle isoform of the adenine nucleotide translocator. Nat Genet 16, 226-234.

Hoyt, M.A., Stearns, T., and Botstein, D. (1990). Chromosome instability mutants of Saccharomyces cerevisiae that are defective in microtubule-mediated processes. Mol Cell Biol 10, 223-234.

Karbowski, M., and Youle, R.J. (2003). Dynamics of mitochondrial morphology in healthy cells and during apoptosis. Cell Death Differ 10, 870-880.

Koshiba, T., Detmer, S.A., Kaiser, J.T., Chen, H., McCaffery, J.M., and Chan, D.C. (2004). Structural basis of mitochondrial tethering by mitofusin complexes. Science 305, 858-862.

Labrousse, A.M., Zappaterra, M.D., Rube, D.A., and van der Bliek, A.M. (1999). C. elegans dynamin-related protein DRP-1 controls severing of the mitochondrial outer membrane. Mol Cell 4, 815-826.

Lee, J.-Y., Kapur, M., Li, M., Choi, M.-C., Choi, S., Kim, H.-J., Kim, I., Lee, E., Taylor, J.P., and Yao, T.-P. (2014). MFN1 deacetylation activates adaptive mitochondrial fusion and protects metabolically challenged mitochondria. J Cell Science 127, 4954-4963.

Li, Y., Kelly, W.G., Logsdon, J.M., Jr., Schurko, A.M., Harfe, B.D., Hill-Harfe, K.L., and Kahn, R.A. (2004). Functional genomic analysis of the ADP-ribosylation factor family of GTPases: phylogeny among diverse eukaryotes and function in C. elegans. FASEB J 18, 1834-1850.

Liu, C.M., and Meinke, D.W. (1998). The titan mutants of Arabidopsis are disrupted in mitosis and cell cycle control during seed development. The Plant journal : for cell and molecular biology 16, 21-31.

McElver, J., Patton, D., Rumbaugh, M., Liu, C., Yang, L.J., and Meinke, D. (2000). The TITAN5 gene of Arabidopsis encodes a protein related to the ADP ribosylation factor family of GTP binding proteins. Plant Cell 12, 1379-1392.

Mishra, P., Carelli, V., Manfredi, G., and Chan, David C. (2014). Proteolytic Cleavage of Opa1 Stimulates Mitochondrial Inner Membrane Fusion and Couples Fusion to Oxidative Phosphorylation. Cell Metabolism 19, 630-641.

Mourier, A., Motori, E., Brandt, T., Lagouge, M., Atanassov, I., Galinier, A., Rappl, G., Brodesser, S., Hultenby, K., Dieterich, C., and Larsson, N.G. (2015). Mitofusin 2 is required to maintain mitochondrial coenzyme Q levels. J Cell Biol 208, 429-442.

Newman, L.E., Zhou, C.-j., Mudigonda, S., Mattheyses, A.L., Paradies, E., Marobbio, C.M.T., and Kahn, R.A. (2014). The ARL2 GTPase Is Required for Mitochondrial Morphology, Motility, and Maintenance of ATP Levels. PLoS One 9, e99270.

Pich, S., Bach, D., Briones, P., Liesa, M., Camps, M., Testar, X., Palacin, M., and Zorzano, A. (2005). The Charcot-Marie-Tooth type 2A gene product, Mfn2, up-regulates fuel oxidation through expression of OXPHOS system. Hum Mol Genet 14, 1405-1415.

Radcliffe, P.A., Vardy, L., and Toda, T. (2000). A conserved small GTP-binding protein Alp41 is essential for the cofactor-dependent biogenesis of microtubules in fission yeast. FEBS Lett 468, 84-88.

Rambold, A.S., Kostelecky, B., Elia, N., and Lippincott-Schwartz, J. (2011). Tubular network formation protects mitochondria from autophagosomal degradation during nutrient starvation. Proc Natl Acad Sci U S A 108, 10190-10195.

Santel, A., Frank, S., Gaume, B., Herrler, M., Youle, R.J., and Fuller, M.T. (2003). Mitofusin-1 protein is a generally expressed mediator of mitochondrial fusion in mammalian cells. J Cell Sci 116, 2763-2774.

Sauvanet, C., Duvezin-Caubet, S., di Rago, J.P., and Rojo, M. Energetic requirements and bioenergetic modulation of mitochondrial morphology and dynamics. Semin Cell Dev Biol 21, 558-565.

Schrepfer, E., and Scorrano, L. (2016). Mitofusins, from Mitochondria to Metabolism. Mol Cell 61, 683-694.

Sharer, J.D., and Kahn, R.A. (1999). The ARF-like 2 (ARL2)-binding protein, BART. Purification, cloning, and initial characterization. J Biol Chem 274, 27553-27561.

Sharer, J.D., Shern, J.F., Van Valkenburgh, H., Wallace, D.C., and Kahn, R.A. (2002). ARL2 and BART enter mitochondria and bind the adenine nucleotide transporter. Mol Biol Cell 13, 71-83.

Smirnova, E., Griparic, L., Shurland, D.L., and van der Bliek, A.M. (2001). Dynamin-related protein Drp1 is required for mitochondrial division in mammalian cells. Mol Biol Cell 12, 2245-2256.

Song, Z., Chen, H., Fiket, M., Alexander, C., and Chan, D.C. (2007). OPA1 processing controls mitochondrial fusion and is regulated by mRNA splicing, membrane potential, and Yme1L. J Cell Biol 178, 749-755.

Stearns, T., Hoyt, M.A., and Botstein, D. (1990). Yeast mutants sensitive to antimicrotubule drugs define three genes that affect microtubule function. Genetics 124, 251-262.

Tammineni, P., Anugula, C., Mohammed, F., Anjaneyulu, M., Larner, A.C., and Sepuri, N.B. (2013). The import of the transcription factor STAT3 into mitochondria depends on GRIM-19, a component of the electron transport chain. J Biol Chem 288, 4723-4732.

Tapper, D.P., Van Etten, R.A., and Clayton, D.A. (1983). Isolation of mammalian mitochondrial DNA and RNA and cloning of the mitochondrial genome. Methods Enzymol 97, 426-434.

Tian, G., Thomas, S., and Cowan, N.J. (2010). Effect of TBCD and its regulatory interactor Arl2 on tubulin and microtubule integrity. Cytoskeleton (Hoboken) 67, 706-714.

Tondera, D., Grandemange, S., Jourdain, A., Karbowski, M., Mattenberger, Y., Herzig, S., Da Cruz, S., Clerc, P., Raschke, I., Merkwirth, C., Ehses, S., Krause, F., Chan, D.C., Alexander, C., Bauer, C., Youle, R., Langer, T., and Martinou, J.C. (2009). SLP-2 is required for stress-induced mitochondrial hyperfusion. EMBO J 28, 1589-1600.

Toyama, E.Q., Herzig, S., Courchet, J., Lewis, T.L., Losón, O.C., Hellberg, K., Young, N.P., Chen, H., Polleux, F., Chan, D.C., and Shaw, R.J. (2016). AMP-activated protein kinase mediates mitochondrial fission in response to energy stress. Science 351, 275-281.

Wegrzyn, J., Potla, R., Chwae, Y.J., Sepuri, N.B., Zhang, Q., Koeck, T., Derecka, M., Szczepanek, K., Szelag, M., Gornicka, A., Moh, A., Moghaddas, S., Chen, Q., Bobbili, S., Cichy, J., Dulak, J., Baker, D.P., Wolfman, A., Stuehr, D., Hassan, M.O., Fu, X.Y., Avadhani, N., Drake, J.I., Fawcett, P., Lesnefsky, E.J., and Larner, A.C. (2009). Function of mitochondrial Stat3 in cellular respiration. Science 323, 793-797.

Wick, A.N., Drury, D.R., Nakada, H.I., Wolfe, J.B., Britton, W.t.t.a.o.B., and Grabowski, R. (1957). Localization of the primary metabolic block produced by 2-deoxyglucose. J Biol Chem 224, 963-969.

Zhang, C.J., Bowzard, J.B., Anido, A., and Kahn, R.A. (2003). Four ARF GAPs in Saccharomyces cerevisiae have both overlapping and distinct functions. Yeast 20, 315-330.

Zhang, C.J., Cavenagh, M.M., and Kahn, R.A. (1998). A family of Arf effectors defined as suppressors of the loss of Arf function in the yeast Saccharomyces cerevisiae. J Biol Chem 273, 19792-19796.

Zhou, C., Cunningham, L., Marcus, A.I., Li, Y., and Kahn, R.A. (2006). Arl2 and Arl3 regulate different microtubule-dependent processes. Mol Biol Cell 17, 2476-2487.

Zuchner, S., Mersiyanova, I.V., Muglia, M., Bissar-Tadmouri, N., Rochelle, J., Dadali, E.L., Zappia, M., Nelis, E., Patitucci, A., Senderek, J., Parman, Y., Evgrafov, O., Jonghe, P.D., Takahashi, Y., Tsuji, S., Pericak-Vance, M.A., Quattrone, A., Battaloglu, E., Polyakov, A.V., Timmerman, V., Schroder, J.M., and Vance, J.M. (2004). Mutations in the mitochondrial GTPase mitofusin 2 cause Charcot-Marie-Tooth neuropathy type 2A. Nat Genet 36, 449-451.

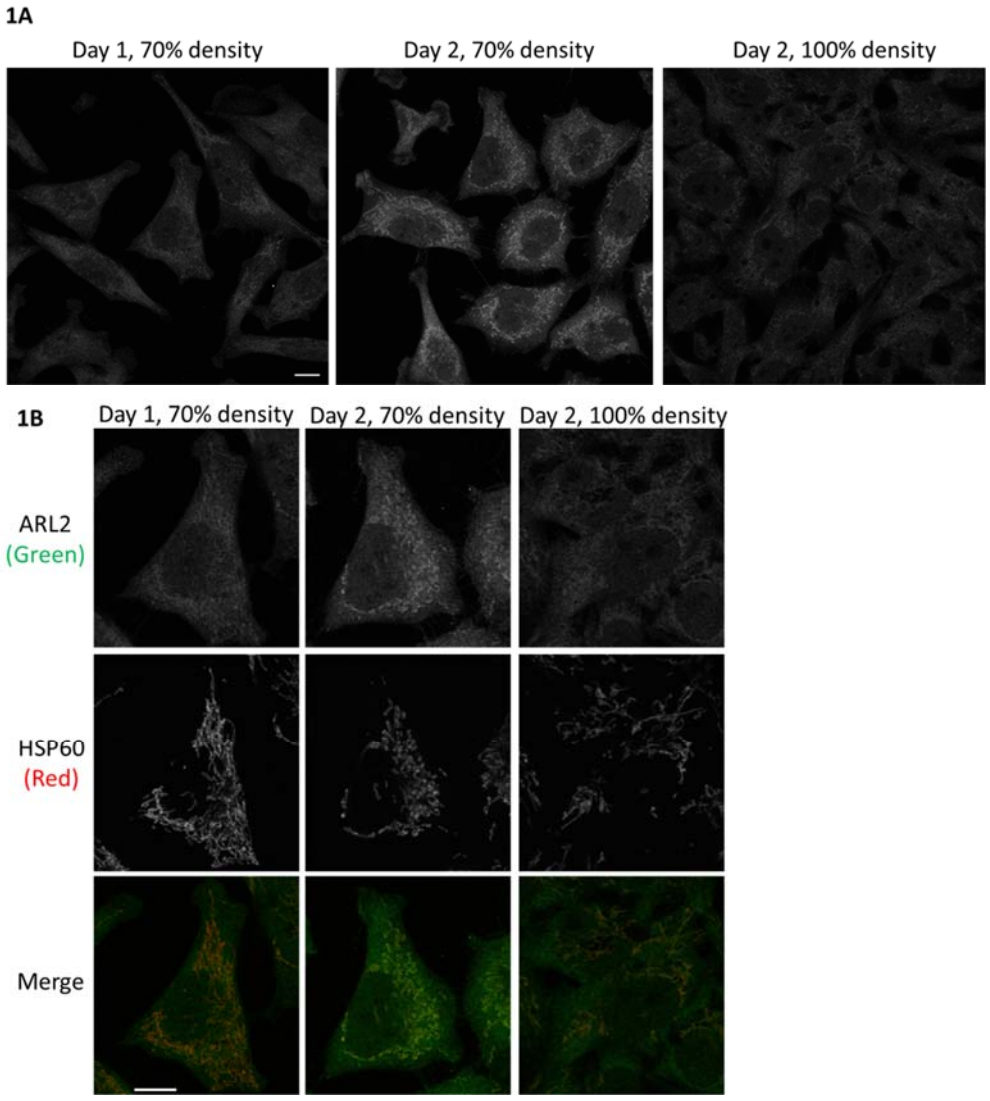

Figure 1: Mitochondrial staining of ARL2 increases with days after plating but diminishes at high cell densities. HeLa cells were seeded onto coverslips and fixed either one (left panels) or two days (middle panels) later, at ~70% confluence. To compare cells at lower and higher density, an additional plate was seeded with more cells and fixed on day 2 at 100% density (right panels). Cells were fixed and stained for ARL2 and HSP60, as described under Methods. (A) A field of cells stained for ARL2 for each condition is shown. (B) One cell from each field in A was selected and enlarged to help identify mitochondria. ARL2 (top panels) and HSP60 staining (middle panels) are shown separately, with merged images of the two channels on the bottom. Images are single planes acquired by confocal microscopy. Scale bar = 10 μm.

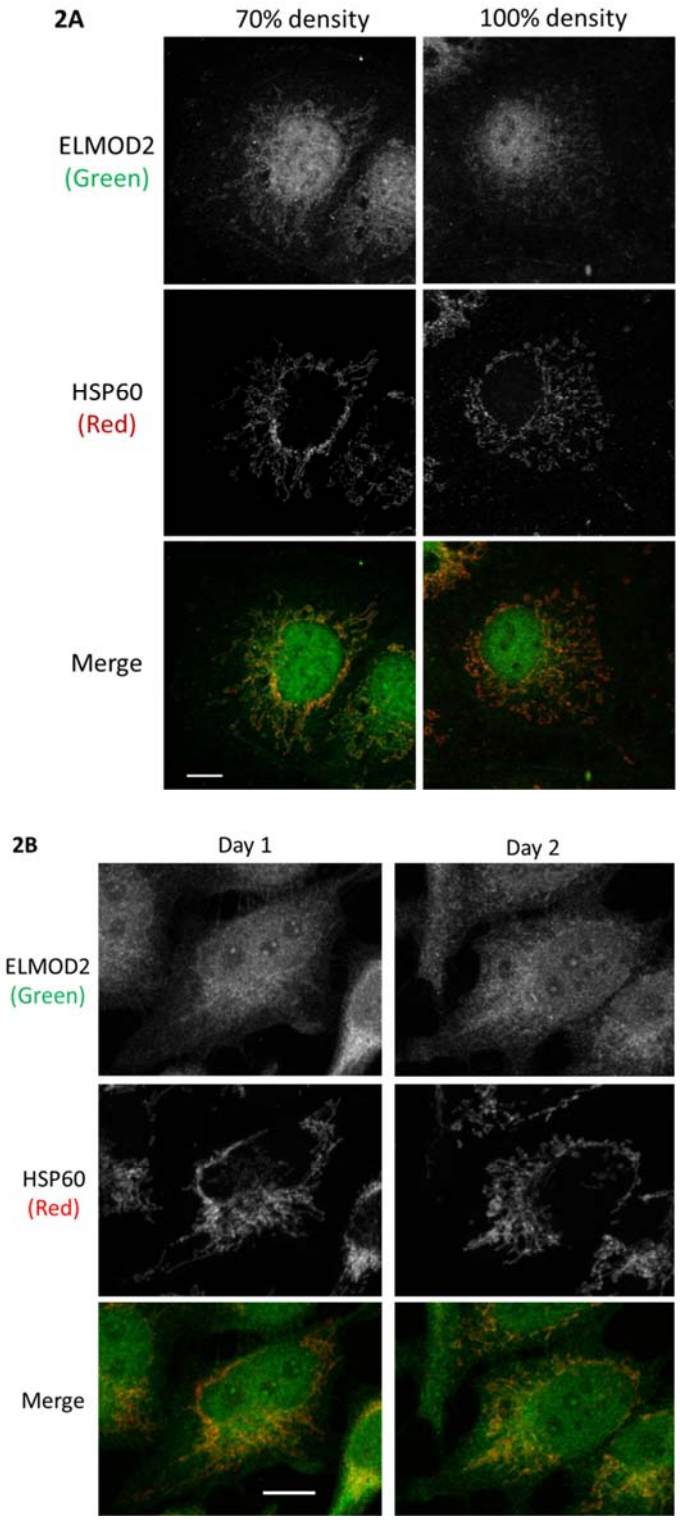

Figure 2: Mitochondrial staining of ELMOD2 diminishes upon approaching confluence but is unchanged with days after plating. (A) To compare cells at 70% and 100% (confluent) densities cells were seeded at different densities and imaged 2 days later. (B) HeLa cells were seeded onto

coverslips and fixed either one or two days later, at 70% confluence. All cells were fixed and stained for ELMOD2 and HSP60. ELMOD2 (top panels) and HSP60 staining (middle panels) are shown separately, with merged images of the two channels on the bottom. Images are single planes acquired by confocal microscopy. Note that the nuclear staining of ELMOD2 is non-specific, as described in the text. Scale bar = 10 μm.

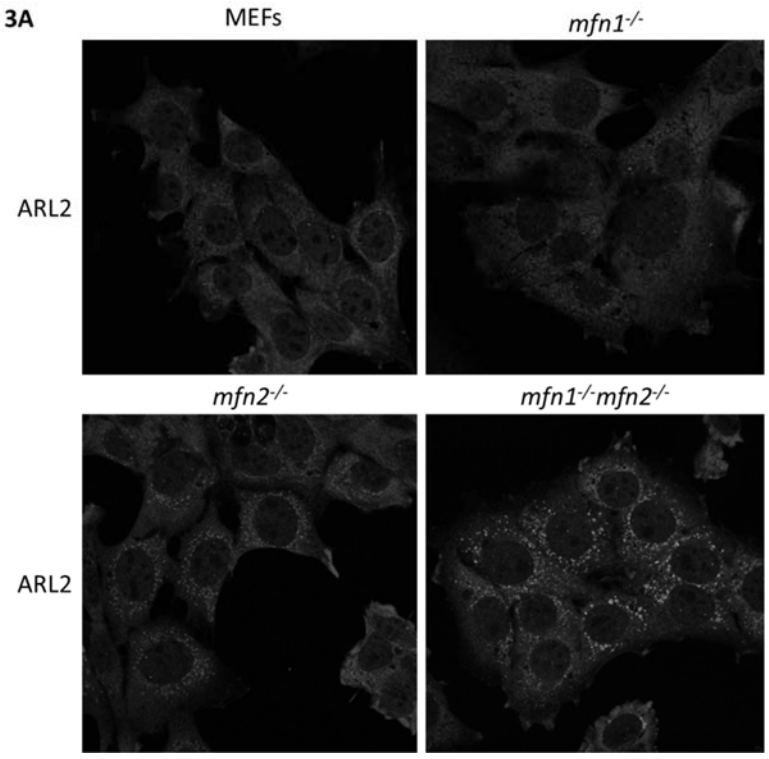
3A
MEFs
mfn1-/-
ARL2
mfn2-/-
mfn1-/-mfn2-/-
ARL2

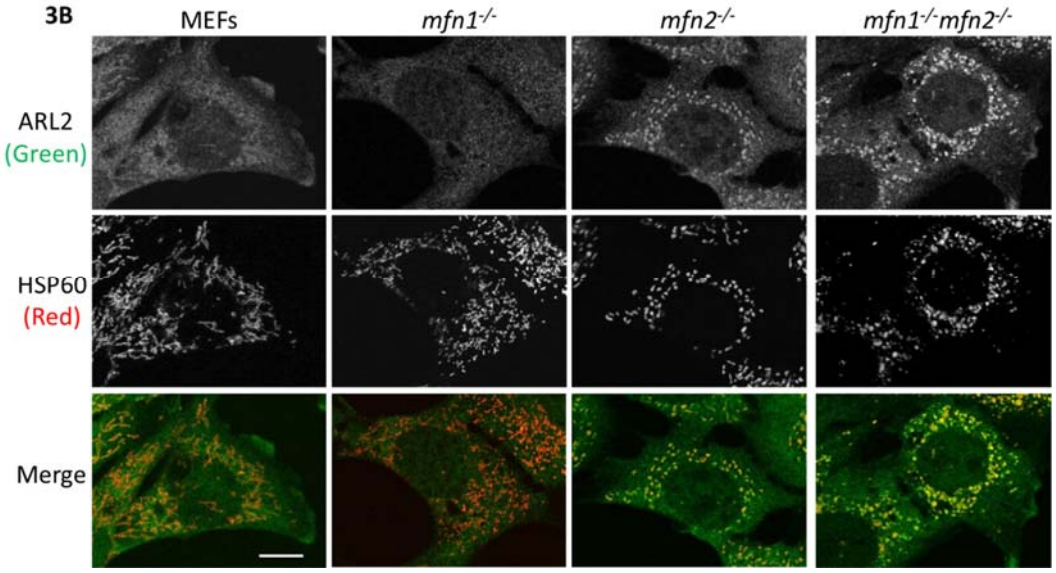
3B
MEFs
mfn1-/-
mfn2-/-
mfn1-/-mfn2-/-
ARL2
(Green)
HSP60
(Red)
Merge

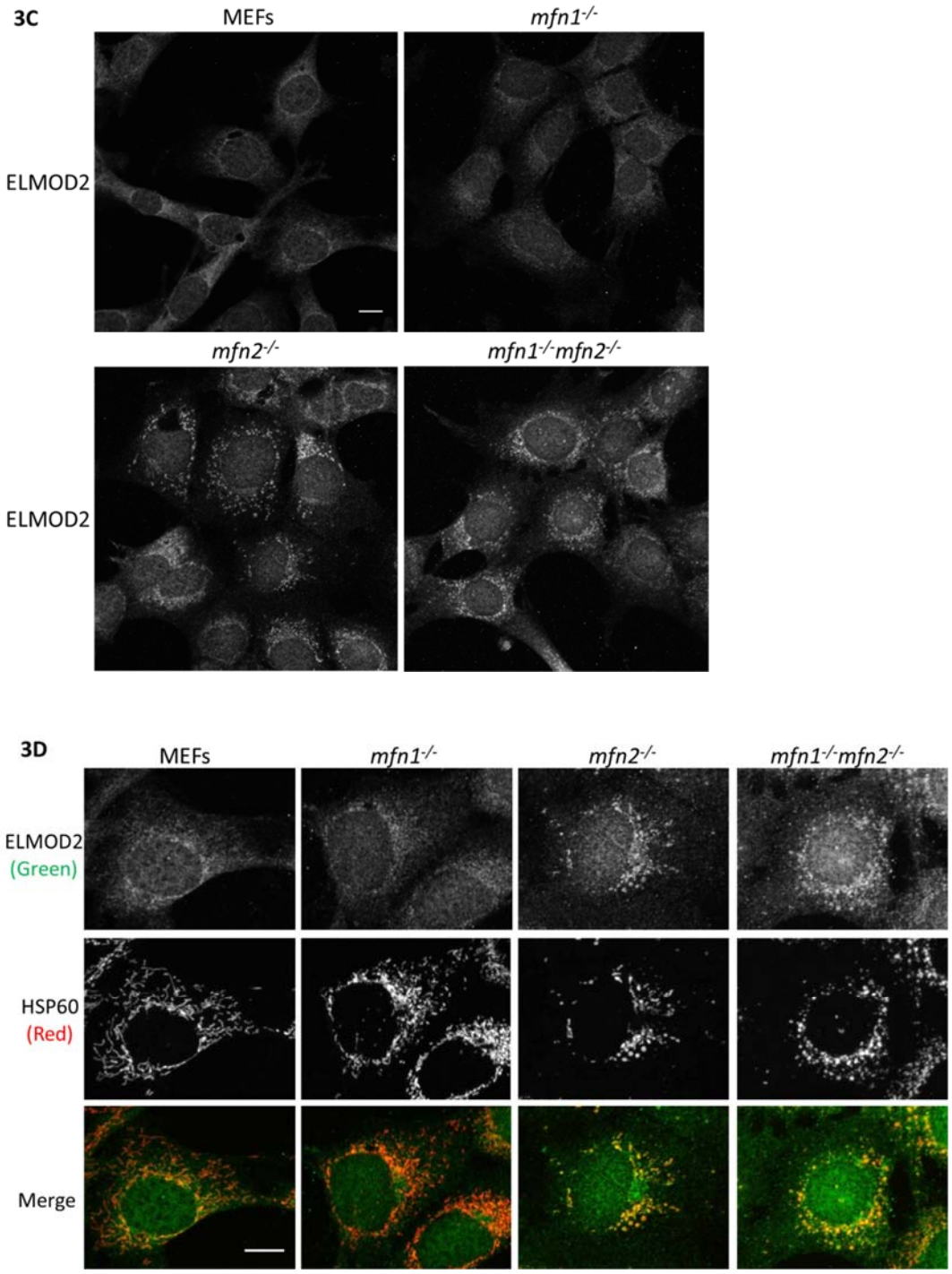

Figure 3: Mitochondrial staining of ARL2 and ELMOD2 is increased in MEFs deleted for MFN2. Wild type, *mfn1*$^{-/-}$, *mfn2*$^{-/-}$, or *mfn1*$^{-/-}$*mfn2*$^{-/-}$ MEFs were plated and one day later were fixed (50% density) and stained with antibodies to ARL2 or HSP60. (A) A field of cells stained for ARL2 for each MEF strain is shown. (B) Higher magnifications of single cells stained for

ARL2 (top panels) and HSP60 (middle panels) are shown. The bottom panels show the overlap, to better highlight mitochondrial morphology and staining. Single z planes are shown. (C) Same as A, except MEFs were stained for ELMOD2. Z stack projections are shown. (D) Same as B, except MEFs stained with ELMOD2 and HSP60. Scale bar = 10 μm. For both ARL2 and ELMOD2, similar results were obtained one and two days after plating.

4A

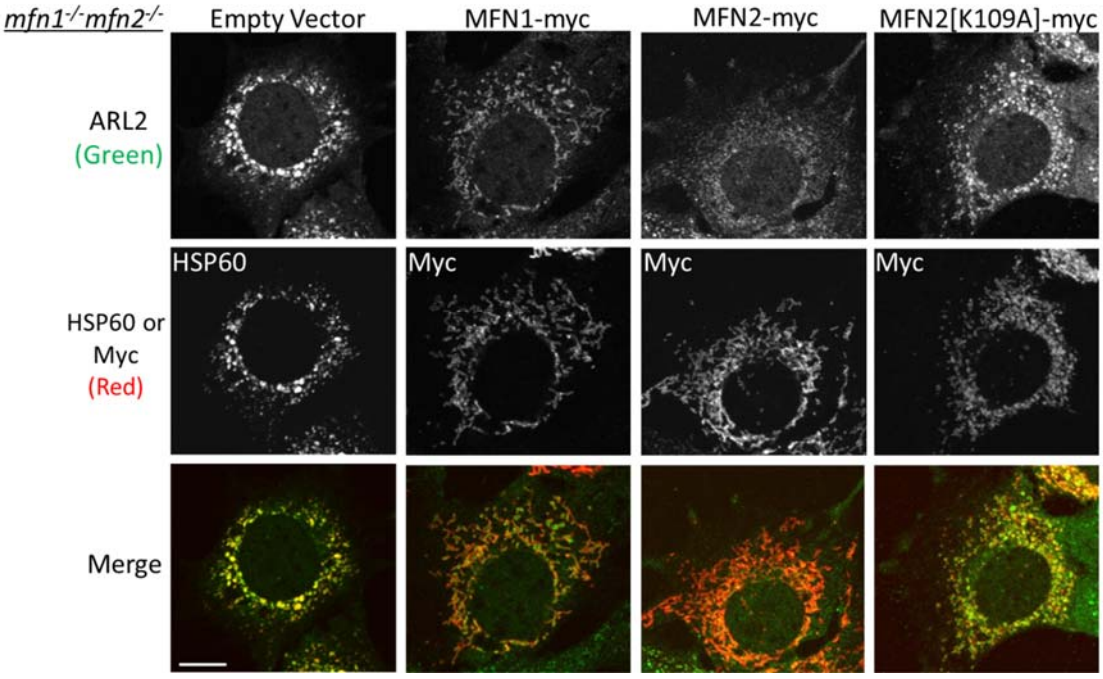
mfn1-/-mfn2-/-
Empty Vector
MFN1-myc
MFN2-myc
MFN2[K109A]-myc
ARL2
(Green)
HSP60 or
Myc
(Red)
HSP60
Myc
Myc
Myc
Merge

4B

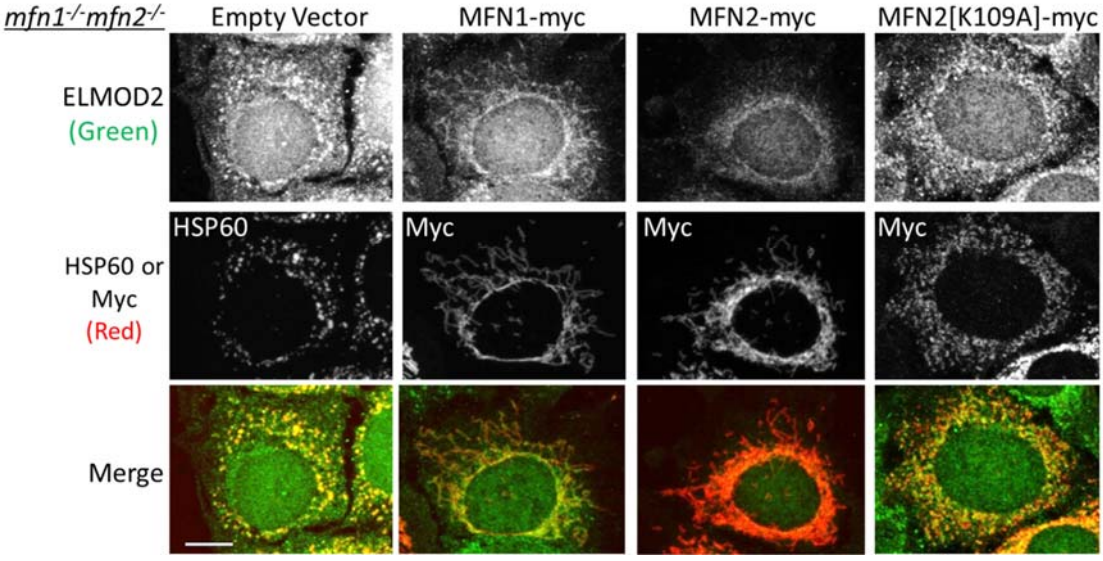
mfn1-/-mfn2-/-
Empty Vector
MFN1-myc
MFN2-myc
MFN2[K109A]-myc
ELMOD2
(Green)
HSP60 or
Myc
(Red)
HSP60
Myc
Myc
Myc
Merge

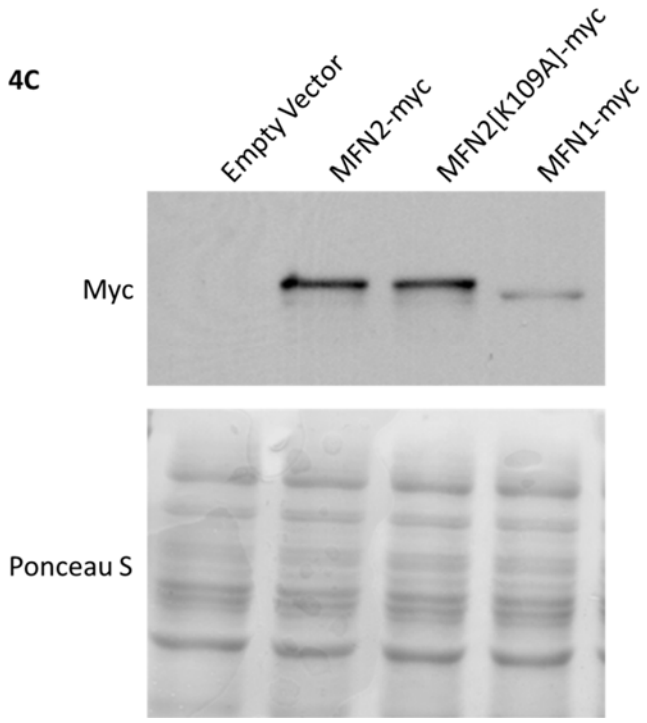

Figure 4: Increased ARL2 and ELMOD2 mitochondrial staining is reversed with expression of MFN2-myc, but not MFN2[K109A]-myc or MFN1-myc, in *mfn1*$^{-/-}$*mfn2*$^{-/-}$ MEFs. (A) *mfn1*$^{-/-}$ *mfn2*$^{-/-}$ MEFs were transfected with empty vector, or the same vector directing expression of MFN1-myc, MFN2-myc, or MFN2[K109A]-myc. MEFs were fixed 48 hours later and stained for ARL2 (top panels) and either HSP60 (empty vector) or myc (MFN1-myc, MFN2-myc, MFN2[K109A]-myc) (middle panels). Merged images are shown (bottom panels). Single planes are shown. (B) Same as A, except cells were stained for ELMOD2. Z stack projections are shown. Scale bar = 10 μm. For both ARL2 and ELMOD2, similar results were obtained 24 and 48 hours after transfection. (C) *mfn1*$^{-/-}$*mfn2*$^{-/-}$ MEFs were transfected with empty vector, MFN1-myc, MFN2-myc, or MFN2[K109A]-myc, and harvested 24 hours later. Total cell lysates (20 μg) were resolved by SDS-PAGE, transferred to nitrocellulose, and probed with an antibody specific to the myc epitope (upper panel), as described under Methods. Ponceau S staining (lower panel) was performed immediately after transfer, shows equal protein loaded across all lanes.

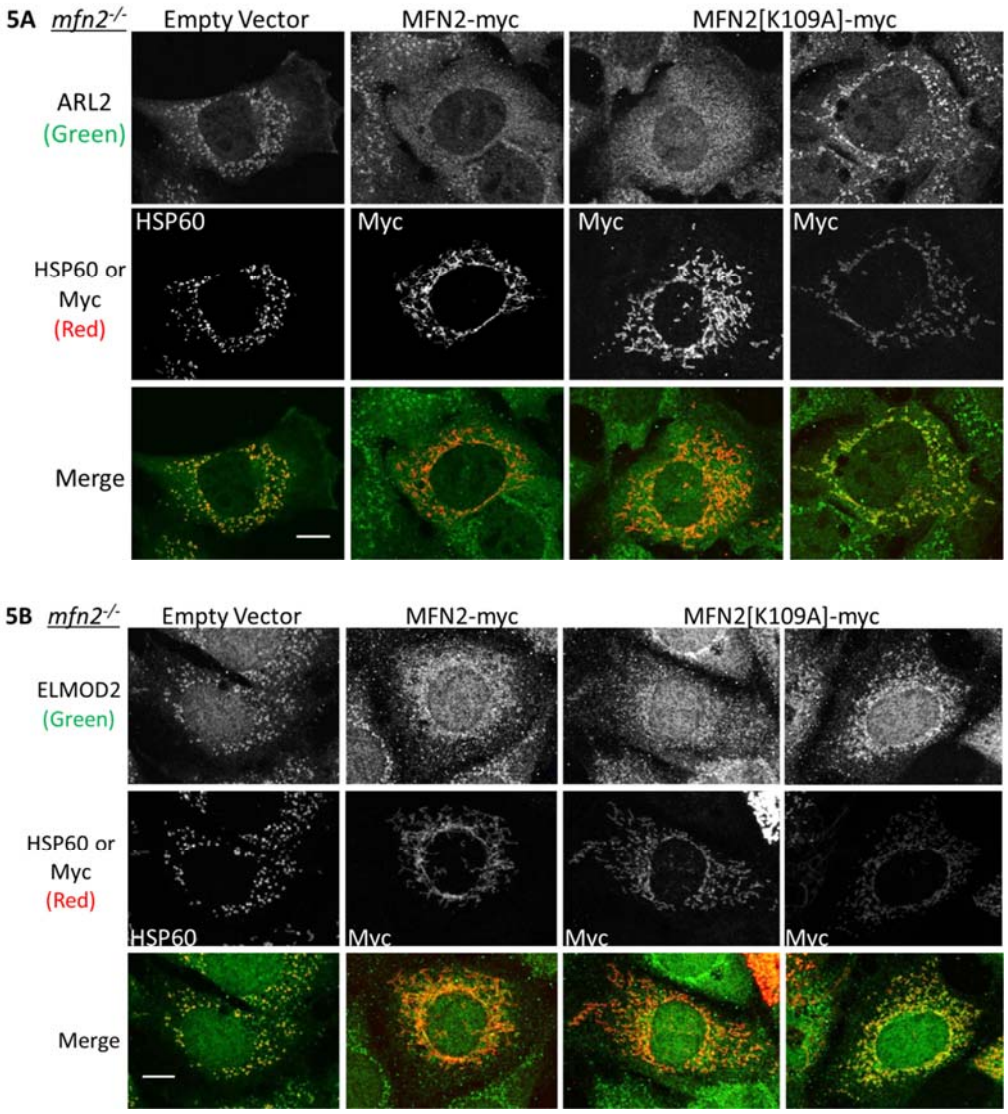

Figure 5: Increased ARL2 and ELMOD2 mitochondrial staining is reversed with expression of MFN2-myc and MFN2[K109A]-myc in *mfn2*$^{-/-}$, MEFs. (A) *mfn2*$^{-/-}$ MEFs were transfected with empty vector, MFN2-myc, or MFN2[K109A]-myc. MEFs were fixed 48 hours later and stained for ARL2 (top panels) and either HSP60 (empty vector) or myc (MFN2-myc, MFN2[K109A]-myc) (middle panels). Merged images are shown in the bottom panels. Single planes are shown. (B) Same as A, except cells were stained for ELMOD2. Z stack projections are shown. Scale bar = 10 μm. For both ARL2 and ELMOD2, similar results were obtained 24 and 48 hours after transfection.

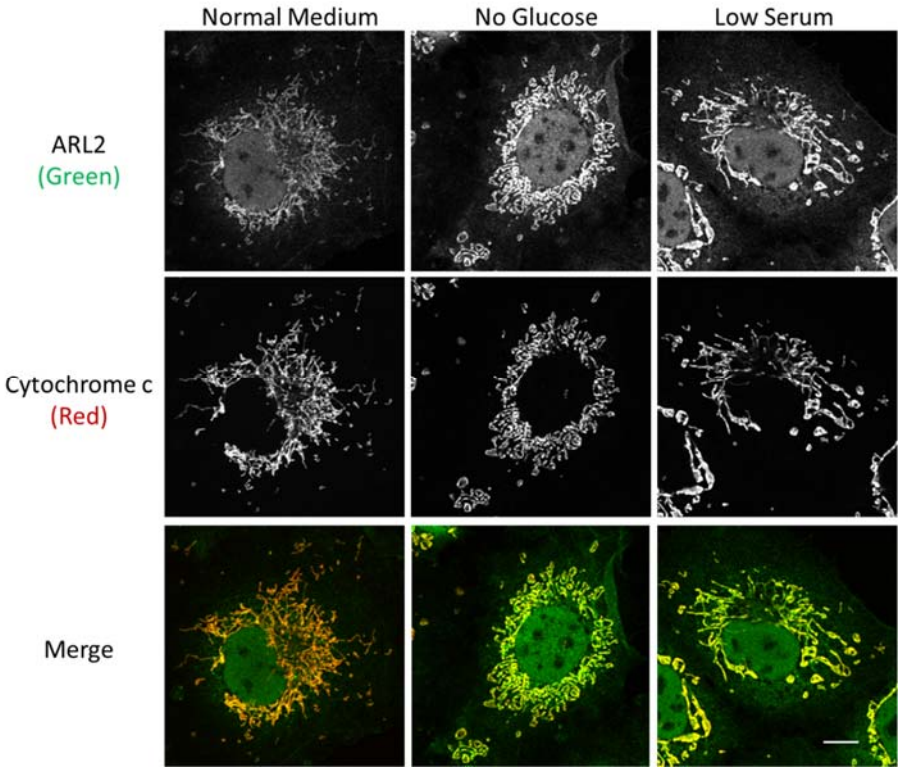

Figure 6: Mitochondrial staining of ARL2 increases in cells cultured in medium with no glucose or low serum. COS7 cells were cultured for 48 hours in normal medium (25 mM glucose, 10% FBS), 0 glucose medium (0 mM glucose, 10% FBS), or low serum medium (25 mM glucose, 2% FBS), and fixed and stained for ARL2 (top panels) and cytochrome c (middle panels) at ~50% confluence. Merged images of ARL2 and cytochrome c are shown (bottom panels). Images are single planes acquired by confocal microscopy. Scale bar = 10 μm.

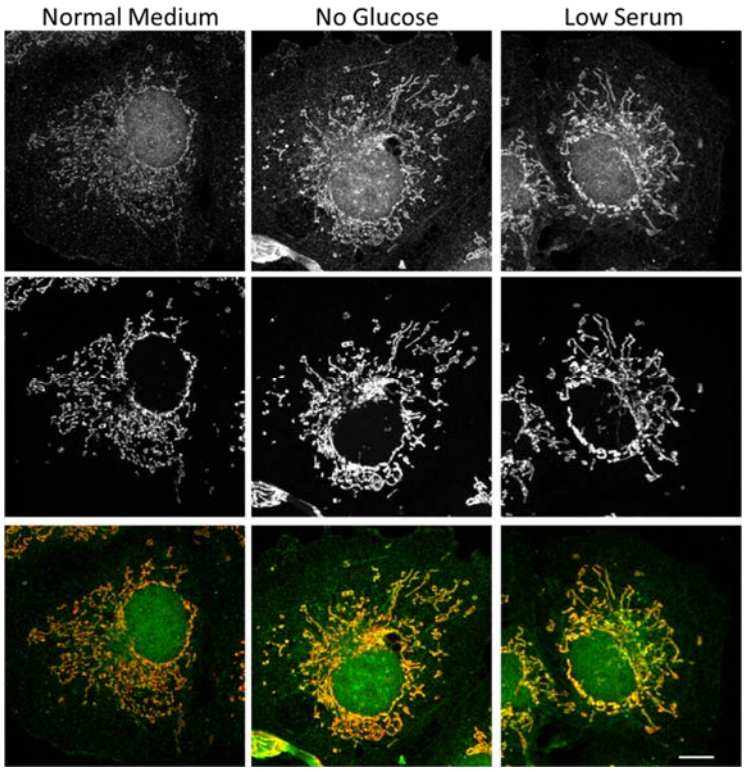

Figure 7: Mitochondrial staining of ELMOD2 increases in cells cultured in medium with no glucose or low serum. COS7 cells were cultured for 48 hours in normal medium (25 mM glucose, 10% FBS), 0 glucose medium (0 mM glucose, 10% FBS), or low serum medium (25 mM glucose, 2% FBS), and fixed and stained for ELMOD2 (top panels) and cytochrome c (middle panels). Merged images of ELMOD2 and cytochrome c are shown (bottom panels). Images are z stack projections acquired by confocal microscopy. Scale bar = 10 μm.

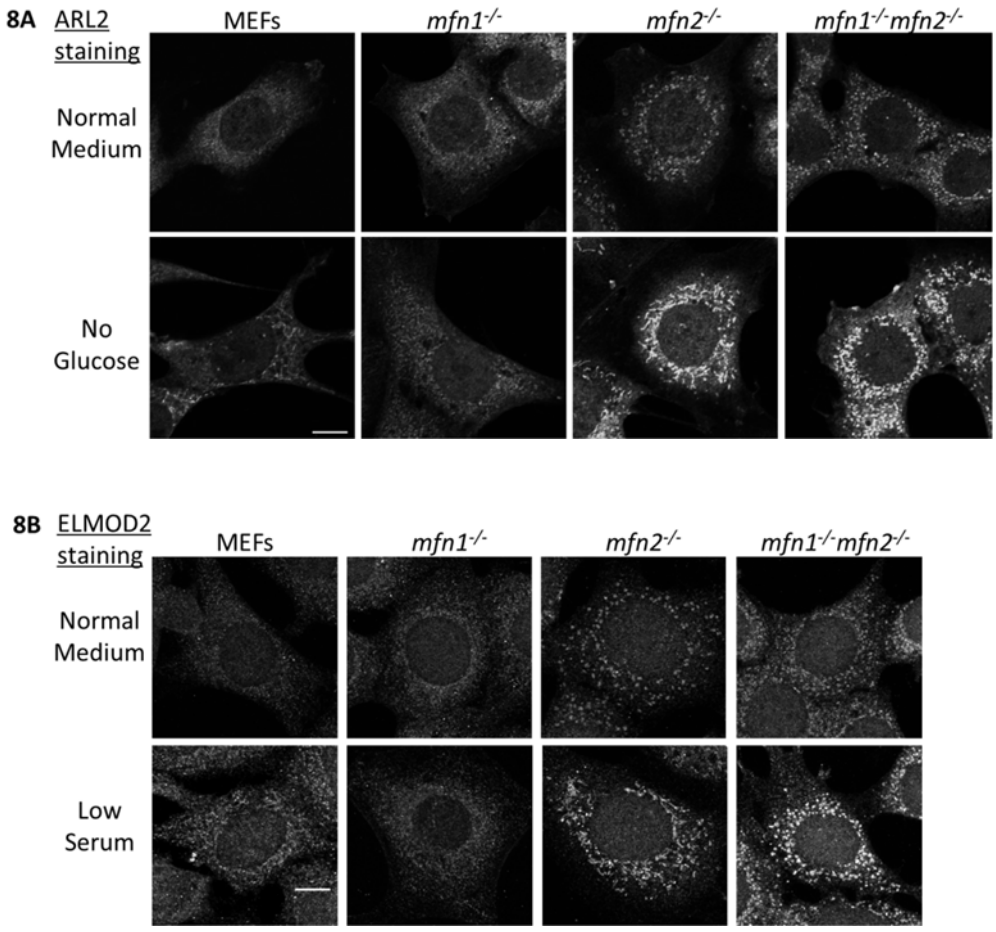

Figure 8: Glucose or serum deprivation increases ARL2 and ELMOD2 staining in wild type, *mfn2*$^{-/-}$, or *mfn1*$^{-/-}$*mfn2*$^{-/-}$ MEFs, but not *mfn1*$^{-/-}$ MEFs. MEFs were cultured for 48 hours in normal medium, 0 glucose medium, or low serum medium, and fixed and stained for ARL2 (A) or ELMOD2 (B). Single planes are shown in (A) and z stack projections are shown in (B). Scale bar = 10 μm.

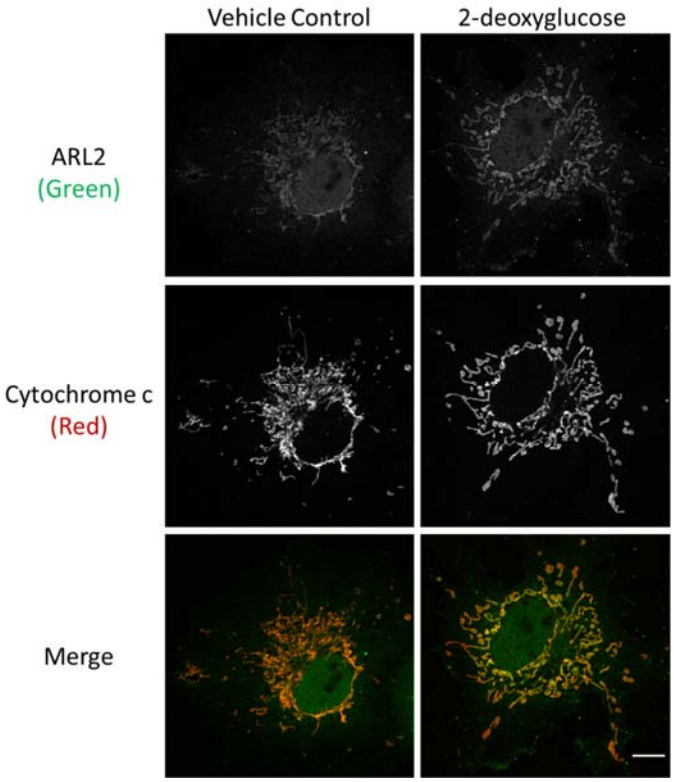

Figure 9: Mitochondrial staining of ARL2 is increased by treatment with 2-deoxyglucose. COS7 cells were cultured in normal medium or medium in which the 25 mM glucose was replaced with 25 mM 2-deoxyglucose. The next day (16 hours), cells were fixed and stained for ARL2 (top panels) and cytochrome c (middle panels). Merged images of ARL2 and cytochrome c are shown (bottom panels). Images are single planes acquired by confocal microscopy. Scale bar = 10 µm.

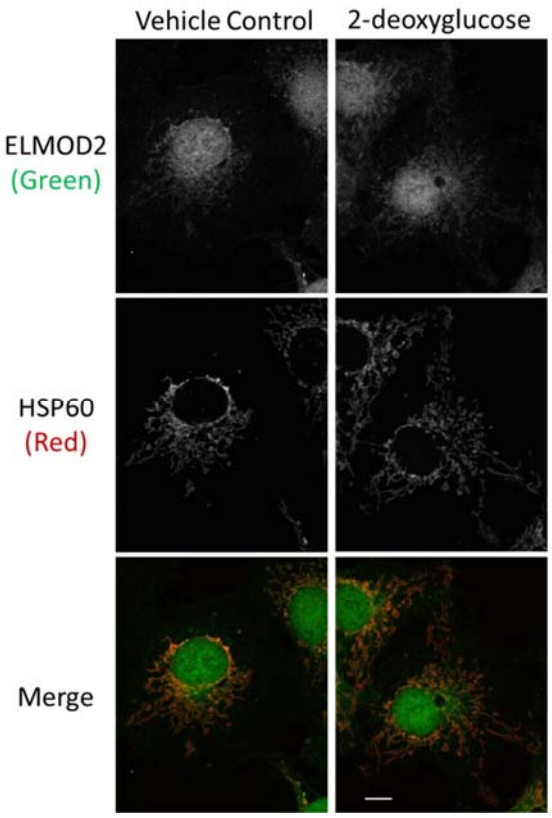

Figure 10: Mitochondrial staining of ELMOD2 does not change with 2-deoxyglucose treatment. COS7 cells were cultured in normal medium or medium with 25 mM 2-deoxyglucose added, as described under Methods. Cells were fixed 16 hr later and stained for ELMOD2 (top panels) and HSP60 (middle panels). Merged images of ELMOD2 and HSP60 are shown (bottom panels). Images are z stack projections acquired by confocal microscopy. Scale bar = 10 μm.

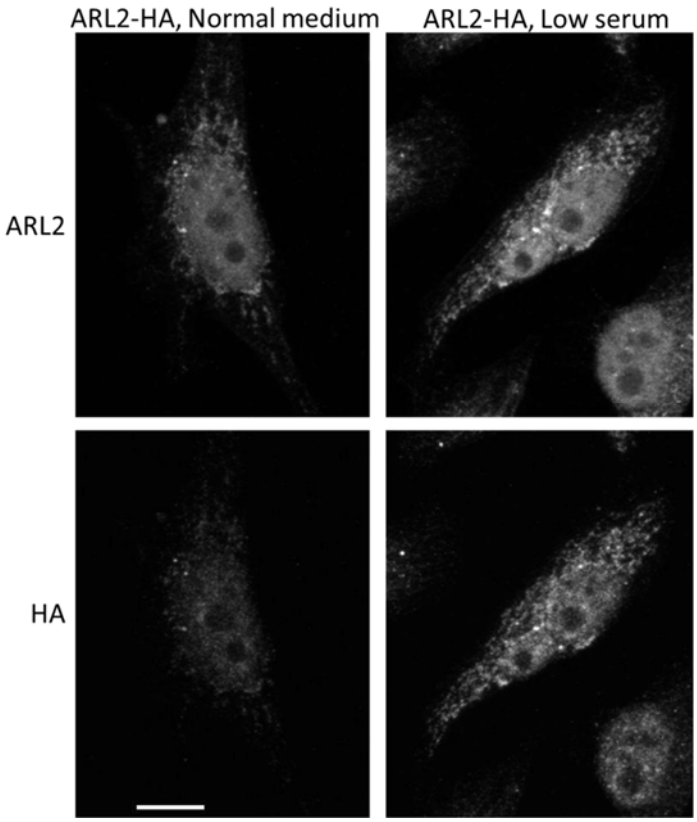

Figure 11: Both ARL2 and HA staining increase in stressed cells expressing ARL2-HA. HeLa cells were transfected with ARL2-HA and replated onto coverslips following transfection. After allowing 4 hours for cells to attach, the medium was changed to either normal medium (25 mM glucose, 10% FBS) or low serum medium (25 mM glucose, 2% FBS). Two days later, cells were permeabilized with 0.5% saponin in PBS immediately prior to fixation, to remove cytosolic ARL2-HA. Cells were then stained for ARL2 and HA. Images are z stack projections acquired by confocal microscopy. Scale bar = 10 μm.

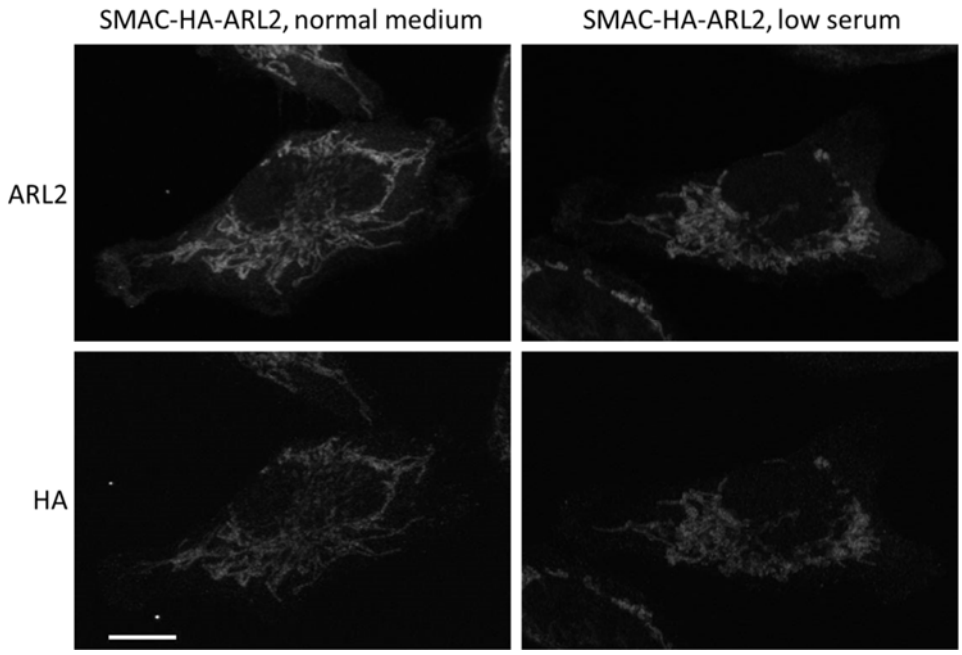

Figure 12: Neither ARL2 nor HA staining increases in stressed cells expressing SMAC-HA-ARL2. HeLa cells were transfected with SMAC-HA-ARL2 and replated onto coverslips following transfection. After allowing 4 hours for cells to attach, the medium was changed to either normal medium (25 mM glucose, 10% FBS) or low serum medium (25 mM glucose, 2% FBS). Two days later, cells were fixed and stained for ARL2 and HA. Images are single planes acquired by confocal microscopy. Scale bar = 10 μm.

Table I. Summary of the effects of energetic stressors on mitochondrial staining of ARL2 or ELMOD2. See text for details. + indicates an increase in staining intensity was observed, over that seen in cells grown in DMEM medium with 25 mM glucose and 10% FBS. NC indicates no changes in staining intensities were evident.

Stressor	Duration of stress	ARL2 staining	ELMOD2 staining	Effect on mitochondrial morphology	Cell lines
0 mM glucose + 10% FBS	24, 48 hours	+	+	Elongation	COS7, HeLa, MEFs
25 mM glucose + 2% FBS	24, 48 hours	+	+	Elongation	COS7, HeLa, MEFs
10 mM galactose	24, 48 hours	+	+	Elongation	COS7, HeLa, MEFs
25 mM 2-deoxyglucose	16 hours	+	NC	Partial fragmentation	COS7, HeLa, MEFs
10 µM oligomycin	16 hours	+	NC	Fragmentation	COS7, HeLa, MEFs
10 µM antimycin A	16 hours	+	NC	Fragmentation	COS7, HeLa, MEFs
10 µM rotenone	16 hours	+	NC	Fragmentation	COS7, HeLa, MEFs
10 µM menadione	1 hour	+	NC	No change	COS7, HeLa

Table II. Summary of effects of MFN deletions on ARL2/ELMOD2 staining in MEF lines. See text for details. NC, no change compared to wild type MEFs. +, - indicate clearly increased or decreased mitochondrial staining, respectively.

MEF line	**Transfected plasmid (Protein expressed)**	**ARL2 staining relative to wild type MEFs**	**ELMOD2 staining relative to wild type MEFs**
Wild type	N/A	NC	NC
mfn1$^{-/-}$	N/A	-	-
mfn2$^{-/-}$	N/A	+	+
mfn1$^{-/-}$*mfn2*$^{-/-}$	N/A	+	+
mfn2$^{-/-}$	Empty vector	+	+
mfn2$^{-/-}$	MFN1-myc	+	+
mfn2$^{-/-}$	MFN2-myc	-	-
mfn2$^{-/-}$	MFN2[K109A]-myc	-	-
mfn1$^{-/-}$*mfn2*$^{-/-}$	Empty vector	+	+
mfn1$^{-/-}$*mfn2*$^{-/-}$	MFN1-myc	+	+
mfn1$^{-/-}$*mfn2*$^{-/-}$	MFN2-myc	-	-
mfn1$^{-/-}$*mfn2*$^{-/-}$	MFN2[K109A]-myc	+	+
mfn1$^{-/-}$*mfn2*$^{-/-}$	MFN2[R94Q]-myc	+	+
mfn1$^{-/-}$*mfn2*$^{-/-}$	MFN2[V69F]-myc	-	-
mfn1$^{-/-}$*mfn2*$^{-/-}$	MFN2[L76P]-myc	-	-
mfn1$^{-/-}$*mfn2*$^{-/-}$	MFN2[R274Q]-myc	-	-

Chapter 6: Studies of mitochondrial functions of ARL2

Abstract

Here, I summarize unpublished data regarding ARL2 functions in mitochondria. I show that the ARL2/HSP60 complex does not change with ARL2 siRNA or metabolic stress, making it an unlikely mediator of any effects of ARL2 on mitochondria. I examined the activity of the electron transport chain and found no defects in function. By examining cristae morphology, I provide preliminary data that ARL2 siRNA leads to a loss in mitochondrial cristae. Cristae density is unaltered in cells expressing ARL2[T30N] or ARL2[Q70L], consistent with cristae density affected only when ATP levels are challenged by ARL2 siRNA. With Cara Schiavon, I identified point mutants in ARL2 that allow for dissection of its roles in microtubule and mitochondrial dynamics. Finally, using immunofluorescence I show that MIROs are present in puncta that align with ARL2 puncta, providing further evidence for a role of ARL2 in regulation of mitochondrial motility.

Materials and Methods

Cell culture: Human cervical carcinoma (HeLa) cells were grown in DMEM supplemented with 10% fetal bovine serum (Invitrogen, Carlsbad, CA) and 2 mM glutamine at 37°C in the presence of 5% CO_2. Cells were originally obtained from the ATCC. Cells were screened for mycoplasma regularly by staining with Hoechst 33342 DNA dye, usually in conjunction with immunofluorescence experiments (described below). Cells were not cultured for more than 30 passages.

Plasmids: ARL2, ARL2[T30N], and ARL2[Q70L] in pcDNA3.1 were made in our lab and described previously (Zhou et al., 2006). [I6R], [F50A] and [L3A] mutations were introduced into ARL2, ARL2[T30N], and ARL2[Q70L] using the QuickChange (Stratagene) kit and protocol and sequence-verified; this was done by Cara Schiavon. Mito-GFP was a gift from

James Zheng (Emory University), and myc-MIRO1, myc-MIRO2, and GRIF1-HA in pRK5 were a gift from Pontus Aspenstrom (Karolinska Institute).

Antibodies: Antibodies to ARL2, BART, and ELMOD2 were generated in our lab and characterized previously (Newman et al., 2014; Sharer et al., 2002). The following antibodies were obtained from commercial sources: Complex V subunit alpha (Mitosciences MS502), NDUFA9 (Mitosciences MS111), UQCRC2 (Mitosciences MS304), HA (Covance MMS-101P), HSP60 (Enzo Life Sciences ADI-SPA-807), alpha tubulin (Sigma T9026), myc (Invitrogen R950-25), KIF5B (Millipore MAB1613).

Blue native polyacrylamide gel electrophoresis (BN-PAGE) and western blotting: Cells were harvested by rinsing twice with phosphate buffered saline (PBS; 140 mM NaCl, 3 mM KCl, 10 mM Na_2HPO_4, 2 mM KH_2PO_4, pH 6.75), collected by incubation in 5 mM EDTA in PBS, and pelleted in a microfuge (14,000 rpm, 4°C). Cells were lysed in 1% CHAPS, 50 mM Bis Tris, 6N HCl, 50 mM NaCl, 10% w/v glycerol, 0.001% Ponceau S, pH 7.2, and protease inhibitors (Sigma #P-2714) at room temperature for 30 minutes, and the S14 was obtained by clarifying lysates by centrifugation for 30 minutes (16,873xg, 4°C). Protein concentrations were determined by Bradford Assay (Bio-Rad) using bovine serum albumin as standard. Protein samples (20 µg/well) were separated on BN-PAGE gels (4-16%) obtained commercially (Invitrogen) and used according to manufacturer's instructions. Molecular weight standards for native gels were purchased from Invitrogen (cat#LC0725). Following electrophoresis, lysates were wet-transferred to PVDF membranes (Immobilon #IPVH00010) at 70V for 2.5 hours. Western blotting procedures were carried out at room temperature. Membranes were blocked in blotto (5% (w/v) dry milk, 50 mM Tris pH 8, 2 mM $CaCl_2$, 80 mM NaCl, 0.2% (v/v) Tween-20, 0.02% sodium azide) for 1 hour. Membranes were then incubated with primary antibody in blocking buffer at 4°C overnight. Removal of excess primary antibody was carried out by washing the

membranes in PBST (PBS with 0.1% Tween-20) three times for 10 min each. Secondary antibodies (GE cat #NA934V, #NA931V) were diluted 1:5,000 in PBST and incubated with the membrane for 1 hour at room temperature. Excess secondary antibody was removed by washing the membranes in PBST 3 times for 10 min each. Blots were incubated in luminol containing solution (0.1 mM Tris-HCl pH 8.0, 1.2 mM luminol, 0.2 mM p-coumaric acid, 0.009% hydrogen peroxide) for 1 min prior to exposure to film. The ARL2 antibody was used in western blotting at a 1:2000 dilution.

siRNAs: Individual siRNAs were obtained from Dharmacon (Lafayette, CO). Catalog numbers are as follows: ARL2 siRNA #1 J-011585-05, ARL2 siRNA #2 J-011585-06.

Transfection with siRNA and plasmids: For siRNA transfection, cells were grown in six-well culture dishes to 40-50% confluence. siRNAs (25 nM) were transfected into HeLa cells using Dharmafect transfection reagent #1 (Dharmacon, Lafayette, CO) following the company's instructions. Transfections using siRNAs were carried out for 24 hours, after which cells were typically trypsinized and replated, and harvested either 24 or 48 hours later. We consistently observed at least 70% transfection efficiency, using expression of fluorescence-tagged proteins to score.

For plasmid transfection, cells at 90% density or higher were transfected in 6 well plates using the following protocols. Both the amount of DNA and the ratio of Lipofectamine: DNA were separately optimized for ARL2 expression in HeLa and COS7 cells. A ratio of 2 µg Lipofectamine: 1 µg DNA yielded the highest transfection efficiency. ARL2 plasmids (2 µg) were diluted in 250 µL Opti-MEM (Invitrogen). Lipofectamine 2000 (4 µg; Invitrogen) was diluted in a separate tube containing 250 µL Opti-MEM, vortexed briefly, and incubated at room temperature for 5 minutes. The tubes were mixed and incubated 20 minutes. Cell culture medium was changed to 1 ml of fresh medium, and transfection complexes (500 µL) were added dropwise

to the cells. After 24 hours, cells were trypsinized and replated, typically at a 1:4 split. This transfection typically resulted in ~70% of cells overexpressing ARL2 and ~50% expressing ARL2[T30N] or ARL2[Q70L] when assayed 48 hours from the start of transfection.

Immunofluorescence: Cells were grown on matrigel (BD Biosciences #356231) coated coverslips. Cells were fixed in a pre-warmed (37°C) solution of 4% paraformaldehyde in PBS (140 mM NaCl, 3 mM KCl, 10 mM Na_2HPO_4, 2 mM KH_2PO_4, pH 6.75), and permeabilized with 0.1% (v/v) Triton X-100 in PBS for 10 minutes at room temperature. Incubation with primary antibodies was carried out in filtered PBS containing 1% (w/v) BSA at 4°C overnight, followed by 4 x 5 minute washes in PBS. Secondary antibodies (1:500, Alexa fluorophores, Invitrogen) were incubated in the same buffer for 1 hour at room temperature, following 4 x 5 minute washes in PBS. Secondary antibody was removed by 2 x 5 minute washes in PBS. DNA was then stained with Hoechst 33342 for 4 minutes, followed by 2 x 5 minutes washes in PBS and mounting onto slides using Prolong Antifade (Invitrogen). Images were acquired using an Olympus FV1000 microscope and Olympus Fluoview v1.7 software, using 488 and 543 laser excitation and a 100x oil objective (1.45 NA). The following antibody dilutions were used: ARL2 (1:2000), HSP60 (1:5000), myc (1:1000), HA (1:2000), alpha tubulin (1:2000).

Seahorse Assays: Respiration measurements were essentially collected as described, using the Seahorse XF96 analyzer (Nicholls et al., 2010). HeLa cells were transfected as described above, in 6 well plates. One day later cells were replated (3.5×10^4 cells per well) into 96 well plates containing growth medium (DMEM + 10% FBS) supplemented with penicillin and streptomycin. Cells were typically ~90% confluent at 48 hours following transfection, at which point they were used. Cells were placed in DMEM Running Medium (Seahorse #100965-000) and incubated at 37°C without CO_2. Respiration was measured following prior (basal) or after sequential injections of oligomycin (10 μM final concentration), FCCP (3 μM) plus pyruvate (50 mM), and antimycin

A (10 μM) plus rotenone (10 μM). Wells that had a cell density of less than 90% or were on the outer edge of the 96 well plate were excluded from analysis, due to "edge effects". Following analysis, protein concentrations were determined by Bradford assay or cell number by Cyquant (Invitrogen), to allow normalization to either parameter.

Electron microscopy: Fixation, staining, and imaging were performed by Hong Yi at the Robert P. Apkarian Integrated Electron Microscopy Core at Emory University.

Structured Illumination Microscopy (SIM): For SIM experiments, the minimal amount of transfected DNA was determined for each construct for both optimal expression and minimal effects on mitochondrial morphology. COS7 cells were transfected with 1 μg myc-MIRO1 or 0.25 μg of myc-MIRO2. A ratio of 2 μg Lipofectamine 2000: 1 μg DNA was used for all constructs. Cells were imaged on a Nikon N-SIM using three dimensional SIM using a 100X (NA 1.49) oil objective. Cells were selected based on an apparently normal mitochondrial morphology, and a range of expression for each construct was examined. Fluorophores were excited by 488 and 561 laser lines. For each cell, a widefield image was obtained in addition to raw SIM data. Reconstruction was achieved using the Nikon Elements software, and reconstruction parameters suggested by the software were adjusted with reference to the widefield image, to avoid previously described artifacts (for examples see http://www.gelifesciences.com/gehcls_images/GELS/Pdf%20documents/2015-05-06-Pellett-Bitesizebio-Seminar.pdf).

Results

The ARL2/HSP60 complex is unresponsive to metabolic poisons or ARL2 siRNA

Previously, we documented the presence of ARL2 in a ~500 kDa complex visualized by BN-PAGE. Following fractionation, this complex was enriched in the 7,000xg pellet along with

mitochondrial markers. Mass spectrometry revealed the presence of HSP60 in this complex, with the ~500 kDa size consistent with the HSP60 heptamer (Cheng et al., 1989). Incubation of partially purified ARL2/HSP60 complex in 10 mM ATP caused dissociation of the HSP60 heptamer (Levy-Rimler et al., 2001) and loss of ARL2 from the ~500 kDa immunoreactive band, confirming physical association of the two proteins (Chapter 4; Newman et al., manuscript submitted). I also observed that the ARL2/HSP60 complex was less stable on ice, in agreement with previously published results (Levy-Rimler et al., 2001).

I tested if loss of ARL2 by siRNA could promote dissociation of the ARL2/HSP60 complex. ARL2 siRNA causes mitochondrial fragmentation, a loss in plus end directed mitochondrial motility, and decreased cellular ATP levels (Newman et al., 2014). Loss of this complex with ARL2 siRNA might indicate its role in one of the phenotypes caused by ARL2 siRNA. HeLa cells were transfected with no siRNA or ARL2 siRNA #1, and cells were harvested 24, 48, and 72 hours after transfection and lysates analyze by BN-PAGE. ARL2 siRNA caused loss of ARL2 from the ARL2/Cofactor D complex, which migrates at a size consistent with its apparent molecular weight of ~200 kDa in BN-PAGE (Figure 1) (Francis et al., manuscript in preparation). In contrast, ARL2 siRNA caused no change in the amount of ARL2 in the ARL2/HSP60 ~500 kDa complex, even 72 hours after transfection of ARL2 siRNA (Figure 1). Given that mitochondrial fragmentation and clustering are observed 24 hours after ARL2 siRNA transfection and ATP loss occurs 48 hours after siRNA transfection (Newman et al., 2014), the ARL2/HSP60 complex appears stable and persists while other phenotypes resulting from loss of ARL2 occur.

To assay a potential functional role for this complex, I asked if its abundance changed in response to metabolic stressors. ARL2 abundance in mitochondria increases with metabolic stress (Newman & Schiavon et al., manuscript submitted), so we would predict ARL2's abundance in this complex to increase, which might indicate a role for the ARL2/HSP60 complex in that process. HeLa cells were stressed with 25 mM 2-deoxyglucose (which inhibits glycolysis) or 1

μM antimycin A (complex III inhibitor), alongside a vehicle control. Each inhibitor leads to robust increases in mitochondrial ARL2 by immunofluorescence (Newman & Schiavon et al., manuscript submitted). Two time points were chosen: 16 hours, when the increase in mitochondrial ARL2 is strongest, and 3 hours, when the increase is first observed. No changes in the amount of ARL2 present in the ARL2/HSP60 complex were observed (Figure 2), even after 16 hours of either drug. This experiment was done once; it should be repeated prior to publication. These results suggest that the ARL2/HSP60 complex does not change in response to metabolic stressors.

Finally, we later found that the ARL2/HPS60 complex contains several mitochondrial proteins. By immunoblotting, I found that the ~500 kDa HSP60 complex also contained ANT, ELMOD2, BART, Complex I subunit NDUFA9, Complex III subunit UQCRC2, and Complex V subunit alpha. We also submitted the 500 kDa band for mass spectrometry and did not detect ARL2. The low abundance of ARL2 in this complex and the presence of several other mitochondrial proteins supports the role of this complex as a chaperone for proteins imported into the matrix.

Loss of ARL2 increases basal cellular respiration

The fact that the ARL2/HSP60 complex persists in ARL2 siRNA cells suggests that it is not the site of action of ARL2 in affecting ATP levels. To gain a better understanding of how loss of ARL2 impacts ATP production, we performed the BOFA assay: mock or ARL2 siRNA treated cells were assayed for **b**asal rates of respiration and then treated sequentially with **o**ligomycin (10 μM; Complex V inhibitor), **F**CCP (3 μM; an electron transport chain uncoupler) with 50 mM pyruvate addition, and **a**ntimycin A (10 μM) plus rotenone (10 μM) (electron transport chain complex III and I inhibitors, respectively), with continuous, real-time measurement of oxygen consumption using the Seahorse XF analyzer, as described under Materials and Methods. This protocol is designed to measure properties related to mitochondrial functions in the same cell

populations; basal respiration, coupled respiration (difference between basal respiration and respiration after oligomycin), spare respiratory capacity (difference between basal respiration and respiration after FCCP), and proton leak (difference between respiration after oligomycin and respiration after antimycin A/rotenone), respectively.

I found that cells transfected with siRNA #1 had a 26.9 ± 15% higher oxygen consumption than did controls at 48 hours post-transfection when normalized to cell number, indicative of a higher basal respiration rate (Figure 3). I assayed cells 48 hours after transfection because this is when we observe a ~50% reduction in cellular ATP (Newman et al., 2014). To control for off-target effects, I also later performed this experiment using ARL2 siRNA #2, a sequence independent siRNA that also depletes ARL2 and causes mitochondrial defects (Newman et al., 2014), and obtained similar results. This higher basal respiration was highly significant ($p<0.001$), reproducible (with a total of 24 replicates in three different experiments) and was consistent at least at plating densities of 30-40,000 cells/well. Results were essentially the same when oxygen consumption was normalized to total cell protein or cell number. In contrast, I found no statistically significant differences between control and ARL2 siRNA cells in their response to the different drug treatments (Figure 3). Thus, depletion of ARL2 in HeLa cells results in a significant increase in oxygen consumption, but no effects were observed on coupled respiration, spare respiratory capacity, or proton leak. In addition, extracellular acidification rate, which is a measure of glycolysis, was also measured using the Seahorse instrument. I observed no differences in extracellular acidification between control and knockdown cells (data not shown), suggesting no differences in the rates of glycolysis and consistent with the model that mitochondrial ATP production is impaired in ARL2 knockdown cells.

Loss of ARL2 results in a loss in cristae density

Though we have documented that loss of ARL2 results in a loss in cellular and mitochondrial ATP levels, no evidence exists that loss of ARL2 causes defects in the electron

transport chain. No changes were observed in any of the respiratory complexes when analyzed by BN-PAGE (Newman et al., 2014), and the increase in basal respiration with no concomitant changes in uncoupled respiration, spare respiratory capacity, or proton leak led us to rule out any gross abnormalities in the electron transport chain. As I began to hypothesize that ARL2 regulates mitochondrial fusion, I wondered if ARL2 may be involved in the same pathways as OPA1. OPA1 regulates fusion of the inner mitochondrial membrane, but is also regulates cristae morphology (Cipolat et al., 2004; Griparic et al., 2004). Cristae are invaginations of the inner mitochondrial membrane specialized for ATP production, and loss of OPA1 leads to a loss in mitochondrial cristae with negative consequences for ATP production (Griparic et al., 2004; Patten et al., 2014). Therefore, I asked if loss of ARL2 might also affect cristae morphology.

Initially, I performed experiments on cells transfected with ARL2 siRNA and fixed at 48 hours, when ATP loss is first observed (Newman et al., 2014). For these experiments, cells were transfected for a total of 24 hours, after which they were trypsinized, replated, and fixed 24 hours later. The results of these initial experiments were inconclusive, as cells receiving mock siRNA transfections had extremely variable cristae and an overall low density of cristae in mitochondria, making it difficult to ascertain a potential loss in cristae. For my second experiment, I allowed more time for cells to grow on plates. I transfected cells for 24 hours, then replated cells and fixed 48 hours later (72 hours after start of siRNA transfection). With this experiment, I observed a higher cristae density in mock treated cells. Because of these results, I ensured that cells were plated at least 2 days prior to fixation for the rest of the experiments described in this chapter.

To assay potential changes in cristae with ARL2 siRNA, HeLa cells were transfected for 24 hours with either no siRNA (mock) or ARL2 siRNA #1, replated immediately after transfection, and fixed 48 hours later and processed for electron microscopy. Cells receiving mock siRNA treatment had several visible cristae per mitochondrion (Figure 4). We imaged cells in the ARL2 siRNA cell population by expected phenotype: cells with obvious fragmentation and perinuclear clustering were chosen for analysis. When we observed these cells, we could see an

obvious decrease in cristae density in ARL2 siRNA cells by visual inspection. Round, fragmented mitochondria in mock treated cells typically had 3-4 cristae, whereas similarly sized fragmented mitochondria in cells receiving ARL2 siRNA typically had 0-2 cristae (Figure 4).

I used two metrics to quantify cristae density. One metric was to count the number of visible cristae in mitochondria and normalize to the size of mitochondria by measuring the total length of the outer membrane (Figure 5B). The other metric was to measure the total cristae length within mitochondria and normalize to the length of the outer membrane (Figure 5C). Three mock cells and two ARL2 siRNA cells were analyzed, with a total of 52 (mock transfected) or 37 (ARL2 siRNA) mitochondria measured. Cells not showing the expected phenotype for ARL2 siRNA (mitochondrial fragmentation and perinuclear clustering) were excluded from analysis. ARL2 siRNA cells have 36% fewer cristae/μm outer membrane length (1.68 +/- 0.77 vs 1.08 +/- 0.77) and 54% less cristae membrane length (0.75 +/- 0.37 vs 0.34 +/- 0.25) compared to mock treated cells (2 cells analyzed per condition). These differences were not significant due to large error bars resulting from the low number of cells analyzed, though may reach significance as more cells are analyzed.

Loss of cristae density may be secondary to mitochondrial fragmentation. To determine if loss of cristae density was specific to ARL2 siRNA, I analyzed cristae density in cells expressing ARL2[T30N]. ARL2[T30N] causes mitochondrial fragmentation and perinuclear clustering, similar to ARL2 siRNA, but does not cause a loss in cellular ATP, unlike ARL2 siRNA (Newman et al., 2014). Cells were transfected with empty vector (pcDNA3.1), ARL2, or ARL2[T30N] on day one after plating, and transfected for 24 hours. Cells were then fixed immediately after transfection, two days after plating without any further replating. Over-expression of ARL2 has no effect on mitochondrial morphology (Newman et al., 2014). Control cells receiving empty vector appeared similar to cells expressing ARL2 and had a similar cristae density (data not shown). As with ARL2 siRNA, we selected cells from the ARL2[T30N] population displaying the expected phenotype of fragmentation and perinuclear clustering. When

we compared cells expressing ARL2 with cells expressing ARL2[T30N], there were no obvious differences in cristae density when judged by visual inspection (Figure 6). These results were repeated once with similar results, though quantification also needs to performed prior to publication. These preliminary results support the conclusion that loss of cristae density due to ARL2 siRNA is not a secondary consequence of changes in mitochondrial morphology.

To further differentiate between the effects of ARL2 on mitochondrial morphology and cristae, I decided to analyze cristae density in cells expressing ARL2[Q70L]. Expression of ARL2[Q70L] causes mitochondrial elongation (Newman et al., manuscript submitted). I transfected ARL2 or ARL2[Q70L] in cells for 24 hours, then replated and fixed cells 48 hours later. Consistent with the previous experiment examining ARL2[T30N] (Figure 6), cells expressing ARL2 had several cristae per mitochondrion (Figure 7). Cells expressing ARL2[Q70L] were selected for imaging based on the presence of elongated mitochondria, and these cells showed no obvious differences in cristae morphology or density, compared to cells expressing ARL2 as judged by visual inspection (Figure 7). Therefore, elongation of mitochondria by ARL2[Q70L] has no obvious effect on cristae morphology. More quantification of these effects and lack of effects in controls is required before publishing these observations.

Point mutations of ARL2 abrogate phenotypes caused by ARL2[Q70L] and ARL2[T30N]

ARL2 regulates not only mitochondrial morphology, motility, and ATP levels, but also plays a role in tubulin dynamics (Bhamidipati et al., 2000; Tian et al., 2010; Zhou et al., 2006). Both ARL2[Q70L] and ARL2[T30N] cause microtubule loss, as well as altering mitochondrial morphology when expressed in cells (Newman et al., 2014; Zhou et al., 2006). Therefore, in order to gain a better understanding of these functions of ARL2, we attempted to dissociate these phenotypes from each other. We generated a series of point mutants with the goal of disrupting binding of ARL2 to a subset of effectors, based on crystal structures of ARL2 bound to two known effectors, BART and PDEδ (Bhamidipati et al., 2000; Hanzal-Bayer et al., 2002; Zhang et

al., 2009). Using site-directed mutagenesis, Cara Schiavon introduced these mutations into ARL2, ARL2-HA, ARL2[Q70L], and ARL2[T30N], as part of her rotation project. Together, we transfected these constructs into HeLa cells, and assayed for the ability of ARL2[Q70L] constructs to cause microtubule loss 48 hours after transfection, as well as ARL2[T30N] constructs for the ability to cause mitochondrial fragmentation and perinuclear clustering. Later, I tested the ARL2[Q70L] constructs for their ability to promote mitochondrial elongation. The results of these experiments are summarized in Figure 8.

By visual inspection, we found that ARL2[Q70L, L3A] and ARL2[Q70L, F50A] were unable to cause microtubule destruction to the same extent as ARL2[Q70L] (Figure 9A). Similarly, we found that [Δ1-9]ARL2[Q70L] was unable to cause any microtubule loss (data not shown). The [I6R] mutation, however, had no effect on microtubule density (Figure 9A). I quantified microtubule density using three categories: (1) normal, microtubules appear similar to untransfected cells, (2) intermediate, a clear reduction in microtubule density is observed, but some microtubules are still visible, and (3) severe, no microtubules are visible (shown in Figure 9B). Note that I did not quantify the effects of [Δ1-9]ARL2[Q70L] expression on microtubules; this needs to be performed before this data is published. After scoring cells, I found that only 26% of cells expressing ARL2[Q70L] had normal microtubule density, compared to 100% of cells expressing ARL2 or receiving empty vector (Figure 9C). In contrast, the majority of cells expressing ARL2[Q70L, F50A] (84%) or ARL2[Q70L, L3A] (90%) retained normal microtubule density. However, only 18% of cells expressing ARL2[Q70L, I6R] had normal microtubule density (Figure 9C). To rule out the possibility that the [L3A] or [F50A] caused lowered expression levels of ARL2[Q70L], we performed immunoblots on lysates of cells expressing ARL2[Q70L], ARL2[Q70L, F50A], ARL2[Q70L, L3A] and ARL2[Q70L, I6R]. We found that ARL2[Q70L, F50A], ARL2[Q70L, L3A] and ARL2[Q70L, I6R] all express to similar levels, and that ARL2[Q70L, F50A], ARL2[Q70L, L3A] and ARL2[Q70L, I6R] all express to higher levels than ARL2[Q70L] (Josh Francis, unpublished data, not shown). Therefore, these results are

consistent with [L3A] and [F50A] disrupting interaction of ARL2 to an effector, which we propose is Cofactor D, and preventing its actions on microtubules (Francis et al., manuscript in preparation).

Because ARL2[T30N] also causes microtubule loss (Newman et al., 2014), Cara and I also expressed ARL2[T30N] constructs and visually inspected cells for microtubule density. However, transfection efficiency for this experiment was low, making it difficult for us to find transfected cells to inspect. I have since optimized our transfection protocols, so this experiment should be repeated. However, the results of this experiment were inconclusive.

Next, we assayed ARL2[T30N] constructs for mitochondrial fragmentation 24 hours after transfection and found that neither ARL2[T30N, L3A] nor ARL2[T30N, I6R] were able to cause mitochondrial fragmentation to the same degree as ARL2[T30N]. We also assayed these constructs for perinuclear clustering, and found that ARL2[T30N, L3A] and ARL2[T30N, I6R] were not able to cause perinuclear clustering. We also found that [Δ1-9]ARL2[T30N] was unable to promote either mitochondrial fragmentation and perinuclear clustering. We did not quantify fragmentation or perinuclear clustering, but the reduction was obvious by visual inspection. This experiment was done once and needs to be repeated and quantified prior to publication. Later, I tested if these two mutations could also reverse mitochondrial elongation caused by ARL2[Q70L]. I found that all of the ARL2 double mutants ([L3A], [I6R], and [F50A]) were able to promote mitochondrial elongation, to a similar extent as ARL2[Q70L] (Newman et al., manuscript submitted). However, [Δ1-9]ARL2[Q70L] was unable to promote mitochondrial elongation (data not shown, summarized in Figure 8).

The mutations that reverse mitochondrial fragmentation, [L3A] and [I6R], might prevent import of ARL2 into mitochondria. We hypothesize that the N terminus of ARL2 may contain its MLS, as addition of an HA tag to the N terminus of ARL2 prevents its import into mitochondria (Newman et al., manuscript submitted), and exogenous [Δ1-9]ARL2 appears diffuse 2-3 days after transfection, despite the fact that overexpressed ARL2 appears mitochondrial at the same

time points (data not shown). Therefore, I tested if [L3A] and [I6R] prevent import of ARL2 into mitochondria. HA-ARL2, ARL2-HA, ARL2[L3A]-HA, and ARL2[I6R]-HA were expressed in cells. One day later, cells were permeabilized (0.5% saponin in PBS) immediately prior to fixation, to remove cytosolic ARL2 and allow for easier visualization of mitochondrial ARL2. Cells were then fixed and stained for HA in order to visualize exogenous ARL2. I found that addition of an HA tag to the C terminus of ARL2 did not prevent its import into mitochondria, but addition of an HA tag to the N terminus of ARL2 did prevent its import (Figure 9) (Newman et al., manuscript submitted). In cells expressing ARL2-HA, HA staining appeared mitochondrial and co-localized with mito-GFP. In contrast, cells expressing HA-ARL2 had no mitochondrial HA staining (Figure 10). Similar to ARL2-HA, HA staining in cells expressing ARL2[L3A]-HA or ARL2[I6R]-HA appeared associated with mitochondria and overlapped with mito-GFP (Figure 10). This experiment has been repeated with similar results. Therefore, [L3A] and [I6R] do not interfere substantially with import of ARL2 into mitochondria.

While I was quantifying ARL2[Q70L, L3A] and ARL2[Q70L, F50A] for mitochondrial elongation, I noted a change in mitochondrial distribution in transfected cells, where mitochondria were not only elongated but also seemed to extend into the periphery, which was rarely observed in cells expressing ARL2[Q70L] or ARL2 or receiving empty vector. This effect appears similar to previously published phenotypes associated with overexpression of myc-MIRO1 and GRIF1-HA (Fransson et al., 2006; Saotome et al., 2008). This phenotype has been repeated by Rachel Turn, and she is in the process of studying and optimizing this phenotype (data not shown). Thus, it appears that the same two mutations that eliminate effects of the dominant, [Q70L], mutation on microtubule density also results in greater plus-end directed motility of mitochondria and distribution to the cell periphery.

ELMOD2 and mitochondrial motility machinery also align with ARL2 puncta

I previously described that ARL2 localizes to puncta along mitochondria, and that these puncta align with MFN1 and MFN2 (Newman et al., manuscript submitted). Because we model ELMOD2 as an ARL2 effector for mitochondrial morphology (Newman et al., 2014), I asked if ELMOD2 also localized to puncta along mitochondria. Using structured illumination microscopy (SIM), I imaged both HeLa and COS7 cells stained for ELMOD2, and found that it also shows a similar punctate pattern along mitochondria. Cara Schiavon has since repeated these data and showed that ELMOD2 also aligns with MFN1 and MFN2 puncta, similar to ARL2 (data not shown), suggesting that ELMOD2 puncta overlap with ARL2 puncta. Thus, ARL2 and the ARL2 GAP ELMOD2 align with MFNs at discrete puncta that display regular spacing along mitochondria (Newman et al., manuscript submitted).

Given that loss of ARL2 activity causes a loss in plus end directed motility (Newman et al., 2014), I asked if any of the mitochondrial motility machinery also aligns with ARL2. First, I examined MIRO. I expressed myc-MIRO1 and myc-MIRO2 in HeLa cells, and fixed and stained with myc and ARL2. When I imaged cells using SIM, I found that myc staining for both MIRO1 and MIRO2 formed puncta that also aligned with ARL2 puncta (Figure 11). These puncta often appeared adjacent to ARL2 puncta, consistent with the localization of MIROs to the outer membrane and ARL2 to the IMS. These data have been repeated twice – I performed the pilot experiment, and the repeat experiment was performed by Rachel Turn under my supervision.

Because ARL2 aligned with MIRO, I next examined other mitochondrial motility proteins. I expressed GRIF1-HA in cells, and stained with HA and ARL2. Despite repeated attempts using variable plasmid concentrations for transfection, I was unable to show that GRIF1-HA had a punctate localization along mitochondria. When expressed, GRIF1-HA was only weakly mitochondrial and appeared mostly diffuse, consistent with previous studies (MacAskill et al., 2009), and did not appear mitochondrial when 3D SIM data was reconstructed (data not shown). Next, I stained COS7 cells for ARL2 and KIF5B. I observed that staining of KIF5B was punctate and diffuse, also consistent with previous studies (Pfister et al., 1989). When KIF5B was

associated with mitochondria, it appeared adjacent to ARL2 puncta the majority of the time. This is in contrast to other punctate staining I've imaged, including DRP1-YFP and GFP-MFF, which appeared both next to and in between ARL2 puncta equally (data not shown). Though KIF5B appears punctate and associates with mitochondria, KIF5B puncta do not align the length of mitochondria as myc-MIROs do. Therefore, we may need to perform some type of quantitiative analysis to determine how often KIF5B associates with ARL2 puncta, to determine if my initial impressions are supported. Rachel Turn and I are in the process of repeating this data and generating figures.

Discussion

In this chapter, I summarize my unpublished data concerning ARL2's roles in mitochondria, and attempted to uncover the mechanism by which ARL2 regulates ATP levels. I first focused on the ARL2/HSP60 complex present in mitochondria. The ARL2 in this complex persisted for several days after initiation of ARL2 knockdown, suggesting that the ARL2/HSP60 complex is unaffected by ARL2 siRNA and not the site of action for ARL2 effects on ATP levels. I performed the BOFA assay on ARL2 siRNA cells and found no obvious defects in the activity of the electron transport chain, compared to mock transfected controls. Next, I examined cristae morphology in ARL2 siRNA cells and found trends toward lower cristae density, though this result requires greater N numbers to achieve statistical significance and a clear conclusion. This decrease in cristae density was not observed in cells expressing either ARL2[T30N] or ARL2[Q70L], suggesting that ARL2 may regulate ATP via cristae morphology and that this is a separate site of action from its regulation of mitochondrial morphology. Along with Cara Schiavon, I identified point mutants of ARL2 that allow dissociation of ARL2's effects on mitochondria and microtubules. Finally, I provided data that ELMOD2 and MIROs align with ARL2 puncta along mitochondria.

Using BN-PAGE, we found that ARL2 is present in a complex with HSP60 (Newman et al., submitted). HSP60 is a chaperone in the mitochondrial matrix, so the presence of the ARL2/HSP60 complex supports our observations that a pool of ARL2 resides in the matrix (Newman et al., 2014; Sharer et al., 2002). We examined a potential role for this complex in mitochondrial functions of ARL2. Treatment with metabolic stressors increases mitochondrial ARL2 pools, as determined by immunofluorescence (Newman & Schiavon, manuscript in preparation); however, these treatments did not increase the amount of ARL2 in the ARL2/HSP60 complex. A second test of functionality was to knock down ARL2 and examine the ARL2/HSP60 complex. ARL2 was not depleted from the ARL2/HSP60 complex with knockdown, suggesting that (1) ARL2 in the complex has a long half-life and (2) depletion of ARL2 from the complex is not correlated with phenotypes caused by ARL2 siRNA. We believe that the amount of ARL2 in the complex may be very small: samples run on BN-PAGE where we can detect ARL2 in the HSP60 complex, when run on SDS-PAGE have undetectable ARL2 (Michael East, unpublished observations). Therefore, BN-PAGE appears to be substantially more sensitive than SDS-PAGE for ARL2 immunoblotting. Additionally, we were unable to estimate the amount of ARL2 in the ARL2/HSP60 complex because we were unable to resolve purified ARL2, which runs at 20 kDa, on the same native gel as the complex. Taken together, these results argue against a role for this complex in mitochondrial functions of ARL2. Instead, this complex may represent a folding intermediate of ARL2 imported into the matrix or perhaps destined for degradation. This model is consistent with the function of HSP60 and the fact that we detect several other mitochondrial proteins co-migrating with the HSP60 complex at ~500 kDa. Thus, we conclude that while a small pool of ARL2 is present in the mitochondrial matrix, based upon its presence in a complex containing the matrix protein HSP60, though this pool is not functional in any of the effects of ARL2 on mitochondria examined to date in our lab.

After ruling out a role for the ARL2/HSP60 complex in ARL2 regulation of ATP levels, I chose to test for defects of the electron transport chain. Using BN-PAGE, I found no differences

in the abundance of any of the respiratory complexes (Newman et al., 2014). Therefore, I used the BOFA assay to measure the activity of the electron transport chain. I found that basal respiration was increased in ARL2 siRNA cells, suggesting increased overall activity of the electron transport chain. However, ARL2 siRNA cells responded to sequential drug additions (oligomycin, CCCP, and antimycin A/rotenone) indistinguishably from mock transfected cells, suggesting no abnormalities in electron transport chain activity. While presenting my work at a poster session at a meeting, I learned that a defect in the electron transport chain may have been masked because I culture cells in DMEM with 25 mM glucose. Therefore, a defect in the electron transport chain might emerge if ARL2 siRNA cells are instead cultured in a lower concentration of glucose (5 mM was recommended). However, the increased basal respiration without any changes in response to respiratory inhibitors suggests that the electron transport chain is functioning normally, and may have increased activity to compensate for the lowered ATP levels in ARL2 siRNA cells.

With no obvious defects in the electron transport chain, I decided to examine cristae morphology as a possible mechanism for decreased ATP levels in ARL2 siRNA cells. I found that cristae morphology was obviously diminished in ARL2 siRNA cells, compared to mock transfected cells receiving no siRNA. When quantified, ARL2 siRNA cells have 36% fewer cristae/μm outer membrane length and 54% less cristae membrane length. A limitation of this analysis is that my error bars are large due to only analyzing mitochondria from 2 cells per condition. Because the analysis is time-consuming, I would advise anyone wanting to follow up to contact the ICI core here at Emory about making a macro to perform and speed analysis. As a result of the small sample size, it is premature to make any hard conclusions on these effects.

The lower cristae density in ARL2 siRNA cells does not appear to be secondary to fragmented mitochondria, by visual inspection. Fragmented mitochondria in mock treated cells appeared to have more cristae than cells receiving ARL2 siRNA (Figure 4), and my analysis (Figure 5) normalizes cristae to outer membrane length as a measure of mitochondrial size.

Furthermore, I examined cristae in cells expressing ARL2[T30N], and cristae density appeared similar to controls, despite the fact that mitochondria in these cells are fragmented. We have also observed that ELMOD2 siRNA causes mitochondrial fragmentation but does not affect cristae morphology (Cara Schiavon, unpublished data), further supporting our conclusion that loss of cristae is not secondary to mitochondrial fragmentation. Similar to the data with ARL2 siRNA described above, quantification of cristae density will be required to solidify this conclusion.

My preliminary data on mitochondrial cristae support the hypothesis that ARL2 regulates ATP levels through regulation of cristae morphology. We previously found that only ARL2 siRNA leads to ATP loss; ATP levels are unchanged with ELMOD2 siRNA or expression of ARL2[T30N], despite the fact that all three treatments cause mitochondrial fragmentation (Newman et al., 2014). These data led us to model two sites of action for ARL2 in mitochondria: one regulating mitochondrial fusion through ELMOD2, and another regulating ATP levels without ELMOD2. Loss in cristae density is observed with ARL2 siRNA but not with ARL2[T30N] or ELMOD2 siRNA. Additionally, expression of ARL2[Q70L] causes mitochondrial elongation but has no effect on cristae morphology or ATP levels. These data are consistent with the model that ARL2 regulates ATP levels through cristae morphology, and that this pathway is independent of ELMOD2 and its role(s) in fusion.

Along with Cara Schiavon, I identified point mutants in ARL2 that allow for dissection of effects on mitochondria from effects on microtubules. Both [F50A] and [L3A] reverse microtubule loss associated with ARL2[Q70L], whereas [L3A] and [I6R] reverse mitochondrial fragmentation and perinuclear clustering associated with ARL2[T30N]. The observation that [F50A] only affects microtubule loss and [I6R] only affects mitochondrial morphology supports the conclusion that these are independent pathways regulated by ARL2. Similarly, my data that [L3A] and [I6R] do not reverse mitochondrial elongation associated with ARL2[Q70L] (Newman et al., manuscript submitted), despite the fact that they reverse fragmentation associated with ARL2[T30N], suggests that ARL2 mediates mitochondrial fragmentation and elongation through

two different pathways. Mitochondrial fragmentation and motility, however, could be mediated by one ARL2 effector, as [L3A] and [I6R] reverse both fragmentation and perinuclear clustering caused by ARL2[T30N]. I also discovered a phenotype associated with ARL2[Q70L, L3A] and ARL2[Q70L, F50A], in that mitochondria extend into the cell periphery, phenocopying overexpression of MIRO1. I did not observe this phenotype with ARL2[Q70L], likely because the majority of ARL2[Q70L] cells are missing microtubules (Zhou et al., 2006), which might interfere with mitochondrial movement to the cell periphery.

Finally, I show that ELMOD2 and MIROs align with ARL2 puncta along mitochondria. ELMOD2 also localizes to puncta along mitochondria, and these puncta align with MFN puncta (Cara Schiavon, unpublished data), suggesting that ELMOD2 exists in the same puncta as ARL2. We model ELMOD2 as the ARL2 effector for mitochondrial fusion, so its localization to puncta along with ARL2 and MFNs supports this hypothesis. I also show that MIRO1, MIRO2, and possibly KIF5B align with ARL2 puncta. The association of mitochondrial motility machinery with mitochondrial fusion machinery is exciting, because it suggests that these proteins coordinate fusion and motility processes. This idea is supported by the observations that MFNs co-immunoprecipitate with MIRO1 and MIRO2, and that deletion of MFN2 affects mitochondrial motility (Chen et al., 2003; Misko et al., 2010). Therefore, ARL2 (and ELMOD2) may coordinate mitochondrial fusion and mitochondrial motility, which will be explored in future studies.

References

Bhamidipati, A., S.A. Lewis, and N.J. Cowan. 2000. ADP ribosylation factor-like protein 2 (Arl2) regulates the interaction of tubulin-folding cofactor D with native tubulin. J Cell Biol. 149:1087-1096.

Chen, H., S.A. Detmer, A.J. Ewald, E.E. Griffin, S.E. Fraser, and D.C. Chan. 2003. Mitofusins Mfn1 and Mfn2 coordinately regulate mitochondrial fusion and are essential for embryonic development. J Cell Biol. 160:189-200.

Cheng, M.Y., F.U. Hartl, J. Martin, R.A. Pollock, F. Kalousek, W. Neupert, E.M. Hallberg, R.L. Hallberg, and A.L. Horwich. 1989. Mitochondrial heat-shock protein hsp60 is essential for assembly of proteins imported into yeast mitochondria. Nature. 337:620-625.

Cipolat, S., O.M. de Brito, B. Dal Zilio, and L. Scorrano. 2004. OPA1 requires mitofusin 1 to promote mitochondrial fusion. Proc Natl Acad Sci U S A. 101:15927-15932.

Fransson, S., A. Ruusala, and P. Aspenstrom. 2006. The atypical Rho GTPases Miro-1 and Miro-2 have essential roles in mitochondrial trafficking. Biochem Biophys Res Commun. 344:500-510.

Griparic, L., N.N. van der Wel, I.J. Orozco, P.J. Peters, and A.M. van der Bliek. 2004. Loss of the intermembrane space protein Mgm1/OPA1 induces swelling and localized constrictions along the lengths of mitochondria. J Biol Chem. 279:18792-18798.

Hanzal-Bayer, M., L. Renault, P. Roversi, A. Wittinghofer, and R.C. Hillig. 2002. The complex of Arl2-GTP and PDE delta: from structure to function. EMBO J. 21:2095-2106.

Levy-Rimler, G., P. Viitanen, C. Weiss, R. Sharkia, A. Greenberg, A. Niv, A. Lustig, Y. Delarea, and A. Azem. 2001. The effect of nucleotides and mitochondrial chaperonin 10 on the structure and chaperone activity of mitochondrial chaperonin 60. Eur J Biochem. 268:3465-3472.

MacAskill, A.F., K. Brickley, F.A. Stephenson, and J.T. Kittler. 2009. GTPase dependent recruitment of Grif-1 by Miro1 regulates mitochondrial trafficking in hippocampal neurons. Mol Cell Neurosci. 40:301-312.

Misko, A., S. Jiang, I. Wegorzewska, J. Milbrandt, and R.H. Baloh. 2010. Mitofusin 2 is necessary for transport of axonal mitochondria and interacts with the Miro/Milton complex. J Neurosci. 30:4232-4240.

Newman, L.E., C.-j. Zhou, S. Mudigonda, A.L. Mattheyses, E. Paradies, C.M.T. Marobbio, and R.A. Kahn. 2014. The ARL2 GTPase Is Required for Mitochondrial Morphology, Motility, and Maintenance of ATP Levels. PLoS One. 9:e99270.

Nicholls, D.G., V.M. Darley-Usmar, M. Wu, P.B. Jensen, G.W. Rogers, and D.A. Ferrick. 2010. Bioenergetic profile experiment using C2C12 myoblast cells. J Vis Exp.

Patten, D.A., J. Wong, M. Khacho, V. Soubannier, R.J. Mailloux, K. Pilon-Larose, J.G. MacLaurin, D.S. Park, H.M. McBride, L. Trinkle-Mulcahy, M.E. Harper, M. Germain, and R.S. Slack. 2014. OPA1-dependent cristae modulation is essential for cellular adaptation to metabolic demand.

Pfister, K.K., M.C. Wagner, D.L. Stenoien, S.T. Brady, and G.S. Bloom. 1989. Monoclonal antibodies to kinesin heavy and light chains stain vesicle-like structures, but not microtubules, in cultured cells. J Cell Biol. 108:1453-1463.

Saotome, M., D. Safiulina, G. Szabadkai, S. Das, A. Fransson, P. Aspenstrom, R. Rizzuto, and G. Hajnoczky. 2008. Bidirectional Ca2+-dependent control of mitochondrial dynamics by the Miro GTPase. Proc Natl Acad Sci U S A. 105:20728-20733.

Sharer, J.D., J.F. Shern, H. Van Valkenburgh, D.C. Wallace, and R.A. Kahn. 2002. ARL2 and BART enter mitochondria and bind the adenine nucleotide transporter. Mol Biol Cell. 13:71-83.

Tian, G., S. Thomas, and N.J. Cowan. 2010. Effect of TBCD and its regulatory interactor Arl2 on tubulin and microtubule integrity. Cytoskeleton (Hoboken). 67:706-714.

Zhang, T., S. Li, Y. Zhang, C. Zhong, Z. Lai, and J. Ding. 2009. Crystal Structure of the ARL2-GTP-BART Complex Reveals a Novel Recognition and Binding Mode of Small GTPase with Effector. Structure (London, England : 1993). 17:602-610.

Zhou, C., L. Cunningham, A.I. Marcus, Y. Li, and R.A. Kahn. 2006. Arl2 and Arl3 regulate different microtubule-dependent processes. Mol Biol Cell. 17:2476-2487.

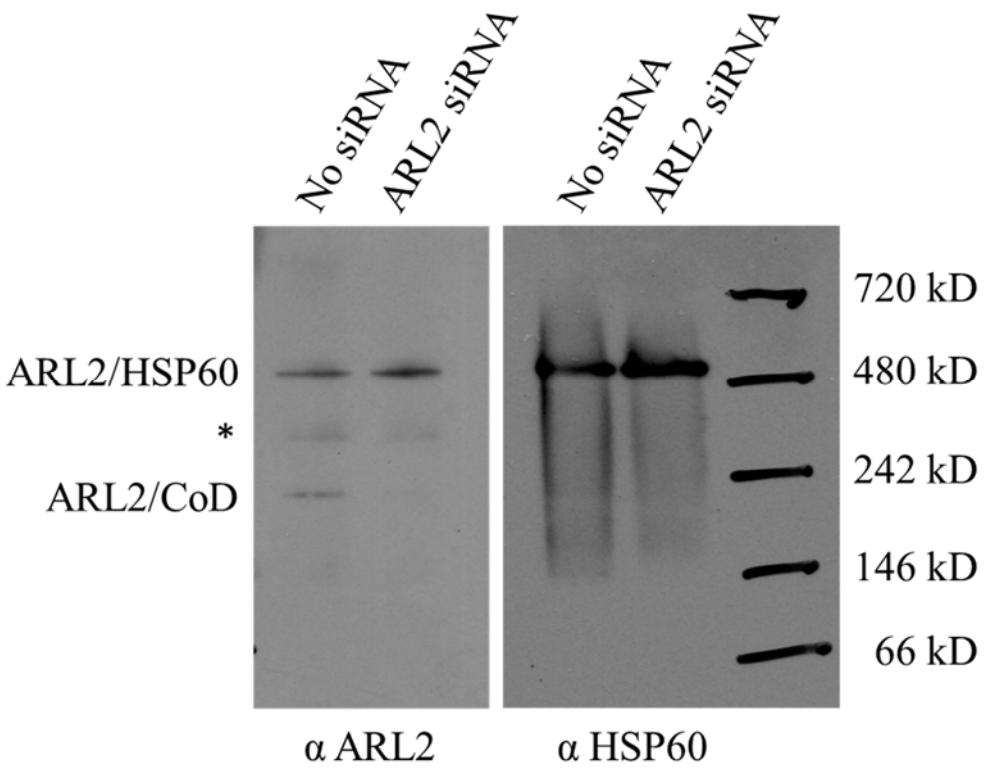

Figure 1. The ARL2/HSP60 complex is unchanged by knockdown of ARL2. HeLa cells were transfected with no siRNA or ARL2 siRNA, and harvested 24 hours later. Cells were lysed and resolved on 4-16% BN-PAGE gel, followed by blotting for ARL2 or HSP60. No differences in the amount of ARL2/HSP60 complex running at ~500 kDa were observed, despite the disappearance of the cytosolic, ARL2/Cofactor D complex at ~200 kDa. Similar results were obtained 48 and 72 hours after transfection. Asterisk indicates a non-specific band that is not competed with antigen. This experiment has been repeated several times with similar results.

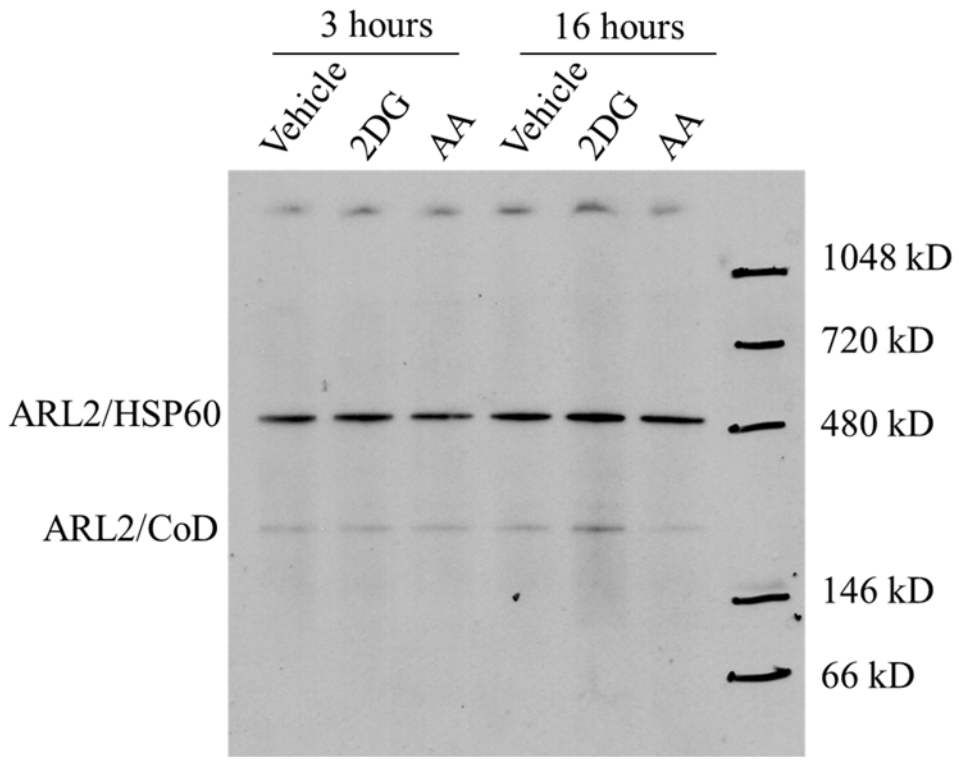

Figure 2. The ARL2/HSP60 complex does not change with metabolic stressors. HeLa cells were treated for either 3 hours or 16 hours with 25 mM 2-deoxyglucose, 1 μM antimycin A, or vehicle control. Cells were lysed and resolved in a 4-16% BN-PAGE gel, followed by immunoblotting for ARL2. No change in the levels of the ARL2/HSP60 complex at ~500 kDa is evident. This experiment was done once and needs to be repeated prior to publication.

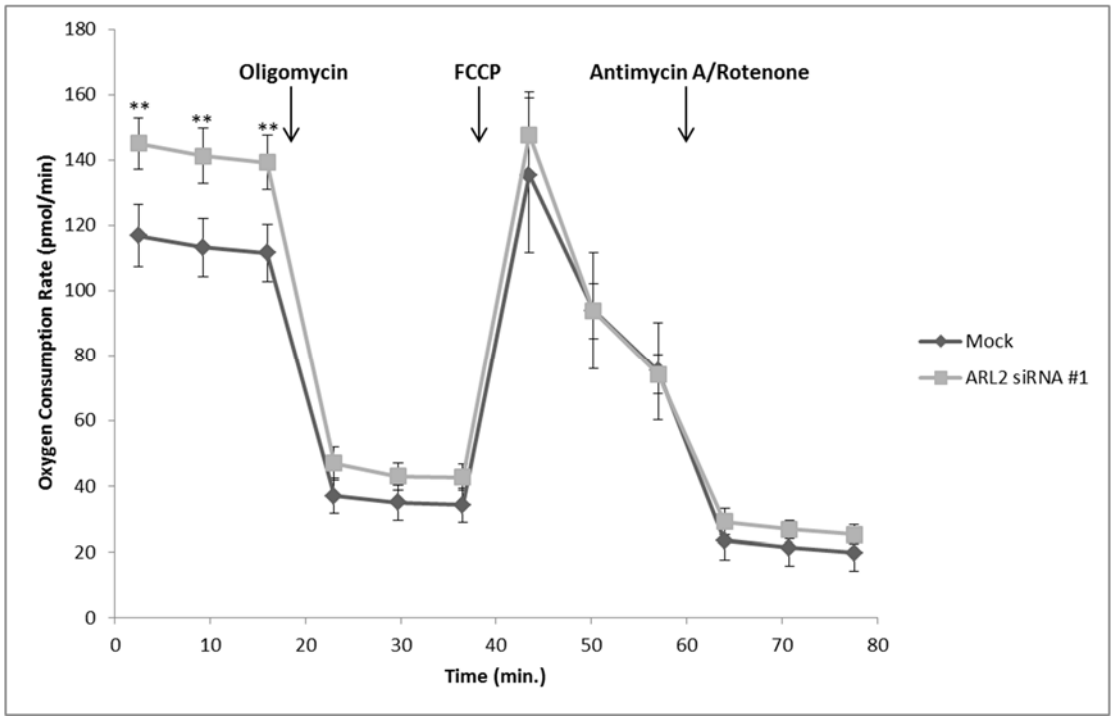

Figure 3. Basal cell respiration is increased in HeLa cells depleted of ARL2. HeLa cells were transfected with no siRNA (Mock) or ARL2 siRNA #1. Oxygen consumption was measured after sequential addition of oligomycin (10 μM), FCCP (3 μM) plus pyruvate (50 mM), and antimycin A (10 μM) plus rotenone (10 μM) at 18, 39, and 59 minutes after the start of the assay, respectively. Measurements were made with a Seahorse XF analyzer 48 hours after transfection, and normalized to cell number using the Cyquant assay. This experiment has been repeated three times with a total of 24 replicates; shown is a representative experiment with eight replicates per condition. Double asterisks indicate statistically significant differences ($p<0.01$). This experiment has been repeated twice with similar results.

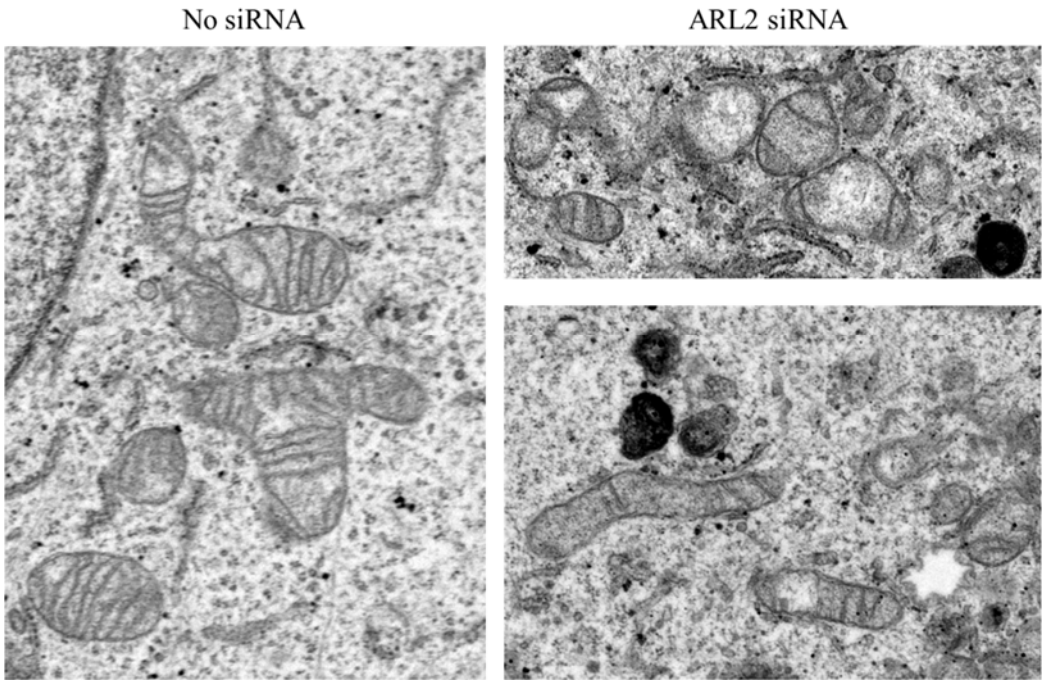

Figure 4. Knockdown of ARL2 causes a loss in cristae density. HeLa cells were transfected with either no siRNA (left) or ARL2 siRNA (right), and re-plated 24 hours later. Seventy-two hours after transfection, cells were fixed and processed for electron microscopy. Representative images are shown. This experiment has been repeated once with similar results.

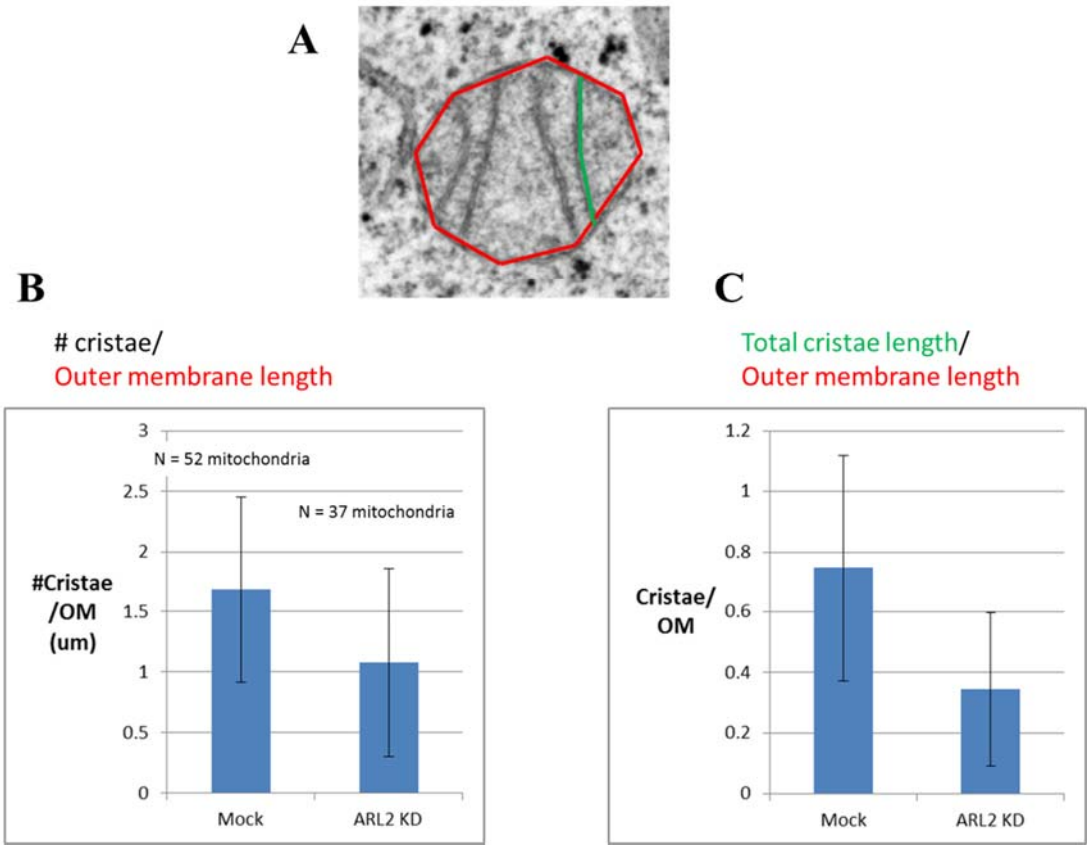

Figure 5. ARL2 siRNA leads to fewer number and length of cristae per mitochondrion. (**A**) Schematic showing analysis of cristae. The outer mitochondrial membrane (red) and the cristae membranes (green) were traced using ImageJ to measure the length in μm. The number of cristae per mitochondrion were counted. (**B**) When the average number of cristae was normalized to the length of the outer mitochondrial membrane, ARL2 siRNA cells have 36% fewer cristae (average of 1.68 cristae/mitochondrion in control cells vs 1.08 cristae/mitochondrion in ARL2 siRNA cells). (**C**) When the length of cristae was normalized to the length of the outer membrane, ARL2 siRNA cells have 54% less cristae (0.75 μm for control cells, 0.34 μm for ARL2 siRNA cells).

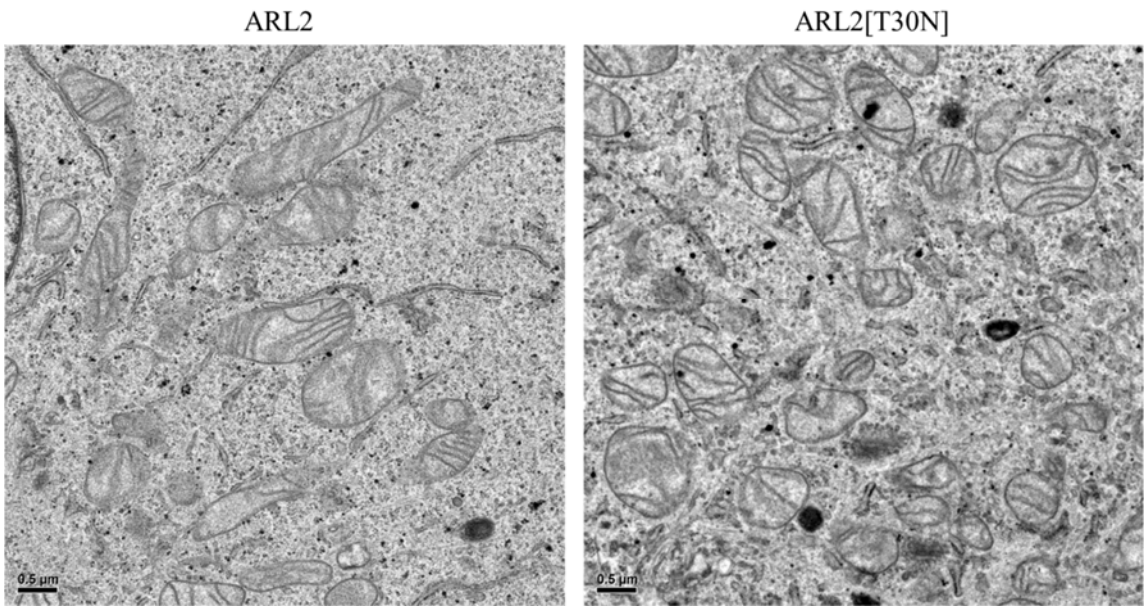

Figure 6. Expression of ARL2[T30N] does not affect cristae density. HeLa cells were transfected with either ARL2 (left) or ARL2[T30N] (right). Twenty-four hours after transfection, cells were fixed and processed for electron microscopy. Representative images are shown. This experiment has been repeated with similar results. Scale bar = 0.5 µm.

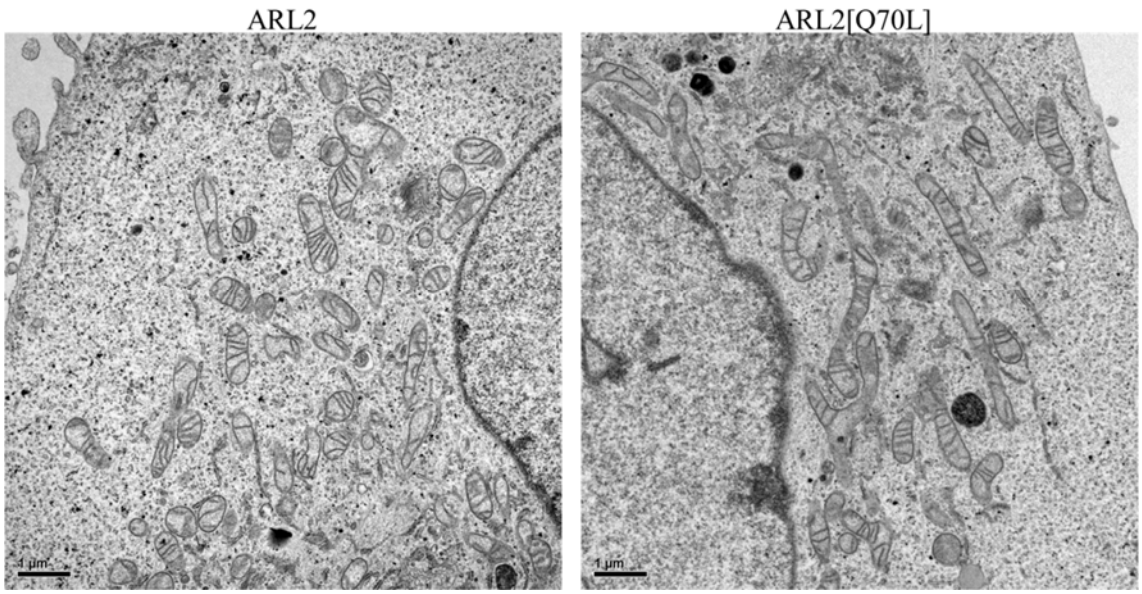

Figure 7. Expression of ARL2[Q70L] does not affect cristae density. HeLa cells were transfected with either ARL2 (left) or ARL2[Q70L] (right). Seventy-two hours after transfection, cells were fixed and processed for electron microscopy. Representative images are shown. This experiment has been repeated with similar results. Scale bar = 1 um.

Microtubule loss	
ARL2	-
ARL2[Q70L]	+
[Δ1-9] ARL2[Q70L]	-
ARL2[Q70L, L3A]	**-**
ARL2[Q70L, I6R]	+
ARL2[Q70L, F50A]	**-**

Mitochondrial Elongation	
ARL2	-
ARL2[Q70L]	+
[Δ1-9] ARL2[Q70L]	-
ARL2[Q70L, L3A]	+
ARL2[Q70L, I6R]	+
ARL2[Q70L, F50A]	+

Mitochondrial fragmentation and perinuclear clustering	
ARL2	-
ARL2[T30N]	+
[Δ1-9] ARL2[T30N]	-
ARL2[T30N, L3A]	**-**
ARL2 [T30N, I6R]	**-**
ARL2[T30N, F50A]	+

Figure 8. Summary of mutations that reverse phenotypes caused by expression of dominant ARL2 mutants. The mutations described above were introduced into ARL2[Q70L] and ARL2[T30N]. The resulting constructs were expressed in HeLa cells. Cells transfected with ARL2[Q70L]-derived constructs were assayed for microtubule destruction or mitochondrial elongation 48 hours after transfection. Cells transfected with ARL2[T30N]-derived constructs were assayed for mitochondrial fragmentation and perinuclear clustering 24 hours after transfection. Mitochondrial fragmentation and perinuclear clustering data are preliminary, based on visual inspection of one experiment, and need to be repeated and quantified prior to publication.

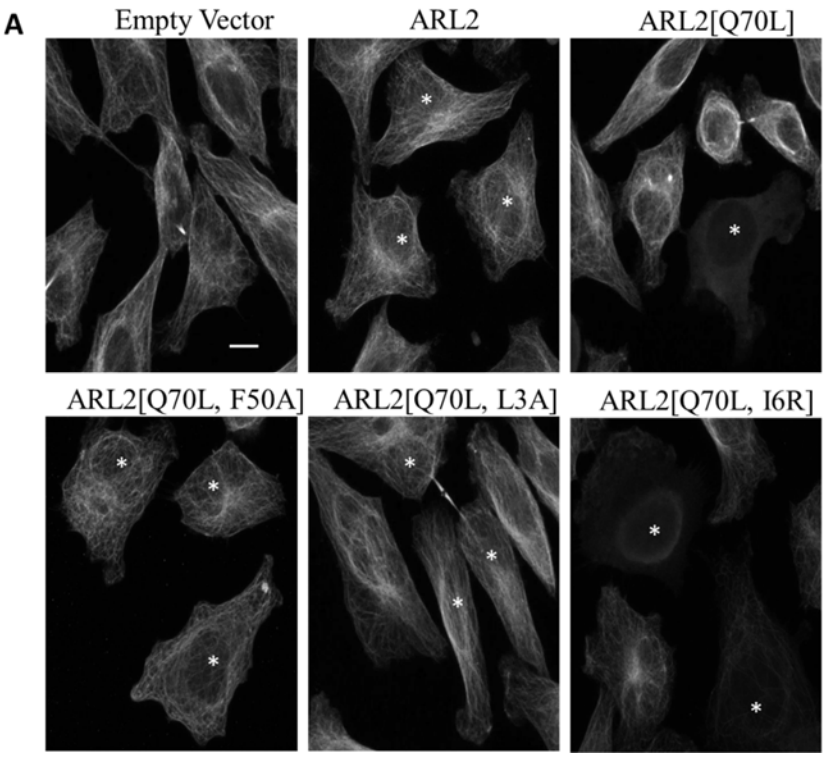
A
Empty Vector
ARL2
ARL2[Q70L]
ARL2[Q70L, F50A]
ARL2[Q70L, L3A]
ARL2[Q70L, I6R]

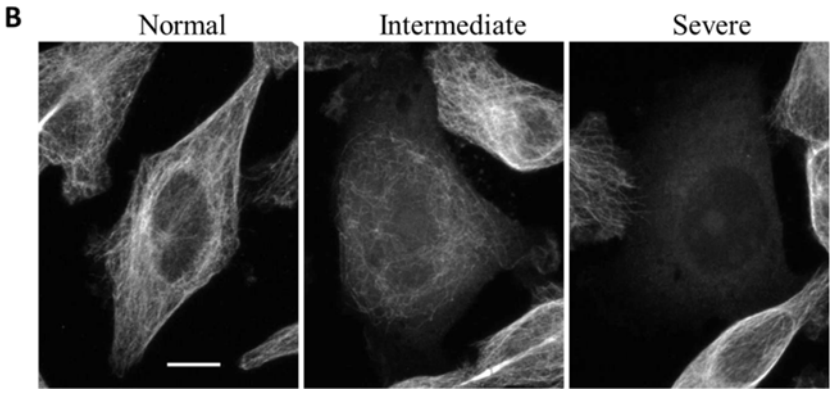
B
Normal
Intermediate
Severe

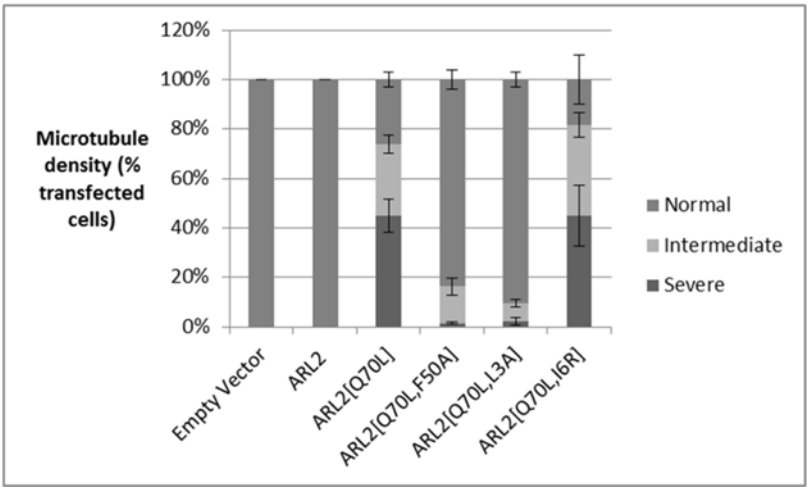
C
Microtubule density (% transfected cells)
120%
100%
80%
60%
40%
20%
0%
Empty Vector
ARL2
ARL2[Q70L]
ARL2[Q70L,F50A]
ARL2[Q70L,L3A]
ARL2[Q70L,I6R]
Normal
Intermediate
Severe

Figure 9. [L3A] and [F50A] mutations reverse microtubule destruction caused by ARL2[Q70L]. A) Plasmids directing expression of empty vector (pcDNA3.1), ARL2, ARL2[Q70L], ARL2[Q70L, F50A], ARL2[Q70L, L3A], or ARL2[Q70L, I6R] were transfected into HeLa cells. Cells were fixed 72 hours later and stained for ARL2, to identify transfected cells, and α tubulin, to visualize microtubules. Z stack projections are shown. Asterisk (*) indicates transfected cell. Scale bar = 10 μm. B) Examples of categories used to score cells are shown. Scale bar = 10 μm. C) Cells were transfected, fixed, and stained as in A, and scored for microtubule density using the categories shown in B. Results shown are means of three independent experiments, with at least 200 cells counted per condition, per experiment. Error bars represent standard deviation.

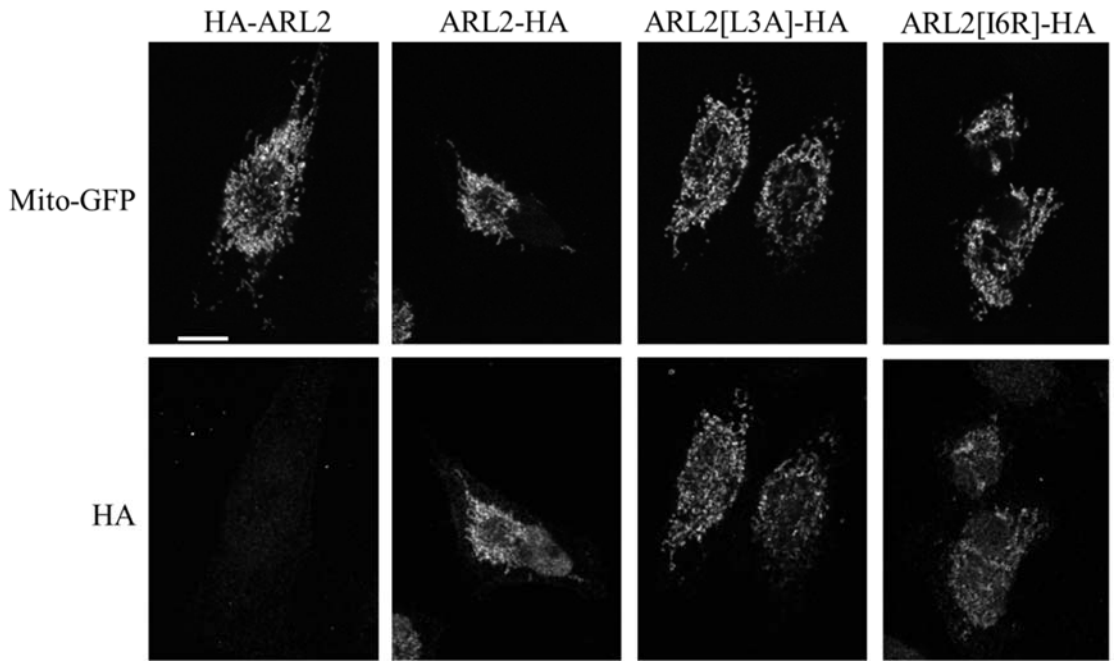

Figure 10. [L3A] and [I6R] do not prevent import of ARL2 into mitochondria. HeLa cells were co-transfected with 0.5 µg of mito-GFP (to mark transfected cells) as well as 2 µg of either HA-ARL2, ARL2-HA, ARL2[L3A]-HA, or ARL2[I6R]. Twenty-four hours after transfection, cells were permeabilized with ice-cold 0.5% saponin in PBS immediately prior to fixation in cold 4% PFA in PBS. Coverslips were then stained for HA. Representative, single plane confocal images are shown. This experiment was repeated once with similar results. Scale bar = 10 µm.

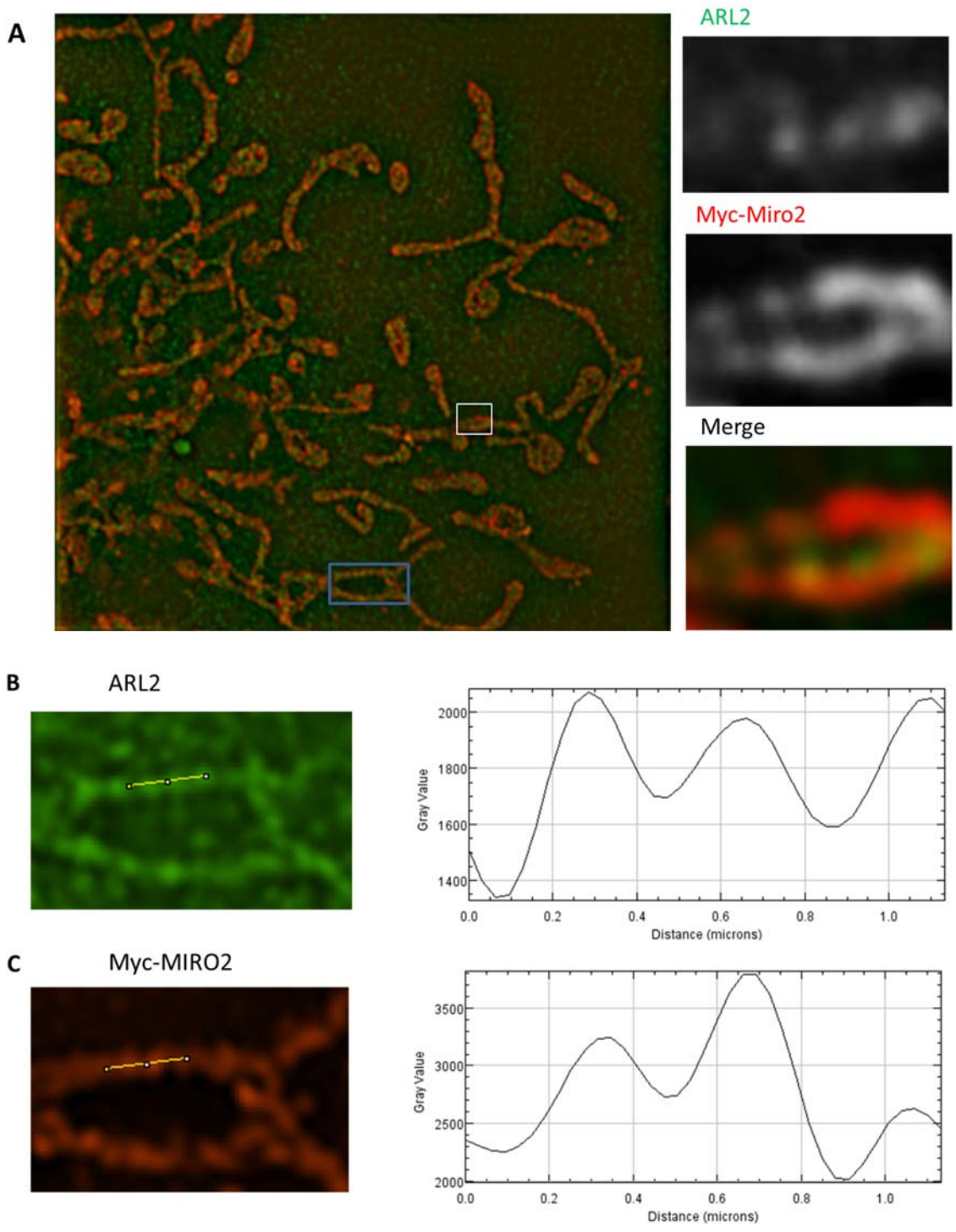

Figure 11: MIROs localize to puncta that align with ARL2 puncta. COS7 cells were transfected with myc-MIRO2, stained for ARL2 and myc, and imaged using three-dimensional SIM. A) Myc staining (red) localizes to puncta along the outer membrane that align with endogenous ARL2 puncta, consistent with its proposed localization in the IMS. Images are

enlarged from the white inset shown on the larger image. Similar results were obtained for myc-MIRO1 (not shown). This experiment has been repeated once with similar results while working with Rachel Turn. B) Line scan analysis was performed through a portion of mitochondria enlarged from the blue inset, using ARL2 staining. The graph (ARL2 staining) shows pixel intensity along the line. C) Line scan analysis was performed for myc-MIRO2, using the same line. The graph on the right shows pixel intensity of myc-MIRO2 staining along the line.

Chapter 7: Studies of phosphorylation of ARL2

Abstract

In this chapter, I explore roles of phosphorylation in ARL2 signaling. Because ARL2 localizes to distinct sites and its import into mitochondria changes in response to a variety of stressors, we speculated that one or more post-translational modifications on ARL2 may be important in the regulation of its localization. On-line resources identified serine 45 as a site of phosphorylation that is quite often found in high throughput proteomics (e.g., see Phosphosite Plus). Thus, I first tested for a functional role of serine-45 phosphorylation in a number of the assays established in our lab for ARL2 functions. Unfortunately, expression of ARL2[S45A] or ARL2[S45D] had no obvious phenotypes in cells. I then performed radiolabeling of live cells with $^{32}P_i$, followed by IP of ARL2, and found $^{32}P_i$ incorporation into ARL2, suggesting that ARL2 is indeed phosphorylated in HeLa cells. However, I also found $^{32}P_i$ incorporation into ARL2[S45A] to a similar extent as wild type ARL2, indicating that the bulk of the phosphorylation was likely not on serine-45. Mass spectrometry failed to identify any phosphorylation sites in ARL2, despite good coverage. However, I found diminished $^{32}P_i$ incorporation into ARL2 under a subset of conditions that lead to increased import of ARL2 into mitochondria. Therefore, this phosphorylation site may have functional significance under conditions that lead to increased mitochondrial ARL2, and further studies will be needed to elucidate this role.

Introduction

As demonstrated in previous chapters, ARL2 has several important functions within mitochondria, including fusion, motility, and ATP production. Interestingly, the amount of ARL2 in mitochondria is increased in response to several cellular stressors (Newman & Schiavon et al., manuscript submitted). Therefore, we hypothesize that import of ARL2 into mitochondria is regulated in response to cellular stressors. However, we estimate that only 5-10% of ARL2 is

mitochondrial, the bulk of the remaining ~90% of cytosolic ARL2 is bound to the tubulin folding chaperone Cofactor D. (Bhamidipati et al., 2000; Sharer et al., 2002; Shern et al., 2003). In order for cytosolic ARL2 to reroute to mitochondria or interact with effectors, it must dissociate from Cofactor D. Because our in vitro data suggest a long half-life of ARL2-Cofactor D complexes, we speculate that dissociation requires either a dissociation factor or post-translational modification that results in the loss of binding to Cofactor D. Several phosphoproteomics studies have identified ARL2 as a phosphoprotein. Though several putative phosphorylation sites have been found only once, one site of phosphorylation, serine-45, has been found repeatedly (Choudhary et al., 2009; Dephoure et al., 2008; Gauci et al., 2009; Humphrey et al., 2013; Huttlin et al., 2010; Klammer et al., 2012; Lundby et al., 2012; Mayya et al., 2009; Mertins et al., 2013; Trinidad et al., 2012; Weber et al., 2012; Weintz et al., 2010; Wisniewski et al., 2010; Wu et al., 2012; Zanivan et al., 2008; Zhou et al., 2013). Serine-45 is located in switch I, which is conserved in GTPases and changes conformation in response to the nucleotide bound in order to facilitate interactions with effectors (Kahn et al., 2006). As shown in Figure 1, serine-45 (purple) is located at the interface of ARL2 (green) bound to PDEδ (blue), an ARL2 effector. Addition of a phosphate group to serine-45 is predicted to negatively influence binding of ARL2 to effectors that use switch I. Therefore, phosphorylation of ARL2 could play an important role in ARL2 signaling by altering its ability to bind to effectors, including Cofactor D. Consequently, phosphorylated ARL2 would be free to have other effects on the cell, including possible import into mitochondria. Stated another way, the localization of a protein kinase or phosphatase that acts on ARL2 could be a determinant in the ultimate distribution of ARL2 in cells. In this chapter, I tested for a role of serine-45 in ARL2 signaling and also showed that ARL2 is phosphorylated in cells, likely at a novel site.

Materials and Methods

Cell culture: Human cervical carcinoma (HeLa) cells were grown in DMEM supplemented with 10% fetal bovine serum (Invitrogen, Carlsbad, CA) and 2 mM glutamine at 37°C in the presence of 5% CO_2.

Antibodies: Rabbit polyclonal antibodies directed against human ARL2 were generated in our lab and have been described previously (Sharer et al., 2002). Characterization of the specificity of these reagents has included comparisons to pre-immune serum and antigen competition in both immunoblots and indirect immunofluorescence. The following antibodies were obtained from commercial sources: HSP60 (Enzo Life Sciences ADI-SPA-807), alpha-tubulin (Sigma T9026).

Plasmids: Phosphomimetic [S45D] and phosphonull [S45A] mutations were introduced by site-directed mutagenesis into ARL2, ARL2[Q70L], or ARL2[T30N] in pcDNA3.1, which were described previously (Zhou et al., 2006). Mutations were made by Oskar Laur in the Cloning Core at Emory.

Transfection: Cells were plated for 24 hours and transfected at a density of 70-80% in 6 well plates. DNA (2 µg) was diluted in 100 µl of OPTIMEM (Invitrogen), and 6 µl of Plus reagent (Invitrogen) was then added. The DNA/Plus mixture was incubated for 15 minutes at room temperature. During incubation, 4 µl of Lipofectamine (Invitrogen) was diluted in 100 µl of OPTIMEM. The two tubes were combined and allowed to incubate for another 15 minutes at room temperature. Cell culture medium was changed to 0.8 ml OPTIMEM per well, prior to addition of 0.2 ml of transfection complexes drop wise to each well, after which cells were returned to the incubator. Four hours later, the medium was either changed back to growth media, or cells were split 1:2 on matrigel (BD Biosciences #356231) coated coverslips for immunofluorescence.

Immunofluorescence: To visualize mitochondria, cells were fixed in 4% paraformaldehyde in PBS, and permeabilized with 0.1% (v/v) Triton X-100 in PBS for 10 minutes at room

temperature. Incubation with primary antibodies was carried out in PBS containing 1% (w/v) BSA, at 4°C overnight. Secondary antibodies (Alexa fluorophores, Invitrogen) were incubated in the same buffer for 1 hour at room temperature at a 1:500 dilution. To visualize microtubules, we used PHEMO fixation (3.7% (v/v) paraformaldehyde, 0.05% (v/v) glutaraldehyde, 0.5% (v/v) Triton X-100 in 68 mM PIPES, 25 mM HEPES, 15 mM EGTA, 3 mM $MgCl_2$, 10% (v/v) dimethylsulfoxide, pH 6.8) for 10 minutes at room temperature, as described previously (Mabjeesh et al., 2003). Cells were then stained and imaged as described above. Antibody dilutions used for immunofluorescence were as follows: ARL2 (1:1000), HSP60 (1:5000), alpha tubulin (1:1000).

Immunoprecipitation: Cells were washed twice with ice cold PBS, and the PBS was aspirated before cells were frozen in a dry ice/acetone bath. Once the cells were frozen, 100 µl of 2% SDS was added per well, and cells were scraped to collect and lyse. RIPA buffer without SDS (1.9 ml; 150 mM NaCl, 1% NP-40, 0.5% DOC, 50 mM Tris pH 8) was then added (final SDS concentration = 0.1%). I did not determine concentration of radiolabeled lysates; in optimization experiments my lysates were typically 3-4 mg/ml by DC assay, and I ensured that varying the concentration of lysate did not affect the IP of ARL2. The 2 ml of cell lysate was split into two tubes, and 10 µl of ARL2 antiserum (R86336, exsanguination) or control serum (anti-ELMOD2, D7489 bleed 2) was added to 1 ml of lysate (or no serum for beads alone control). Tubes were rotated for one hour at 4°C. Protein G Sepharose beads (GE Healthcare) were washed once in 0.5 M EDTA pH 8, then twice in RIPA buffer, and 20 µl of bead slurry was added to each tube. After another hour of rotation, beads were pelleted by centrifugation and washed 2 times in cold RIPA buffer. The above protocol was optimized for endogenous ARL2; for mass spectrometry experiments, I found that 15 µl of serum per 1 ml lysate was optimal for IP of exogenous ARL2.

Western blotting: Proteins were separated in 15% polyacrylamide gels and wet-transferred to nitrocellulose membranes (Bio-Rad #162-0112) at 70V for 2.5 hours. Western blotting procedures were carried out at room temperature. Membranes were blocked in blotto (5% (w/v) dry milk, 50 mM Tris pH 8, 2 mM $CaCl_2$, 80 mM NaCl, 0.2% (v/v) Tween-20, 0.02% sodium azide) for 1 hour. When probing for ARL2 (1:1000 dilution), membranes were blocked in an alternate blocking buffer (10% goat serum, 5% Tween-20 in PBS), freshly filtered through a 0.2 µm membrane. Membranes were then incubated with primary antibody in blocking buffer at 4°C overnight. Removal of excess primary antibody was carried out by washing the membranes in PBST (PBS with 0.1% Tween-20) three times for 10 min each. HRP-conjugated secondary antibodies (GE cat #NA934V, #NA931V) were diluted 1:5,000 in PBST and incubated with the membrane for 1 hour at room temperature. Excess secondary antibody was removed by washing the membranes in PBST 3 times for 10 min. each, then incubated in luminol containing solution (0.1 mM Tris-HCl pH 8.0, 1.2 mM luminol, 0.2 mM p-coumaric acid, 0.009% hydrogen peroxide) for 1 min. prior to exposure to film.

Radiolabeling: I followed a modified protocol from David Brautigan to radiolabel and lyse cells. Cells were washed three times in serum-free DMEM with no phosphates (Invitrogen) then incubated in the same medium for an hour. [^{32}P]orthophosphate (Perkin Elmer) was added to phosphate-free medium to a final concentration of 1 mCi/ml, and was added to cells (final volume = 1 ml in one well of a six well plate). Cells were labeled for 3 hours at 37°C, 5% CO_2. Calyculin A (50 nM) was added for the last 4 minutes of labeling. Cell lysis and IPs were then performed as described above. Following IP, 30 µl of 2x sample buffer was added, and tubes were incubated on ice for 30 minutes (instead of boiling) prior to loading onto a 15% gel. The gel was dried overnight and exposed to film at -80^{0}C.

Mass spectrometry: Immunoprecipitations were performed as described above on ARL2 overexpressing cells, without radiolabeling. For the first experiment, 50 mM NaF and 1 mM sodium orthovanadate were added to the lysis buffer, and the ARL2 band at 20 kD was cut out and digested with either trypsin or chymotrypsin. For the second experiment, a commercial phosphatase inhibitor cocktail (Halt, Thermo Fisher #78420) was added to the lysis buffer, and three samples were given to the core: a cell pellet from one well, one IP that hadn't been loaded onto a gel, and one IP that had been resolved by SDS-PAGE. Mass spectrometry was performed by the core facility at Emory University.

Results

Expression of ARL2[S45A] or ARL2[S45D] has no effect on microtubule density or mitochondrial morphology

We first asked if phosphomimetic (S45D) or phosphonull (S45A) mutations of serine-45 might alter activity of ARL2 in cells. ARL2 regulates microtubule density (Zhou et al., 2006) as well as mitochondrial morphology (Newman et al., 2014), so I chose to examine microtubules or mitochondria in ARL2[S45A] or ARL2[S45D] expressing cells. HeLa cells were transfected with plasmids directing expression of ARL2[S45A] or ARL2[S45D], plated onto coverslips following transfection, and fixed and stained for ARL2, along with markers for either microtubules (α tubulin) or mitochondria (HSP60). Negative controls included pcDNA3.1 (empty vector) and wild type ARL2, which has no obvious mitochondrial or microtubule phenotypes and is used as a control for overexpression. Transfected cells were identified on the basis of ARL2 staining. No obvious mitochondrial or microtubule defects were obvious by visual inspection, and cells transfected with either ARL2[S45A] or ARL2[S45D] were indistinguishable from cells over-expressing wild type ARL2. Similar results were obtained 24, 48, and 72 hours after transfection, and these experiments were repeated at least twice (data not shown).

We then wondered if combining the [S45A] or [S45D] mutations with dominant ARL2 mutants might alter their phenotypes. Previously, we had observed that the dominant active mutant (ARL2[Q70L]) caused a strong reduction in microtubules (Zhou et al., 2006), and that the dominant negative mutant (ARL2[T30N]) causes both a loss in microtubules and mitochondrial fragmentation (Newman et al., 2014). A total of four constructs were transfected in cells: ARL2[Q70L, S45A], ARL2[Q70L, S45D], ARL2[T30N, S45A], and ARL2[T30N, S45D]. Mitochondrial fragmentation was assayed 24 hours after transfection, and microtubule loss was assayed 48 hours after transfection. Combination of [S45A] or [S45D] had no effect on dominant phenotypes by visual inspection: microtubule loss was observed with each construct, and mitochondrial fragmentation was observed with both ARL2[T30N, S45A] and ARL2[T30N, S45D]. These results were repeated with similar results.

ARL2 is phosphorylated in cells

In order to detect phosphorylation of ARL2, I first optimized immunoprecipitation (IP) of endogenous and exogenous ARL2, with the goal of performing radiolabeling followed by IP. Initially, I attempted to IP ARL2 under non-denaturing conditions by lysing cells in RIPA buffer. I was unable to detect any endogenous ARL2 in my IPs, and only able to IP about 10-15% of exogenous ARL2. Additionally, I found that I could not IP ARL2 from CHAPS or cholate containing buffers, as exogenous ARL2 was precipitated in the beads alone control under those conditions, without any ARL2 antibody added. However, I was able to successfully immunoprecipitate ARL2 under denaturing conditions. Cells were lysed by freezing and scraping cells in 2% SDS. Lysate in 2% SDS was then diluted in RIPA buffer without SDS to a final concentration of 0.1% SDS, and ARL2 was immunoprecipitated with our ARL2 rabbit polyclonal antibody. After some optimization (described under Materials and Methods), I was able to IP almost all endogenous ARL2 (Figure 2). I was only able to IP ARL2 with our polyclonal ARL2

antibody under these conditions; none of the nine monoclonal antibodies generated in the Emory antibody core facility was able to IP ARL2.

To determine if ARL2 is phosphorylated in cells, I performed radiolabeling of live cells with $^{32}P_i$. I labeled both untransfected cells as well as cells overexpressing ARL2 for 3 hours (1 mCi/ml) in serum free, phosphate free DMEM. After labeling, ARL2 was immunoprecipitated as described under Materials and Methods. Proteins were then resolved in SDS-PAGE gels, which were later dried and exposed to film. In both IPs of ARL2 overexpressing cells as well as untransfected cells, I found $^{32}P_i$ incorporation in a band that ran at ~20 kDa, the molecular weight for ARL2 (Figure 3). This signal was absent from the beads alone control without ARL2 antibody, suggesting that this 20 kDa signal represented ARL2. I observed $^{32}P_i$ incorporation into a 20 kDa band in the IP from untransfected HeLa cells, suggesting that endogenous ARL2 might be phosphorylated. The $^{32}P_i$ intensity was stronger in ARL2 overexpressing cells compared to untransfected cells, consistent with the stronger $^{32}P_i$ intensity at 20 kDa representing more $^{32}P_i$ incorporation in overexpressed ARL2.

$^{32}P_i$ is incorporated into ARL2[S45A]

I then asked if the ARL2 phosphorylation detected by $^{32}P_i$ incorporation was predominantly the result of modifying serine-45. I tested if $^{32}P_i$ incorporation seen when wild type ARL2 was over-expressed might be prevented if I instead expressed ARL2[S45A]. I expressed ARL2[S45A] or ARL2 in HeLa cells, labeled as before, and immunoprecipitated as described above. I found no change in $^{32}P_i$ incorporation between wild type ARL2 and ARL2[S45A] (Figure 4). Both wild type ARL2 and ARL2[S45A] express to similar levels (data not shown), suggesting that the presence of [S45A] had no effect on $^{32}P_i$ incorporation into the 20 kDa ARL2 band. The background in Figure 3 is noticeably higher than the background in Figure 2. I tested a variety of conditions, including adding phosphate to the washes, and found that the

number of washes of the IP is a key determinant of this background. Though I stopped working on this project before I could optimize the number of washes, I know that the optimal number of washes is somewhere between 2 and 5 using RIPA buffer. I encourage anyone following up on phosphorylation of ARL2 to first optimize the number of washes after radiolabeling and IP.

Given that the site of ARL2 phosphorylation was probably not due to incorporation of $^{32}P_i$ at serine-45, I turned to mass spectrometry in an attempt to identify novel sites of phosphorylation in ARL2 in this system. Because I obtained the strongest $^{32}P_i$ incorporation with overexpressed ARL2, I optimized my immunoprecipitation of overexpressed ARL2, and was able to detect ~0.5 ug of ARL2 on a gel, based upon visual inspection of Coomassie blue staining intensity (Figure 5). Despite this, mass spectrometry was unsuccessful in identifying any phosphorylation sites, although ARL2 peptides were found. Immunoprecipitation was performed as described above, with a mock radiolabeling period of 3 hours in serum free, phosphate free medium to mimic previous experiments. A variety of conditions for mass spectrometry were tried. First, ARL2 IPs were run on SDS-PAGE and Coomassie stained (Figure 5), and the ARL2 band was digested with either trypsin or chymotrypsin, eluted from the gel, and processed for mass spectrometry. To rule out the possibility that ARL2 peptides possibly containing the phosphorylation site were not eluting from the gel, the Emory Proteomics Core also attempted to digest the ARL2 IP without SDS-PAGE, as well as analyzing HeLa cells overexpressing ARL2. None of the attempts were successful at identifying any sites of ARL2 phosphorylation, despite obtaining good coverage of ARL2.

$^{32}P_i$ incorporation into ARL2 is diminished when cells are treated with metabolic inhibitors

Finally, I tested for functional significance of ARL2 phosphorylation. Treatment of cells with metabolic inhibitors causes increased ARL2 within mitochondria (Newman & Schiavon et al., manuscript submitted). Therefore, I tested whether ARL2 phosphorylation changed in

response to any of these metabolic inhibitors. HeLa cells were transfected with plasmids directing expression of ARL2, and treated with either vehicle control, 1 μM oligomycin (complex V inhibitor), 25 mM 2-deoxyglucose (glycolysis inhibitor), or 1 μM antimycin A (complex III inhibitor) for 3 hours simultaneously with radiolabeling. I previously observed that mitochondrial staining of ARL2 begins to increase noticeably after three hours of treatment with metabolic inhibitors (Newman & Schiavon et al., manuscript submitted). Following radiolabeling, immunoprecipitation, SDS-PAGE, and exposure to film was performed, as described above. As before, I observed $^{32}P_i$ incorporation into ARL2. However, in cells treated with metabolic inhibitors, the amount of $^{32}P_i$ incorporation into ARL2 was diminished (Figure 6). These results indicate that metabolic inhibition leads to a reduction in $^{32}P_i$ incorporation into ARL2, though repeating and testing other conditions that increase mitochondrial ARL2, e.g., deletion of MFNs, is required.

Discussion

In this chapter, I demonstrate that ARL2 is phosphorylated when overexpressed in HeLa cells, along with preliminary, suggestive data that endogenous ARL2 is also phosphorylated. I showed that this phosphorylation may be inversely correlated with conditions in the cell that increase ARL2 in mitochondria. However, this phosphorylation does not appear to be linked to serine-45. I also found no changes in phenotypes associated with expression of ARL2[S45A] or ARL2[S45D] either alone or when combined with the dominant active [Q70L] mutation. Thus, the functional significance of the phosphorylation of serine-45 on ARL2, reported more than 50 times in high throughput proteomics, remains to be determined. I was unable to identify any other putative phosphorylation sites on ARL2 by mass spectrometry, hampering further studies, though the correlation between the extent of phosphorylation of ARL2 and metabolic stressors argues that further studies should be performed.

I used an *in vivo* radiolabeling approach to demonstrate that overexpressed ARL2 is phosphorylated in HeLa cells. I observed $^{32}P_i$ incorporation into a ~20 kDa band in IPs that was enriched over IP from untransfected cells as well as IP without ARL2 antibody, consistent with $^{32}P_i$ incorporation occurring on ARL2. My data also suggest that endogenous ARL2 is phosphorylated, because a band running at the same size as overexpressed ARL2 also shows $^{32}P_i$ incorporation. However, several $^{32}P_i$ -containing bands were present in that IP (Figure 3), suggesting that other phosphoproteins were being precipitated with the ARL2 antibody. Therefore, controls such as antigen competition will be necessary to confirm that the 20 kDa band in the IP of untransfected cells corresponds to endogenous ARL2.

I showed in preliminary data that $^{32}P_i$ incorporation into overexpressed ARL2 was diminished with treatment of metabolic inhibitors. These metabolic inhibitors increase the amount of ARL2 in mitochondria (Newman & Schiavon et al., submitted). Therefore, these data suggest that the same conditions that increase ARL2 in mitochondria may also decrease ARL2 phosphorylation. An alternate interpretation of these results is that because these inhibitors lower ATP levels, incorporation of $^{32}P_i$ into the cellular ATP pool may be diminished, leading to less $^{32}P_i$ incorporation into ARL2. Overall $^{32}P_i$ signal along the entire lane appeared lower in IPs from metabolically challenged cells, supporting this interpretation. Therefore, future experiments should include several different treatments that increase ARL2 within mitochondria, such as serum starvation or deletion of MFN2 in MEFs, to minimize these concerns (Newman & Schiavon et al., manuscript submitted).

ARL2 has been shown to be phosphorylated at serine-45 by several mass spectrometry studies (17 studies according to Phosphosite Plus, as of September 2016). Therefore, I tested for a functional significance of serine-45 phosphorylation by generating phosphomimetic and phosphonull mutants of ARL2. The mutations [S45A] and [S45D] were introduced into ARL2, ARL2[Q70L], or ARL2[T30N]. Ultimately, neither [S45A] nor [S45D] had any effect on the

phenotypes caused by ARL2, ARL2[Q70L], or ARL2[T30N]. Microtubule loss and mitochondrial fragmentation were assayed; the mitochondrial hyperfusion phenotype caused by ARL2[Q70L] (Newman et al., manuscript submitted) had not yet been discovered so was not assayed. Data generated by another lab member, Josh Francis, indicates that serine-45 phosphorylation may be important for ARL2 binding to Cofactor D. While I was unable to detect any phosphorylation sites by mass spectrometry, Josh Francis did find serine-45 phosphorylation by mass spectrometry of the ARL2/Cofactor D/β tubulin complex, and did not observe serine-45 on purified ARL2 in a parallel experiment (unpublished data). Additionally, he found that ARL2[S45A] had a slight reduction in binding to Cofactor D, while ARL2[S45D] had a slight increase in binding to Cofactor D (Josh Francis, unpublished data). Because the majority of overexpressed ARL2 does not bind Cofactor D (Francis et al., manuscript in preparation), ARL2[S45A] or ARL2[S45D] may have yielded no phenotypes because the majority of exogenous protein is not bound to Cofactor D. The ARL2/Cofactor D complex is likely important for centrosomes (Cunningham and Kahn, 2008; Zhou et al., 2006), so it may be worth expressing ARL2[S45A] or ARL2[S45D] and inspecting centrosomes, which I did not assay. Finally, ARL2 localizes to and has functions in the nucleus (Muromoto et al., 2008); serine-45 phosphorylation may play a role in those functions. Therefore, a function for serine-45 phosphorylation in ARL2 biology remains to be determined.

The phosphorylation of ARL2 that I observed is likely not at serine-45, as I observed $^{32}P_i$ incorporation into ARL2[S45A]. Therefore, we wanted to identify other sites of phosphorylation on ARL2. After several attempts, we were ultimately unsuccessful in finding other sites of ARL2 phosphorylation, despite good coverage of ARL2. The percentage of overexpressed ARL2 in the cell that is phosphorylated may be small. If the $^{32}P_i$ positive 20 kDa band immunoprecipitated from untransfected cells is actually endogenous phosphorylated ARL2, then the fold increase of $^{32}P_i$ signal with ARL2 overexpression is much less than the fold increase in ARL2 protein with

overexpression, which we estimate to be 200-300 fold. Testing a range of cell lines may reveal one showing more ARL2 phosphorylation than that observed in HeLa cells. Finally, one might test for a functional significance for this ARL2 phosphorylation. Metabolic inhibitors may decrease ARL2 phosphorylation, but other treatments, such as cell cycle synchronization, may increase the amount of phosphorylation and improve probability of detection.

To summarize, I showed that ARL2 is indeed phosphorylated in cells, though in my HeLa cell model I could not confirm serine-45 as the site, despite extensive data from high throughput proteomics suggesting it to be the predominant site of phosphorylation. Further testing and optimization will be required to identify the site of phosphorylation and begin to test for functional significance. Additionally, the site of phosphorylation I identified is probably not serine-45, and the functional significance of serine-45 phosphorylation remains to be determined. Though based upon a large amount of preliminary data, I hypothesize that ARL2 binding to cofactor D is linked to phosphorylation. Therefore, the reduction in ARL2 phosphorylation may be correlated with conditions that lead to increased import of ARL2 into mitochondria, making phosphorylation a plausible mechanism for regulated import. The fact that only a small fraction of ARL2 is involved and that ARL2 is not expressed to very high levels endogenously makes testing of this model challenging, but no less important.

References

Bhamidipati, A., S.A. Lewis, and N.J. Cowan. 2000. ADP ribosylation factor-like protein 2 (Arl2) regulates the interaction of tubulin-folding cofactor D with native tubulin. J Cell Biol. 149:1087-1096.

Choudhary, C., J.V. Olsen, C. Brandts, J. Cox, P.N. Reddy, F.D. Bohmer, V. Gerke, D.E. Schmidt-Arras, W.E. Berdel, C. Muller-Tidow, M. Mann, and H. Serve. 2009. Mislocalized activation of oncogenic RTKs switches downstream signaling outcomes. Mol Cell. 36:326-339.

Cunningham, L.A., and R.A. Kahn. 2008. Cofactor D functions as a centrosomal protein and is required for the recruitment of the gamma-tubulin ring complex at centrosomes and organization of the mitotic spindle. J Biol Chem. 283:7155-7165.

Dephoure, N., C. Zhou, J. Villen, S.A. Beausoleil, C.E. Bakalarski, S.J. Elledge, and S.P. Gygi. 2008. A quantitative atlas of mitotic phosphorylation. Proc Natl Acad Sci U S A. 105:10762-10767.

Gauci, S., A.O. Helbig, M. Slijper, J. Krijgsveld, A.J. Heck, and S. Mohammed. 2009. Lys-N and trypsin cover complementary parts of the phosphoproteome in a refined SCX-based approach. Anal Chem. 81:4493-4501.

Humphrey, S.J., G. Yang, P. Yang, D.J. Fazakerley, J. Stockli, J.Y. Yang, and D.E. James. 2013. Dynamic adipocyte phosphoproteome reveals that Akt directly regulates mTORC2. Cell Metab. 17:1009-1020.

Huttlin, E.L., M.P. Jedrychowski, J.E. Elias, T. Goswami, R. Rad, S.A. Beausoleil, J. Villen, W. Haas, M.E. Sowa, and S.P. Gygi. 2010. A tissue-specific atlas of mouse protein phosphorylation and expression. Cell. 143:1174-1189.

Kahn, R.A., J. Cherfils, M. Elias, R.C. Lovering, S. Munro, and A. Schurmann. 2006. Nomenclature for the human Arf family of GTP-binding proteins: ARF, ARL, and SAR proteins. J Cell Biol. 172:645-650.

Klammer, M., M. Kaminski, A. Zedler, F. Oppermann, S. Blencke, S. Marx, S. Muller, A. Tebbe, K. Godl, and C. Schaab. 2012. Phosphosignature predicts dasatinib response in non-small cell lung cancer. Mol Cell Proteomics. 11:651-668.

Lundby, A., A. Secher, K. Lage, N.B. Nordsborg, A. Dmytriyev, C. Lundby, and J.V. Olsen. 2012. Quantitative maps of protein phosphorylation sites across 14 different rat organs and tissues. Nat Commun. 3:876.

Mabjeesh, N.J., D. Escuin, T.M. LaVallee, V.S. Pribluda, G.M. Swartz, M.S. Johnson, M.T. Willard, H. Zhong, J.W. Simons, and P. Giannakakou. 2003. 2ME2 inhibits tumor growth and angiogenesis by disrupting microtubules and dysregulating HIF. Cancer Cell. 3:363-375.

Mayya, V., D.H. Lundgren, S.I. Hwang, K. Rezaul, L. Wu, J.K. Eng, V. Rodionov, and D.K. Han. 2009. Quantitative phosphoproteomic analysis of T cell receptor signaling reveals system-wide modulation of protein-protein interactions. Sci Signal. 2:ra46.

Mertins, P., J.W. Qiao, J. Patel, N.D. Udeshi, K.R. Clauser, D.R. Mani, M.W. Burgess, M.A. Gillette, J.D. Jaffe, and S.A. Carr. 2013. Integrated proteomic analysis of post-translational modifications by serial enrichment. Nat Methods. 10:634-637.

Muromoto, R., Y. Sekine, S. Imoto, O. Ikeda, T. Okayama, N. Sato, and T. Matsuda. 2008. BART is essential for nuclear retention of STAT3. International Immunology. 20:395-403.

Newman, L.E., C.-j. Zhou, S. Mudigonda, A.L. Mattheyses, E. Paradies, C.M.T. Marobbio, and R.A. Kahn. 2014. The ARL2 GTPase Is Required for Mitochondrial Morphology, Motility, and Maintenance of ATP Levels. PLoS One. 9:e99270.

Sharer, J.D., J.F. Shern, H. Van Valkenburgh, D.C. Wallace, and R.A. Kahn. 2002. ARL2 and BART enter mitochondria and bind the adenine nucleotide transporter. Mol Biol Cell. 13:71-83.

Shern, J.F., J.D. Sharer, D.C. Pallas, F. Bartolini, N.J. Cowan, M.S. Reed, J. Pohl, and R.A. Kahn. 2003. Cytosolic Arl2 is complexed with cofactor D and protein phosphatase 2A. J Biol Chem. 278:40829-40836.

Trinidad, J.C., D.T. Barkan, B.F. Gulledge, A. Thalhammer, A. Sali, R. Schoepfer, and A.L. Burlingame. 2012. Global identification and characterization of both O-GlcNAcylation and phosphorylation at the murine synapse. Mol Cell Proteomics. 11:215-229.

Weber, C., T.B. Schreiber, and H. Daub. 2012. Dual phosphoproteomics and chemical proteomics analysis of erlotinib and gefitinib interference in acute myeloid leukemia cells. J Proteomics. 75:1343-1356.

Weintz, G., J.V. Olsen, K. Fruhauf, M. Niedzielska, I. Amit, J. Jantsch, J. Mages, C. Frech, L. Dolken, M. Mann, and R. Lang. 2010. The phosphoproteome of toll-like receptor-activated macrophages. Mol Syst Biol. 6:371.

Wisniewski, J.R., N. Nagaraj, A. Zougman, F. Gnad, and M. Mann. 2010. Brain phosphoproteome obtained by a FASP-based method reveals plasma membrane protein topology. J Proteome Res. 9:3280-3289.

Wu, X., L. Tian, J. Li, Y. Zhang, V. Han, Y. Li, X. Xu, H. Li, X. Chen, J. Chen, W. Jin, Y. Xie, J. Han, and C.Q. Zhong. 2012. Investigation of receptor interacting protein (RIP3)-dependent protein phosphorylation by quantitative phosphoproteomics. Mol Cell Proteomics. 11:1640-1651.

Zanivan, S., F. Gnad, S.A. Wickstrom, T. Geiger, B. Macek, J. Cox, R. Fassler, and M. Mann. 2008. Solid tumor proteome and phosphoproteome analysis by high resolution mass spectrometry. J Proteome Res. 7:5314-5326.

Zhou, C., L. Cunningham, A.I. Marcus, Y. Li, and R.A. Kahn. 2006. Arl2 and Arl3 regulate different microtubule-dependent processes. Mol Biol Cell. 17:2476-2487.

Zhou, H., S. Di Palma, C. Preisinger, M. Peng, A.N. Polat, A.J. Heck, and S. Mohammed. 2013. Toward a comprehensive characterization of a human cancer cell phosphoproteome. J Proteome Res. 12:260-271.

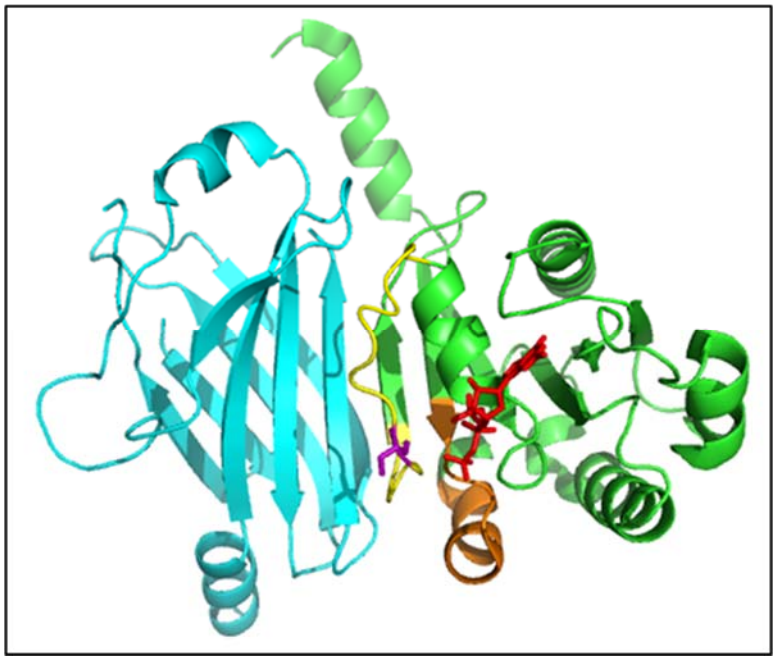

Figure 1. Serine-45, a predicted site of phosphorylation, interfaces with effectors. The crystal structure of ARL2 (green) bound to PDE-delta (pale blue), an effector, is shown (PDB: 1KSG). A phosphate group on serine-45 (purple), located within switch I (yellow), a conserved region that mediates binding to effectors, is predicted to disrupt binding of ARL2 to this and other effectors that utilize direct contacts with switch I.

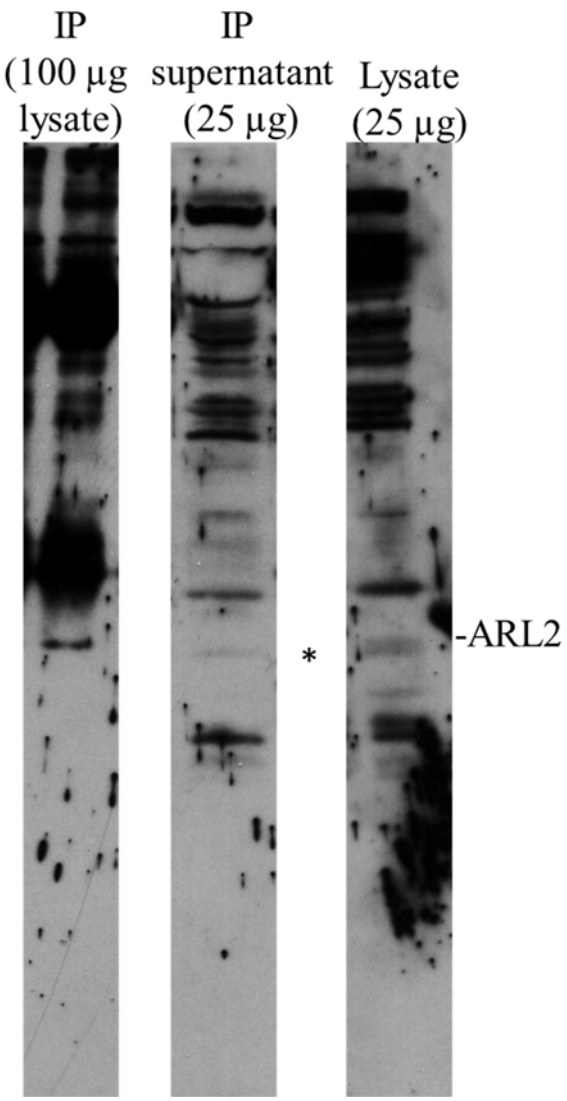

Figure 2. Immunoprecipitation (IP) of ARL2. ARL2 was immunoprecipitated from HeLa lysates prepared under denaturing conditions, resolved by SDS-PAGE, and blotted for ARL2, as described under Materials and Methods. Lane 1 (IP) is the total ARL2 immunoprecipitated from 100 µg of lysate. Lane 2 (Supernatant) is 25 µg of IP supernatant, and Lane 3 (Input) is 25 µg of the lysate used for the IP. The majority of ARL2 is immunoprecipitated from the input and is not detected in the supernatant. Nonadjacent lanes from the same blot are shown. Asterisk (*) indicates nonspecific band. This experiment was performed several times with similar results.

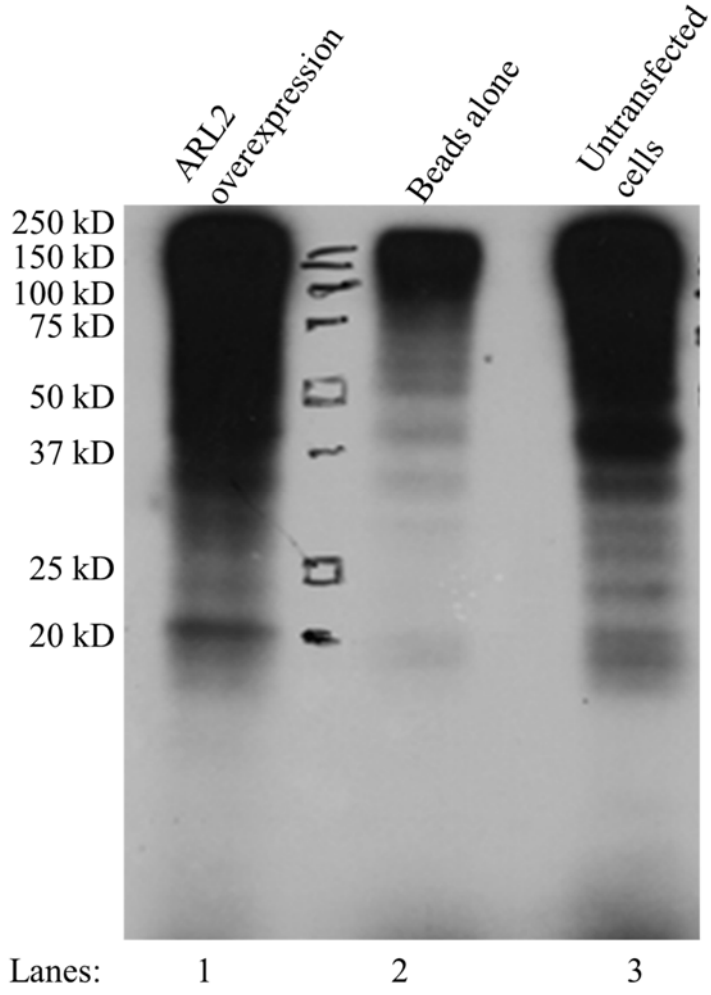

Figure 3. ARL2 is phosphorylated in cells. Untransfected or ARL2-overexpressing HeLa cells were labeled with $^{32}P_i$ for three hours, beginning 21 hours after transfection. ARL2 was immunoprecipitated from HeLa lysates prepared under denaturing conditions and resolved in an SDS gel, which was later dried and exposed to film for 19.5 hours, as described under Materials and Methods. Lane 1 is the ARL2 IP from HeLa cells overexpressing ARL2. Lane 2 is an IP without ARL2 antibody (beads alone) from untransfected HeLa lysate. Lane 3 (Input) is an ARL2 IP from untransfected lysate. In both ARL2 IPs, a ~20 kD band is observed that is absent from the beads alone negative control. The IP from cells overexpressing ARL2 has been repeated several times, while the IP of endogenous ARL2 requires further optimization and needs to be repeated.

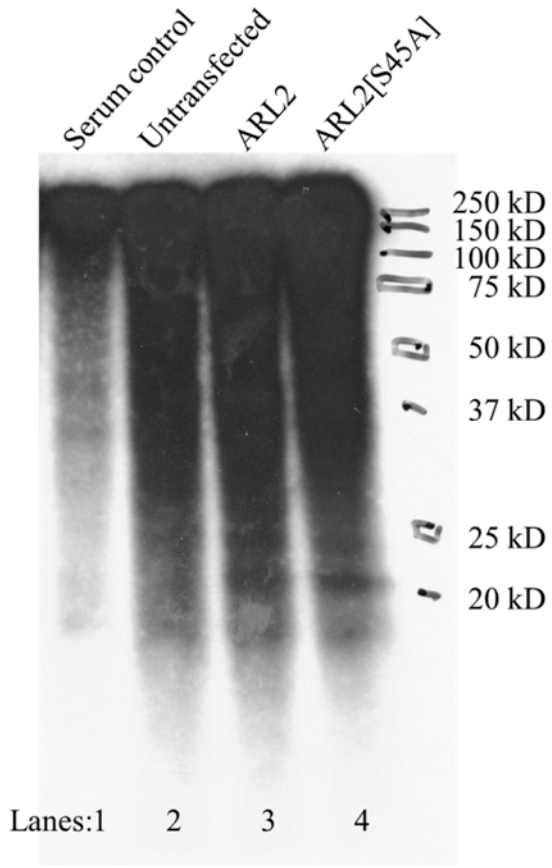

Figure 4. Both ARL2 and ARL2[S45A] are phosphorylated in cells. Untransfected cells (Lanes 1 and 2) and HeLa cells expressing ARL2 or ARL2[S45A] (Lanes 3 and 4) were subjected to radiolabeling and IP and exposed to film for 6.5 hours, as described under Materials and Methods. Lane 1 shows an IP from untransfectd HeLa cells using anti-ELMOD2 rabbit serum, and Lane 2 is an IP using ARL2 rabbit serum. Lane 3 is an ARL2 IP from cells overexpressing ARL2, and Lane 4 is an ARL2 IP from cells expressing ARL2[S45A]. A ~20 kD band is present in both lanes 3 and 4, suggesting that $^{32}P_i$ is incorporated into both ARL2 and ARL2[S45A]; this experiment was repeated a total of two times, with similar results. Lane 2 was an attempt to IP endogenous ARL2, which was difficult to discern due to high background. Data from other experiments suggest that the number of times the IP is washed prior to loading on the gel contributes to the background, and this needs to be further optimized.

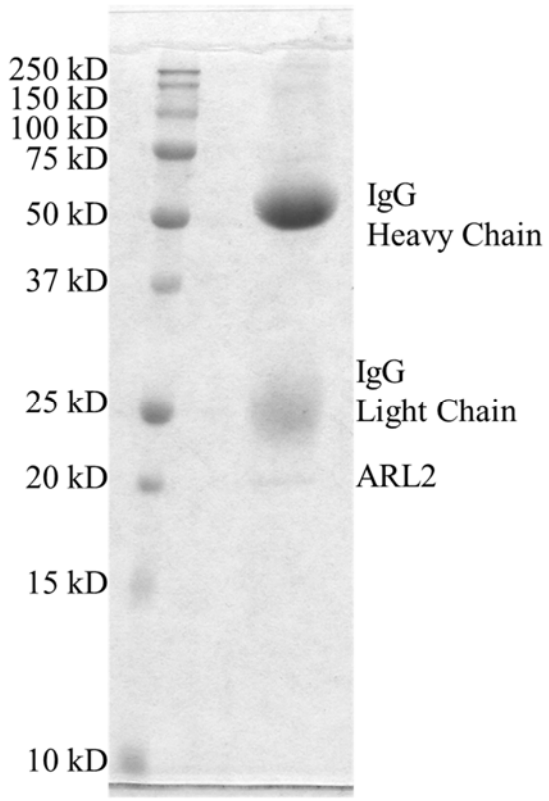

Figure 5. Optimized IP of overexpressed ARL2 for mass spectrometry. Lysates of HeLa cells were prepared and ARL2 IPs were performed as described under Materials and Methods. IPs were resolved by SDS-PAGE, and the gel was stained with Coomassie blue. ARL2 is (barely) visible by Coomassie staining as a ~20 kD band.

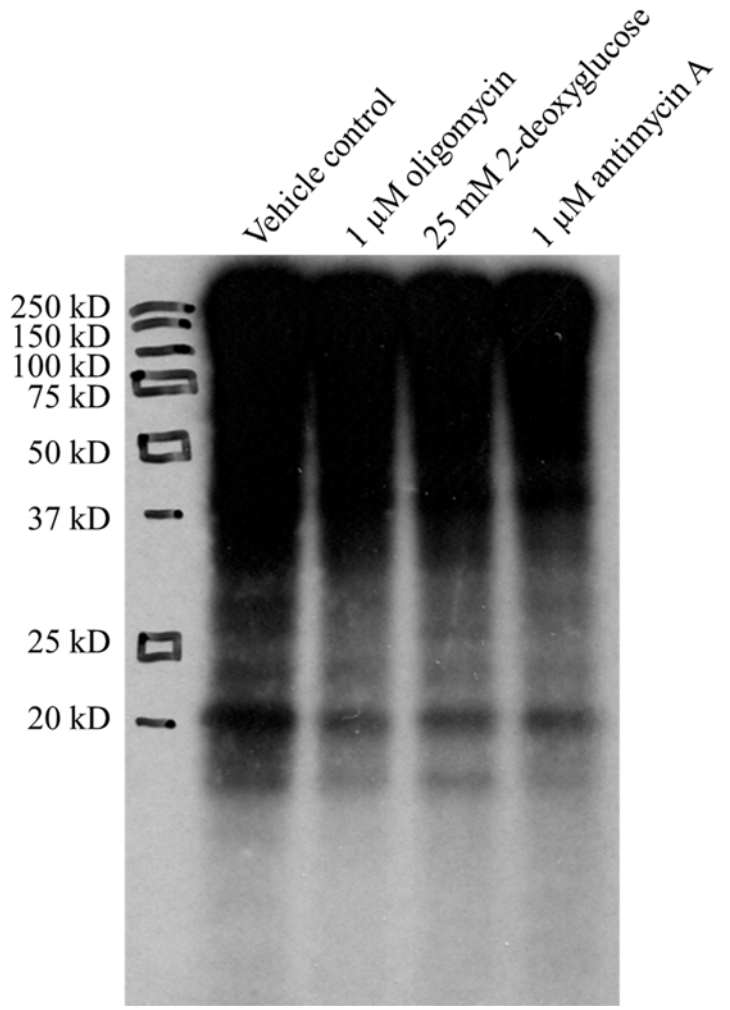

Figure 6. Treatment with metabolic inhibitors diminishes $^{32}P_i$ incorporation into ARL2. HeLa cells overexpressing ARL2 were subjected to vehicle control, oligomycin (1 μM), 2-deoxyglucose (25 mM), or antimycin A (1 μM) for 3 hours simultaneously with $^{32}P_i$ labeling. IPs were resolved by SDS-PAGE and exposed to film for 16 hours, as described under Materials and Methods. $^{32}P_i$ was incorporated into a ~20 kD band. In the metabolic inhibitor conditions, it appears that $^{32}P_i$ incorporation is diminished, both in the ~20 kD band as well as along the entire lane. This experiment was performed once and needs to be repeated.

Chapter 8: Discussion

Summary

Mitochondria provide several important functions for the cell, and constantly modify their morphology to adapt to the needs of the cell. Previous work by David Chan, Luca Scorrano, Jodi Nunnari, and others revealed that mitochondrial shape is regulated in part by mitochondrial fusion, and they have identified the key players (the large, dynamin-related GTPases MFN1, MFN2, and OPA1). However, how fusion and these GTPases are regulated remain open questions. In this dissertation, I show that ARL2 and ELMOD2 are novel regulators of mitochondrial fusion (Figure 1). Initially, we showed that ARL2 and ELMOD2 are each required for mitochondrial morphology (chapter 2). I later show that ARL2 regulates mitochondrial morphology by regulating fusion, and that it does so from the IMS, upstream of the mitofusins (chapter 4). Expanding on these studies, we show that the amount of ARL2 and ELMOD2 in mitochondria is responsive to cellular stress, as well as the fusogenic activity of MFN2 (chapter 5). These observations further support the conclusion that ARL2 and ELMOD2 are involved in and regulate mitochondrial fusion. In addition to its role in fusion, I provide preliminary data that ARL2 is phosphorylated in cells, and also that it regulates ATP levels via cristae morphology (chapters 7 and 6, respectively). Finally, published and preliminary data support the existence of a novel structure containing ARL2, ELMOD2, MFNs, and MIROs. Based on these data, we hypothesize that there is a complex important for coordination of mitochondrial fusion and motility, which will require more work to confirm. My research identifying ARL2 and likely ELMOD2 as novel regulators of fusion lays the groundwork for a better understanding of how fusion is regulated in response to cellular demands.

In chapter 2, I document that ARL2 is important for several mitochondrial functions. Loss of ARL2 causes mitochondrial fragmentation, a loss in plus-end directed motility, and a dramatic loss in cellular ATP. Expression of dominant inactive ARL2[T30N] also caused fragmentation and loss in motility but had no effect on ATP levels. These observations suggest

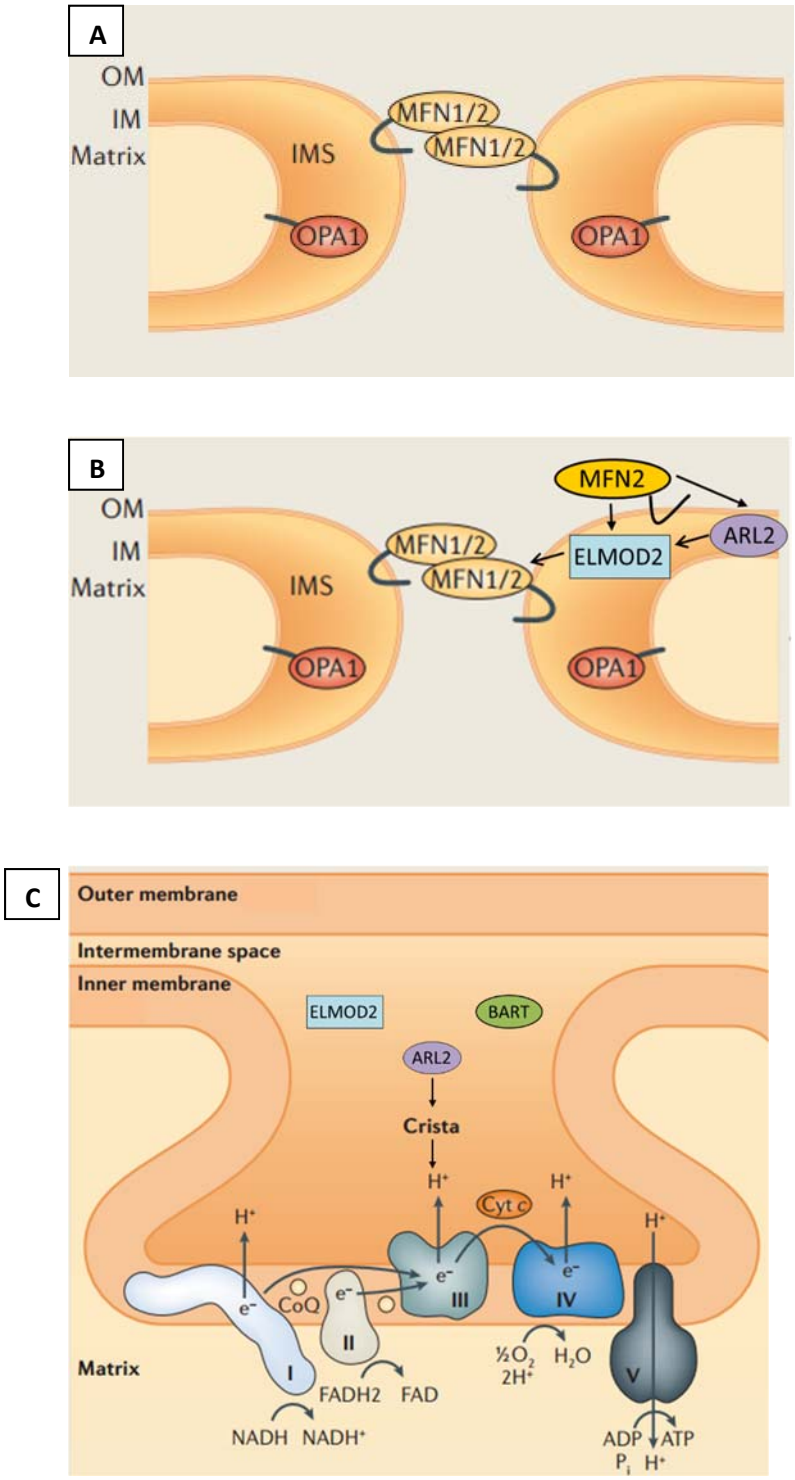

Figure 1. ARL2 and ELMOD2 are novel regulators of mitochondrial fusion. A) Prior to my work, the key players of mitochondrial fusion are identified, along with a basic mechanism. B) My work adds ARL2 as a regulator of fusion upstream of the mitofusins. My research also

implicates ELMOD2 as another novel regulator of mitochondrial fusion. C) In addition to mitochondrial fusion, I propose a second site of action for ARL2 in mitochondria, in regulation of ATP levels via cristae morphology, not involving either of its effectors ELMOD2 or BART. Outstanding questions arising from my research include: (1) Can ELMOD2 also stimulate MFN1 and MFN2 activity from the IMS? (2) What is the mechanism by which ARL2 and ELMOD2 stimulate MFN activity? Do they do so directly, or are other proteins downstream of ARL2/ELMOD2 and also upstream of MFNs? (3) What is the mechanism by which MFN2 regulates ARL2/ELMOD2 abundance in mitochondria? (4) Is increased ARL2/ELMOD2 in mitochondria a result of increased import or decreased degradation? (5) Does ARL2 regulate ATP production through cristae morphology, and if so, what is the mechanism? Figure adapted from Boxes 1and 2 in Mishra and Chan, 2014. Reprinted with permission (details at end of dissertation).

that ARL2 regulates two mitochondrial pathways: one regulating morphology/motility, and the other regulating ATP levels. In addition, we found that knockdown of ELMOD2 causes fragmentation and perinuclear clustering, but has no effect on ATP levels. These data suggest that ELMOD2 acts as an ARL2 effector rather than a GAP. To date, almost all ARF GAPs have also been shown to be effectors (East and Kahn, 2011). Therefore, we conclude there are two sites of action within mitochondria for ARL2, and that ELMOD2 is the ARL2 effector for its effects on mitochondrial morphology and motility.

Research from our lab demonstrates that ARL2 localizes to both the IMS as well as the matrix (Sharer et al., 2002). Therefore, we sought a way to target ARL2 to the IMS or matrix, in order to study its functions in each location. To this end, we used mitochondrial localization sequences from OCT and SMAC to drive ARL2 into either location (Horwich et al., 1985; Horwich et al., 1986; Ozawa et al., 2007; Sabharwal et al., 2013). These MLSs were chosen because they are cleaved after mitochondrial import, allowing us to assess the degree of processing (and thereby import) by immunoblot. In addition, we were worried about targeting exogenous ARL2 to the IMS and matrix since both are small compartments, particularly the IMS. To minimize this issue, we used a series of vectors containing truncated CMV promoters (Morita et al., 2012), to attenuate the expression of ARL2. By inserting the sequences for OCT and SMAC MLSs into these vectors, we generated a series of plasmids allowing for attenuated protein expression in each compartment, and have made these plasmids available to others via Addgene. Importantly, we documented that two proteins, GFP and ARL2, are expressed from these vectors, migrate on immunoblots as expected, and are targeted to the correct compartment. These plasmids allowed us to study the effects of exogenous ARL2 when targeted to the IMS and matrix (chapter 4).

In chapter 4, I expanded upon regulation of morphology by ARL2, and show that it regulates mitochondrial fusion. Dominant active and inactive mutants of ARL2 have opposite

effects on mitochondrial morphology, suggesting that increased ARL2 activity is associated with increased fusion. Using plasmids developed in chapter 3, I show that ARL2 regulates mitochondrial fusion from the IMS. I also found that dominant active ARL2[Q70L] can stimulate fusion through either MFN1 or MFN2. These findings are novel for several reasons. First, few regulators of mitochondrial fusion have been identified, and this is the first small GTPase identified as a regulator of fusion. ARL2 is also the first identified regulator of MFNs that acts from the IMS, as the previously described regulators of MFNs act from the cytosolic face of the outer membrane. Therefore, ARL2 likely plays a role in transmitting signals from the IMS to the outer membrane. ARL2 is also the first soluble regulator of fusion in the IMS; the other known fusion regulators are transmembrane proteins of the inner membrane that cleave OPA1. Finally, only two other proteins have been shown to reverse fragmentation in MFN null MEFs. Bax reverses fragmentation in *mfn1*$^{-/-}$ MEFs (Hoppins et al., 2011b), while OPA1 overexpression reverses fragmentation in *mfn2*$^{-/-}$ MEFs (Cipolat et al., 2004). To my knowledge, ARL2 is the first protein to reverse fragmentation in both *mfn1*$^{-/-}$ and *mfn2*$^{-/-}$ MEFs, further heightening the novelty. These observations build on our hypothesis that there is an ARL2-driven pathway in the mitochondrial IMS, regulating fusion independently of previously described pathways.

Chapter 5 further establishes roles for ARL2 and ELMOD2 in mitochondrial fusion, and that the levels of ARL2 and ELMOD2 in mitochondria are sensitive to the fusogenic activity of MFN2. MFN2 depletion increases mitochondrial ARL2 and ELMOD2, and this increase is only reversed with re-expression of MFN2 and restoration of tubular mitochondrial morphology. The fact that ARL2/ELMOD2 levels change in response to loss of MFN2, and not MFN1, is interesting because MFN2 is thought to have additional metabolic and signaling roles not shared with MFN1 (Bach et al., 2003; Chen et al., 2005; Pich et al., 2005; de Brito and Scorrano, 2008; Mourier et al., 2015), suggesting that these roles of MFN2 may be upstream of ARL2/ELMOD2. We show that the amounts of ARL2 and ELMOD2 in mitochondria increase in response to

cellular stress conditions that also result in mitochondrial elongation. Conditions that increase ARL2/ELMOD2 show substantial overlap with stress-induced mediated hyperfusion, suggesting that ARL2 and ELMOD2 play a role in this process (Tondera et al., 2009). Finally, we show that the amount of ARL2 and ELMOD2 are increased in mitochondria under these conditions. These results suggest that either import or degradation of ARL2 and ELMOD2 in mitochondria is regulated, though more work will be required to test this hypothesis.

In addition to its role in fusion, I also studied a role for ARL2 in ATP production. Based on data presented in chapter 2, we model the regulation of ATP as a separate site of action for ARL2 in mitochondria, not shared by ELMOD2. Previously, we showed that activated (GTP-bound) ARL2, complexed with its effector BART, binds ANT1. A potential relationship between ARL2 and ANT1 was supported by the fact that deletion of ANT1 led to increased mitochondrial ARL2 in heart and skeletal muscle (Sharer et al., 2002). Therefore, we hypothesized that ARL2 may regulate ATP levels through the ARL2/BART/ANT1 complex. However, in chapter 2 we found that knockdown of BART had no effect on ATP levels, and that neither ARL2 nor BART regulated ANT1 activity in vitro, arguing against this hypothesis. Testing of electron transport chain abundance (chapter 2) or function (chapter 6) revealed no obvious defects. Instead, I hypothesize that ARL2 regulates ATP levels via effects on cristae morphology. In chapter 6, I show preliminary data that ARL2 siRNA causes a loss in cristae density. Because cristae are domains of the inner membrane specialized for ATP production (Cogliati et al., 2016), loss in cristae could explain the loss of ATP caused by ARL2 siRNA. In support of this hypothesis, neither ARL2[T30N] nor ELMOD2 siRNA, which do not affect ATP levels, cause a reduction in cristae. A major limitation of these data is the lack of quantitative analysis, which should be performed before these data are published. However, based on preliminary data, I model that ARL2, in concert with ELMOD2, regulates fusion and also has a separate site of action in cristae morphology. In this regard, knockdown of ARL2 phenocopies knockdown of OPA1, which also

leads to a loss in fusion and cristae morphology (Cipolat et al., 2004; Griparic et al., 2004). Therefore, further study of a potential relationship between ARL2 and OPA1 may be warranted.

Future Directions

1. ELMOD2

In this dissertation, I present evidence that ELMOD2 regulates mitochondrial fusion and is thought to do so in concert with ARL2. Knockdown of ELMOD2 causes mitochondrial fragmentation, phenocopying ARL2[T30N] (chapter 2). Additionally, ELMOD2 levels in mitochondria are elevated in response to MFN2 depletion and are reversed by restoration of the fusogenic activity of MFN2, again phenocopying ARL2 (chapter 5). I also show that ELMOD2 localizes to puncta along mitochondria, and Cara Schiavon has shown that these puncta align with exogenously expressed MFN-myc containing puncta, similar to ARL2 (chapter 6). In addition, Cara Schiavon has shown that expression of ELMOD2-myc/his in *mfn2*$^{-/-}$ MEFs reverses mitochondrial fragmentation observed in that cell line, again similar to ARL2. Interestingly, ELMOD2[R167]-myc/his, a GAP dead mutant, also restores tubular morphology in *mfn2*$^{-/-}$ MEFs, to a similar extent as ELMOD2-myc/his (Cara Schiavon, unpublished data). These data support our model that ELMOD2 also regulates mitochondrial fusion, and that ELMOD2 is acting as an ARL2 effector rather than as a GAP. However, more work needs to be done, such as using the mito-PAGFP assay of fusion, to solidify a role for ELMOD2 in fusion.

2. ARL2/ELMOD2/MFN puncta

In chapters 4 and 6, Cara Schiavon and I provide data that ARL2, ELMOD2, and MFNs localize to puncta along mitochondria. Importantly, several mitochondrial proteins (summarized in chapter 4) do not show a similar localization pattern along mitochondria, suggesting that these puncta represent a novel structure involved in mitochondrial fusion. Based on the presence of these puncta as well as other data, I model that ELMOD2 binds GTP-bound

ARL2 to recruit components of a complex required for mitochondrial fusion. If our hypothesis is correct, then physical and functional characterization of these puncta is expected to lead to identification of novel components of the mitochondrial fusion machinery and their mechanisms of action. In particular, by identifying putative interacting partners of ARL2 and ELMOD2, we may find more IMS-localized regulators of MFNs. We plan to use a proximity labeling/BioID approach using APEX2 (Lam et al., 2015; Hung et al., 2016), combined with the plasmids generated in chapter 3, likely alongside co-immunoprecipitation to identify novel components of these puncta and test their activities. Cara Schiavon is currently generating these plasmid constructs and optimizing protocols to perform these experiments. There is a long history of protein complex identification from mitochondria leading to substantial increases in our understanding of mitochondrial functions; from the five complexes involved in the ETC, to the more recent MICOS and ERMES complexes, implicated in cristae morphology (Harner et al., 2011; Hoppins et al., 2011a; von der Malsburg et al., 2011; Alkhaja et al., 2012) and ER-mitochondrial contacts (Kornmann et al., 2009), respectively.

3. ARL2 and regulation of mitochondrial motility

We showed that loss of ARL2 and ELMOD2 also causes perinuclear clustering of mitochondria. Using ARL2[T30N] and ARL2 siRNA, we show that perinuclear clustering results from a loss in plus-end directed motility (chapter 2). Since then, I have generated additional preliminary data that ARL2 also regulates mitochondrial motility. In the experiments described in chapter 4, I observe that IMS-directed, (but not matrix or cytosol localized ARL2) caused fragmentation. I also observed that only IMS-directed ARL2[T30N] caused perinuclear clustering. This result suggests that ARL2 regulates plus-end directed motility from the IMS, though requires further optimization to quantify. Expression of ARL2[Q70L, F50A] or ARL2[Q70L, L3A], dominant active ARL2 mutants that are unable to cause microtubule destruction, causes extension of mitochondria to the cell periphery, similar to expression of

dominant active MIRO (Fransson et al., 2003; Fransson et al., 2006; Saotome et al., 2008). Another lab member, Rachel Turn, has repeated and is currently optimizing this phenotype. Strikingly, this phenotype is opposite from the perinuclear clustering caused by ARL2[T30N], and suggests that ARL2 activity within mitochondria regulates mitochondrial motility as well as fusion. In addition, I found that immunofluorescent imaging of myc-MIRO also revealed puncta that align with ARL2 puncta, suggesting a physical and functional relationship between the two. More work is required to elucidate if ARL2 regulates motility, and if ARL2 might regulate cross-talk between motility and fusion machinery. Excitingly, if our hypothesis that ARL2 also regulates motility is correct, identification of novel binding partners of ARL2/ELMOD2 discussed above may also yield novel regulators of mitochondrial motility.

Concluding remarks

Work pioneered by several mitochondrial labs has elucidated key players of mitochondrial fusion, as well as aspects of their fundamental mechanisms (Figure 1A). Additionally, several disease links have been identified, including links to dominant optic atrophy and Charcot-Marie-Tooth type 2A (Alexander et al., 2000; Delettre et al., 2000; Zuchner et al., 2004), highlighting the importance of mitochondrial fusion to human health. While mechanistic details are missing and still need to be addressed, the key questions that I believe will yield the most important gains in our understanding in the next decade are those involving regulation of the basic mechanisms described by the leading mitochondria labs. Given that mitochondria regulate several important cellular processes and modify their morphology to a wide variety of stressors (Tondera et al., 2009), several of these regulators will likely have roles in other cellular processes. For example, SMAD2, a recently identified activator of MFN2, already has well-established roles in signaling and gene expression in the nucleus (Kumar et al., 2016). Therefore, goals should include not only identification of novel regulators, but a better understanding of how these regulators integrate mitochondrial morphology with other pathways in the cell. It may prove

challenging to dissect multiple functions of these regulators. Here, I have identified ARL2 as a novel regulator of mitochondrial fusion, but ARL2 has several additional functions, including microtubule polymerization (Bhamidipati et al., 2000; Sharer et al., 2002; Shern et al., 2003; Zhou et al., 2006; Tian et al., 2010), gene expression (Muromoto et al., 2008), and trafficking (Ismail et al., 2011). However, tools described in this dissertation (CMVΔ0-6 SMAC-HA-ARL2, chapter three; [L3A], [I6R], and [F50A], chapter 6) have allowed us to begin dissecting the multiple roles of ARL2. If successful with our studies of ARL2, we will possess a better understanding of how mitochondrial fusion is integrated with microtubules, centrosomes, and the nucleus. Improved knowledge of regulation of mitochondrial fusion in context with the cell and stressful conditions will be important to understanding the pathology of the several human diseases linked to mitochondrial dynamics and are predicted to identify currently unknown targets for potential pharmacological intervention.

References

Alexander, C., Votruba, M., Pesch, U.E., Thiselton, D.L., Mayer, S., Moore, A., Rodriguez, M., Kellner, U., Leo-Kottler, B., Auburger, G., Bhattacharya, S.S., and Wissinger, B. (2000). OPA1, encoding a dynamin-related GTPase, is mutated in autosomal dominant optic atrophy linked to chromosome 3q28. Nat Genet 26, 211-215.

Alkhaja, A.K., Jans, D.C., Nikolov, M., Vukotic, M., Lytovchenko, O., Ludewig, F., Schliebs, W., Riedel, D., Urlaub, H., Jakobs, S., and Deckers, M. (2012). MINOS1 is a conserved component of mitofilin complexes and required for mitochondrial function and cristae organization. Mol Biol Cell 23, 247-257.

Bach, D., Pich, S., Soriano, F.X., Vega, N., Baumgartner, B., Oriola, J., Daugaard, J.R., Lloberas, J., Camps, M., Zierath, J.R., Rabasa-Lhoret, R., Wallberg-Henriksson, H., Laville, M., Palacin, M., Vidal, H., Rivera, F., Brand, M., and Zorzano, A. (2003). Mitofusin-2 determines

mitochondrial network architecture and mitochondrial metabolism. A novel regulatory mechanism altered in obesity. J Biol Chem 278, 17190-17197.

Bhamidipati, A., Lewis, S.A., and Cowan, N.J. (2000). ADP ribosylation factor-like protein 2 (Arl2) regulates the interaction of tubulin-folding cofactor D with native tubulin. J Cell Biol 149, 1087-1096.

Chen, H., Chomyn, A., and Chan, D.C. (2005). Disruption of fusion results in mitochondrial heterogeneity and dysfunction. J Biol Chem 280, 26185-26192.

Cipolat, S., de Brito, O.M., Dal Zilio, B., and Scorrano, L. (2004). OPA1 requires mitofusin 1 to promote mitochondrial fusion. Proc Natl Acad Sci U S A 101, 15927-15932.

Cogliati, S., Enriquez, J.A., and Scorrano, L. (2016). Mitochondrial Cristae: Where Beauty Meets Functionality. Trends Biochem Sci 41, 261-273.

de Brito, O.M., and Scorrano, L. (2008). Mitofusin 2 tethers endoplasmic reticulum to mitochondria. Nature 456, 605-610.

Delettre, C., Lenaers, G., Griffoin, J.M., Gigarel, N., Lorenzo, C., Belenguer, P., Pelloquin, L., Grosgeorge, J., Turc-Carel, C., Perret, E., Astarie-Dequeker, C., Lasquellec, L., Arnaud, B., Ducommun, B., Kaplan, J., and Hamel, C.P. (2000). Nuclear gene OPA1, encoding a mitochondrial dynamin-related protein, is mutated in dominant optic atrophy. Nat Genet 26, 207-210.

East, M.P., and Kahn, R.A. (2011). Models for the functions of Arf GAPs. Semin Cell Dev Biol 22, 3-9.

Fransson, A., Ruusala, A., and Aspenstrom, P. (2003). Atypical Rho GTPases have roles in mitochondrial homeostasis and apoptosis. J Biol Chem 278, 6495-6502.

Fransson, S., Ruusala, A., and Aspenstrom, P. (2006). The atypical Rho GTPases Miro-1 and Miro-2 have essential roles in mitochondrial trafficking. Biochem Biophys Res Commun 344, 500-510.

Griparic, L., van der Wel, N.N., Orozco, I.J., Peters, P.J., and van der Bliek, A.M. (2004). Loss of the intermembrane space protein Mgm1/OPA1 induces swelling and localized constrictions along the lengths of mitochondria. J Biol Chem 279, 18792-18798.

Harner, M., Korner, C., Walther, D., Mokranjac, D., Kaesmacher, J., Welsch, U., Griffith, J., Mann, M., Reggiori, F., and Neupert, W. (2011). The mitochondrial contact site complex, a determinant of mitochondrial architecture. EMBO J 30, 4356-4370.

Hoppins, S., Collins, S.R., Cassidy-Stone, A., Hummel, E., Devay, R.M., Lackner, L.L., Westermann, B., Schuldiner, M., Weissman, J.S., and Nunnari, J. (2011a). A mitochondrial-focused genetic interaction map reveals a scaffold-like complex required for inner membrane organization in mitochondria. J Cell Biol 195, 323-340.

Hoppins, S., Edlich, F., Cleland, M.M., Banerjee, S., McCaffery, J.M., Youle, R.J., and Nunnari, J. (2011b). The soluble form of Bax regulates mitochondrial fusion via MFN2 homotypic complexes. Mol Cell 41, 150-160.

Horwich, A.L., Kalousek, F., Fenton, W.A., Pollock, R.A., and Rosenberg, L.E. (1986). Targeting of pre-ornithine transcarbamylase to mitochondria: Definition of critical regions and residues in the leader peptide. Cell 44, 451-459.

Horwich, A.L., Kalousek, F., Mellman, I., and Rosenberg, L.E. (1985). A Leader Peptide Is Sufficient to Direct Mitochondrial Import of a Chimeric Protein. Embo Journal 4, 1129-1135.

Hung, V., Udeshi, N.D., Lam, S.S., Loh, K.H., Cox, K.J., Pedram, K., Carr, S.A., and Ting, A.Y. (2016). Spatially resolved proteomic mapping in living cells with the engineered peroxidase APEX2. Nat Protoc 11, 456-475.

Ismail, S.A., Chen, Y.-X., Rusinova, A., Chandra, A., Bierbaum, M., Gremer, L., Triola, G., Waldmann, H., Bastiaens, P.I.H., and Wittinghofer, A. (2011). Arl2-GTP and Arl3-GTP regulate a GDI-like transport system for farnesylated cargo. Nat Chem Biol 7, 942-949.

Kornmann, B., Currie, E., Collins, S.R., Schuldiner, M., Nunnari, J., Weissman, J.S., and Walter, P. (2009). An ER-mitochondria tethering complex revealed by a synthetic biology screen. Science 325, 477-481.

Kumar, S., Pan, Christopher C., Shah, N., Wheeler, Sarah E., Hoyt, Kari R., Hempel, N., Mythreye, K., and Lee, Nam Y. (2016). Activation of Mitofusin2 by Smad2-RIN1 Complex during Mitochondrial Fusion. Molecular Cell 62, 520-531.

Lam, S.S., Martell, J.D., Kamer, K.J., Deerinck, T.J., Ellisman, M.H., Mootha, V.K., and Ting, A.Y. (2015). Directed evolution of APEX2 for electron microscopy and proximity labeling. Nat Methods 12, 51-54.

Morita, E., Arii, J., Christensen, D., Votteler, J., and Sundquist, W.I. (2012). Attenuated protein expression vectors for use in siRNA rescue experiments. Biotechniques 0, 1-5.

Mourier, A., Motori, E., Brandt, T., Lagouge, M., Atanassov, I., Galinier, A., Rappl, G., Brodesser, S., Hultenby, K., Dieterich, C., and Larsson, N.G. (2015). Mitofusin 2 is required to maintain mitochondrial coenzyme Q levels. J Cell Biol 208, 429-442.

Muromoto, R., Sekine, Y., Imoto, S., Ikeda, O., Okayama, T., Sato, N., and Matsuda, T. (2008). BART is essential for nuclear retention of STAT3. International Immunology 20, 395-403.

Ozawa, T., Natori, Y., Sako, Y., Kuroiwa, H., Kuroiwa, T., and Umezawa, Y. (2007). A Minimal Peptide Sequence That Targets Fluorescent and Functional Proteins into the Mitochondrial Intermembrane Space. ACS Chemical Biology 2, 176-186.

Pich, S., Bach, D., Briones, P., Liesa, M., Camps, M., Testar, X., Palacin, M., and Zorzano, A. (2005). The Charcot-Marie-Tooth type 2A gene product, Mfn2, up-regulates fuel oxidation through expression of OXPHOS system. Hum Mol Genet 14, 1405-1415.

Sabharwal, S.S., Waypa, G.B., Marks, J.D., and Schumacker, P.T. (2013). Peroxiredoxin-5 targeted to the mitochondrial intermembrane space attenuates hypoxia-induced reactive oxygen species signalling. Biochem J 456, 337-346.

Saotome, M., Safiulina, D., Szabadkai, G., Das, S., Fransson, A., Aspenstrom, P., Rizzuto, R., and Hajnoczky, G. (2008). Bidirectional Ca2+-dependent control of mitochondrial dynamics by the Miro GTPase. Proc Natl Acad Sci U S A 105, 20728-20733.

Sharer, J.D., Shern, J.F., Van Valkenburgh, H., Wallace, D.C., and Kahn, R.A. (2002). ARL2 and BART enter mitochondria and bind the adenine nucleotide transporter. Mol Biol Cell 13, 71-83.

Shern, J.F., Sharer, J.D., Pallas, D.C., Bartolini, F., Cowan, N.J., Reed, M.S., Pohl, J., and Kahn, R.A. (2003). Cytosolic Arl2 is complexed with cofactor D and protein phosphatase 2A. J Biol Chem 278, 40829-40836.

Tian, G., Thomas, S., and Cowan, N.J. (2010). Effect of TBCD and its regulatory interactor Arl2 on tubulin and microtubule integrity. Cytoskeleton (Hoboken) 67, 706-714.

Tondera, D., Grandemange, S., Jourdain, A., Karbowski, M., Mattenberger, Y., Herzig, S., Da Cruz, S., Clerc, P., Raschke, I., Merkwirth, C., Ehses, S., Krause, F., Chan, D.C., Alexander, C., Bauer, C., Youle, R., Langer, T., and Martinou, J.C. (2009). SLP-2 is required for stress-induced mitochondrial hyperfusion. EMBO J 28, 1589-1600.

von der Malsburg, K., Muller, J.M., Bohnert, M., Oeljeklaus, S., Kwiatkowska, P., Becker, T., Loniewska-Lwowska, A., Wiese, S., Rao, S., Milenkovic, D., Hutu, D.P., Zerbes, R.M., Schulze-Specking, A., Meyer, H.E., Martinou, J.C., Rospert, S., Rehling, P., Meisinger, C., Veenhuis, M., Warscheid, B., van der Klei, I.J., Pfanner, N., Chacinska, A., and van der Laan, M. (2011). Dual role of mitofilin in mitochondrial membrane organization and protein biogenesis. Dev Cell 21, 694-707.

Zhou, C., Cunningham, L., Marcus, A.I., Li, Y., and Kahn, R.A. (2006). Arl2 and Arl3 regulate different microtubule-dependent processes. Mol Biol Cell 17, 2476-2487.

Zuchner, S., Mersiyanova, I.V., Muglia, M., Bissar-Tadmouri, N., Rochelle, J., Dadali, E.L., Zappia, M., Nelis, E., Patitucci, A., Senderek, J., Parman, Y., Evgrafov, O., Jonghe, P.D., Takahashi, Y., Tsuji, S., Pericak-Vance, M.A., Quattrone, A., Battaloglu, E., Polyakov, A.V., Timmerman, V., Schroder, J.M., and Vance, J.M. (2004). Mutations in the mitochondrial GTPase mitofusin 2 cause Charcot-Marie-Tooth neuropathy type 2A. Nat Genet 36, 449-451.

Licence agreement (For figures in introduction and discussion chapters)